University of Stavanger

**Faculty of Science and Technology**

# MASTER'S THESIS

| Study program/Specialization:<br><br>Master of Science in Engineering Structures and Materials | Spring semester, 2021<br><br>Open |
|---|---|
| Writer:<br>Gösta Elin Johanna Graneland | |
| Faculty supervisor: Samindi Samarakoon<br><br>External supervisor(s): | |
| Thesis title:<br>Flexural behavior of cracked reinforced concrete beams with externally bonded CFRP plates | |
| Credits (ECTS): 30 | |
| Key words:<br>Concrete<br>CFRP<br>Strengthening system<br>Sika | Pages: 151<br>+ enclosure: 83<br><br>Stavanger, 10/07/21<br>Date/year |

# Preface

This Master thesis concludes the last requirement to fulfill a degree in Master of Science in Engineering Structures and Material at the University of Stavanger, Faculty of Science and Technology, Norway.

The thesis covers 30 ECTS and was carried out spring semester of 2021.

I would like to express my gratitude to my supervisor at the University of Stavanger, Samindi Samarakoon for guidance and consultation throughout the duration of the thesis. Her dedication and support in all stages of the thesis, from planning to performing of the laboratory testing, as well as analysis of final result have been highly appreciated.

I would also like to express my gratitude to Sika Norge AS, for providing the carbon fiber plates and structural adhesive used for the laboratory testing, and Åge Rettvin for consultation and advice regarding the use of the material.

Gratitude is also extended to Geir Nuland and Chem-Con AS for practical advice regarding application of the strengthening system, Ronny Hansen and Polygon Stavanger for supplying a concrete grinder, Arnt-Henning from HBK Services and Solutions for practical advice regarding installation of strain gauges onto fiber reinforced composites.

In addition, I would like to thank the laboratory staff at the University of Stavanger for assistance of the practical part of the thesis, including Jarle Berge, Samdar Kakay, Jan-Tore Jakobsen and Swen Roemer. Additional muscle power and experience have been much appreciated in areas where my physical capacities were not sufficient.

# Abstract

The purpose of this thesis is to perform an experimental study of the flexural behavior of damaged reinforced concrete beams strengthened with externally bonded Carbon Fiber Reinforced Polymer (CFRP) plates. Damage have been simulated by applying different pre-load prior to installation of the strengthening system. The effect of existing cracks and different degree of damage have been evaluated from failure test under a 4-point load arrangement of the strengthened members. Same reinforcement configuration of the externally bonded CFRP plates will be used for eight different test specimens subjected do different degree of preload with corresponding different degree of crack formation in the concrete substrate.

The resulting failure capacity have been evaluated and compared to theoretical predictions. Different national guidelines and codes for FRP strengthened concrete structures have been reviewed to compare different design parameters and the corresponding theoretical capacity. The experimental work will give a greater understanding of the failure behavior of concrete beams reinforced with CFRP and the accuracy of current guidelines for CFRP design can be validated with the test results.

The results obtained from experimental testing revealed a lower capacity of the strengthened beams compared to the theoretical prediction. Failure mode for all the test specimen were governed by formation of flexural cracks within constant bending zone followed by sudden debonding of the CFRP plates from the concrete substrate. To prevent debonding, strain limits of the FRP are implemented in the design. During test, the developed strain in the CFRP plates were monitored and recorded with strain gauges. The results from the test revealed neither theoretical failure load nor theoretical strain limit were reached.

Despite the lower ratio of experimental over theoretical result, a capacity increase between 70-80% were found for the CFRP strengthened beams and the result demonstrated the vast potential of capacity enhancement possible to attain by externally bonded CFRP reinforcement.

# Table of contents

# List of figures

# List of tables

# 1 Introduction

## 1.1 Background

Deterioration and damage of existing structures are unavoidable, and material degradation along with damage accumulation will affect the structural integrity of any structure over time. Concrete structures are in general designed for a long service life and continuous maintenance and repair are vital in order to fulfill the design requirements of a structure throughout the service life.

Various reasons may affect the need for repair or retrofitting of an existing concrete structure. Material deterioration may be attributed to general ageing, environmental impact, accidental events, errors during construction or poor initial, design which may result in an insufficient structural capacity. During the service life, changes in the use of a structure or changes of applied load may lead to load situations exceeding the initial design loads and thereby change the demand on the structural capacity [1, p.57].

Different techniques are used for strengthening or retrofitting of existing concrete structures. Traditionally this was accomplished using conventional construction materials and techniques. Externally bonded steel plates, steel or concrete jackets, or external post-tensioning are some of the traditional techniques. [2, p.3] Strengthening of concrete structures by bonding steel plates to the surface of the tension zone with adhesive and bolts were developed in the 1960s [3, p.1] and were shown to be a viable technique to increase the flexural strength of the member [2, p.10].

However, due to the corrosive nature of steel, the adhesive bond between the steel and concrete deteriorates over time. Installation procedure of externally bonded steel plates are also difficult due to the relatively high weight of the material and the equipment needed for installation [2, p.10]. The length of steel plates is generally limited and strengthening of longer spans might require joint [3, p.9]. Fiber reinforced polymer materials were therefore introduced as an alternative to steel plates for external reinforcement.

The initial development of externally bonded FRP systems for retrofitting of concrete structures occurred in the 1980s in both Europe and Japan. [2, p.10] Application of Fiber Reinforced Polymers (FRP) on existing structures are today an acknowledged method to improve the load bearing capacity of a structure in service. FRP are used both as a repair method and to reinforce structures in need of strengthening. The material properties of FRP makes it superior to the use of steel plates with a high strength to weight ratio, chemical resistance as well as the ease of application.

## 1.2 Objective

The objective of the thesis is to study the flexural behavior of damaged reinforced concrete beams reinforced with Carbon Fiber Reinforced Polymer (CFRP) plates. The reinforced concrete beams have been damaged by applying different degree of load to induce different extent of crack formation in the beams prior to installation of the CFRP plates. By experimental evaluation, the effect of existing cracks has been evaluated with respect to the ultimate capacity of the CFRP strengthened member.

The flexural behavior of the beams will be evaluated both analytically and through experimental work, and the theoretical calculations are compared to actual results from laboratory testing.

The reinforced concrete beams used for the experiment has been casted at the University of Stavanger. The strengthening system was provided from Sika Norway consisting of CFRP plates, Sika CarboDur S512, to be used in conjunction with the structural adhesive Sikadur 30. Application of the strengthening system has also been performed at the University of Stavanger.

## 1.3 Limitations

The scope of the thesis is limited to flexural strengthening using CFRP plates, consideration of other types fiber reinforcement or other types of strengthening will not be included.

Another limitation is the performance of the installation of the strengthening system. Referring to the Method Statement of Sika CarboDur system, the limitations listed for the use of the strengthening system expresses: *"All the works must be carried out as directed by qualified engineer as the Supervising Officer"* [4]. Also defined in the Product Data Sheet for both the CFRP plates and the adhesive, specifications regarding the use of the product expresses: *"Sika CarboDur S/Sikadur 30 may only be used by experienced professionals"* [5][6]. Since the application of the strengthening system was executed without any prior experience in the field, some uncertainties regarding the performance of the installation must be considered.

Some unexpected difficulties occurred during casting, affecting the concrete surface quality of the beams. Additional surface repair was therefore required to be able to proceed with the intended test program. This should also be considered a limitation due to the associated uncertainty of the repair work performed.

## 1.4 Thesis overview

The thesis is outlined as illustrated in Table 1.1. Chapter 2. is a literature review and serves as a foundation for the approach used for the conducted experiment. First a theoretical introduction of FRP composites and the mechanical properties of the material are described. Followed by the advantages and disadvantages associated with the material and its use as reinforcement material for structural applications. The theoretical approach for flexural strengthening is reviewed with respect to different available guidelines followed by the application process of the strengthening system used for the experiment.

Chapter 3. describes the performance of the experiment, including casting of the reinforced concrete beam, surface preparation and installation of the CFRP plates. Result from the capacity test of the four reference beams are presented to determine the load limits used for the preloading of the CFRP strengthened beams. To evaluate the actual strength of concrete at time of testing, compression strength, tensile splitting strength and E-modulus tests are performed. The results from the tests are presented to define the actual concrete strength parameters used for the theoretical derivation of ultimate capacity. Lastly, the theoretical prediction of the strengthened capacity is derived, based approach defined in Chapter 2, with the actual concrete strength found from test.

Chapter 4. presents the result of the capacity test of the CFRP strengthened beams with the associated failure mode. The results from the test are discussed and evaluated. Due to failure mode governed by delamination of all the plates, theoretical derivation of the different FRP separation criteria are performed in Chapter 5. Different initiation mechanism for delamination are evaluate using the actual failure load found in Chapter 4. Further a verification of the theoretical approach used are compared and verified with the results given Sika CarboDur FRP Design software.

Table 1.1 Outline of thesis

| **Theory** | |
|---|---|
| **Chapter 2:** | FRP composite material<br>Design approach for flexural strengthening using FRP reinforcement<br>Application method for externally bonded CFRP plates |
| **Method and Materials** | |
| **Chapter 3:** | Preparation of test specimen<br>Test and result of concrete strength properties<br>Theoretical prediction of strengthened capacity |
| **Experimental result** | |
| **Chapter 4:** | Result from capacity test of strengthened beams |
| **Discussion of theoretical and experimental capacity** | |
| **Chapter 5:** | Evaluation of experimental result with debonding criteria |
| **Discussion about failure behavior and debonding** | |
| **Chapter 6:** | **Conclusion** |

# 2 Theory

## 2.1 Fiber reinforced polymers

Composites are collective notation for materials made up of two or more components, combined in order to enhance the physical or chemical properties. By combining different materials, the properties of the composite can be tailored to different needs. The advantage of composite action can be exemplified by reinforced concrete, where the tension strength of steel is utilized to strengthen the concrete section.

Fiber reinforced polymer (FRP), are a composite material consisting of high strength fiber embedded in a polymer matrix. The fibers in the composite are the load bearing component, while the polymer matrix transfer the stresses between the fibers and provides protection from the environment. Utilizing the fact that most materials are stronger and stiffer in fibrous form compared to bulk material [7, p.7], fiber reinforced polymers can attain a very high strength-to-weight ratio, making it an ideal material in many engineering disciplines.

The mechanical properties of the FRP can be alternated and tailored to its intended use, and therefore the propertied of FRP have large variation for different application. For structural applications of FRP, unidirectional stiffness and strength are often emphasized [8, p.5-6]. Although the strength and stiffness of FRP are governed by the fibers, the overall material properties of the composite depend on several factors. The material properties of the FRP composite are dependent on the composition of the constituents, the mechanical properties of the constituent materials themselves, the relative proportions of fiber and matrix, as well as the orientation of the fibers within the matrix and the method of manufacture [8, p.8].

### 2.1.1 Fiber

There are mainly three types of fibers used in FRP composites for strengthening applications. Glass fibers, carbon fibers and aramid fibers. [10, p.12] Characteristic for all the fibers is a high strength compared to conventional construction material. All the fibers display linear elastic behavior up to rupture. Figure 2.1 below illustrates typical properties for different unidirectional fiber types compared to the stress strain diagram for mild steel.

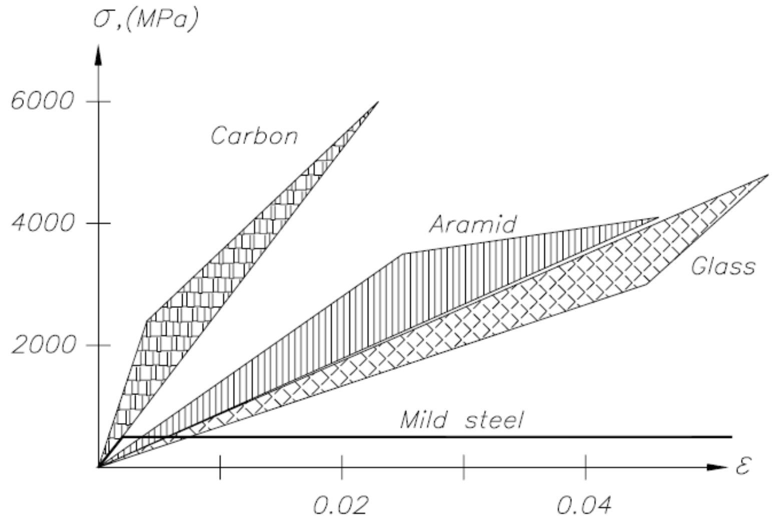


Figure 2.1 Stress-strain diagram for different fibers [10]

The type of fiber used in a particular application depends on different factors. The type of structure, the expected loading and the environmental condition needs to be considered, as well as the required strength, stiffness, durability and economical limitations [3, p.18].

Characteristic for structural FRP applications are continuous fibers oriented in specified direction, yielding orthotropic properties, where strength and stiffness are higher in the fiber directions [8, p.5]. In civil engineering applications, regarding strengthening of existing concrete structures, CFRP, are the most used FRP [9, p.15]. The high strength and E-modulus, low density and resistance to thermal, chemical and environmental effect makes it an attractive choice for structural strengthening where weight and deflection are critical factors [8, p.6].

### 2.1.2 Matrix

While the fibers provide the strength and stiffness of a FRP composite, the matrix binds the fibers together, to form composite action between the constituents. The matrix is essential to transfer the forces between the fibers, protect the fibers from the environment impact and redistribute the forces if a fiber is fractured [10, p.10].

Polymer matrices are either thermoset or thermoplastic. For structural application, thermoset polymers are most often used. These polymers display good thermal stability at service temperatures, good chemical resistance and low creep and relaxation properties in comparison to thermoplastics. Epoxy resin, polyester and vinylester are the three most common used thermosetting resins for manufacturing structural composites [8, p.4].

Due to the ease of processing and relative low cost, polyester is a commonly used matrix material for many fiber reinforced composites. Vinylester are used in manufacture if FRP reinforcing bars due to the resistivity to alkalis. Epoxy resin are often used for applications of FRP plates and sheets used for structural rehabilitation due to the high toughness and great adhesion properties [8, p.5]. In general, epoxy resin has better mechanical properties than both polyester and vinylester, but also, the more expensive material [7, p.7].

### 2.1.3 Adhesive

The adhesive between the concrete surface and the FRP composite are a crucial part of the strengthened system as the adhesive provides the shear load path between the components, enabling the development of composite action. The adhesive used for structural strengthening needs to have documented properties suitable for use of externally bonded reinforcement [10, p.37]. For structural applications, two-component epoxy adhesive are mainly used, consisting of an epoxy resin mixed with a hardener [7, p.5].

### 2.1.4 Advantage and disadvantage of FRP

**Advantages**

FRP composites are a relatively expensive material, which often are a governing factor for material selection. For retrofitting and strengthening of existing structures however, the speed and ease of installation of FRP composites, makes it an attractive option to more conventional strengthening techniques. For locations where space and accessibility are limited or projects where installation time are critical, strengthening system with FRP composites are particularly advantageous [3, p.7].

Since strengthening by externally bonded FRP systems were developed as an alternative to traditional external reinforcement techniques, the advantages of using FRP composites compared to steel are listed below [3, p8-9] [8, p.2].

- FRP have higher ultimate strength and lower density than steel, yielding a high strength to weight ratio
- Lower weight of FRP composites makes handling and installation of strengthening system significantly easier than steel
- Flexibility of FRP composites enables installation on curved profiles, steel plates would have to be pre-bent to required radius
- FRP materials are available in long lengths while steel plates often have limited lengths
- Ability to tailor mechanical properties by appropriate choice and direction of fibers
- High chemical resistance

**Disadvantages**

However, several disadvantages are also associated with the use of FRP composites and needs to be carefully considered.

Two disadvantages associated with externally bonded FRP composites are the vulnerability to mechanical damage and fire exposure. Since externally bonded reinforcement are exposed and the FRP material itself are brittle [9, p.8], the risk of damage due to accidental event, vandalism or impact must be considered.

The epoxy adhesive used for bonding of the strengthening system are also vulnerable to elevated temperatures, as epoxy resin have a glass transition temperature $T_g$ in range between 50°C and 65°C [3, p.24]. The glass transition temperature defines a change in the characteristics of the adhesive where the polymer transforms from a solid state to less stiff state resulting in degradation of the adhesive bond [3, p.24].

Considerations regarding loss of composite action must therefore be implemented in the design of a strengthened system, to ensure damage of the externally bonded reinforcement does not lead to partial or complete collapse of the structure.

Other disadvantages concern the high initial material cost of FRP material, which can be several times higher than steel [8, p.2].

Documented long-term durability of FRP strengthened structures are limited [3, p.12] Even though FRP composites have been used in the aerospace industry for over 50 years the application and requirements for FRP material are different [10, p.1]. Civil engineering structures are designed for long service life with high statical loading whereas aerospace industry is subjected to dynamic loading over relative short period of time [10, p.1]. Therefore, long term properties for FRP used in civil engineering structures have limited verification.

## 2.2 Design approaches for FRP strengthening

There is currently no common design method for the design of FRP reinforced concrete structures in Europe. Initiative have been made to prepare and develop a new Eurocode to provide a common design criteria and methodology for FRP reinforced structures under the aegis of CEN/TC250, [11, p.6] the European Committee for Standardization technical committee.

However, various national design guidelines are available with detailing rules and design manuals for FRP reinforcement. Design and execution of rehabilitation and strengthening projects often rely on these existing manuals, as well as specification and guidelines from material suppliers and FRP manufacturers.

There are various ways of FRP strengthening of existing structures, as well as different material choices any techniques used for strengthening. To limit the scope of the thesis, the literature review will focus on strengthening of flexural members, with strengthening system applied by externally bonded CFRP plates. The design approach given in this chapter will provide the theoretical base for the experimental setup and test results.

### 2.2.1 Available guidelines on FRP strengthening

During this thesis, the theoretical derivation is based on the approach given by Concrete Society Technical Report No. 55, *Design guidance for strengthening concrete structures using fibre composite material, 3rd edition.*

The TR55 guidance has been written to be used in conjunction with the Eurocodes for structural design, in particular BS EN 1990 *Basis for structural design*, BS EN 1991 *Action on structures* and BS EN 1992 *Design of concrete structures* [3, p.52].

Theoretical approach and considerations will also be compared with following codes:

Swedish design guideline *Kompositförstärkning av betong* [12], and a former design guideline *FRP Strengthening of Existing Concrete structures* [9], technical report *FiB bulletin 14 Externally bonded FRP reinforcement for RC structures* [7] and the American code *Guide for the Design and Construction of Externally Bonded FRP Systems for Strengthening Concrete Structures, ACI 440.2R-17* [2] by American Concrete Institute.

The fundamental theory of calculating the strengthened moment capacity is similar when comparing the different codes. Whereas parameters regarding the FRP, as well as partial factors for the materials differs between different codes. "*The design process is based to great extent on design of reinforced concrete with special consideration to the FRP plate bonding part"* [9, p.25]. The moment capacity is established based on moment of the forces in the section, when equilibrium of forces is achieved. [3, p.74].

### 2.2.2 Strengthening limits

Strengthening of concrete structures with externally bonded CFRP plates is an effective strengthening method, and great capacity enhancement can be achieved. However, the strengthened system relies on the composite action of the adherents and if composite action is not achieved, the strengthening effect is lost [9, p.24].

An important part of the design of FRP strengthening system is to consider the level of strengthening that can be achieved as well as the associated failure mode Considerations regarding failure mode are essential since strengthening against one mode of failure may increase the probability of failure for another failure mode. The characteristics of a failure may also be altered, a beam with previous ductile failure mode may display brittle failure behavior after strengthening [3, p.16].

For the design of a strengthened member, consideration with the risk associated with partial or complete loss of composite action due to accidental events must be careful considered, to ensure that failure of the composite will not lead to failure of the structure.

This issue is addressed in different guidelines with implemented strengthening limits in the design. The limits ensure sufficient capacity of the member to support a specified amount of service load in case of loss of strengthening due to construction error, severe environmental impact, damage, vandalism or fire [13, p.36].

The condition of the existing structure must be evaluated prior to strengthening, and sections should only be considered for strengthening if the resistance of the unstrengthen member displays sufficient capacity to withstand factored load effects. This ensures that even in the event of removal of the FRP strengthening due to unforeseen events, catastrophic collapse of the structure is prevented [3, p.71].

The strengthening limits defined by TR55 in accordance with Eurocode evaluate the ultimate resistance on the unstrengthen member derived with partial factors for accidental design situations according to EN 1992.1.2 section 2.4.2.4. The resistance of the member must exceed the load effect derived by frequent load combination of actions according to EN 1990 clause A.1.4.1 and A.1.4.2 [14].

The design aspect must also consider the accidental event of fire, due to the reduction of bond strength at high temperatures. The resistance of the unstrengthen member are evaluated with the unfactored strength assuming partial factors for the material $\gamma_{M,fi} = 1.0$. The resistance must exceed the load combination of actions due to exposure of fire according to EN 1991.1.2 clause 4.3.1 [14].

These verifications impose effective limits on the additional load that can be applied to the strengthened member with respect to safety of the structure [14].

### 2.2.3 Design for flexural strengthening

#### 2.2.3.1 General

The design for a strengthened system is based on limit state principles and both ultimate limit states (ULS) and serviceability limit state (SLS) verifications should be performed during design. ULS to the safety of the structure and are implemented to prevent partial or complete collapse of the structure, whereas SLS relates to the durability and the performance of the structure. In addition, further verifications should be performed associated with the FRP to concrete interface with verifications regarding debonding [3, p.53].

The design approach given in below section are following the TR55 guideline by Concrete Society, developed to be used in conjunction with the Eurocodes for structural design.

#### 2.2.3.2 Partial factors for material

The design approach regarding reinforced concrete structures the are specified by EN 1992-1-1 [15]. The design strength of steel and concrete are determined based on the partial factors according to EN 1992-1-1 Table 2.1N, illustrated in Table 2.1 below. For ULS verification, the characteristic material properties are divided with partial factors of safety.

Table 2.1 Partial factors materials for ultimate limit state [15]

| Design situations | $\gamma_C$ for concrete | $\gamma_S$ for reinforcing steel | $\gamma_S$ for prestressing steel |
|---|---|---|---|
| Persistent & Transient | 1,5 | 1,15 | 1,15 |
| Accidental | 1,2 | 1,0 | 1,0 |

Partial factors for FRP materials are implemented to account for the uncertainties associated with the material itself and for its use in the structure. The design parameters for FRP are a combination of safety factors regarding both the material and the method of manufacture [3, p.58]. The relation between characteristic and design properties regarding stress and strain are illustrated in Figure 2.2 below.

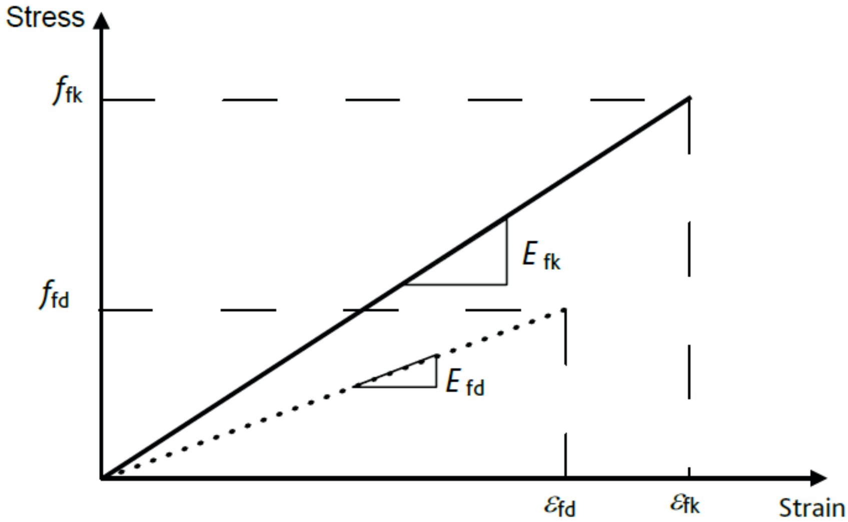


Figure 2.2 Stress and strain relation for FRP [3, p.60]

As FRP does not have any ability to undergo plastic deformation but behaves elastic up until rupture, the stiffness of the FRP are important to consider for the design. The modulus of elasticity for FRP may vary according to the method of manufacture as the orientation of the fibers within the FRP which have a significant influence of the stiffness. Uncertainties regarding long term properties are also considered, as modulus of elasticity may change over time [3, p.58].

The design modulus of elasticity is therefore derived to account for uncertainties regarding both the material and the method of manufacture, with corresponding partial factors illustrated in Table 2.2 and 2.3 below.

$$E_{fd} = \frac{E_{fk}}{\gamma_{FRP,m}\gamma_{FRP,E}}$$

Table 2.2 Partial factor Young's modulus [3, p.59]

| Material | Factor of safety, $\gamma_{\mathrm{FRP,E}}$ |
|---|---|
| Carbon FRP | 1.1 |
| Aramid FRP | 1.1 |
| AR glass FRP | 1.6 |
| E-glass FRP | 1.8 |
| Basalt FRP | 1.8 |

Table 2.3 Partial factor method of manufacture and application [3, p.59]

| Type of system (and method of application or manufacture) | Additional partial safety factor, $\gamma_{\mathrm{FRP,m}}$ |
|---|---|
| **Plates** | |
| Pultruded | 1.05 |
| Prepreg | 1.05 |
| Preformed | 1.1 |
| **Sheets or tapes** | |
| Machine-controlled application | 1.05 |
| Vacuum infusion | 1.1 |
| Wet lay-up | 1.2 |
| **Prefabricated (factory-made) shells** | |
| Filament winding | 1.05 |
| Resin transfer moulding | 1.1 |
| Hand lay-up | 1.2 |
| Hand-held spray application | 1.5 |

From durability test, the long-term behavior of FRP materials have displayed a reduction of ultimate strain [3, p.59]. The design value for ultimate strain of the FRP are therefore derived in a similar manner with a combination of both the method of manufacture and the material used, with the partial factors regarding strain given in Table 2.4.

$$\varepsilon_{fd} = \frac{\varepsilon_{fk}}{\gamma_{FRP,m}\gamma_{FRP,\varepsilon}}$$

Table 2.4 Partial factor FRP strain [3, p.59]

| Material | Partial safety factor, $\gamma_{FRP,\varepsilon}$ |
|---|---|
| Carbon FRP | 1.25 |
| Aramid FRP | 1.35 |
| AR glass FRP | 1.85 |
| E-glass FRP | 1.95 |
| Basalt FRP | 1.95 |

The design strength of FRP are derived by the design values for the elastic modulus and the strain.

$$f_{fd} = E_{fd}\varepsilon_{fd}$$

### 2.2.3.3 Assumptions

For the design of members strengthened in flexure, following assumptions are made [3, p.72]:

- Plane sections remain plane, i.e. strain in the cross section varies linearly and no longitudinal slip between the or within the components of the section
- The concrete compression stresses are derived from stress-strain curves given in EN 1992-1-1 clause 3.1.7, with maximum compressive strain limited to $\varepsilon_{cu2}$ or $\varepsilon_{cu3}$ dependent on the stress-strain diagram used
- The tensile strength of concrete is ignored
- The stresses in the steel reinforcement are derived from stress-strain curves given in EN 1992-1-1 clause 3.2
- The initial strains of the cross section prior to strengthening should be accounted for when determining the final strain of the cross section.
- The FRP material behaves linearly elastic until rupture, the stress development in the FRP are derived from the level of strain in the FRP.
- Separation failure will occur if longitudinal shear stresses exceeds the limiting stress
- Rupture of the FRP will occur when strain exceeds rupture strain.

### 2.2.3.4 Failure mode

The maximum flexural strength of a section is limited by the on the controlling failure mode. The definitions of the associated failure modes vary slightly between different guidelines [2, p.17] [9, p.38] [7, p.28].

However, all failure modes are defined by the same basic theory and can be summarized into two categories, failure while full composite action is maintained or failure due to loss of composite action.

Assuming full composite action, three associated failure modes should be evaluated:

- Crushing of concrete before yielding of the steel reinforcement.
- Yielding of steel reinforcement followed by crushing of concrete.
- Yielding of steel reinforcement followed by rupture of the FRP laminate.

For best utilization of FRP strengthening, the desired behavior of the section is yielding of the tensile reinforcement [9, p.39]. Failure mode by concrete crushing are normally associated with section with high reinforcement ratios, where the compressive strain in the concrete compression zone are exceeded before the steel yields [7, p.29]. According to TR.55, a section should normally be designed such that yielding steel reinforcement precedes both compressive failure of the concrete and tensile failure of the FRP [3, p.71].

Due to the elastic behavior of FRP until rupture, the associated strain can be relatively large. In cases where the FRP theoretically reach its design tensile strain before the concrete compressive strain is exceeded, failure normally occurs due to delamination of the FRP plate rather than rupture [3, p.71]. In order to prevent debonding, limiting strain of the FRP are implemented in the design of a strengthened section, which will be further discussed in Chapter 2.2.6.1.

Delamination and FRP separation failure are categorized as failure mode due to loss of composite action and a detailed design procedure to avoid FRP plate separation will be discussed in chapter below.

### 2.2.4 Moment capacity of a strengthened section

Based on the assumptions listed previous, the flexural capacity of a strengthened section can be determined by a stepwise process in accordance with the guidelines given in TR55 [3, p.73].

Since analytical expression for the entire procedure are not included in the TR55 guideline, supplementary explanation of the parameters is attained from previous mentioned guidelines in Chapter 2.2.1, and a worked example based on TR55 approach [17].

**a) Initial strain condition**

For the design of a strengthened system, the initial condition of the unstrengthen member must be determined. The effect of the initial load acting on a member prior to strengthening impose an initial strain distribution needed for the evaluation of the strengthened member [7, p.28].

The initial strain level in the concrete is determined from elastic analysis of the existing member based on the load at time of strengthening, illustrated in Figure 2.3. The magnitude of initial loading should be considered to evaluate if cracked or uncracked section properties should be assumed. Common assumption of cracked sectional properties are found in various sources [7, p.27] [2, p.51] [16]. To account for the long-term effect of the section properties, modulus of elasticity for the concrete are expressed to account for creep $E_{cm}/(1 + \varphi_{ef})$ [3, p.73].

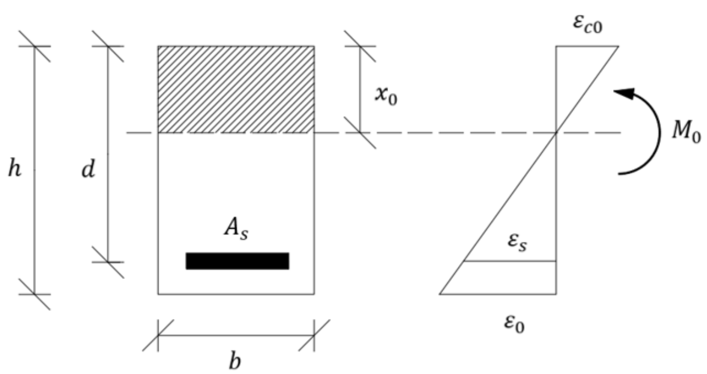


Figure 2.3 Initial strain

The initial strain is derived with following equations [16].

$$\varepsilon_{c0} = \frac{M_0 x_0}{E_c I_{cc}}$$

$$\varepsilon_0 = \varepsilon_{c0} \frac{(h - x_0)}{x_0}$$

Where

$M_0$ = initial load at time of strengthening

$\varepsilon_{c0}$ = the strain in compression

$\varepsilon_0$ = the strain in tension.

$$E_c = \frac{E_{cm}}{1 + \varphi_{ef}}$$

Considering a singly reinforced section, the neutral axis depth $x_0$ and moment of inertia for transformed cracked section $I_{cc}$ are defined according to relation below [16].

Neutral axis depth $x_0$ are determined with the sum of area moment around the neutral axis, illustrated in Figure 2.4.

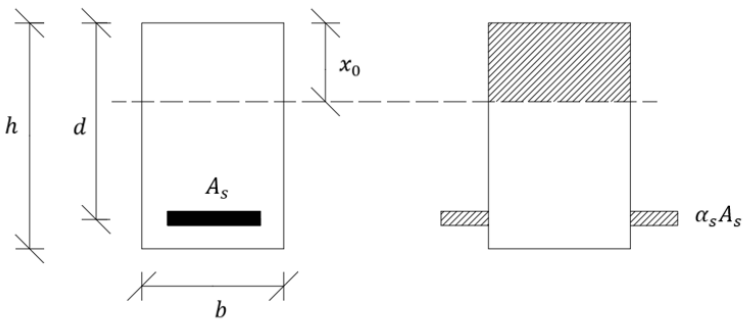


Figure 2.4 Cracked concrete equivalent section

$$\sum A x_0 = 0$$

$$\frac{b {x_0}^2}{2} = \alpha_s A_s (d - x_0)$$

Where $a_s$ are the modular ratio of steel to concrete, $\alpha_s = E_s/E_c$ and to account for creep the modulus of elasticity for concrete can be expressed as $E_c = E_{cm}/(1 + \varphi_{ef})$.

Moment of inertial for the cracked, concrete equivalent section $I_{cc}$ are calculated by:

$$I_{cc} = \frac{b{x_0}^3}{12} + bx_0\left(\frac{x_0}{2}\right)^2 + \alpha_s A_s(d - x_0)^2 \rightarrow \frac{b{x_0}^3}{3} + \alpha_s A_s(d - x_0)^2$$

**b) Determine the governing design strain for the FRP system**

The ultimate design strain, $\varepsilon_{fd}$, derived by partial factors define the design limit for rupture strain of the FRP. However, rupture of the FRP rarely governs the design as debonding failure are normally initiated at strain levels lower than the rupture strain.

The strain limit to avoid debonding, according to TR55 are taken as 0.008, a value based on empirical evidence [3, p,72]. For further reference of this limit, notation $\varepsilon_{f,lim}$ will be used.

The governing design strain for the FRP system should be taken as the smaller of the above mentioned strain values [3, p.72].

$$\varepsilon_{fe} = \min\,(\varepsilon_{fd}, \varepsilon_{f,lim})$$

Where

$$\varepsilon_{fd} = \frac{\varepsilon_{fk}}{\gamma_{FRP,m}\gamma_{FRP,\varepsilon}}$$

$$\varepsilon_{f,lim} = 0.008$$

**c) Calculate applied load**

The applied loads are derived at ultimate limit state for relevant design situations according to EN 1990 [3, p.73].

**d) Estimate required area of FRP**

The additional moment capacity required for the member $M_{add}$ can be used for an initial but potentially non-conservative estimation of the required area of the FRP $A_f$.

By assuming the neutral axis position remaining approximately at the same location as the unstrengthen member, the area of FRP required to carry the additional moment $M_{add}$ can be estimated with formula below [3, p.72].

$$A_f = \frac{M_{add}}{\varepsilon_{fe} E_{fd} z}$$

Where $\varepsilon_{fe} E_{fd}$ are the design stresses in the FRP governed by the effective design strain in FRP determined in step b) and $z$ are the lever arm of the steel reinforcement for the unstrengthen member [3, p.71].

**e) Initial assumption of concrete compressive strain**

Maximum concrete compressive strain can be initially assumed to $\varepsilon_{cu2}$ or $\varepsilon_{cu3}$ depending on stress stain diagram used [3, p.73].

**f) Assume initial position of neutral axis $x_i$**

A reasonable position of neutral axis is assumed for the initial value.

**g) Determine forces in the cross section**

By the assumption that concrete reaches maximum strain, the forces in the section can be derived. The stress state of the steel reinforcement is limited to the yield stress of steel, force contribution from steel are thereby governed by the yield strength.

The forces in FRP are derived from the strain level, assuming perfectly elastic behavior in the composite. The strain in FRP should be evaluated by subtracting the initial strain in the section $\varepsilon_{ct0}$ and derived with the assumed position of neutral axis $x_i$ and concrete compression strain $\varepsilon_{cu}$ [3, p.73].

Expression for the resulting FRP strain are demonstrated below [7, p.35] [2, p.26].

$$\varepsilon_f = \varepsilon_{cu} \frac{h - x_i}{x_i} - \varepsilon_0$$

With strain levels determined for the assumed neutral axis depth $x_i$, force equilibrium of the section should be verified by checking the initial assumption of neutral axis depth $x_i$ [3, p.73].

Force equilibrium for a singly reinforced section are demonstrated below.

$$0.8xbf_{cd} = f_{yd}A_s + \varepsilon_f E_{fd} A_f$$

Corresponding location of neutral axis to fulfill force equilibrium.

$$x_{1+n} = \frac{f_{yd}A_s + \varepsilon_f E_{fd} A_f}{0.8bf_{cd}}$$

## h) Iteration process to achieve equilibrium of forces

Iterative adjust the location of neutral axis and recalculate corresponding stress and strain in the section until force equilibrium is attained and a force balanced section is achieved [3, p.73].

## i) Verification of stresses and strains

The calculated stress and strains must be verified against following criteria [3, p.74].

- Compressive strain in concrete shall not exceed the ultimate compression strain limit $\varepsilon_{cu2}$ or $\varepsilon_{cu3}$ depending on stress stain diagram used.
- Strain in the FRP should be verified against strain limits.
  The resulting strain after equilibrium of forces in the section are achieved should be less than the governing design strain $\varepsilon_{fe}$ defined in b) in order to prevent debonding.

$$\varepsilon_f = \varepsilon_{cu} \frac{h - x_i}{x_i} - \varepsilon_0 \leq \varepsilon_{fe}$$

Evaluating the equation above, the associated failure mode can be determined. By initially assuming concrete reached ultimate strain $\varepsilon_{cu}$ the relation $\varepsilon_f \leq \varepsilon_{ef}$ will determine the behavior.

If $\varepsilon_f$ is smaller than $\varepsilon_{fd}$, crushing of concrete will be governing failure mode. The strain state of the steel can be derived by similar triangles, with a maximum stress limited by the yield stress for steel [2, p.52].

$$\varepsilon_s = (\varepsilon_f + \varepsilon_0)\left(\frac{d - x_i}{h - x_i}\right)$$

$$\sigma_s = \varepsilon_s E_s \leq f_{yd}$$

For $\varepsilon_f \geq \varepsilon_{fe}$ governing failure mode will be due to FRP rupture or debonding, dependent in the governing parameter in the definition of $\varepsilon_{fe}$ determined in b).

When maximum tensile strain in FRP, $\varepsilon_f$, exceeds the governing design strain $\varepsilon_{fe}$, concrete will not reach its ultimate strain $\varepsilon_{cu}$. Maximum FRP strain will govern the design and the design process should be repeated from step f) to find force equilibrium [3, p.74].

The corresponding strain on concrete $\varepsilon_c$, are derived from maximum strain in the FRP and the neutral axis depth. Force in the concrete can be derived from stress-strain diagrams according to EN 1991-1-1 clause 3.1.7 with truncated strain limits. Rectangular stress blocks should not be used since it is only valid if the concrete reaches its ultimate strain [3, p.74].

In addition, the longitudinal shear stresses should be checked and verified against the limiting shear stress in order to prevent shear stress induced debonding [3, p.73]. These limits, and other initiation mechanisms for FRP plate debonding will be further described in Chapter 2.2.5.

**j) Bending resistance**

When stress, strain and forces of the section are determined, and force equilibrium attained, the bending resistance of the section can be calculated based on the moment of the forces in the section [3, p.74].

To verify the capacity of the section, the bending resistance should exceed the applied moment with a corresponding steel strain larger than $0.002 + f_{yk}/E_s\gamma_s$, or having a bending resistance exceeding the applied moment by a factor of 1.15.

Capacity verification [3. P.74]:

$$M_{Rd,st} \geq 1.15 M_{Ed}$$

If above criteria are not fulfilled the section should be checked with criterion below.

$$M_{Rd} > M_{Ed}$$

$$\varepsilon_s \geq 0.002 + \frac{f_{yk}}{E_s \gamma_s}$$

If capacity verifications are fulfilled the design of strengthening system are suitable. If the section does not fulfill above criteria the amount of FRP should be increased and the process repeated from step e) [3, p.74].

With above design procedure the theoretical design capacity of the section can be determined. However, the strength of the section is dependent on the adhesive bond to maintain the composite action. The behavior of the interface between the FRP and the concrete surface is crucial to the performance of the strengthened structure [3, p.74].

According to TR55, based on analysis of 23 different studies of reinforced concrete beams with externally bonded FRP reinforcement, over 60% of the beams failed due to delamination and loss of composite action [3, p.74]. TR55 further declares that, in agreement with other studies it shows that separation of FRP from the concrete is the most prevalent failure mode of FRP strengthened beams [3, p.74].

Similar acknowledgment is also found in FiB bulletin 14, stating that most failures observed in flexural test of reinforced concrete members with externally bonded reinforcement are caused by peeling off of the externally bonded element [7, p.33].

### 2.2.5 Design process to avoid delamination of FRP

To address FRP delamination failure, different initiation mechanisms of FRP separation must be considered. A design procedure to account for FRP separation failure is developed by TR55 with six design criteria to be verified [3, p.74]. These criteria are illustrated in Figure 2.5 and relates to different initiation mechanisms for FRP separation.

Debonding criteria for flexural strengthened structural members are treated differently in different guidelines. From the reviewed guidelines, the most detailed approach was found in TR55, the design procedure, A-F, demonstrated below are directly referred to the procedure given in TR55 section 6.3.3.

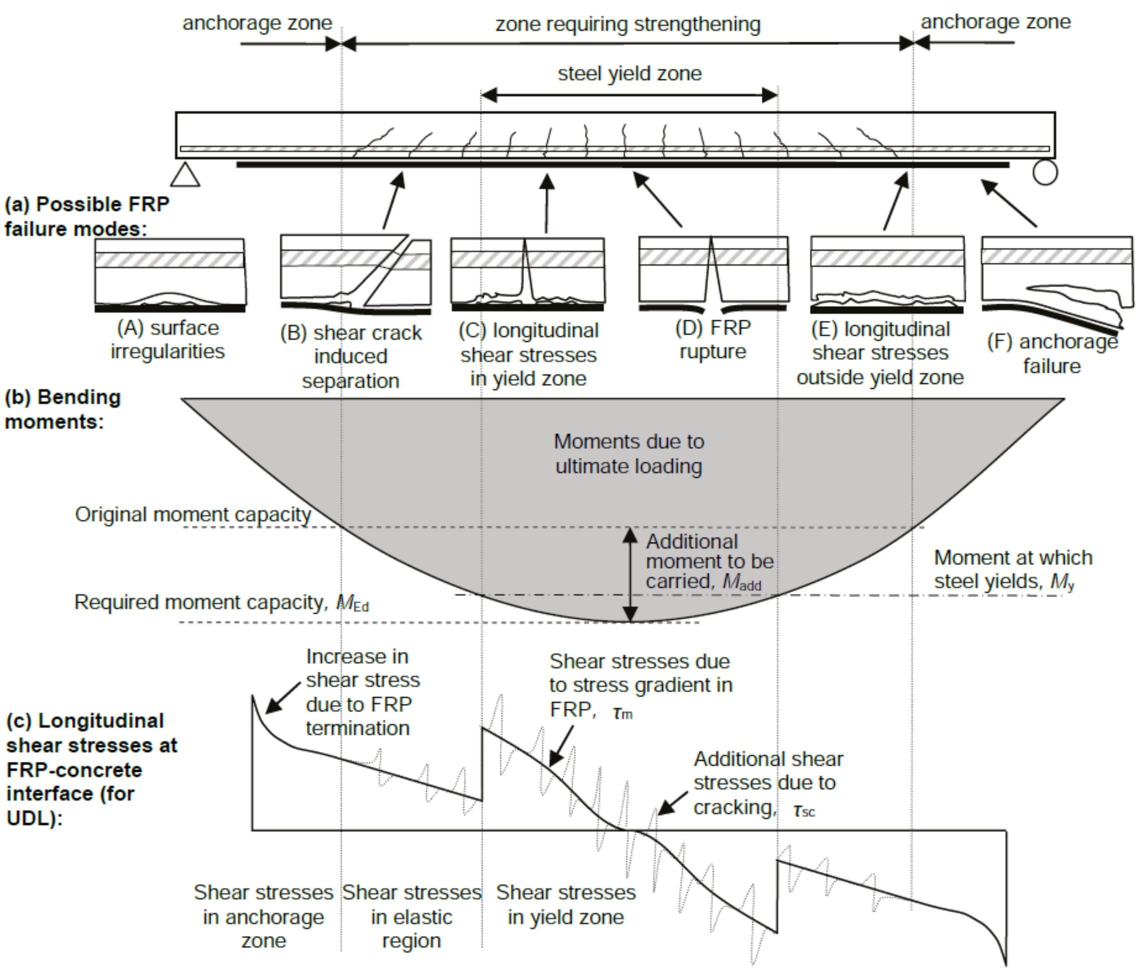


Figure 2.5 Initiation mechanisms for FRP separation [3, p.75]

A. **Surface irregularity induced FRP separation**

Concave irregularities of the soffit will lead to development of transverse tensile stresses as the FRP tries to straighten under load. These stresses may promote the initiation of FRP separation. The tolerance for the surface profile for plate-based systems are a curvature om 3 mm in 1 m [3, p.76].

B. **Shear-crack induced FRP separation**

Formation of significant shear cracks will affect the bond behavior. The presence of shear cracks leads to development of significant transverse tensile stresses in the adhesive and concrete surface which can result in initiation of FRP separation. To ensure no shear crack induced separation the design shear force $V_{Ed}$ should be lower than the capacity of the section to resist formation of significant shear crack $V_{Rd,crack}$ [3, p.77].

The maximum shear resistance to avoid significant shear cracks is defined as $67\%$ of the ultimate shear resistance of the section $V_{Rd,s}$ governed by a maximum value from the combined shear resistance without stirrups $V_{Rd,c}$ and the effective contribution form the stirrups $V_{S,eff}$. The capacity to resist shear cracks of the strengthened section are calculated according to following conditions [3, p.77]:

- $V_{Rd,crack}$ should be no greater than $V_{Rd,c} + V_{S,eff}$
- For members with shear reinforcement but no shear strengthening, $V_{Rd,crack}$ should be no greater than $0.67V_{Rd,s}$
- For members with shear strengthening, $V_{Rd,crack}$ should be no greater than $V_{Rd,s,f}$
- However, in all cases, $V_{Rd,crack}$ need not be taken as less than $(2d/a_v)V_{Rd,c}$ where $a_v < 2d$ or $V_{Rd,c}$ where $a_v \geq 2d$

Where

$V_{Rd,c}$= shear strength of concrete section without required shear reinforcement, according to EC 1992-1-1 clause 6.2.2

$V_{Rd,s}$ = shear strength of concrete section with shear reinforcement required, according to EC 1992-1-1 clause 6.2.3, assuming variable angle truss analogy. If shear strengthening is included $V_{Rd,s}$ can be replaced with $V_{Rd,s,f}$

$V_{S,eff}$ = effective shear resistance from steel reinforcement

$a_v$ = shear span

$d$ = effective depth of the section

The effective shear resistance provided by steel stirrups, $V_{S,eff}$, is given by [3, p.78]:

$$V_{S,eff} = \frac{d}{s} A_{sw} E_s \varepsilon_{sv,eff}$$

Where effective strain in shear reinforcement are defined according to formula below [3, p.78].

$$\varepsilon_{sv,eff} = \frac{10^{-5}}{\sqrt{\alpha_{flex}\alpha_w \left(\frac{E_{fd}}{E_{cm}}\right)\left(\frac{t_f}{d}\right)^{1.3}}} \leq \varepsilon_y$$

With a conservative lower bound $\varepsilon_{sv,eff} = 0.00025$ [3, p.78].

$$\alpha_{flex} = \frac{I_{cs} - I_{cc}}{I_{cc}}$$

$$\alpha_w = \frac{b}{b_f} \leq 3$$

$I_{cc}$ = moment of inertia for unstrengthen, transformed cracked section

$I_{cs}$ = moment of inertia for strengthen, transformed cracked section

$s$ = spacing of steel stirrups

$t_f$ = thickness FRP

$b_f$ = width of FRP

$A_{sw}$ = cross sectional area of steel shear reinforcement

$E_s$ = E-modulus steel

$E_{cm}$ = E-modulus concrete

$E_{fd}$ = design E-modulus FRP

If $V_{Ed} \geq V_{Rd,crack}$ the section is at risk for shear crack induced FRP separation. Additional transverse anchorage by U-wrap of the FRP should be applied at both ends in order to prevent delamination [3, p.79].

**C. Longitudinal shear stress in the yield zone**

The longitudinal shear stress developed in the yield zone of the section must be checked and verified towards a limiting allowable shear stress $\tau_{lim,y}$ [3, p.80].

The longitudinal shear stresses are derived with direct proportionality to the rate of change of the axial stresses of the FRP. Considering the elastic zone of a section, where the resulting moment are lower than the moment at which steel yields $M_y$, an increase of applied moment will in this section will be resisted by a combination of both steel and FRP. Due to this, the axial force gradient along the FRP are low to moderate, hence the longitudinal shear stresses are small. However, along the yield lines, illustrated in Figure 2.3 above, steel has limited ability to carry additional stresses beyond the yield stress and an increased moment along the yield lines are resisted almost exclusively by the FRP. Consequently, the rate of change of axial stress in the FRP are high when proceeding from the elastic zones to the yield zones along the beam resulting in higher longitudinal shear stresses [2, p.80].

The longitudinal shear stresses may also be influenced by local effects, such as stress concentration in the proximity of flexural cracks. The total longitudinal stress is therefore derived as a combination of these two contributing factors [3, p.80].

The derivation of the longitudinal stress is based on following assumptions [3, p.80]:

- Complete composite action, i.e. perfect bond
- Plane sections remain plane, i.e. linear strain distribution
- Concrete in tension has no contributing strength
- Tensile strength of concrete is lower than tensile strength of adhesive

The total longitudinal stresses are determined following a stepwise process [3, p.80.81]:

1. Determine the moment at which the steel reinforcement reaches yield stress $M_y$, with the associated nominal stress in the FRP $\sigma_y$.
2. Determine maximum design moment within the yield zone $M_{Ed}$, with the associated stress and strain in the FRP, $\sigma_{fmax}$ and $\varepsilon_{fmax}$. The strain in the FRP should be limited by a maximum of 0.008.
3. Determine the distance $\Delta x$, between the yield moment $M_y$ and the maximum moment $M_{Ed}$ for the applied loading.
4. Calculate $\tau_m$, the mean longitudinal stress due to the gradient of nominal axial stress in the FRP between the minimum and maximum moment locations along the yield zone.

$$\tau_m = t_f[\frac{\sigma_{fmax} - \sigma_{fy}}{\Delta x}]$$

Where $t_f$ are the thickness of the FRP plate.

5. Calculate $\tau_{sc}$, the additional longitudinal shear stress due to stress concentration in the proximity of flexural cracks.

$$\tau_{sc} = 7.8\left[1.1 - \frac{M_y}{M_{Ed}}\right] f_{ctk}$$

Where $f_{ctk}$ are the characteristic tensile strength of concrete.

6. Determine the total longitudinal shear stress $\tau_t$ within the yield zone.

$$\tau_t = \tau_m + \tau_{sc}$$

7. Verify the longitudinal shear stress to ensure no initiation of FRP separation

$\tau_t$ should be smaller than the limiting shear stress of concrete $\tau_{\mathrm{lim,y}}$, which is assumed to be the weakest link in the bond between the materials.

$$\tau_t \leq \tau_{lim,y} = 4.5\frac{f_{ctk}}{\gamma_c}$$

## D. Strain in the FRP

Rupture failure in the FRP can occur if the strain in the FRP exceeds the design rupture strain of the FRP. Rupture of FRP is rarely a governing failure mode for externally bonded FRP, since delamination normally occurs at strain values lower than the design rupture strain [3, p.81].

However, increase in strain due to cracks may lead to rupture of the FRP and needs to be verified. Maximum strain $\varepsilon_{mt}$, is calculated as the maximum strain due to bending combined with local strain contribution at crack locations [3, p.81].

$$\varepsilon_{mt} = \varepsilon_{fmax} + 0.114\frac{\tau_{sc}}{\sqrt{E_{fd}t_f}}$$

Maximum strain in the FRP must be less than the design rupture strain $\varepsilon_{fd}$ [3, p.81].

$$\varepsilon_{mt} \leq \varepsilon_{fd}$$

Where

$$\varepsilon_{fd} = \frac{\varepsilon_{fk}}{\gamma_{FRP,\varepsilon}\gamma_{FRP,m}}$$

## E. Longitudinal shear stress near ends of FRP

For externally bonded FRP, the longitudinal stresses close to the plate ends should be checked. For sections outside the yield zone, both concrete, steel and FRP are assumed to behave linearly elastic, and the longitudinal shear stress $\tau$ can be calculated according to formula below [3, p.82].

$$\tau = \frac{V_{add}\alpha_f A_f(h-x)}{I_{cs}b_a}$$

Where

$V_{add}$ = the difference between ultimate shear force and the applied shear force when the strengthening is installed

$\alpha_f$ = modular ratio of FRP to concrete $E_{fd}/E_{cm}$

$A_f$ = area FRP

$x$ = neutral axis strengthened section

$I_{cs}$ = moment of inertia, strengthened equivalent cracked section

$b_a$ = width of adhesive layer

$h$ = depth of section

The definition of $\tau$ assumes no local increase in shear stress due to cracks, the limiting shear stress is therefore limited by $\tau_{lim,c}$ [3, p.82].

$$\tau_{lim,c} = 0.8\frac{f_{ctk}}{\gamma_c}$$

**F. Anchorage design**

A sufficient anchorage length of the FRP must be provide in order to activate the bond force. Anchorage design are performed to determine the location in the span where FRP are no longer required [3, p.83].

The characteristic bond failure force $F_k$ increases with an increase in anchorage length $l_t$ up until a threshold value $l_{t,max}$ where further increase in anchorage length does not contribute to increased load bearing capacity [3, p.83]. Maximum ultimate bond force $T_{k,max}$ with corresponding maximum anchorage length $l_{t,max}$ are illustrated in Figure 2.6 below.

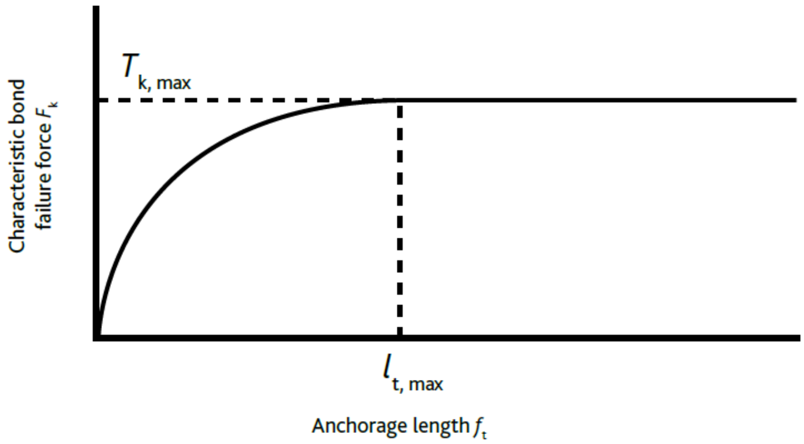


Figure 2.6 Bond force and anchorage length [3, p.83]

The maximum ultimate bond force and anchorage length are defined with below equations [3, p.83].

$$T_{k,max} = 0.5 k_b b_f \sqrt{E_{fd} t_f f_{ctk}}$$

Where

$$k_b = 1.06 \sqrt{\frac{2 - \frac{b_f}{b}}{1 + \frac{b_f}{400}}} \geq 1.0$$

$b_f$ = width of FRP laminates

$b$ = width of beam

$t_f$ = thickness FRP

$E_{fd}$ = design E-modulus of FRP

$f_{ctk}$ = characteristic tensile strength of FRP

The corresponding maximum anchorage length are defined with following expression.

$$l_{t,max} = 0.7 \sqrt{\frac{E_{fd} t_f}{f_{ctk}}} \geq 500\ mm$$

However, a minimum anchorage length of 500 mm is recommended for design [3, p.83].

If provided anchorage length $l_t$ are smaller than $l_{t,max}$ the bond force is reduced and calculated according to expression below [3, p.83].

$$T_k = (\frac{T_{k,max} l_t}{l_{t,max}})(2 - \frac{l_t}{l_{t,max}})$$

$l_t$= provided anchorage length $l_t < l_{t,max}$

FRP strengthened structures does also need to be verified for accidental events, such as fire, explosion, impact damage of the FRP and seismic loading. These verifications are of great importance in order to avoid partial or complete collapse of the structure if the strengthening mechanism provided by the FRP are compromised.

With regards to limitation of the thesis, and laboratory testing focusing on failure load and failure behavior, verification for accidental events and strengthening limits will not be included in the analysis.

### 2.2.6 Different parameter definition between different guidelines

When comparing different guidelines, specifically two parameters impose conflict in the theoretical derivation for the laboratory testing, as they are defined differently in different codes. These parameters are the limiting strain to prevent debonding and the required anchorage length of the FRP plates. The different code definitions are explained below.

### 2.2.6.1 Debonding strain

When equilibrium of forces is determined for a section strengthened with FRP, the moment capacity is derived based on the forces in the section.

The force contribution from the FRP are evaluated based on the assumption of elastic behavior up to rupture. Due to the linear elastic behavior, the level of strain will govern the developed force in FRP, limited by the smaller of rupture strain and debonding strain.

To avoid premature delamination of the FRP, strain limits are implemented to limit the effective strain in the FRP. This strain limit is however defined differently in different guidelines, which results in inconsistent theoretical prediction of the strengthened capacity when comparing different guidelines. Table 2.5 below illustrates the different strain limits defined in guidelines reviewed.

Table 2.5 Debonding strain limit according to different guidelines

| **Guideline** | **Debonding strain limit** | **Comment** |
|---|---|---|
| TR55 [3, p.72] | $\varepsilon_{f.lim} = 0.008$ | Based on empirical evidence [3, p.72] |
| ACI 440.2R-17 [2, p.24] | $\varepsilon_{fd} = 0.41\sqrt{\frac{f_c'}{nE_f t_f}} \leq 0.9\varepsilon_{fu}$ | $f_c'$ = characteristic compression strength<br>$n$ = layers of plates<br>0.41 = best fit coefficient based on empirical data [2, p.24] |
| FiB bulletin 14 [7, p.51] | $\varepsilon_{f,lim} = 0.0065 - 0.0085$ | |
| Kompositförstärkning av betong [12, p.43] | $\varepsilon_{fd,ic} = 0.41\sqrt{\frac{f_{cd}}{nE_f t_f}} \leq 0.9\varepsilon_{fu}$ | Based on ACI definition [12, p.43]<br>Design value used for concrete compression strength and FRP E-modulus. |

### 2.2.6.2 Anchorage length

The anchorage length of the externally bonded FRP plates are an important aspect with respect to the developed anchorage force of the FRP plates, and insufficient anchorage length reduce the effect of the strengthening system. The definition and application of anchorage length are also found different in different guidelines which will be described below.

According to TR55, anchorage design is conducted by determining the point in the span where FRP are no longer required. This location coincides with the location in the span where applied moment exceeds the unstrengthen moment capacity, illustration of the anchorage zone is found in Figure 2.5. The force developed in the FRP at this location should be less than the ultimate bond force $T_{k,max}$ and sufficient anchorage is provided by extending the FRP plate by an anchorage length $l_{t,max}$ beyond this point [3, p.83].

The anchorage length is defined according to formula below, with are recommended minimum anchorage length of 500 mm. Illustrated in Figure 2.6 the development of ultimate bond force $T_{k,max}$ are dependent on the anchorage length $l_{t,max}$ displayed by a parabolic relation [3, p.83].

$$l_{t,max} = 0.7\sqrt{\frac{E_{fd}t_f}{f_{ctk}}} \geq 500mm$$

Reviewing different codes, the same relation between the ultimate bond force and associated anchorage length are implemented. Referring to numerous different laboratory test [9, p.51] same conclusion is found, that there is a threshold anchorage length over which increase of anchorage length does not contribute further to increased bond force [2, p.44] [9, p.51] [7, p.54]. Same parabolic curvature relation between bond force and anchorage length are found in the other codes, Figure 2.7 shows the relation described in FiB bulletin 14, Approach 2.

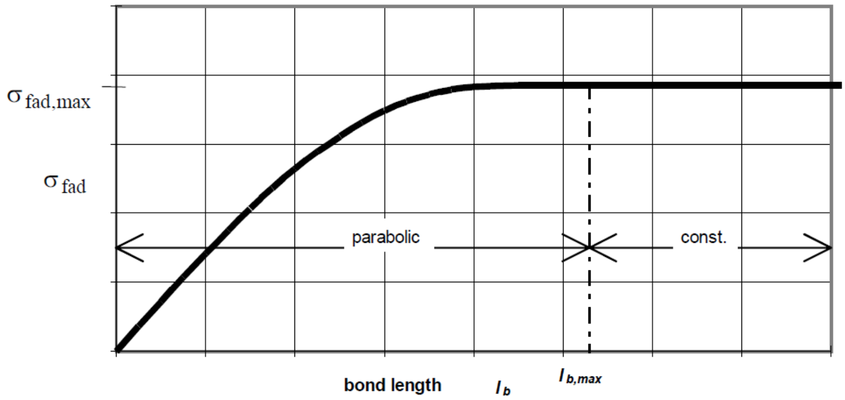


Figure 2.7 Parabolic relation between bond force and anchorage length [7, p.55]

However, as opposed to TR55 where the anchorage length are extended beyond point where applied moment exceeds unstrengthen moment capacity, both ACI, FiB bulletin 14 and the Swedish guideline Kompositförstärkning av betong, defines the anchorage length as the extension of the FRP plates beyond the location of the last crack in the cross section [2, p.44] [7, p.54] [12, p.48].

According to a publication by J.F. Chen and J.G. Teng [17], bond behavior and the force transfer of the bonded plate are related to the crack formation of the beam. Where cracking of the concrete near the applied loads will shift the active bond zone to areas further away from the loading point. The shift of the active bond zone implies that only part of the bond is effective at a given time, and as cracking of the concrete propagates, the bond resistance is gradually lost in the area near the applied load [17].

To develop sufficient bond force, the anchorage length must be extended beyond the last crack in the cross section as illustrated in Figure 2.8. Sufficient anchorage of the CFRP plates are then provided by extending the plates at least a distance equal to the anchorage length past the point along the span corresponding to the cracking moment $M_{cr}$ [12, p.48] [2, p.44] [7, p.54].

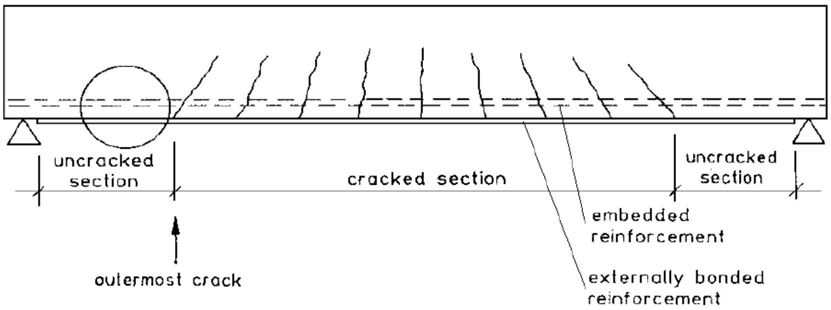


Figure 2.8 Anchorage zone beyond location of last crack [7, p.54]

Table 2.6 gives an overwide of the anchorage length defined by different guidelines.

Table 2.6 Anchorage length according to different codes

| Guideline | Anchorage length | Remark |
|---|---|---|
| TR55 [3, p.83] | $l_{t,max} = 0.7\sqrt{\frac{E_{fd}t_f}{f_{ctk}}} \geq 500mm$ | * |
| ACI 440.2R-17 [2, p.44] | $l_{df} = \sqrt{\frac{nE_f t_f}{\sqrt{f_c'}}}$ | ** |
| FiB bulletin 14 Approach 1 [7, p.51] | $l_{b,max} = \sqrt{\frac{E_f t_f}{c_2 f_{ctm}}}$ <br> $c_2 = 2$ | ** |
| FiB bulletin 14 Approach 2 [7, p.54] | $l_{b,max} = c_2\sqrt{\frac{E_f t_f}{\sqrt{f_{ck}f_{ctm}}}}$ <br> $c_2 = 1.44$ | ** |
| Kompositförstärkning av betong [12, p.48] | $l_{ef} = \sqrt{\frac{E_f t_f}{2f_{ctm}}}$ | ** |
| *Beyond location where applied moment exceed unstrengthen capacity <br> **Beyond location of last crack | | |

### 2.2.6.3 Experimental evaluation of the parameters

To evaluate the behavior with respect to these two parameters, physical measurements were recorded during the testing. Strain gauges were mounted on the CFRP to evaluate the development of strain in the CFRP plates and crack propagation and measured distance to last first crack from support was documented during testing.

## 2.3 Strengthening system for laboratory testing

The strengthening system used for the laboratory testing was provided from Sika Norway.

Sika CarboDur system is a structural strengthening system used for post construction reinforcement of buildings and civil engineering structures or element [4]. The strengthening system consists of CarboDur CFRP plates to be used in conjunction with Sikadur-30 adhesive, a two-component structural adhesive based on epoxy resin with special fillers [6].

Sika CarboDur plates are pultruded, carbon fiber reinforced polymers with an epoxy matrix [4] [5]. The plates are available in three different categories, S, M and H, correlated to the mechanical properties, the plates are also available in various cross sections.

The CarboDur plates used for the laboratory testing is CarboDur S512. Notation 512, relates to the cross-sectional dimensions with a plate width of 50 mm and thickness of 1.2 mm. Notation S, corresponds to the mechanical properties given in Table 2.7, the properties in the table are the values along the longitudinal direction of the fibers. Mechanical properties for the adhesive Sikadur 30 are found in Table 2.8 below.

Table 2.7 Mechanical properties CarboDur S512 [5]

**TECHNICAL INFORMATION**

| | | | |
|---|---|---|---|
| **Laminate Tensile Strength** | Mean value | 3 100 N/mm² | (EN 2561) |
| | 5 % fractile-value | 2 900 N/mm² | |
| | Values in the longitudinal direction of the fibres | | |
| **Laminate Tensile Modulus of Elasticity** | Mean value | 170 000 N/mm² | (EN 2561) |
| | 5 % Fractile-value | 165 000 N/mm² | |
| | Values in the longitudinal direction of the fibres | | |
| **Laminate Elongation at Break** | Strain mean value | 1.80 % | (EN 2561) |
| | Values in the longitudinal direction of the fibres | | |
| **Glass Transition Temperature** | >100 °C | | (EN 61006) |

Table 2.8 Mechanical properties Sikadur 30 [6]

**TECHNICAL INFORMATION**

| | | | | | |
|---|---|---|---|---|---|
| **Compressive Strength** | **Curing Time** | **Curing Temperature** | | | (EN 196) |
| | | **+10 °C** | **+35 °C** | | |
| | 12 hours | - | ~85 N/mm$^2$ | | |
| | 1 day | ~55 N/mm$^2$ | ~90 N/mm$^2$ | | |
| | 3 days | ~70 N/mm$^2$ | ~90 N/mm$^2$ | | |
| | 7 days | ~75 N/mm$^2$ | ~90 N/mm$^2$ | | |
| **Modulus of Elasticity in Compression** | ~9 600 N/mm$^2$ (at 23 °C) | | | | (ASTM D 695) |
| **Tensile Strength** | **Curing Time** | **Curing Temperature** | | | (DIN EN ISO 527-3 |
| | | **+15 °C** | **+35 °C** | | |
| | 1 day | ~20 N/mm$^2$ | ~26 N/mm$^2$ | | |
| | 3 days | ~23 N/mm$^2$ | ~27 N/mm$^2$ | | |
| | 7 days | ~26 N/mm$^2$ | ~29 N/mm$^2$ | | |
| **Tensile Modulus of Elasticity** | ~11 200 N/mm$^2$ (+23 °C) | | | | (ISO 527) |
| **Tensile Adhesion Strength** | Curing time | Substrate | Curing temperature | Adhesion strength | (EN ISO 4624, EN 1542, EN 12188) |
| | 7 days | Concrete dry | +23 °C | > 4 N/mm$^2$ * | |
| | 7 days | Steel | +23 °C | >21 N/mm$^2$ | |
| | *100% concrete failure | | | | |
| **Shear Strength** | **Curing time** | **Curing Temperature** | | | (FIP 5.15) |
| | | **+15 °C** | **+23 °C** | **+35 °C** | |
| | 1 day | ~4 N/mm$^2$ | - | ~17 N/mm$^2$ | |
| | 3 days | ~15 N/mm$^2$ | - | ~18 N/mm$^2$ | |
| | 7 days | ~16 N/mm$^2$ | 18 N/mm$^2$ (1) | ~18 N/mm$^2$ | |
| | Concrete failure (~15 N/mm$^2$)<br>(1) (DIN EN ISO 4624) | | | | |
| **Shrinkage** | 0.04 % | | | | (FIP: Fédération Internationale de la Précontrainte) |
| **Coefficient of Thermal Expansion** | 2.5 x 10$^{-5}$ per °C (Temperature range: −20 °C to +40 °C) | | | | (EN 1770) |
| **Glass Transition Temperature** | **Curing time** | **Curing temperature** | **TG** | | (EN 12614) |
| | 30 days | +30 °C | +52 °C | | |

## 2.3.1 Installation procedure

Installation procedure of a FRP system should be performed in accordance with the guidelines given by the manufacturer, as installation procedures often differ between different systems [3, p.153].

Application of the CFRP plates used for the experiment was performed in accordance with the guidelines given in the Method Statement for Sika CarboDur systems [4].

The Method statement emphasis the requirements prior to installation, recommended equipment, procedure of application as well as quality control before, during and after application.

#### 2.3.1.1 Surface preparation

A major factor for the effect of the strengthened system is the quality of the concrete substrate. A thorough inspection of the concrete surface should therefore be performed prior to strengthening. Any unsound material, such as weak or damaged concrete, and any problem associated with the concrete substrate that can compromise the integrity of the adhesive bond between the CRFP plates and the concrete must be addressed prior to surface preparation [4].

For areas where repair of the concrete surface is necessary it is essential that the repair materials are compatible with the adhesive used as well as being suitable to be used in structural situations [4]. Choice of repair material often depends on the timeframe of a project, therefore the curing time for the material must be considered. For fast repair in small areas, epoxy resin-based material such as the adhesive can be used. For larger areas, cement-based repair mortar is more suitable as long as it is compatible with the adhesive [4].

#### 2.3.1.2 Surface leveling

Before the adhesive is applied, the concrete surface must be cleaned and leveled. Any protrusions, such as formwork joints or other out-of-plane variations should be leveled by either concrete grinder or high-pressure blasting [4]. Sika refers to FiB Bulletin 14 for definition of the tolerance for permissible unevenness of the surface, illustrated in Figure 2.9.

| Type of FRP EBR | 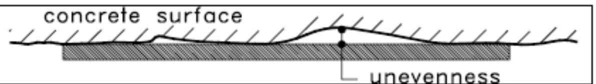  | |
|---|---|---|
| | Permissible unevenness on a 2.0 m base (mm) | Permissible unevenness on a 0.3 m base (mm) |
| "Prefab", thickness > 1 mm | 10 | 4 |
| "Prefab", thickness < 1 mm | 6 | 2 |
| "Cured in situ" | 4 | 2 |

Figure 2.9 Tolerance limits for concrete surface [7, p.98]

The concrete surface should be prepared so that an open texture surface is achieved without lattice layer [5]. The surface should also be cleaned so that it is free from dust, dirt, formwork oil or other contaminants and loose particles that could interfere with the quality of the adhesive bond [4].

Levelling of the concrete surface should be performed shortly before installation of the plates, so that no materials that can interfere with the bond are repositioned on the surface. After levelling, the surface should be cleaned and immediately prior to installation of the plates the surface should be brushed and vacuumed to remove any loose particles [4].

#### 2.3.1.3 Adhesive

Mixing and application of the adhesive should be performed in accordance with manufacturer's instructions. The resin and hardener components of an epoxy adhesive have to be mixed together in defined proportions in order to attain the required properties for the cured adhesive. Therefore, pre-batched quantities of resin and hardener are often used [3, p.158].

When using epoxy adhesive different time concepts needs to be taken into consideration. The pot life of the adhesive defines the time limitation one can work with the adhesive after the resin and hardener are mixed together and before it starts to harden. The open time is the disposable time after the adhesive has been applied to the adherents and before they are joined together [7, p.6].

For Sikadur 30 adhesive the corresponding pot life with respect to temperature is defined in the product data sheet [6], demonstrated in Table 2.9 below.

Table 2.9 Pot life Sikadur 30 [6]

| Pot Life | Temperature | Potlife | Open time | (FIP: Fédération Internationale de la Précontrainte) |
|---|---|---|---|---|
| | +8 °C | ~120 minutes | ~150 minutes | |
| | +20 °C | ~90 minutes | ~110 minuets | |
| | +35 °C | ~20 minutes | ~50 minutes | |

The potlife begins when the resin and hardener are mixed. It is shorter at high temperatures and longer at low temperatures. The greater the quantity mixed, the shorter the potlife. To obtain longer workability at high temperatures, the mixed adhesive may be divided into portions. Another method is to chill components A+B before mixing them (not below +5 °C).

However, the Method Statement for Sika CarboDur systems states: *"The sequence of operation should be planned to ensure that the adhesive cam be applied, the plates bonded and installation completed within one hour of mixing the adhesive, or within 80% of the pot life, whichever comes first"* [4, p.11]. Considering this, effective pot life of 60 minutes was used for application of the CFRP plates for the experiment.

The Sikadur 30 adhesive used for the experiment came in pre-batches units of 6 kg, consisting of component A and B with required mix proportions 3:1. The components should be thoroughly mixed together until a homogeneous consistency are achieved, specified minimum of 3 minutes then poured into a new container and stirred for an additional minute to ensure homogeneous mix [6].

#### 2.3.1.4 Application procedure

Before application of the CFRP plates, the plates should be visually checked for signs of damage. The surface of the plates should be cleaned and degreased with an isopropanol based cleaner to remove any oil, grease or dust. Before applying the adhesive, the solvent must be evaporated and the plates completely dry [4].

To bond the CFRP plates onto the concrete a thin layer of adhesive should first be applied on the prepared concrete surface to fill any small voids and irregularities [4]. Another layer of adhesive is applied on the plates. The adhesive should be applied on the plates with a convex profile across the plates, approximately 1 mm thick on the sides and 2 mm thick in the middle of the plate [4]. The additional thickness along the centerline of the plates helps reduce risk of void formation [3, p.159].

To attain the desired adhesive profile an application tool may be used. A plastic scraper with a profile illustrated in Figure 2.10 mounted on a wooden framework enables a simple and uniform application of the adhesive, by feeding the plates through the application tool [4].

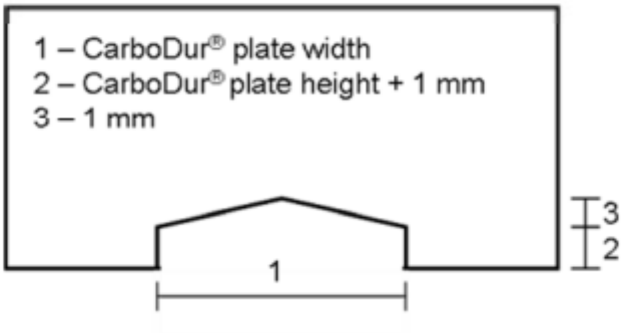


Figure 2.10 Surface profile application scraper [4]

The coated CFRP plates can then be placed onto the prepared concrete surface. Using a hard rubber roller, the plates are presses unto the substrate until adhesive is forced out on both sides of the plate [4].

Full design strength of the adhesive is reached after approximately 7 days of curing at temperatures of 20 °C [4].

#### 2.3.1.5 Quality control after installation

After the installation, ultimately a plate pull-off test should be performed according to procedure described in EN 1542 [4]. As a pull off test is semi destructive, this was not feasible for the laboratory experiment and therefore not described further.

Non-destructive visual inspection of the bond quality should be performed in order to check for air pockets and voids in the adhesive layer. If significant amount of voids are found, the load transfer will not be sufficient and the CFRP plates should be replaced [4].

# 3 Method and Material

## 3.1 Experimental test setup

The experimental study was conducted on 8 reinforced concrete beams subjected to different degree of preload prior to strengthening by externally bonded CFRP plates. The aim of subjecting the beams to preload is to simulate different damage levels in the beams with resulting crack formation prior to installation of the CFRP strengthening system. The aim of the experiment is to investigate the impact of existing cracks with respect to the ultimate capacity of a strengthened member, and whether a member with large extent of crack formation behave differently than members with less or no degree of crack formation.

The degree of preload was determined on basis of expected physical behavior of the beams regarding to crack formation. From a previous experimental study and analysis of the failure behavior of reinforced concrete beams with external CFRP, the damage levels were categorized into four different stages [18, p.560], illustrated in Figure 3.1 below.

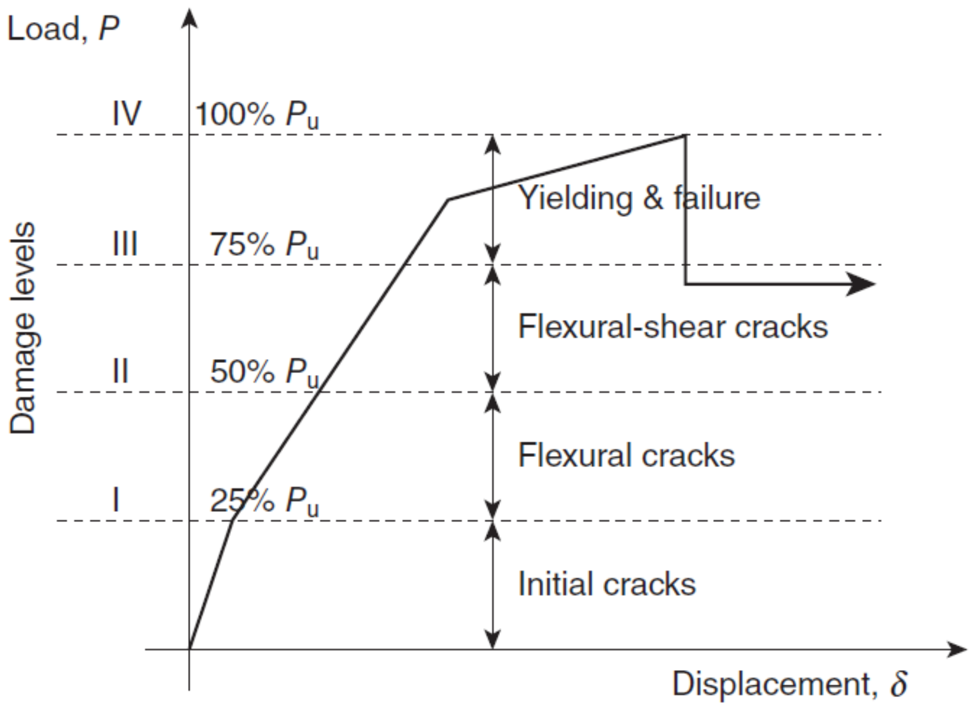


Figure 3.1 Damage level due to applied load [18, p.560]

Applying a similar classification for the damage level of a reinforced beams, the degree of preload was determined to three different load levels.

- $0.3 \cdot P_{fail,us}$
  Expected condition: crack initiation
- $0.5 \cdot P_{fail,us}$
  Expected condition: crack development and expansion of flexural cracks
- $0.7 \cdot P_{fail,us}$
  Expected behavior: Both flexural and shear cracks developed in the specimen.

Where $P_{fail,us}$ is the average failure load for the unstrengthen beam.

Due to limited space, casting of the test specimen were conducted in two batches, hereafter denoted Batch A and Batch B.

12 reinforced concrete beams were assigned to the experiment, with eight specimens strengthened with two externally bonded CFRP plates. Two beams were allocated to each preloading level with two additional control beams without preloading prior to strengthening. To determine the failure load for the unstrengthen beam ($P_{fail,us}$), and the corresponding reference load for the preloading, four reference beams were tested, two from each batch. Table 3.1 summarizes the test program.

Table 3.1 Test program

| | **Beam** | **Batch** | **Preload** | **CFRP** | |
|---|---|---|---|---|---|
| Test 1 | Beam 1 | A | None | None | Reference beams $P_{fail,us}$ |
| | Beam 2 | B | | | |
| | Beam 3 | A | | | |
| | Beam 4 | B | | | |
| Test 3.0 | Beam 5 | A | None | 2 strips | Control beams |
| | Beam 6 | B | | | |
| Test 3.3 | Beam 7 | A | 30% of $P_{fail,us}$ | 2 strips | |
| | Beam 8 | B | | | |
| Test 3.5 | Beam 9 | A | 50% of $P_{fail,us}$ | 2 strips | |
| | Beam 10 | B | | | |
| Test 3.7 | Beam 11 | A | 70% of $P_{fail,us}$ | 2 strips | |
| | Beam 12 | B | | | |

## 3.2 Initial design of reinforced concrete beam

To best utilize the strength increase by CFRP the aim of the experiment was to get failure mode governed by the strain limits of the CFRP. The reinforced concrete beams were therefore designed as an under-reinforced section where yielding of steel precedes compression failure of the concrete.

All the beams were designed with cross sectional dimension 250 mm by 300 mm, and a total length of 2200 mm. For tension reinforcement three 12 mm diameter bars were used with shear reinforcement of 8 mm diameter and 110 mm spacing. The aim of the initial design was to ensure yielding of the tension steel, with sufficient shear resistance of the member to avoid failure governed by the shear strength. Using above reinforcement arrangement these criterions were fulfilled. Detailing rules regarding minimum reinforcement according to EN 1992-1-1 clause 9.2.1.1 were checked and verified [15]. To ensure sufficient shear resistance of the member and suitable spacing, shear reinforcement was chosen according to EN 1992-1-1 clause 9.2.2 (8) and National Annex for Norway [15]. By evaluating the sectional properties against those of a balanced section, the section fulfil criterion to be singly reinforced [19, p.65]. Compression reinforcement is therefore not required but will nevertheless be included to provide stability for the stirrups during casting. Concrete of strength class B35 was used for the reinforced concrete beams. The parameters used for the initial design of the reinforced concrete beam are found in Table 3.2. Detailed derivation of the reinforcement is found in Appendix A.

Table 3.2 Material properties concrete and steel

| **Concrete** | |
|---|---|
| Strength class | B35 (SCC) |
| Compressive strength | $f_{ck} = 35\ MPa$ |
| Cover to the reinforcement | $c_{nom} = 35\ mm$ |
| | |
| **Steel** | |
| Steel class | B500NC |
| Yield strength | $f_{yk} = 500\ MPa$ |
| Longitudinal reinforcement, $Ø_L$ | $Ø_L = 12\ mm$ |
| Shear reinforcement, $Ø_s$ | $Ø_s = 8\ mm$ |

The configuration and reinforcement details of the beams are illustrated in Figure 3.2. The two top bars, 2Ø10 mm, will not be considered structural reinforcement, but merely to keep the stirrups in place. Anchorage is provided by open U-hooks, 2Ø10 mm, at the beam ends extending 300 mm along the reinforcement.

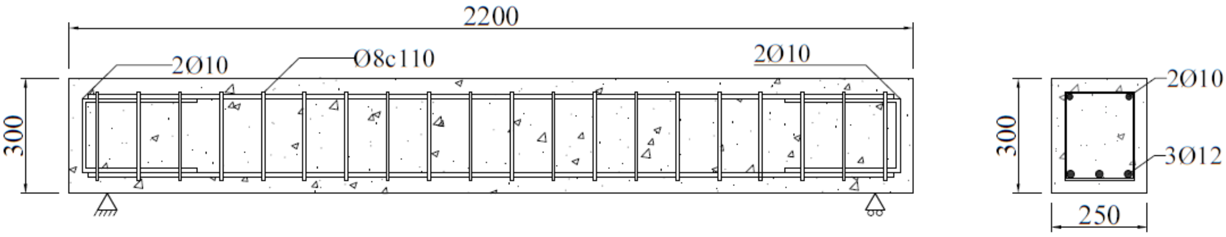


Figure 3.2 Dimension and reinforcement details of beam (All dimensions are given in millimeters)

Analytical prediction of failure load for the unstrengthen capacity were performed by omitting partial factors and derive moment capacity on characteristic strength of the materials. These predictions are used as an initial estimation of capacity. To evaluate the actual concrete compression strength at time of flexural test of the beams, mean compression strength found from compression test will be used for the theoretical calculations.

By omitting the partial factors for the material, a result closer to the actual behavior of the specimen are obtained and will be compared to the experimental results. Derived with respect to the characteristic material properties, moment capacity of the unstrengthen section is calculated by force equilibrium and equivalent rectangular stress block, according to formulas below [19, p.62].

$$0.8xbf_{ck} = f_{yk}A_s$$

$$x = \frac{f_{yk}A_s}{0.8bf_{ck}}$$

$$M_{Rd} = f_{yk}A_s(d - 0.4x)$$

Where

$b = 250\ mm$

$h = 300\ mm$

$d = h - (c_{nom} + \text{Ø}s + \frac{\text{Ø}_L}{2}) = 251\ mm$

$f_{ck} = 35\ MPa$

$f_{yk} = 500\ MPa$

$A_s = 3 \cdot \frac{\pi \text{Ø}_L{}^2}{4} = 339\ mm^2$

Corresponding neutral axis depth and moment capacity for the unstrengthen beams are defined below:

$$x = \frac{500 \cdot 339}{0.8 \cdot 250 \cdot 35} = 24.2\ mm$$

$$M_{Rd,us} = 500 \cdot 339 \cdot (251 - 0.4 \cdot 24.2) = 40.9\ kNm$$

Associated failure load is found by evaluating the bending moment diagram at maximum capacity. For a simplified estimation, self-weight of the beam is neglected, and failure load determined as a function of the shear span, a, between point load and support. Supplementary derivation is found in Appendix A.

$$P_{fail} = \frac{M_{Rd,us} \cdot 2}{a}$$

## 3.3 Load arrangement and CFRP configuration

All beams were tested under four point bending with a load rate set to 10 kN/min. Span length for all the beams was 2000 mm. To ensure the CFRP reinforced beams could be moved and placed in the bending machine without risk of damaging the bonded plates a maximum plate length of 1900 mm were used.

All the specimen reinforced with CFRP plates were installed with two parallel plates on tension side of the beams. The distance between the CFRP plates were chosen with respect to symmetry and for the ease of application. To maintain a relatively large constant bending zone for the test specimens, in order to induce significant crack formation during preloading, while at the same time provide anchorage length as large as possible, distance 750 mm from support to point load was chosen. The setup for the test specimen is illustrated in Figure 3.3, with dimensions and properties for the CFRP plates displayed in Table 3.3.

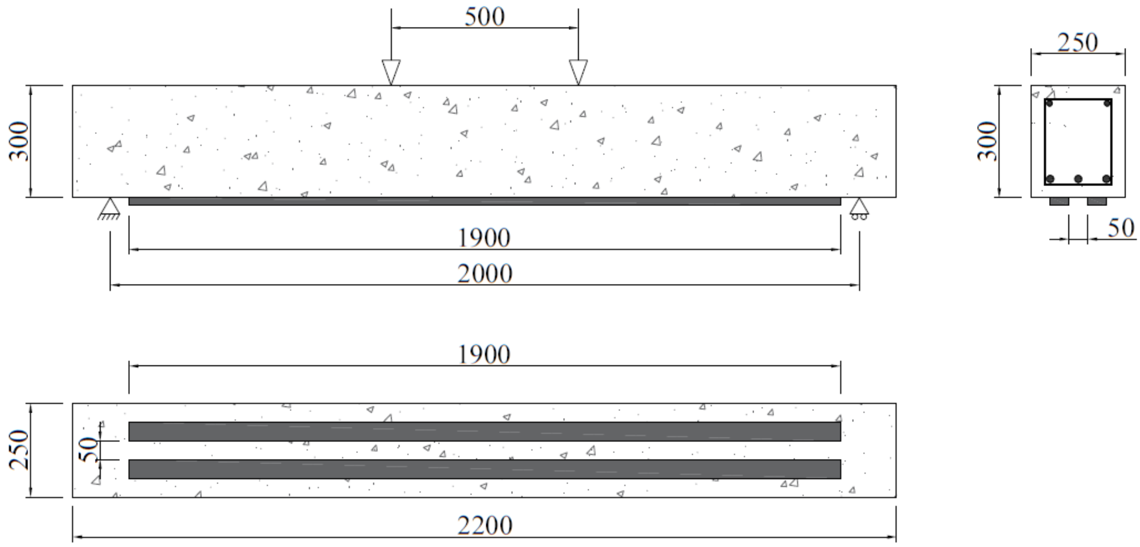


Figure 3.3 Load arrangement and CFRP configuration (All dimensions are given in millimeters)

Table 3.3 Material properties CFRP plates

| | |
|---|---|
| **CarboDur S512** | |
| Dimensions | |
| width | $w_f = 50\ mm$ |
| thickness | $t_f = 1.2\ mm$ |
| Characteristic (5% fractile value) | |
| Modulus of Elasticity $E_{fk}$ | $E_{fk} = 165\ GPa$ |
| Rupture strain $\varepsilon_{fk}$ | $\varepsilon_{fk} = 0.00176$* |
| *Characteristic 5% fractile value retrieved from Sika CarboDur Software since properties given in PDS [5] of CarboDur only displays mean value, ref Table 2.7. | |

## 3.4 Limitations of experiment

A limitation with the performed experiment is the insufficient anchorage length of the test specimen. For a span length of 2 meter with load applied to failure, high forces are developed in a short span and theoretical anchorage length of the CFRP are not sufficient according to guideline defined requirement for anchorage length discussed in Chapter 2.2.6.2

Having a test specimen with span length of 2000 mm, the TR55 criterion for required anchorage length will be hard to satisfy given the anchorage length entail 50% of the entire span, following the recommended minimum anchorage length $l_{t,max} = 500\text{mm}$ [3]. To determine the location of the point loads, for a favorable load configuration for the CFRP and anchorage requirements, other guidelines were reviewed.

Using the section properties for B35 concrete and CarboDur S512 plates, the corresponding required anchorage length defined by different guidelines are demonstrated in Table 3.4 derived from equation given in Chapter 2.2.6.2.

Table 3.4 Corresponding anchorage length

| **Guideline** | **Equation** | **Anchorage length** |
|---|---|---|
| ACI 440.2R-17 [2, p.44] | $l_{df} = \sqrt{\frac{nE_f t_f}{\sqrt{f_c'}}}$ | $l_{df} = 183.0\ mm$ |
| FiB bulletin 14 Approach 1 [7, p.51] | $l_{b,max} = \sqrt{\frac{E_f t_f}{c_2 f_{ctm}}}$ | $l_{b,max} = 176.0\ mm$ |
| FiB bulletin 14 Approach 2 [7, p.54] | $l_{b,max} = c_2 \sqrt{\frac{E_f t_f}{\sqrt{f_{ck} f_{ctm}}}}$ | $l_{b,max} = 197.0\ mm$ |
| Kompositförstärkning av betong [12, p.48] | $l_{ef} = \sqrt{\frac{E_f t_f}{2 f_{ctm}}}$ | $l_{ef} = 176.0\ mm$ |

To evaluate the available anchorage length of the test specimen, distance from support to the cracking moment are derived with below relation from bending moment diagram illustrated in Figure 3.4.

$$\frac{x}{M_{cr}} = \frac{a}{M_{Ed}} \rightarrow x = \frac{M_{cr}}{M_{Ed}} \cdot a$$

Where

$a$ = shear span

$M_{Ed}$ = Applied moment

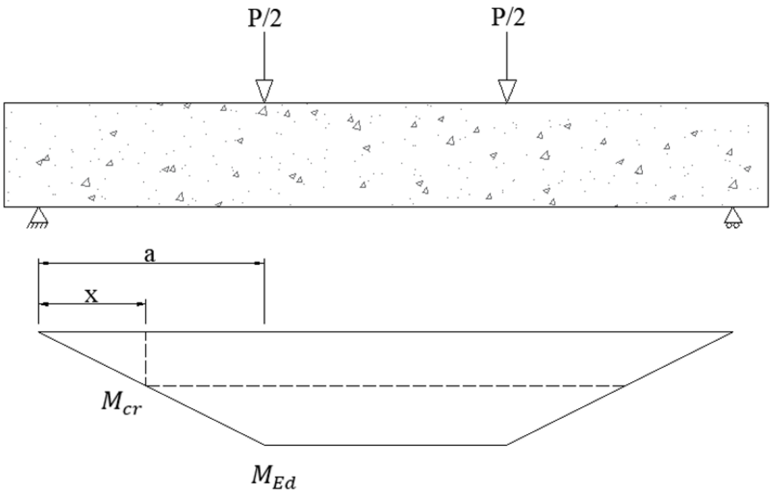


Figure 3.4 Distance to last crack

From elastic bending theory, considering uncracked section properties, the cracking moment, $M_{cr}$, can be derived according to formula below [19, p.144]. With a plate length of 1900 mm used for the experiment, the corresponding provided anchorage length $l_b$ are found by subtracting 50 mm from distance $x$.

$$M_{cr} = \frac{f_{ctm} I_{uc}}{y_t}$$

$$l_b = x - 50\ mm$$

Using above relation, the available anchorage length can be derived with respect to applied load and length of shear span. Evaluated for an applied moment equal to the unstrengthen moment capacity, corresponding anchorage length for different shear spans are demonstrated in Table 3.5. Supplementary derivation is found in Appendix A.

$$M_{cr} = 12.5\ kNm$$

$$M_{Rd,us} = 40.9\ kNm$$

Table 3.5 Available anchorage length

| $a$ | $x = \frac{M_{cr}}{M_{Rd,us}} \cdot a$ | $l_b = x - 50$ |
|---|---|---|
| 600 mm | 187 mm | 134 mm |
| 700 mm | 214 mm | 164 mm |
| 750 mm | 230 mm | 180 mm |
| 800 mm | 245 mm | 195 mm |

Given the results in Table 3.5, and the guideline defined anchorage lengths in Table 3.4, the design criterion for anchorage length will not be satisfied by any guideline definition using the experimental setup used for the experiment. By considering a merely 20% increase in the applied load over the unstrengthen capacity none of the requirements for anchorage are met, demonstrated in Table 3.6.

Table 3.6 Available anchorage length

| $a$ | $x = \frac{M_{cr}}{1.2 \cdot M_{Rd,us}} \cdot a$ | $l_b = x - 50$ |
|---|---|---|
| 600 mm | 153 mm | 103 mm |
| 700 mm | 179 mm | 128 mm |
| 750 mm | 191 mm | 141 mm |
| 800 mm | 204 mm | 154 mm |

The bond force in the anchorage zone will therefore not have the sufficient development length to develop ultimate bond force. This imposes a limitation to the experiment and the experimental setup, since the theoretical failure load of the strengthened beams are significantly higher than the unstrengthen capacity and insufficient anchorage length will reduce the effect of the strengthening system.

Distance of 750 mm were chosen to maintain a relatively large constant bending zone. To evaluate the actual distance to last crack, documentation of the crack extension and measured distance to last crack will be recorded during testing.

## 3.5 Casting of RC beams

Due to limited space, the casting of the beams was performed on two consecutive days. To attain similar properties, fresh concrete was ordered from a local contractor. Same concrete recipe of strength class B35 was used for both batches. Self-compacting concrete was chosen to eliminate the need for manual vibration and compacting of the fresh concrete, since poorly executed compacting can affect the hardened properties.

### 3.5.1 Formwork preparation

Prior to casting, formworks for the beam were prepared. From previous beam testing at the university, four set of formworks with required dimensions were available. To enable the casting to be done in two days, two additional formworks were constructed.

The formwork was constructed of 20 mm thick plywood boards with laminated surfaces to reduce the cohesion between the concrete and formwork and enable easier demolding. Lateral stiffeners were attached along the sides of the formwork to provide support to withstand the lateral pressure of the fresh concrete and sustain the dimensions of the formwork during casting. For additional lateral support, external screw clamps were mounted over the middle of the beam. The formwork for the beams is illustrated in Figure 3.5 below.

Figure 3.5 Formworks used for casting

### 3.5.2 Steel reinforcement

Binding of the reinforcement, an automatic rebar binding machine was primarily used, with some manual correction where required.

To get an indication of the accuracy of the reinforcement, with respect to the geometrical parameters used for theoretical calculations, the actual distance between the bars were measured and compared to the intended distance from the reinforcement drawing. The distance between the top and bottom reinforcement bars were measured for each beam, marked with a and b in Figure 3.6. The distance was recorded at three locations, A, B and C, illustrated in Figure 3.7.

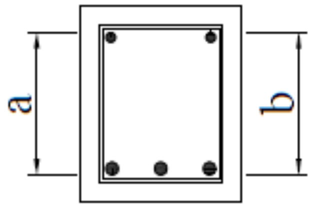


Figure 3.6 Distance between bars

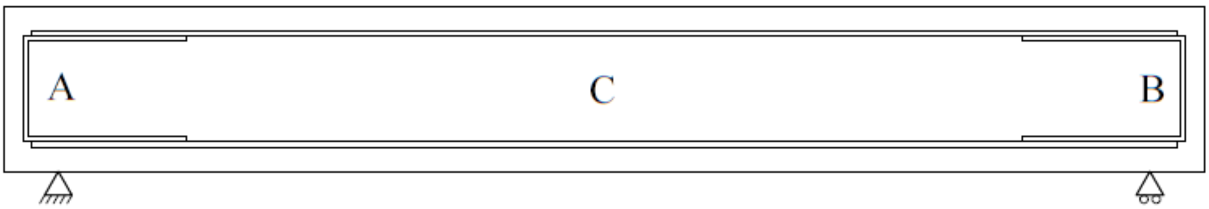


Figure 3.7 Location of measured distance between rebars

According to the reinforcement drawings the corresponding theoretical distance between the rebars should be $h - (2 * c_{nom}) - (2 * Ø_s)$. Considering the stirrup diameter $Ø_s = 8mm$ are the nominal diameter, a factor of 1.25 were used to account for the geometry of ribbed bars [20, p.40]. The theoretical distance becomes: $h - (2 * c_{nom}) - \left(2 * (1.25 * Ø_s)\right) = 210mm$, to be compared to measured distance.

The measured value is overall slightly smaller than the design value. The deviation can be explained by geometrical imperfections of the reinforcement illustrated in Figure 3.8 below, and the variable factor regarding manual labor. The measured distance between the reinforcement bars varied between 197mm - 206mm, with an average distance of 202mm. Example of the recorded measurement for two specimens with corresponding location are shown in Table 3.7 below.

Table 3.7 Measured distance between reinforcement bars

| Beam | | A | B | C | Design |
|---|---|---|---|---|---|
| B.1 | a [mm] | 205 | 205 | 204 | 210 |
| | b [mm] | 205 | 206 | 202 | 210 |
| B.2 | a [mm] | 201 | 205 | 206 | 210 |
| | b [mm] | 202 | 202 | 197 | 210 |

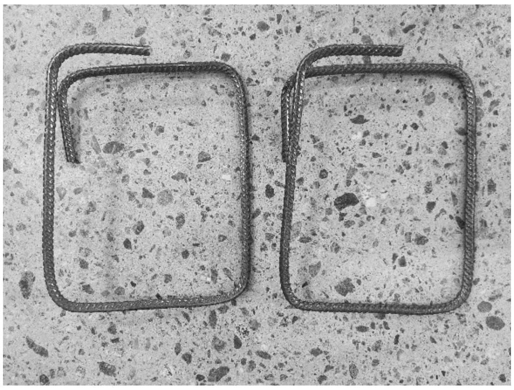

Figure 3.8 Geometrical imperfections in shear reinforcement

For further derivation, the intended theoretical dimensions will be used. Nonetheless, remarks should be made that intended theoretical values does not always correspond to actual values.

### 3.5.3 Casting of Batch A

For Batch A, a quantity of 1.5 $m^3$ was ordered and the concrete was delivered by a concrete truck with a chute. The composition of the concrete mix in found in Appendix B.

Defined by the delivery protocol, the customer has responsibility for the receival control of the concrete [21], including a quality control and control of the workability. Due to the small scale of concrete ordered, no quality control or workability test was performed. By visual appearance, the concrete was fairly thick and viscous. Filling the formworks, the concrete was applied by a chute placed over midsection and manually scooped to the ends of the formwork. Since the concrete was meant to be self-compaction, no additional vibration or compaction was performed to improve the consolidation of the concrete. In addition to the beams, 12 cubes and 4 cylinders were cast for cube compression test, E-modulus test and tensile splitting test.

### 3.5.4 Surface condition Batch A

After 24 hours of hardening the beams from Batch A was demolded and the formworks cleaned and prepared for casting of Batch B. After demolding the beams were covered in plastic and left to cure. The cubes and cylinders were also demolded and placed in water for curing.

During demolding, the surface condition of the beams was assessed, and all of the beams showed signs of poor consolidation with different degree of a honeycomb. During demolding the beams were labeled and the identification will be the reference throughout the thesis. Two of the beams, A.1 and A.6 had honeycomb located on midspan of the beams, more severe on the side of the beam but also on the bottom side. Figure 3.9 and 3.10 illustrates the condition of beam A.6, side view and bottom view.

Figure 3.9 Honeycomb beam A.6

Figure 3.10 Honeycomb, tension side beam A.6

For beam A.2 and A.5, minor areas of honeycomb could be detected on the sides of the beam, bottom side however, were satisfactory for both beams. Beam A.5 showed a smooth and even bottom surface without any signs of surface defects, illustrated in Figure 3.12 and beam A.2 showed some minor honeycomb at one end, illustrated in Figure 3.13.

Figure 3.11 Tension side beam A.5

Figure 3.12 Tension side beam A.2

Beam A.3 and A.4 revealed a greater degree of honeycomb, both along the sides and on the tension side of the beams. Especially on one side of the beams, Figure 3.14 and 3.15 illustrated the surface condition of beam A.4.

Figure 3.13 Beam A.4

Figure 3.14 Beam A.4

Since the surface condition of the concrete are a major factor influencing the adhesive bond between the concrete and CRFP plates, the beams with honeycomb on the tension side will not be suitable for application of the strengthening system in the as-is condition. Table 3.8 below identifies each beam with corresponding extent and location of honeycomb on the tension side of the beams.

Table 3.8 Honeycomb tension side of beams Batch A

| **Beam** | **Midspan** | **Extension** | **End** | **Extension** |
|---|---|---|---|---|
| A.1 | H.C | 35 cm [90-125 cm from end] | - | |
| A.2 | - | | H.C | Minor |
| A.3 | - | | H.C | 25 cm from end |
| A.4 | - | | H.C | 25 cm from end |
| A.5 | - | | - | |
| A.6 | H.C | 20 cm [60-80 cm from end] | - | |

### 3.5.5 Casting of Batch B

For casting of Batch B, a larger quantity of 4.5 $m^3$ concrete was ordered for two additional projects. Due to the larger quantity, the concrete truck was equipped with a pump hose instead of a chute which enabled easier placing in the formworks.

By visual appearance, the concrete was more flowing compared to Batch A, with a much more liquidous consistency. Placing the concrete in the formwork with the hose enabled easier application and a more even filling of the formworks, no additional shoveling needed. Due to the results from Batch A, the concrete of Batch B was manually compacted and poked after filling of the formwork to ensure good consolidation despite the fact the concrete was supposed to be self-compacting. 12 cubes and 4 cylinders were also casted with the concrete from Batch B.

### 3.5.6 Surface condition Batch B

During demolding of Batch B, the surface condition of the beams was assessed. The appearance of all the beams were similar, smooth and even surface with no signs of surface defects. Figure 3.16 below illustrates the surface condition of beam B.6.

Figure 3.15 Beam B.6

After demolding the beams, the beams were covered in plastic and left to cure. The cubes and cylinders from Batch B were placed in water bath for curing.

## 3.6 28 days properties

Since the test specimen were cast in two batches, and small variations in casting and curing conditions can affect the properties of hardened concrete [22], compression test, tensile splitting test and E-modulus test were performed after 28 days of curing, to assess and compare the material properties of the hardened concrete.

### 3.6.1 Compression test

The compressive strength of the hardened concrete is determined in accordance to test method described in NS-EN 12390-3 [23]. Three cube specimen, 100 mm by 100 mm, were tested for each batch. Result from the compression test are found in Table 3.9.

Table 3.9 Cube compression strength

| **Batch** | $\boldsymbol{f_{ci}}$ $[\boldsymbol{N/mm^2}]$ |
|---|---|
| A | 64.73 |
| A | 64.40 |
| A | 65.63 |
| B | 59.46 |
| B | 59.14 |
| B | 59.53 |

The cube compression strength is transformed to cylindrical compression strength by a factor of 0.8. Corresponding mean compression strength for the batches are derived below.

$$f_{cmA} = 0.8\left(\frac{64.73 + 64.40 + 65.63}{3}\right) = 51.9\ MPa$$

$$f_{cmB} = 0.8\left(\frac{59.46 + 59.14 + 59.53}{3}\right) = 47.5\ MPa$$

Evidently, there are deviation in average compression strength between the batches. Treating the results as a single batch, corresponding mean compression strength becomes.

$$f_{cm} = \frac{f_{cmA} + f_{cmB}}{2} = 49.7\ MPa$$

By comparing the results with the associated parameters from Table 3.1 in EN 1992-1-1 for B35 concrete the compression strength found are slightly higher and corresponds better with concrete of strength class B40/B45. Extraction from Table 3.1 are found in Table 3.10 below.

Table 3.10 Table 3.1 EN 1992-1-1 [15]

| | **Strength classes for concrete** | | | | | | | | | | | | | | **Analytical relation / Explanation** |
|---|---|---|---|---|---|---|---|---|---|---|---|---|---|---|---|
| $f_{ck}$ (MPa) | 12 | 16 | 20 | 25 | 30 | 35 | 40 | 45 | 50 | 55 | 60 | 70 | 80 | 90 | |
| $f_{ck,cube}$ (MPa) | 15 | 20 | 25 | 30 | 37 | 45 | 50 | 55 | 60 | 67 | 75 | 85 | 95 | 105 | 2.8 |
| $f_{cm}$ (MPa) | 20 | 24 | 28 | 33 | 38 | 43 | 48 | 53 | 58 | 63 | 68 | 78 | 88 | 98 | $f_{cm} = f_{ck}+8$(MPa) |
| $f_{ctm}$ (MPa) | 1,6 | 1,9 | 2,2 | 2,6 | 2,9 | 3,2 | 3,5 | 3,8 | 4,1 | 4,2 | 4,4 | 4,6 | 4,8 | 5,0 | $f_{ctm}=0,30\times f_{ck}^{(2/3)} \leq$C50/60<br>$f_{ctm}=2,12\cdot\ln(1+(f_{cm}/10))$ > C50/60 |
| $f_{ctk,0,05}$ (MPa) | 1,1 | 1,3 | 1,5 | 1,8 | 2,0 | 2,2 | 2,5 | 2,7 | 2,9 | 3,0 | 3,1 | 3,2 | 3,4 | 3,5 | $f_{ctk;0,05} = 0,7\times f_{ctm}$<br>5% fractile |
| $f_{ctk,0,95}$ (MPa) | 2,0 | 2,5 | 2,9 | 3,3 | 3,8 | 4,2 | 4,6 | 4,9 | 5,3 | 5,5 | 5,7 | 6,0 | 6,3 | 6,6 | $f_{ctk;0,95} = 1,3\times f_{ctm}$<br>95% fractile |
| $E_{cm}$ (GPa) | 27 | 29 | 30 | 31 | 33 | 34 | 35 | 36 | 37 | 38 | 39 | 41 | 42 | 44 | $E_{cm} = 22[(f_{cm})/10]^{0,3}$<br>($f_{cm}$ in MPa) |
| $\varepsilon_{c1}$ (‰) | 1,8 | 1,9 | 2,0 | 2,1 | 2,2 | 2,25 | 2,3 | 2,4 | 2,45 | 2,5 | 2,6 | 2,7 | 2,8 | 2,8 | see Figure 3.2<br>$\varepsilon_{c1}(^0/_{00}) = 0,7\ f_{cm}^{0,31} \leq 2,8$ |
| $\varepsilon_{cu1}$ (‰) | 3,5 | | | | | | | | | 3,2 | 3,0 | 2,8 | 2,8 | 2,8 | see Figure 3.2<br>for $f_{ck} \geq 50$ Mpa<br>$\varepsilon_{cu1}(^0/_{00})=2,8+27[(98-f_{cm})/100]^4$ |
| $\varepsilon_{c2}$ (‰) | 2,0 | | | | | | | | | 2,2 | 2,3 | 2,4 | 2, 5 | 2,6 | see Figure 3.3<br>for $f_{ck} \geq 50$ Mpa<br>$\varepsilon_{c2}(^0/_{00})=2,0+0,085(f_{ck}-50)^{0,53}$ |
| $\varepsilon_{cu2}$ (‰) | 3,5 | | | | | | | | | 3,1 | 2,9 | 2,7 | 2,6 | 2,6 | see Figure 3.3<br>for $f_{ck} \geq 50$ Mpa<br>$\varepsilon_{cu2}(^0/_{00})=2,6+35[(90-f_{ck})/100]^4$ |
| $n$ | 2,0 | | | | | | | | | 1,75 | 1,6 | 1,45 | 1,4 | 1,4 | for $f_{ck} \geq 50$ Mpa<br>$n=1,4+23,4[(90-f_{ck})/100]^4$ |
| $\varepsilon_{c3}$ (‰) | 1,75 | | | | | | | | | 1,8 | 1,9 | 2,0 | 2,2 | 2,3 | see Figure 3.4<br>for $f_{ck} \geq 50$ Mpa<br>$\varepsilon_{c3}(^0/_{00})=1,75+0,55[(f_{ck}-50)/40]$ |
| $\varepsilon_{cu3}$ (‰) | 3,5 | | | | | | | | | 3,1 | 2,9 | 2,7 | 2,6 | 2,6 | see Figure 3.4<br>for $f_{ck} \geq 50$ Mpa<br>$\varepsilon_{cu3}(^0/_{00})=2,6+35[(90-f_{ck})/100]^4$ |

### 3.6.2 E-modulus test

E-modulus test for two cylinders from each batch were performed after 28 days. The test method was performed accordance with Method A defined in NS-EN 12390-13 [24]. The results from the E-modulus test are found in Table 3.11 below.

Table 3.11 Results E-modulus test

| **Specimen** | $\boldsymbol{E_{c,s}}$ $[\boldsymbol{GPa}]$ |
|---|---|
| Batch A | 17.14 |
| Batch A | 14.20 |
| Batch B | 19.32 |
| Batch B | 13.34 |

However, the test procedure was aborted multiple times due to problems with the equipment and error during the procedure and will therefore be regarded inconclusive. E-modulus for the concrete will therefore be derived according to the analytical relation given in Table 3.1, EN 1992-1-1, illustrated in Table 3.10 above.

$$E_{cm} = 22\left[\frac{f_{cm}}{10}\right]^{0.3}$$

### 3.6.3 Tensile splitting test

A splitting tensile test was also performed after 28 days for two cylinders from each batch. The tensile splitting strength of the concrete is determined in accordance with the test method defined in NS-EN 12390-6 [25].

The test is conducted by applying a force along the side of the cylinder, illustrated in Figure 3.17. Compressive force on a narrow region along the length of the test specimen results in tensile forces orthogonal to the applied force, and the load is increased until the specimen fails in tension.

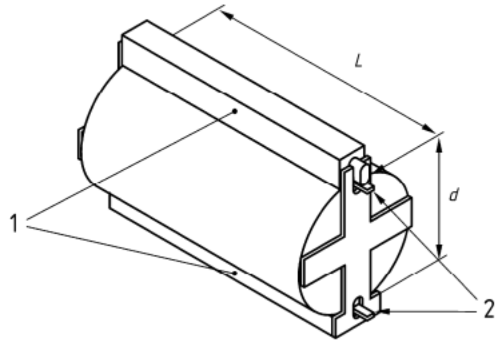


Figure 3.16. Tensile splitting strength setup [25]

The failure load is recorded, and the splitting strength is derived by formula below.

$$f_{ct} = \frac{2F}{\pi L d}$$

Where

$d = 150\ mm$

$L = 300\ mm$

Failure load and associated tensile splitting strength for each specimen are found in Table 3.12.

Table 3.12 Results tensile splitting test

| **Specimen** | $\boldsymbol{F}$ $[\boldsymbol{kN}]$ | $\boldsymbol{f_{ct}}$ $[\boldsymbol{MPa}]$ |
|---|---|---|
| Batch A | 250.99 | 3.55 |
| Batch A | 210.96 | 2.98 |
| Batch B | 234.15 | 3.31 |
| Batch B | 239.81 | 3.39 |

The results from the test does not indicate large deviation between the batches. Since Batch A yields both the highest and lowest strength, the mean value will be derived as the average of the test results from both batches.

According to section 3.1.2 (8) in EN 1992-1-1, the axial tensile strength can be approximated by a factor of 0.9 times the splitting tensile strength [15].

$$f_{ct} = 0.9 f_{ct,sp}$$

The mean value of the axial tensile strength for the concrete $f_{ctm}$, based on the results from the tensile splitting test are defined according to equation below.

$$f_{ctm} = \frac{0.9(3.55 + 2.98 + 3.31 + 3.39)}{4} = 2.98\ MPa$$

## 3.7 Four-point bending test program

Due to the surface condition of the beams from Batch A. The experimental plan had to be adjusted with respect to which beam to be used for which test.

After 28 days of curing, the bottom side of the beams were inspected more thorough. A rubber sledgehammer was used to examine the honeycomb area, to remove loose particles and get a perception of the quality of the hardened concrete in areas with honeycomb.

Beam A.1 and A.6 both had honeycomb along midspan of the beam. Since midspan of the beams will be subjected to highest bending moment, surface defects in this area were assumed to have the greatest impact of the strengthened capacity. To eliminate the need for extensive repair, beam A.1 and A.6 were chosen for Test 1, ultimate load of unstrengthen section.

Beam A.2 and A.5 had none or minor degree of honeycomb along the tension side of the beams. For beam A.2 the small area of honeycomb did not extend into the critical area where the CFRP plates are ending and will therefore not affect the bond of the CFRP plates. These two beams were chosen for test with no preload and 70% preload respectively.

Beams A.3 and A.4 both had honeycomb extending approximately 25 cm from the end of the beam. Surface repair of these beams were therefore required in order to proceed with the planned experiment and to ensure satisfactory surface condition when applying the CFRP plates.

The beams from Batch B were chosen arbitrary for each test since the surface quality were equally satisfactory for all beams. Table 3.13 below gives the final setup for the experiment.

Table 3.13 Test program

| | **Beam** | **Preload** | **CFRP** | |
|---|---|---|---|---|
| Test 1 | Beam A.1 | None | None | Reference beams $P_{fail,us}$ |
| | Beam A.6 | | | |
| | Beam B.1 | | | |
| | Beam B.2 | | | |
| Test 3.0 | Beam A.2 | None | 2 strips | Control beams |
| | Beam B.5 | | | |
| Test 3.3 | Beam A.4 | 30% of $P_{fail,us}$ | 2 strips | |
| | Beam B.4 | | | |
| Test 3.5 | Beam A.3 | 50% of $P_{fail,us}$ | 2 strips | |
| | Beam B.3 | | | |
| Test 3.7 | Beam A.5 | 70% of $P_{fail,us}$ | 2 strips | |
| | Beam B.6 | | | |

## 3.8 Repair of honeycomb in reinforced concrete beams

Before installation of the CFRP plates, surface repair of the tension side of beam A.3 and A.4 was performed. Repair of the honeycomb was necessary since the defects in the concrete extended into the bond zone of the CFRP plates.

Using cement-based repair mortar was not feasible due to the required curing time for the material. After consultation with Sika Norway regarding suitable method and material, the adhesive Sikadur 30 was used for the repair of the damaged beams. The focus of the repair work was to fill the cavities on the tension side of the beam and provide a solid concrete surface in the area where the CFRP plates should be bonded. However, cavities in areas over the support was also filled in order to provide a more compact structure in regions over the support.

Before the repair the surface was be prepared and cleaned in correspondence with the recommendations regarding surface preparation described in Chapter 2.3.1.1. The surface was leveled with a concrete grinder to remove loose particles and remove the laitance layer of the concrete. After grinding the surface was brushed, vacuumed and degreased with Acetone to remove any remains of formwork oil.

Sikadur 30 was injected in the larger cavities and leveled with a wide spatula to get a relatively level surface. Before and after pictures of beam A.3 and A.4 are illustrated in Figure 3.18 - 3.21 below.

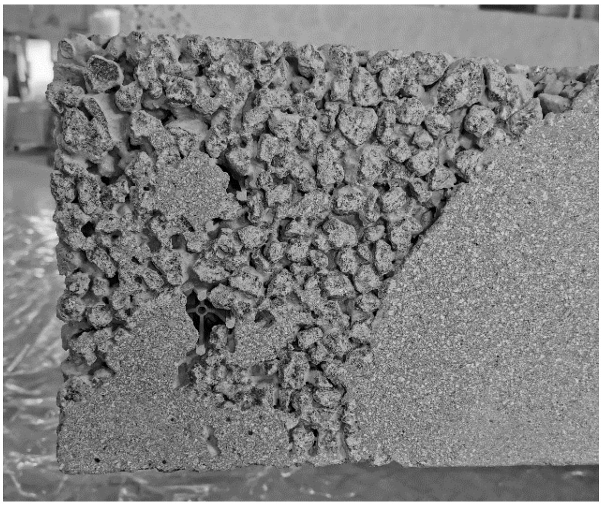

Figure 3.17 Beam A.3 before repair

Figure 3.18 Beam A.3 after repair

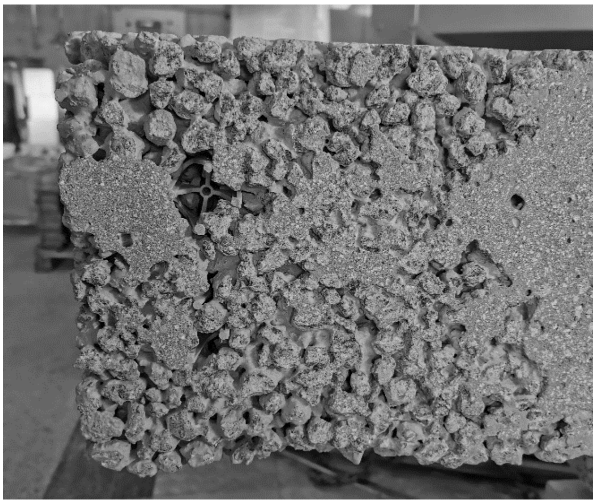

Figure 3.19 Beam A.4 before repair

Figure 3.20 Beam A.4 after repair

## 3.9 Ultimate capacity of unstrengthen reinforced concrete beams

### 3.9.1 Results from 4-point bending test

The same load configuration was used for all the tests, with the load applied at a constant load rate of 10 kN/min. The load vs. deflection curve of the beams for Test 1: Unstrengthen capacity are illustrated in Figure 3.22. The failure load is determined at the knee-point of the graph and the results are found in Table 3.14.

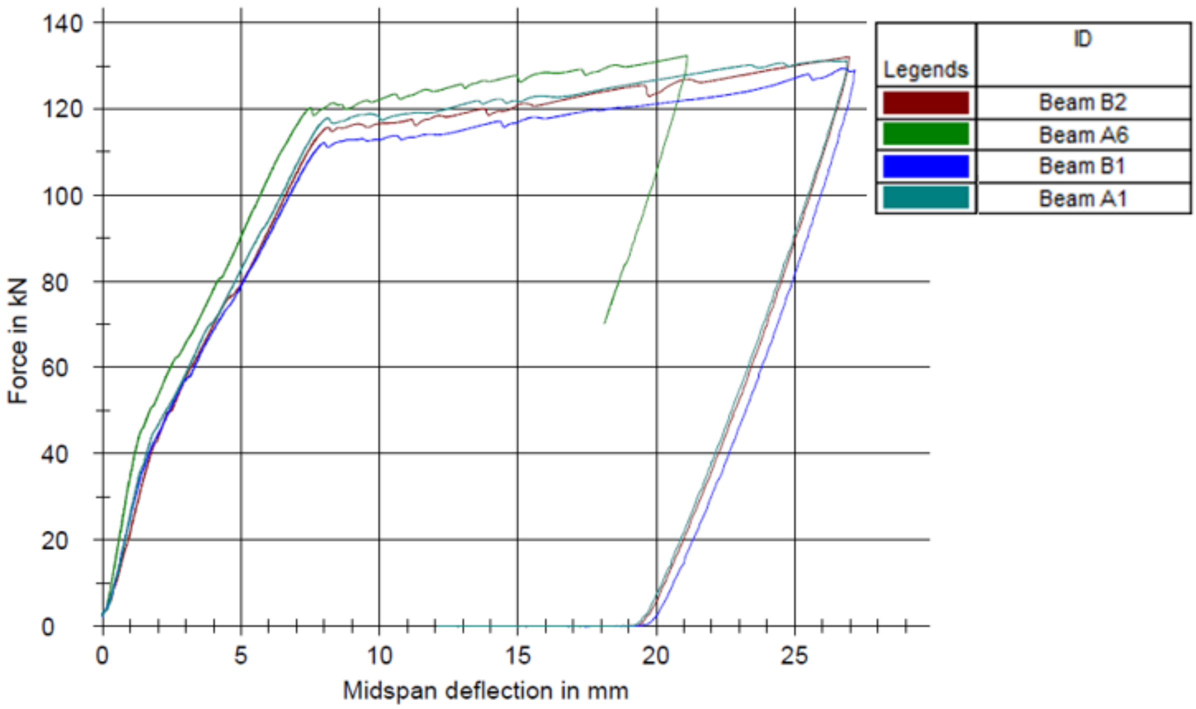


Figure 3.21 Load vs. deflection curve Test 1

Table 3.14 Failure load Test 1

| **Test 1**<br>**Ultimate load unstrengthen beams** | |
|---|---|
| **Beam** | **Failure load** |
| A.1 | 117 kN |
| A.6 | 120 kN |
| B.1 | 112 kN |
| B.2 | 115 kN |

The failure load of the unstrengthen beams, $P_{fail,us}$, are determined with the average value of above results.

$$P_{fail,us} = \sum \frac{P_i}{n} = 116\ kN$$

Corresponding moment capacity found from the experimental failure load, $M_{Rd,ex}$, are derived according to below formula, including the self-weight $q$ of the beam.

$$L = 2\ m$$

$$q = 0.25m \cdot 0.3m \cdot 25\ kN/m^3 = 1.875\ kN/m$$

$$M_{Rd,ex} = \frac{P_{fail,us}}{2} \cdot a + \frac{qL^2}{8} = 44.44\ kNm$$

Evaluating the slope of the load curve in Figure 3.21, all the samples displays similar behavior with a noticeable gradient change at a load of approximately 40 kN. The gradient change of the curve represents the formation of the first crack and the associated changes of the sectional properties of the specimen.

By visual observation crack initiation and propagation of beam A.6 and B.1 were recorded. The first couple of cracks appeared in constant bending zone between the supports for both beams, with new cracks forming progressively towards support at higher applied load. By visual inspection, the majority of the cracks appears to be flexural cracks, as the characteristic diagonal crack pattern of shear cracks was not evident. Figure 3.23 and 3.24 illustrates the crack pattern of beam A.6 and B.1. After failure the distance from support to first crack were measured to evaluate the available anchorage length according to theory described in Chapter 2.2.6.2, results found in Table 3.15.

Table 3.15 First crack Test 1

| Beam | First crack Visually detected [kN] | First crack from graph [kN] | Distance Left support to first crack [cm] | Distance Right support to first crack [cm] |
|---|---|---|---|---|
| A.1 | - | 39 | 42 | 45 |
| A.6 | 48 | 43 | 48 | 32 |
| B.1 | 39 | 37 | 42 | 40 |
| B.2 | - | 42 | 41 | 52 |

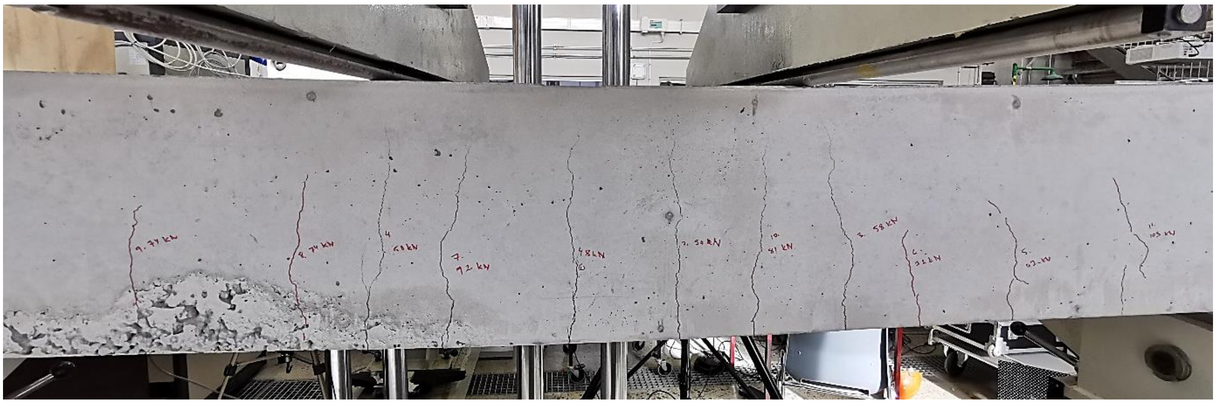

Figure 3.22 Beam A.6

Figure 3.23 Beam B.1

## 3.9.2 Compression test at time of test

To evaluate the actual concrete compression strength at the time of the test, compression test of three concrete cubes from each batch were performed according to same method used to determine the 28 days properties. By Eurocode standardized definition, concrete will normally be specified in terms of the 28-days characteristic strengths [19, p.4]. The strength development is however a continuous process, and concrete generally increases its strength with age even though the strength development declines after 28 days, as illustrated in Figure 3.25. For a more realistic comparison between the theoretical and experimental values, the mean compression strength at time of test were used.

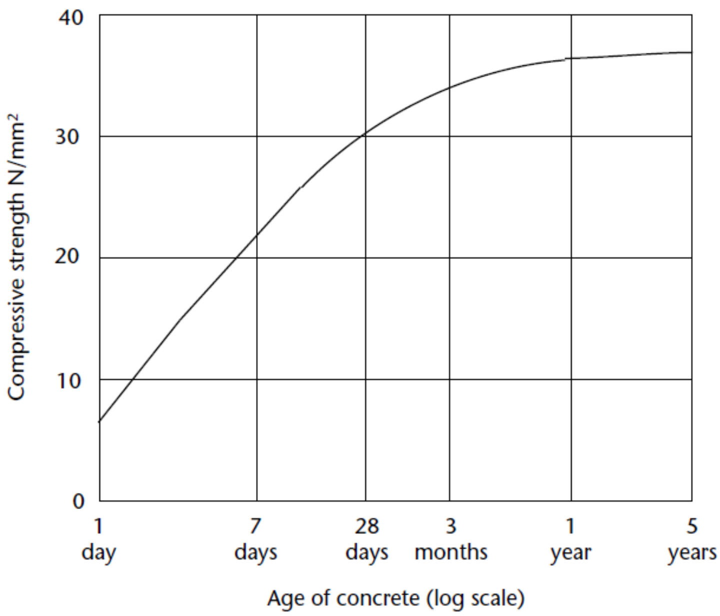


Figure 3.24 Concrete strength development over time [19, p.3]

The compression test was performed 21 days after the first test, where the 28-day properties were determined. Results from the compression test are found in Table 3.16.

Table 3.16 Compression test, Test 1

| **Batch** | $f_{ci}$ $[N/mm^2]$ |
|---|---|
| A | 73.95 |
| A | 73.10 |
| A | 73.59 |
| B | 68.62 |
| B | 67.16 |
| B | 67.01 |

Mean value of concrete cylinder compressive strength $f_{cm}$ for each batch were determined to evaluate relative strength increase between batches and to compare with the 28-day values.

$$f_{cmA} = 0.8\left(\frac{73.95 + 73.10 + 73.59}{3}\right) = 58.8\ MPa$$

$$f_{cmB} = 0.8\left(\frac{68.62 + 67.16 + 67.01}{3}\right) = 54.1\ MPa$$

$$f_{cm} = \frac{f_{cmA} + f_{cmB}}{2} = 56.46\ MPa$$

Comparing the results from both compression test, a strength increase of approximately 13% was found for both batches, demonstrated in Table 3.17.

Table 3.17 Comparison of concrete strength

| | **28 days** | **Test 1** | **Strength increase** |
|---|---|---|---|
| $f_{cmA}$ | 51.9 MPa | 58.5 MPa | 12.7% |
| $f_{cmB}$ | 47.5 MPa | 54.1 MPa | 13.9% |
| $f_{cm}$ | 49.7 MPa | 56.46 MPa | 13.6% |

### 3.9.3 Theoretical calculations

For a better evaluation of the theoretical capacity to be compared with the experimental results, the measured mean compression strength of the concrete $f_{cm}$ at the time of test were used to derive the moment of resistance for the section, results demonstrated below.

$$f_{cm} = 56.47$$

$$x = \frac{f_{yk}A_s}{0.8bf_{cm}} = 15.0\ mm$$

$$M_{Rd,us} = f_{yk}A_s(d - 0.4x) = 41.56\ kNm$$

The theoretical failure load is derived by equation below, including the self-weight $q$ of the beam.

$L = 2\ m$

$q = 0.25m \cdot 0.3m \cdot 25\ kN/m^3 = 1.875\ kN/m$

$$P_t = \left(M_{Rd,us} - \frac{qL^2}{8}\right) \cdot \frac{2}{a} = 108.3\ kN$$

### 3.9.3.1 Evaluation of contribution from top reinforcement

Previously determined, the concrete section is singly reinforced, but top bars are included to provide stability for the stirrups. To evaluate the contribution of the top reinforcement and justify further calculation where the top reinforcement is neglected, moment of resistance is derived with contribution from top reinforcement included.

By first assuming, top reinforcement is yielding in compression zone, the neutral axis depth is found with formula below.

$$A_{s,top} = 2 \cdot \frac{\pi {\O_{10}}^2}{4}$$

$$d_{top} = c_{nom} + \O_s + \frac{\O_{10}}{2}$$

$$x = \frac{f_{yk}A_s - f_{yk}A_{s,top}}{0.8bf_{cm}} = 8.0\ mm$$

Since neutral axis is located above the top reinforcement, the top steel is subjected to tension. Neutral axis is therefore redefined according to formula below.

$$x = \frac{f_{yk}A_s + f_{yk}A_{s,top}}{0.8bf_{cm}} = 22.0\ mm$$

This derivation of neutral axis does however, assume yielding of the top reinforcement, which does not comply with linear strain distribution. The stress and strain in the top reinforcement are found through an iterative process following the sequence below.

Using yield properties for steel as input values.

$$\sigma_y = 500\ MPa$$

$$E_s = 200\ GPa$$

$$\varepsilon_y = \frac{\sigma_y}{E_s} = 0.00025$$

The iteration starts with an initial assumption of $x$ which will be adjusted until it converges.

$$x_i = 22.0\ mm$$

Corresponding strain and stress in top reinforcement from similar triangles and Hooke's law.

$$\varepsilon_i = \varepsilon_y \cdot \frac{d_{top} - x_i}{d - x_i}$$

$$\sigma_i = \varepsilon_i E_s$$

New location of neural axis

$$x_{i+1} = \frac{f_{yk}A_s + \sigma_i A_{s,top}}{0.8bf_{cm}}$$

Adjusting the input parameter $x_i = x_{i+1}$ the iteration continues until convergence. Tabulated result from process are found in Table 3.18.

Table 3.18 Iteration process

| **Iteration, i** | $\varepsilon_i$ | $\sigma_i$ | $x_i$ |
|---|---|---|---|
| 0 (start) | | | 22.0 |
| 1 | 0.00028403 | 56.8073 | 15.8145 |
| 2 | 0.00034212 | 68.4257 | 15.9761 |
| 3 | 0.00034064 | 68.1289 | 15.9720 |
| 4 | 0.00034068 | 68.1365 | 15.9721 |
| 5 | 0.00034068 | 68.1363 | 15.9721 |

The iteration can be considered converged after 5 iterations and the parameters are used to determine the moment of resistance including contribution from top reinforcement demonstrated below.

$\sigma_{top} = 68.136\ MPa$

$x = 15.97\ mm$

$M_{Rd,us(2)} = f_{yk}A_s(d - 0.4x) + \sigma_{top}A_{s,top}\left(d_{top} - 0.4x\right) = 41.94\ kNm$

Evaluating the derived moment of resistance with the moment derived neglecting top reinforcement, the contribution from the top reinforcement are negligible, results demonstrated in Table 3.19. For further calculations the top reinforcement will not be considered. Iteration process and detailed calculations are found in Appendix C.

Table 3.19 Moment capacity considering top reinforcement

| | **Neglecting top reinforcement** | **Including top reinforcement** | $\Delta M_{Rd}$ |
|---|---|---|---|
| $M_{Rd}$ | $M_{Rd,us} = 41.56\ kNm$ | $M_{Rd,us(2)} = 41.94\ kNm$ | $0.38\ kNm$ |

## 3.10 Preload

The preload of the beams was performed with same load rate as the capacity test, 10 kN/min. After reaching target load, the applied load was kept constant for a duration of 15 minutes before unloading. The applied loads for corresponding beams are found in Table 3.20.

Table 3.20 Applied preload

| | **Beam** | **Preload** |
|---|---|---|
| 30% preload | A.4 | $0.3 \cdot P_{fail,us} = 34.8\ kN$ |
| | B.4 | |
| 50% preload | A.3 | $0.5 \cdot P_{fail,us} = 58\ kN$ |
| | B.3 | |
| 70% preload | A.5 | $0.7 \cdot P_{fail,us} = 81.2\ kN$ |
| | B.6 | |

### 3.10.1 Crack formation

Crack initiation and propagation of the beams were recorded, applied load at first crack and distance from the support to first crack in span are found in Table 3.21, as well as number of visual cracks detected.

Table 3.21 Crack formation

| **Applied load** | **Beam** | **First crack Visually detected [kN]** | **No. of visual cracks** | **Distance Left support to first crack [cm]** | **Distance Right support to first crack [cm]** |
|---|---|---|---|---|---|
| 30% preload 34.8 kN | A.4 | *34.8 | 2 | 89 | 82 |
| | B.4 | 29 | 2 | 88 | 75 |
| 50% preload 58 kN | A.3 | 35.5 | 6 | 47 | 59 |
| | B.3 | 32.6 | 7 | 41 | 47 |
| 70% preload 81.2 kN | A.5 | 37 | 9 | 55 | 45 |
| | B.6 | 28 | 11 | 42 | 35 |
| *Crack detected during constant load | | | | | |

The difference in crack pattern between beams are subjected to 30%, 50% and 70% preload are illustrated in Figure 3.26-3.28. For the beams subjected to 30% preload a sparse crack pattern was found with only a few cracks initiated. The beams subjected to 50% and 70% preload had an evident increase of crack formation in the constant bending zone with decreasing crack formation towards the support.

Figure 3.25 Beam B.4 30% preload

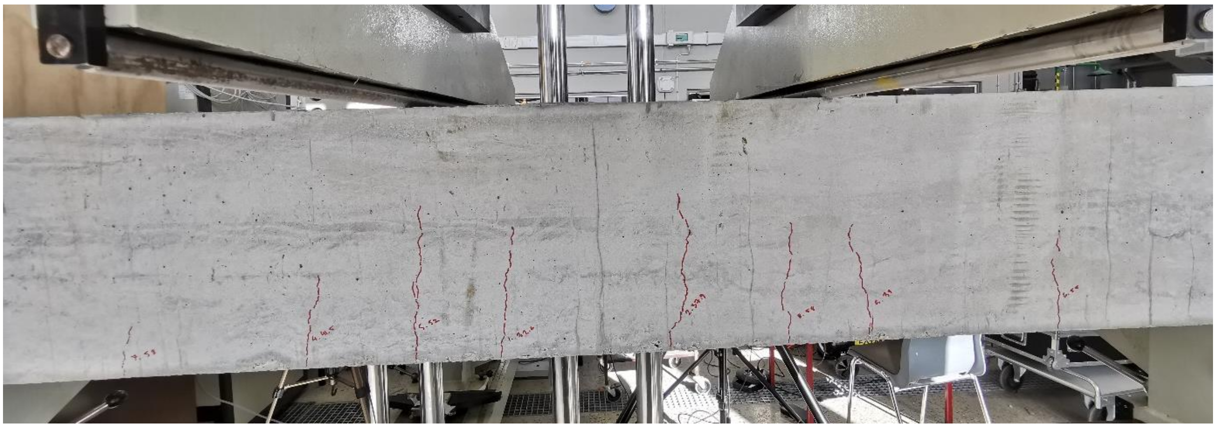

Figure 3.26 Beam B.3 50% preload

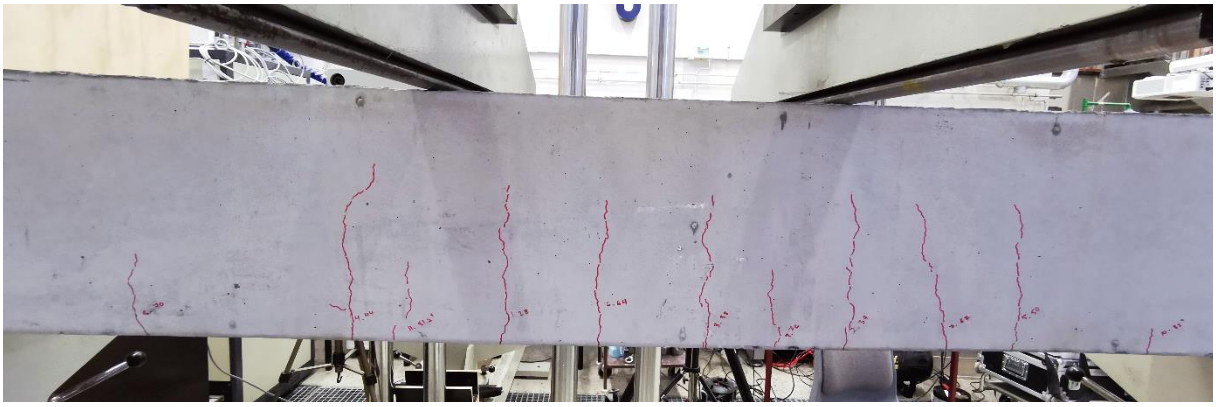

Figure 3.27 Beam B.6 70% preload

## 3.11 Application of CRFP plates

Application of the CFRP plates were performed in accordance with the installation procedure described in Chapter 2.3.2.4 following the guidelines given in the Method Statement for Sika CarboDur system [4].

### 3.11.1 Application method and equipment

The bottom surface of the beams was leveled and prepared with a handheld concrete grinder. The prepared surface was the brushed, vacuumed, and wiped clean with acetone to remove any dust or rest from formwork oil.

For application of the adhesive with the desired convex profile on the CRFP plates, an application tool was constructed. A scraper with the dimensions of the CarboDur S512 plates with additional height of 1 mm on the sides and 2 mm along center, were cut out of a 2 mm MDF board using a laser cutter. The MDF plates were then mounted on a wooden framework, in which the adhesive could be feed, and the CFRP plates pulled through to apply the adhesive. The application tool and scraper used are illustrated in figure 3.29 and 3.30.

Figure 3.28 Application tool

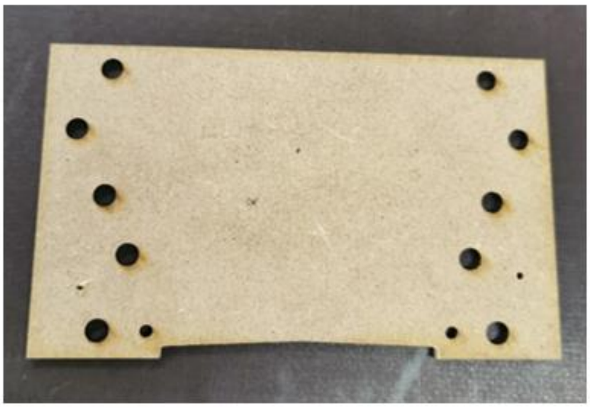

Figure 3.29 Scraper with desired profile

The CFRP plates were cut to designated length by hacksaw, plate ends were inspected after they were cut to length to ensure no damage or splintering of the ends was imposed during sawing. Prior to application, the plates were wiped clean with acetone and left to dry.

A thin layer of adhesive was thereafter applied on the prepared concrete substrate. The exact location where the plates should be applied were marked out with tape, this also enabled easy removal of excess adhesive. Special attention was given to beam A.3 and A.4 where repair of honeycomb had been performed, since small surface irregularities were still present. Procedure for application of the adhesive onto the CFRP plates are illustrated in Figure 3.31.

Figure 3.30 Application of the adhesive

The plates were pressed onto the concrete substrate using a hard rubber roller until the adhesive was forced out on both sides of the plates, illustrated in Figure 3.32. The application procedure was performed two beams at a time, to ensure sufficient time for the installation procedure and complete installation within one hour of mixing the adhesive, as described in Chapter 2.3.1.3. Illustration of the installed plates are found in Figure 3.33. To allow development of full design strength of the adhesive, the strengthen specimen were cured for minimum 7 days.

Figure 3.31 Bonding of the plates onto concrete substrate

Figure 3.32 Installed plates

### 3.11.2 Bond inspection

After curing the bond quality of the strengthen beams were visually inspected. Overall, the majority of the bond interface appeared to be in good condition, with uniformly thickness and hardened edges of the adhesive on both sides of the plates.

However, areas with deficiencies in the bond were also located in a few specimens, where voids between the plate and the concrete were found, illustrated in Figure 3.34.

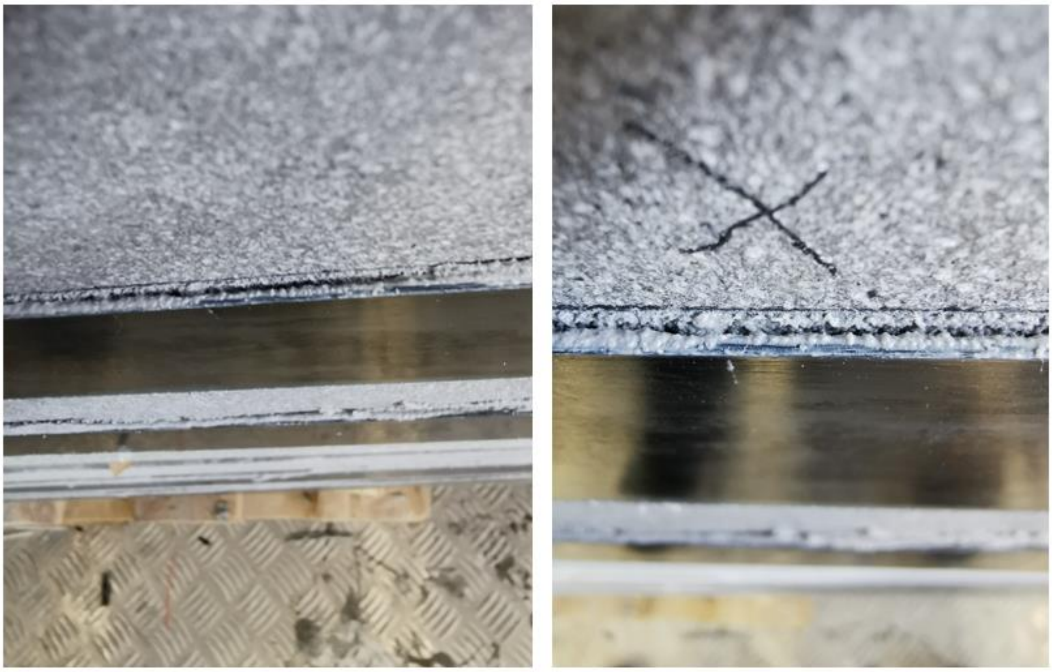

Figure 3.33 Defects in adhesive

The extent of the voids was evaluated by gently tapping on the plate, where difference in resonating sound gives an indication of where the plate is fully bonded and where there are voids within the adhesive layer. Using a thin steel wire, the approximated depth of the bond defect was evaluated, by gently inserting the wire between the CFRP plate and the concrete.

Table 3.22 below summarize the visual bond inspection and the bond defects detected. The extent of the voids are described with notation [length:depth], illustrated in Figure 3.35.

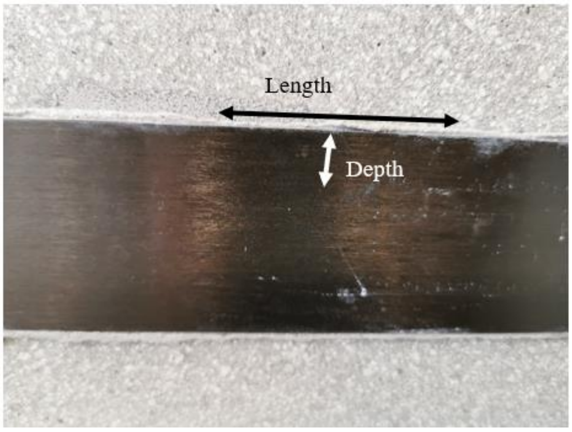


Figure 3.34 Illustration of measured void defects

Table 3.22 Bond inspection

| **Beam** | **Bond condition** |
|---|---|
| A.2 | Good bond quality.<br>Excess adhesive pressed out on both sides of plates.<br>No defects detected by visual inspection |
| B.5 | Good bond quality.<br>Excess adhesive pressed out on both sides of plates.<br>No defects detected by visual inspection |
| A.4 | Good bond quality.<br>Excess adhesive pressed out on both sides of plates.<br>No defects detected by visual inspection |
| B.4 | General good bond quality<br>1 location with void in adhesive layer.<br>[22cm: ~2mm] |
| A.3 | Poor bond quality<br>4 locations with relatively deep voids<br>[8cm: ~9mm]*<br>[9 cm: ~3mm]<br>[8cm: ~4mm]<br>[14cm: ~3mm]<br>*One plate had sunken down approximately 2 cm from intended position, resulting in a large gap and partially unbonded plate at the end with maximum depth of void measured to 9 mm, illustrated in Figure 3.36. |

| | |
|---|---|
| B.3 | Potentially compromised bond quality<br>3 locations with relatively deep voids<br>[10cm: ~3mm]<br>[15cm: ~5mm]<br>[8.5cm: ~6mm] |
| A.5 | General good bond<br>2 locations with void in adhesive layer<br>[3cm: ~1-2mm]<br>[5.5cm: ~2mm] |
| B.6 | General good bond<br>2 locations with void in adhesive layer<br>[3.8cm: ~2mm]<br>[10cm: ~2-3mm] |

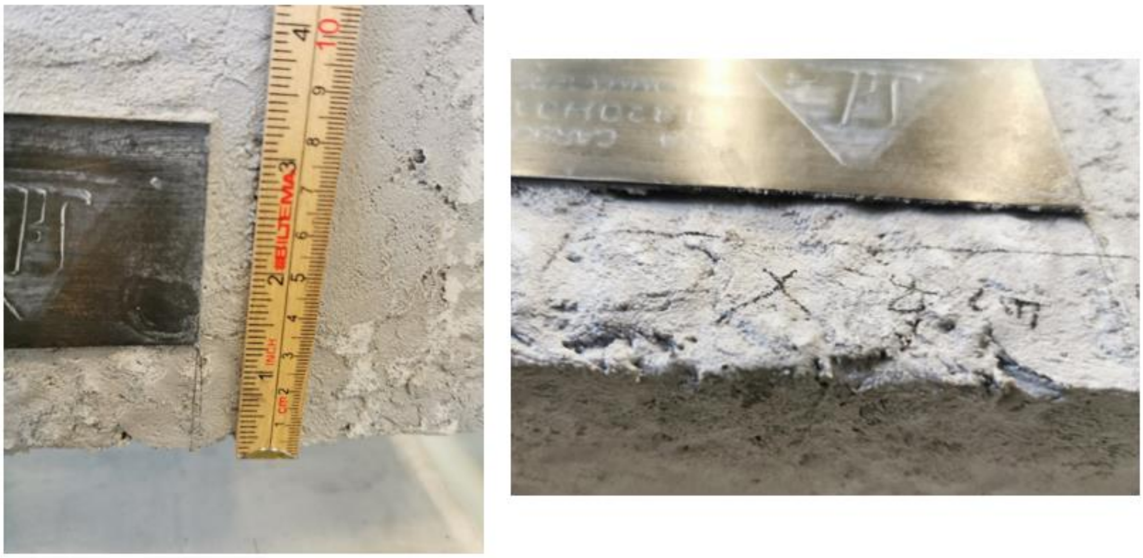

Figure 3.35 Bond defect beam A.3

## 3.12 Mounting of Strain gauges

To evaluate the strain developed in the CFRP plates at failure of the beams and compare the strain value to the different guideline definitions of limiting strain, discussed in Chapter 2.2.6.1 strain gauges were mounted on the CFRP plates. Linear strain gauges with one measuring grid and 120 Ω resistance were used to measure the strain in the directions of the fibers in the CFRP plates.

The location of the strain gauges for beam A.2, A.3, A.4 and A.5 are illustrated in Figure 3.37.

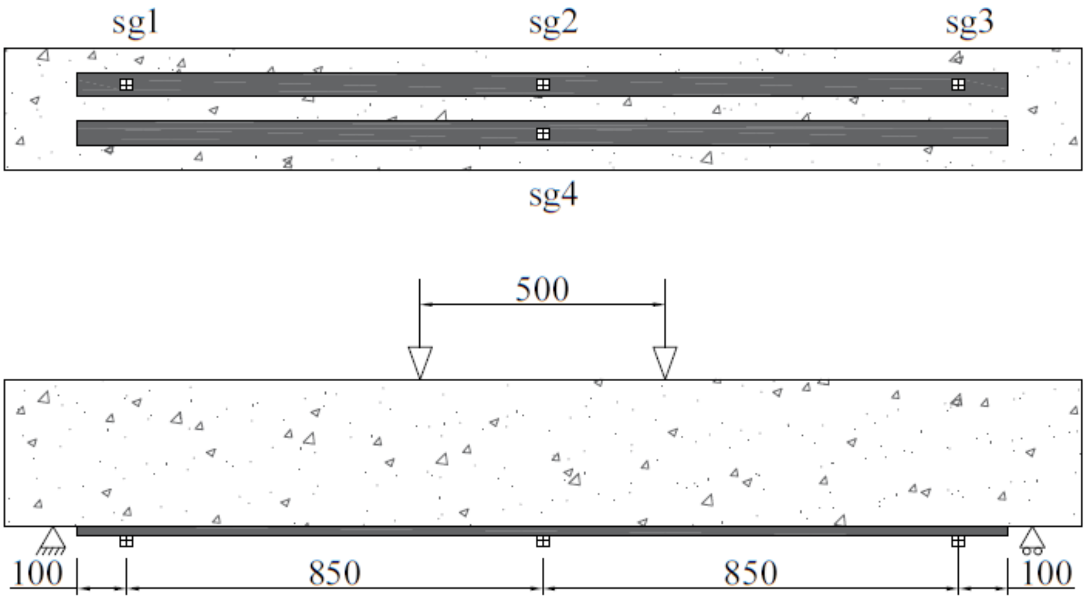


Figure 3.36 Location of strain gauges Beam A.2-4 (All dimensions are given in millimeters)

Beam B.5 and B.6 were mounted with additional strain gauges at location under the point loads and in the span illustrated in Figure 3.38

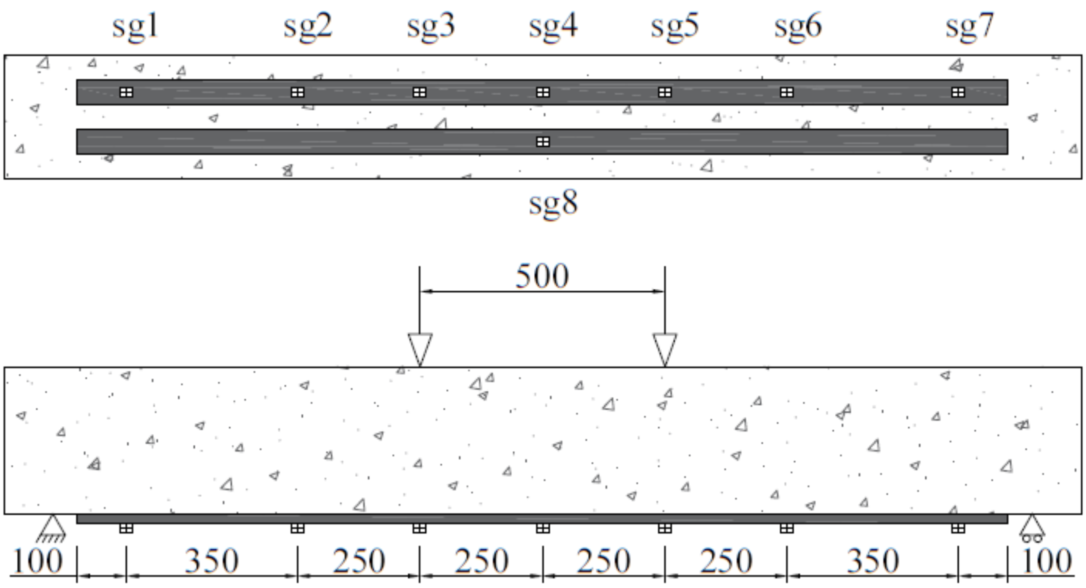


Figure 3.37 Location of strain gauges beam B5-6 (All dimensions are given in millimeters)

Installation of the strain gauges were performed in accordance with recommendation from supplier of the strain gauges [26]. After installation of the strain gauges, all the gauges were checked in unloaded condition to evaluate the connection between the strain gauge and the CFRP plates.

Due to difficulties during installation of the strain gauges, not all strain gauges are of the same type. Few of the gauges displayed drift in the readings and had to be removed and new gauges reinstalled to get reliable data. Due to this, not enough strain gauges were available for all the beams and beam B.3 and B.4 were tested without strain gauges.

The type of strain gauge used for the beams are demonstrated in Table 3.23. Strain gauges from HBM were used for all beams, and the different gauge factors were accounted for in data acquisition software, Catman DAQ, used for post processing of the strain data.

Table 3.23 Type of strain gauges used

| | **Supplier: HBM** | | | | |
|---|---|---|---|---|---|
| **Beam** | **Location (illustrated in Figure 3.37)** | **Type of S.G.** | **Resistance Ω** | **Gauge factor** | **Transverse sensitivity** |
| A.2 | Sg1 | 6/120 LY41 | 120 Ω ± 0.35% | 2.06 ± 1.0% | 0.3% |
| | Sg2 | 6/120 LY41 | 120 Ω ± 0.35% | 2.06 ± 1.0% | 0.3% |
| | Sg3 | 6/120 LY41 | 120 Ω ± 0.35% | 2.06 ± 1.0% | 0.3% |
| | Sg4 | 6/120 LY41 | 120 Ω ± 0.35% | 2.06 ± 1.0% | 0.3% |
| | | | | | |
| A.3 | Same as A.2 | | | | |
| A.4 | | | | | |
| A.5 | | | | | |
| | | | | | |
| **Beam** | **Location (illustrated in Figure 3.38)** | **Type of S.G.** | **Resistance Ω** | **Gauge factor** | **Transverse sensitivity** |
| B.5 | Sg1 | 6/120 LY41 | 120 Ω ± 0.35% | 2.06 ± 1.0% | 0.3% |
| | Sg2 | 3/120ZE LY41 | 120 Ω ± 0.35% | 2.05 ± 1.0% | 0.4% |
| | Sg3 | 6/120 LY41 | 120 Ω ± 0.35% | 2.06 ± 1.0% | 0.3% |
| | Sg4 | 6/120A LY11 | 120 Ω ± 0.35% | 2.11 ± 1.0% | -0.1% |
| | Sg5 | 6/120 LY41 | 120 Ω ± 0.35% | 2.06 ± 1.0% | 0.3% |
| | Sg6 | 3/120ZE LY41 | 120 Ω ± 0.35% | 2.05 ± 1.0% | 0.4% |
| | Sg7 | 6/120 LY41 | 120 Ω ± 0.35% | 2.06 ± 1.0% | 0.3% |
| | Sg8 | 6/120 LY41 | 120 Ω ± 0.35% | 2.06 ± 1.0% | 0.3% |
| | | | | | |
| B.6 | Sg1 | 6/120A LY11 | 120 Ω ± 0.35% | 2.11 ± 1.0% | -0.1% |
| | Sg2 | 6/120A LY11 | 120 Ω ± 0.35% | 2.11 ± 1.0% | -0.1% |
| | Sg3 | 6/120A LY11 | 120 Ω ± 0.35% | 2.11 ± 1.0% | -0.1% |
| | Sg4 | 6/120A LY11 | 120 Ω ± 0.35% | 2.11 ± 1.0% | -0.1% |
| | Sg5 | 6/120A LY11 | 120 Ω ± 0.35% | 2.11 ± 1.0% | -0.1% |
| | Sg6 | 6/120A LY11 | 120 Ω ± 0.35% | 2.11 ± 1.0% | -0.1% |
| | Sg7 | 6/120A LY11 | 120 Ω ± 0.35% | 2.11 ± 1.0% | -0.1% |
| | Sg8 | 6/120A LY11 | 120 Ω ± 0.35% | 2.11 ± 1.0% | -0.1% |

## 3.13 Theoretical approach for strengthened moment capacity

### 3.13.1 Corresponding compression strength at time of test

The concrete compression strength at time of final test were evaluated with compression test of three cubes from each batch. Result from compression test are found in Table 3.24.

Table 3.24 Compression test, Test 3

| **Batch** | $\boldsymbol{f_{ci}\ [N/mm^2]}$ |
|---|---|
| A | 79.22 |
| A | 79.09 |
| A | 78.34 |
| B | 71.76 |
| B | 73.04 |
| B | 71.35 |

Corresponding mean value are found from formulas below.

$$f_{cmA} = 0.8\left(\frac{79.22 + 79.09 + 78.34}{3}\right) = 63.1\ MPa$$

$$f_{cmB} = 0.8\left(\frac{71.76 + 73.04 + 71.35}{3}\right) = 57.6\ MPa$$

$$f_{cm} = \frac{f_{cmA} + f_{cmB}}{2} = 60.4\ MPa$$

The result from all the compression tests and strength increase at final test compared to the 28 days strength are found in Table 3.25, with days from casting indicted in brackets.

Table 3.25 Mean compression strength from compression test

| | **28 days** | **Test 1 (49 days)** | **Test 3 (72 days)** | **Strength increase** |
|---|---|---|---|---|
| $f_{cmA}$ | 51.9 MPa | 58.5 MPa | 63.1 MPa | 21.6% |
| $f_{cmB}$ | 47.5 MPa | 54.1 MPa | 57.6 MPa | 21.3% |
| $f_{cm}$ | 49.7 MPa | 56.46 MPa | 60.4 MPa | 21.5% |

### 3.13.2 Theoretical moment capacity of the strengthened beams

Theoretical capacity for the test specimen were derived in accordance with the design process given in TR55 outlined in Chapter 2.2.4. Few modifications of the process are implemented due to the predetermined area of CFRP and unknown applied load.

To get a theoretical result comparable with the experimental result, design strength of the material is replaced with characteristic strength and actual strength determined from test. All the partial factors for the materials are therefore set to 1.0 in the below calculation.

#### 3.13.2.1 Material properties

The compression strength of concrete used are the actual concrete strength at time of testing, found from compression test. Due to the inconclusive results from the E-modulus test, E-modulus was derived from the analytical relation defined in Chapter 3.5.2, $E_{cm} = 22\left[\frac{f_{cm}}{10}\right]^{0.3}$ [15, Table 3.1].

Since the experiment are performed on newly cast concrete without significant load history prior to failure, creep will not be considered. Tensile strength of concrete is determined by the splitting tensile test determined for the 28-days properties. The properties used for theoretical capacity are defined in Table 3.26.

Table 3.26 Material properties

| **Material properties** | **Dimension** | **Partial factors** |
|---|---|---|
| | | |
| **Concrete** | | |
| $f_{cm} = 60.4\ MPa$ | $b = 250\ mm$ | $\gamma_c$=1.0 |
| $E_{cm} = 37.7\ GPa$ | $h = 300\ mm$ | |
| $f_{ctm} = 2.98\ MPa$ | $c_{nom} = 35\ mm$ | |
| $\varepsilon_{cu} = 0.0035$ | $d = 251\ mm$ | |
| $\gamma = \rho_c \cdot g = 25\ kN/m^3$ | | |
| | | |
| **Steel** | | |
| $f_{yk} = 500\ MPa$ | $\emptyset_L = 12\ mm$ | $\gamma_s = 1.0$ |
| $f_{ywd} = 500\ MPa$ | $\emptyset_s = 8\ mm$ | |
| $E_s = 200\ GPa$ | $A_s = 339\ mm^2$ | |
| | | |
| **CFRP** | | |
| $\varepsilon_{fk} = 0.00176$* | $t_f = 1.2\ mm$ | $\gamma_{FRP,m} = 1.0$ |
| $E_{fk} = 165\ GPa$ | $w_f = 50\ mm$ | $\gamma_{FRP,E} = 1.0$ |
| $\varepsilon_{f,\lim} = 0.008$ | $A_f = 120\ mm^2$ | $\gamma_{FRP,\varepsilon} = 1.0$ |
| | | |
| **Modular ratio** | | |
| $\alpha_s = E_s/E_{cm}$ | | |
| $\alpha_f = E_f/E_{cm}$ | | |
| *Characteristic value retrieved from Sika CarboDur software | | |

### 3.13.2.2 Stepwise procedure

Derivation of theoretical moment capacity and associated failure mode are performed following the stepwise procedure below. Detailed derivation is found in Appendix D.

**i) Initial strain**

The initial state of strain does normally need to be considered for strengthening of existing structures. For the experiment however, the specimen will not be subjected to any load during strengthening and the initial state of strain in the concrete are therefore set to zero.

$\varepsilon_{c0} = 0$

$\varepsilon_0 = 0$

**ii) Governing design strain for CFRP**

Evaluating the strain definitions for the CFRP, the debonding strain limit $\varepsilon_{f,lim}$ are smaller than the design strain $\varepsilon_{fd}$, regardless if partial factors are implemented or not. Illustrated in Table 3.27. Debonding of the system will therefore occur before the CFRP reaches rupture strain and $\varepsilon_{f,lim}$ will be the governing strain limit for the CFRP.

$\varepsilon_{fe} = \min(\varepsilon_{fd}, \varepsilon_{f,lim}) = 0.008$

$\varepsilon_{f,lim} = 0.008$

$$\varepsilon_{fd} = \frac{\varepsilon_{fk}}{\gamma_{FRP,m}\gamma_{FRP,\varepsilon}}$$

Table 3.27 Evaluation of governing strain

| Omitting partial factors | Including partial factors |
|---|---|
| $\gamma_{FRP,m} = 1.0$ | $\gamma_{FRP,m} = 1.05$ |
| $\gamma_{FRP,\varepsilon} = 1.0$ | $\gamma_{FRP,m} = 1.25$ |
| $\varepsilon_{fd} = 0.0176$ | $\varepsilon_{fd} = 0.0134$ |

**Step 1. Assume concrete strain**

Since maximum flexural strength are limited by controlling failure mode, the controlling failure mode for the specimen needs to be determined. The reinforcement ratio for the steel reinforcement were chosen to get ductile failure governed by yielding of the steel reinforcement for the unstrengthen beam. Associate failure mode for the strengthen beam can be determined by evaluating strain condition of the section.

As described in Chapter 2.2.4, by initially assuming concrete reaches maximum compressive strain, the strain in tension can be determined through linear strain relation.

Assume $\varepsilon_{cu} = 0.0035$

**Step 2. Assume initial neutral axis depth $x_i$**

By assuming an initial position of the neutral axis depth $x_i$ the corresponding strain in the CFRP can be determined and the forces in the section derived. By applying an iterative process, the neutral axis is adjusted until force equilibrium are achieved.

Initial neutral axis depth is chosen after recommended value defined in ACI [2, p.57].

$x_i = 0.2d$

**Step 3. Strain in FRP**

Corresponding strain in CRFP are derived by linear strain distribution.

$$\varepsilon_f = \varepsilon_{cu}\left(\frac{h - x_i}{x_i}\right) - \varepsilon_0$$

**Step 4. Calculate internal forces**

The internal forces in the section are derived with the initial values determined in step 2 and 3.

$F_f = \varepsilon_f E_f A_f$

$F_s = f_{yk} A_s$

$F_t = F_f + F_s$

$F_c = 0.8 x_i b f_{cm}$

**Step 5. Evaluate force equilibrium and iterative adjust neutral axis**

Force equilibrium are checked and neutral axis iterative adjusted until force equilibrium is achieved. Step 3 to 5 is repeated until the parameters are converged.

$$x_{i+1} = \frac{f_{yk} A_s + \varepsilon_f E_f A_f}{0.8 b f_{cm}}$$

**Step 6. Parameters at force equilibrium**

The results of the final iteration are demonstrated below

$x = 45.85\ mm$

$\varepsilon_f = 0.0194$

$F_f = 384.132\ kN$

$F_s = 169.5\ kN$

$F_t = 553.632\ kN$

$F_c = 553.627\ kN$

$F_t \approx F_c$

However, strain in the CFRP are limited by the debonding strain limit $\varepsilon_{f,lim}$. Developed strain in the CFRP does therefore need to fulfill criteria below.

$$\varepsilon_f = \varepsilon_{cu}\left(\frac{h - x_i}{x_i}\right) - \varepsilon_0 \leq \varepsilon_{f,lim}$$

For the initial assumption that concrete reaches maximum compressive strain, corresponding strain in CFRP exceeds this limit, $\varepsilon_f = 0.0194 > \varepsilon_{f,\text{lim}} = 0.008$.

Failure mode will therefore be governed by the debonding strain limit of the CFRP, and the process of determining neutral axis and internal forces should be repeated with parameters derived by $\varepsilon_{f,lim}$. Corresponding compressive strain in the concrete are found by the strain in CFRP and the neutral axis depth.

TR55 specifies that rectangular stress block should not be used for cases where the concrete compression strain does not reach ultimate strain [3, p.74]. However, a clear methodology for derivation of concrete forces are not provided. To derive the internal force contribution from concrete when concrete strain does not reach ultimate strain, the approach given in FiB bulletin 14 was used [7, p.36].

The approach implements a reduced stress block area coefficient $\psi$ to replace the 0.8 factor used for rectangular stress block. The stress block centroid $\delta_G$ are also reduced and replaces the 0.4 factor used for rectangular stress block. The coefficients are derived from the compressive strain in the concrete $\varepsilon_c$ following the expression below [7, p.36].

$$\psi = \begin{cases} 1000\varepsilon_c\left(0.5 - \frac{1000}{12}\varepsilon_c\right) & for\ \varepsilon_c \leq 0.002 \\ 1 - \frac{2}{3000\varepsilon_c} & for\ 0.002 \leq \varepsilon_c \leq 0.0035 \end{cases}$$

$$\delta_G = \begin{cases} \frac{8 - 1000\varepsilon_c}{4(6 - 1000\varepsilon_c)} & for\ \varepsilon_c \leq 0.002 \\ \frac{1000\varepsilon_c(3000\varepsilon_c - 4) + 2}{2000\varepsilon_c(3000\varepsilon_c - 2)} & for\ 0.002 \leq \varepsilon_c \leq 0.0035 \end{cases}$$

Same process is repeated to determine force equilibrium through iterative adjusting the neutral axis depts $x_i$, with a few modifications of the parameters. Strain in CFRP plates are limited by $\varepsilon_{f,lim}$ and concrete strain are calculated in step 3.

**Step 2. Assume initial neutral axis depth $x_i$**

$$x_i = 0.2d$$

**Step 3. Strain in concrete**

Corresponding strain in concrete are derived by strain compatibility

$$\varepsilon_c = (\varepsilon_f + \varepsilon_0)\left(\frac{x_i}{h - x_i}\right)$$

**Step 4. Calculate internal forces**

First the coefficients $\psi$ and $\delta_G$ are determined.

For the initial assumed neutral axis depth $x_i$, the corresponding concrete strain are $\varepsilon_c = 0.0016$. Since $\varepsilon_c < 0.002$, below expressions for $\psi$ and $\delta_G$ are used.

$$\psi = 1000\varepsilon_c\left(0.5 - \frac{1000}{12}\varepsilon_c\right)$$

$$\delta_G = \frac{8 - 1000\varepsilon_c}{4(6 - 1000\varepsilon_c)}$$

The internal forces in the section are calculated with expression below.

$$F_f = \varepsilon_{f,lim} E_f A_f$$

$$F_s = f_{yk} A_s$$

$$F_t = F_f + F_s$$

$$F_c = \psi x_i b f_{cm}$$

**Step 5. Evaluate force equilibrium and iterative adjust neutral axis**

Force equilibrium are checked and neutral axis iterative adjusted until force equilibrium is achieved. Step 3 to 5 is repeated until the parameters are converged.

$$x_{i+1} = \frac{f_{yk}A_s + \varepsilon_{f,lim}E_f A_f}{\psi b f_{cm}}$$

**Step 6. Parameters at force equilibrium**

The results of the first 5 iteration are demonstrated in Table 3.28 below, illustrating how the parameters moving towards convergence. Converged result is demonstrated in last row when force equilibrium is attained.

Table 3.28 Iteration procedure

| Iteration | $\boldsymbol{\varepsilon_c}$ | $\boldsymbol{\psi}$ | $\boldsymbol{\delta_G}$ | $\boldsymbol{F_t}$ $[\boldsymbol{kN}]$ | $\boldsymbol{F_c}$ $[\boldsymbol{kN}]$ | $\boldsymbol{x_i}$ $[\boldsymbol{mm}]$ |
|---|---|---|---|---|---|---|
| 0 (start) | | | | | | 50.2 |
| 1 | 0.0016076 | 0.5884 | 0.3638 | 327.9 | 445.863 | 36.918 |
| 2 | 0.0011226 | 0.4563 | 0.3525 | 327.9 | 254.257 | 47.611 |
| 3 | 0.0015091 | 0.5648 | 0.3613 | 327.9 | 405.858 | 38.466 |
| 4 | 0.0011766 | 0.4729 | 0.3537 | 327.9 | 274.581 | 45.935 |
| 5 | 0.0014464 | 0.5488 | 0.3598 | 327.9 | 380.537 | 39.581 |
| | | | | | | |
| Converged | 0.0013143 | 0.5132 | 0.3567 | 327.9 | 327.899 | 42.332 |

The result after final iteration are demonstrated below, converged parameters are used to determine the bending resistance of the section by moment of forces in the section.

$x = 42.33\ mm$ $\quad F_f = 158\ kN$

$\varepsilon_f$ =0.008 $\quad F_s = 169.5\ kN$

$\varepsilon_c = 0.00131$ $\quad F_t = 327.9\ kN$

$\psi = 0.5132$ $\quad F_c = 327.9\ kN$

$\delta_G = 0.3267$ $\quad F_t = F_c$

By evaluating the steel strain for the section, the expected failure mode of the test specimen can be concluded.

$$\varepsilon_s = (\varepsilon_f - \varepsilon_0)\frac{(d-x)}{(h-x)} = 0.0064$$

$$\varepsilon_y = \frac{f_{yk}}{E_s} = \frac{500\ MPa}{200\ GPa} = 0.0025$$

Since steel strain exceeds the yield strain of steel $\varepsilon_s > \varepsilon_y$, expected failure mode for the test specimen, based on above derivation are: yielding of steel reinforcement followed by delamination of CFRP plates and loss of composite action. Moment capacity of the specimen and associated failure load are derived below.

$$M_{Rd,CFRP} = f_{yk}A_s(d - \delta_G x) + \varepsilon_f E_f A_f (h - \delta_G x) = 85.1\ kNm$$

$$P_{fail} = \left(M_{Rd,CFRP} - \frac{qL^2}{8}\right) \cdot \frac{2}{0.75} = 224\ kN$$

# 4 Experimental results

The results from the flexural test of the pre-cracked, CFRP reinforced beams are presented in following chapter. Data of monitored failure behavior including failure load, measured strain in the CFRP and failure mode of the specimen are documented. The bond and fracture surface of the beams are also observed post failure.

## 4.1 Failure mode and failure behavior

First the general behavior of the strengthened beams is presented followed by a more detailed assessment of each beam. The governing failure mode of all the beams was delamination of the CFRP plates. Failure behavior was characterized by flexural crack propagation followed by sudden delamination of the CFRP plates. Graphical representation of the load vs. deflection curve for all the strengthened beams are found in Figure 4.1 where the evident drop in the curve represents the loss of composite action and delamination of the CFRP plates. The extension of the curve after the drop represents the extensive deflection in the beam as a result of the delamination, until manual termination of program.

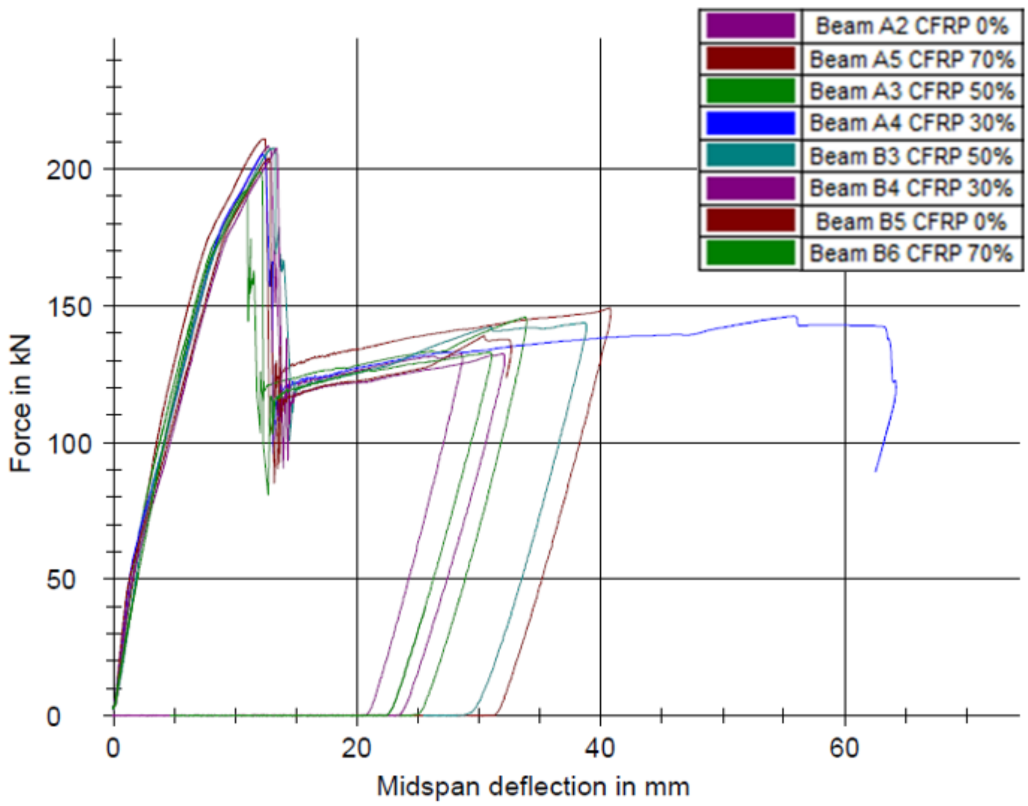


Figure 4.1 Load vs deflection strengthened beams

To demonstrate the different behavior and difference in load response for beams strengthened with CFRP and regular reinforced concrete beams, the load vs. deflection graph of two unstrengthen beams, specimen A.1 and B.2, and two strengthened beams, A.2 and B.5, are illustrated in Figure 4.2. By evaluating of the graph, the beams strengthened with CFRP displays an increased stiffness and a significant increase in load capacity. After the drop representing the delamination of the CFRP, the beams display similar response as the unstrengthen reinforced concrete beams.

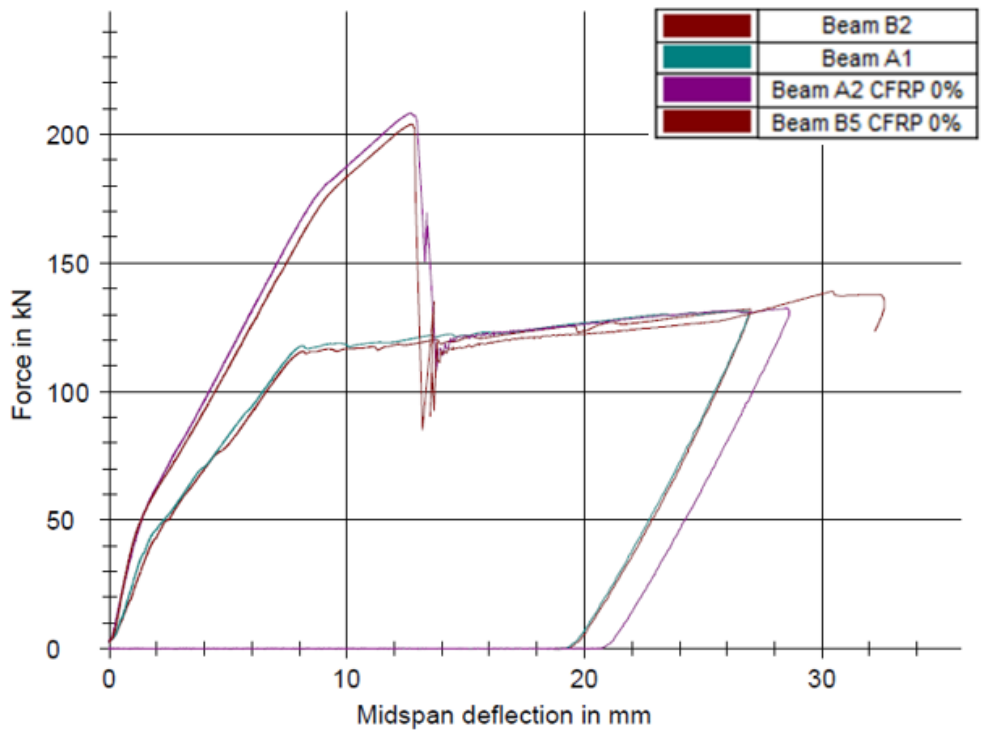


Figure 4.2 Comparison of unstrengthen and strengthened beams

To evaluate the behavior with respect to degree of preloading the observed failure behavior of each beam is summarized in Table 4.1 below.

Table 4.1 Failure behavior

| Beam | Observed failure behavior |
|---|---|
| A.2<br>0% preload | **Behavior**<br>Slight delay of crack initiation compared to unstrengthen beams. Load vs displacement curve of beam A.2 and the unstrengthen beams are illustrated in Figure 4.3 demonstrating the difference in gradient change of the strengthened and unstrengthen beams.<br>**Failure mode**<br>Crack propagation mainly in flexural zone followed by sudden delamination.<br>**Bond condition after failure**<br>Both CFRP plates delaminated from one end. |
| B.5<br>0% preload | **Behavior**<br>Similar to beam A.2 a slight delay of crack initiation was observed.<br>**Failure mode**<br>Crack propagation mainly in flexural zone followed by sudden delamination.<br>**Bond condition after failure**<br>Both CFRP plates delaminated from one end. |
| A.4<br>30% preload | **Behavior**<br>Initiation of new cracks prior to propagation of existing cracks. Slight delay of crack initiation compared to unstrengthen beams.<br>**Failure mode**<br>Crack propagation mainly in flexural zone followed by sudden delamination.<br>**Bond condition after failure**<br>Both CFRP plates delaminated from one end. Plates delaminated from end where repair of honeycomb had been performed. |
| B.4<br>30% preload | **Behavior**<br>Similar to beam A.4.<br>**Failure mode**<br>Crack propagation mainly in flexural zone followed by sudden delamination.<br>**Bond condition after failure**<br>Both CFRP plates completely delaminated. |
| A.3<br>50% preload | **Behavior**<br>Crack propagation of existing cracks followed by new crack formations.<br>**Failure mode**<br>Crack propagation mainly in flexural zone followed by sudden delamination.<br>**Bond condition after failure**<br>Both CFRP plates delaminated from one end. Plates delaminated from end where repair of honeycomb had been performed. |

| | |
|---|---|
| B.3<br>50% preload | **Behavior**<br>Similar to beam A.3.<br>**Failure mode**<br>Crack propagation mainly in flexural zone followed by sudden delamination.<br>**Bond condition after failure**<br>One CFRP plate completely delaminated. One CFRP plate delaminated from one side. |
| A.5<br>70% preload | **Behavior**<br>Crack propagation in existing cracks. Almost no new cracks detected.<br>**Failure mode**<br>Crack propagation mainly in flexural zone followed by sudden delamination.<br>**Bond condition after failure**<br>Both CFRP plates delaminated from one end. |
| B.6<br>70% preload | **Behavior**<br>Similar to A.5.<br>**Failure mode**<br>Crack propagation in mainly flexural zone followed by sudden delamination.<br>**Bond condition after failure**<br>Both CFRP plates delaminated from one end. |

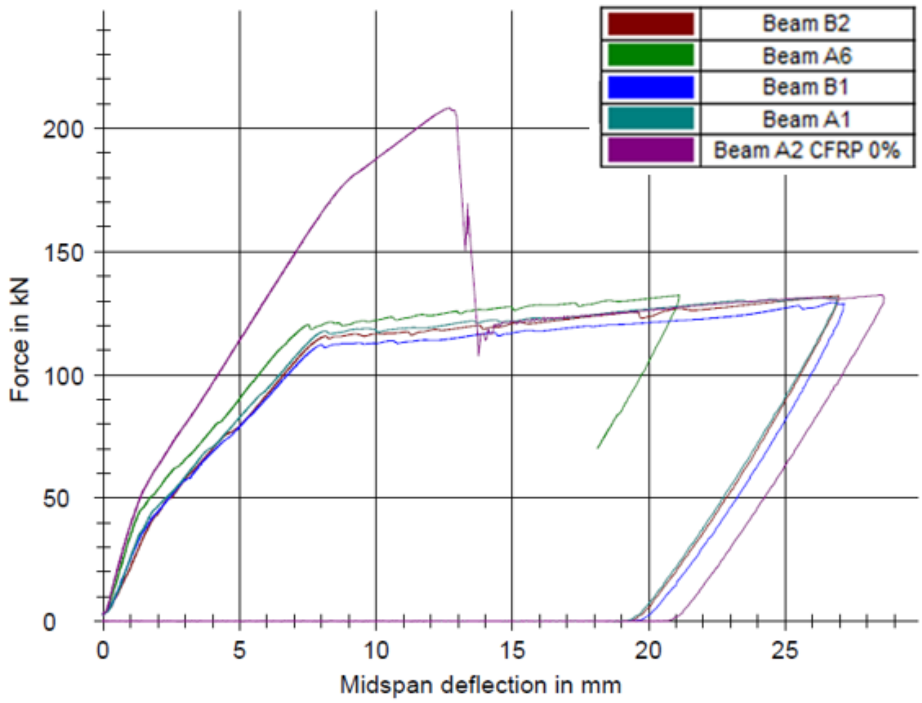


Figure 4.3 Load vs deflection curve of beam A.2 compared to unstrengthen beams

Figure 4.4 – 4.6 below illustrates the different debonding failures occurring during testing, with debonding from one end and complete debonding of entire plate. Figure 4.4 shows beam B.5 where the CFRP plated were deboned from one side. Figure 4.5 shows beam B.4 where one of the plates were completely debonded. Figure 4.6 shows beam B.6 where both plates were debonded simultaneously.

Figure 4.4 B.5 Debonded CFRP plates

Figure 4.5 B.4 Debonded CFRP plates

Figure 4.6 B.6 Debonded CRFP plates

The fracture surface of the beams and deboned CFRP plates is illustrated in Figure 4.7 – 4.9. Along a majority of the CFRP plate length, the fracture surface is distinguished by failure in the concrete with a thin layer of concrete remaining on the CFRP plates.


Figure 4.7 A.5


Figure 4.9 B.5


Figure 4.8 B.6

At the end of the debonded plate the fractures surface displays different behavior with fracture in the adhesive, similar fracture surface was found for all beams. Illustrated in Figure 4.10 – 4.11, the CFRP plates are stripped clean and the adhesive is still attached on the concrete substrate.


Figure 4.10 B.5


Figure 4.11 B.5

## 4.2 Graphical representation of failure behavior

Graphical representation of the load vs. deflection curve for the beams, and the corresponding strain development for beams with strain gauges are found in figure 4.13 – 4.26.

Note! The load vs. deflection curves should only be evaluated up to highest peak. The extension of the graph beyond this point are a representation of the continued loading until manual termination of the test program with excessive deformation as a result of the delamination.

The result from the flexural test displayed similar behavior as illustrated in Figure 4.12, previously described in Chapter 3.1.

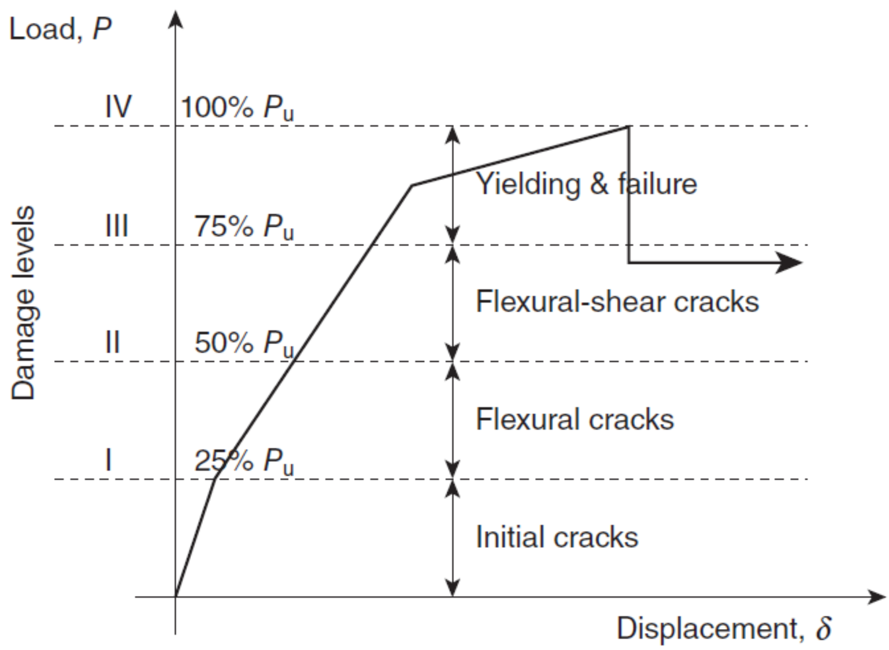


Figure 4.12 Idealized failure behavior [18]

For most of the test specimen, two gradient changes were found in the graphs. First gradient change can be related to the changes in sectional properties when the concrete in tension are cracking. The second gradient change can be assumed to be related to the yielding of the tension steel with similar load response found in the strain readings.

The different gradient changes are illustrated with number 1: crack initiation of concrete and 2: yielding of steel reinforcement, correspondingly in the graphs below.

**No preload**

Beam A.2

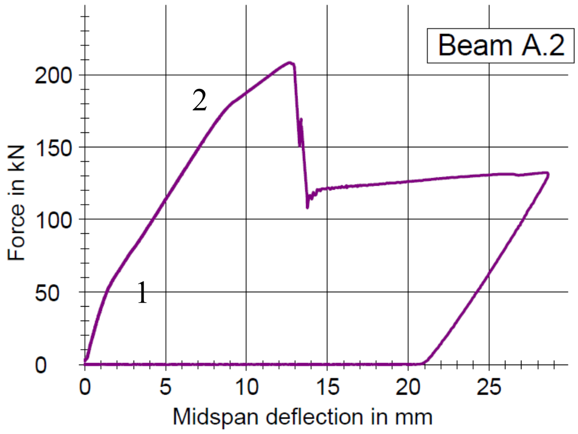


Figure 4.13 A.2 Load vs. deflection

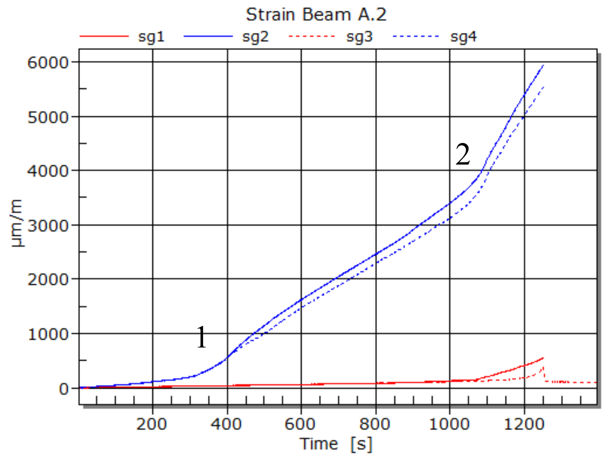


Figure 4.14 A.2 Strain development

Beam B.5

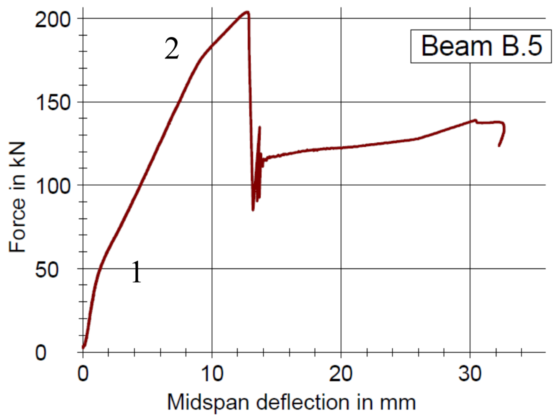


Figure 4.15 B.5 Load vs. deflection

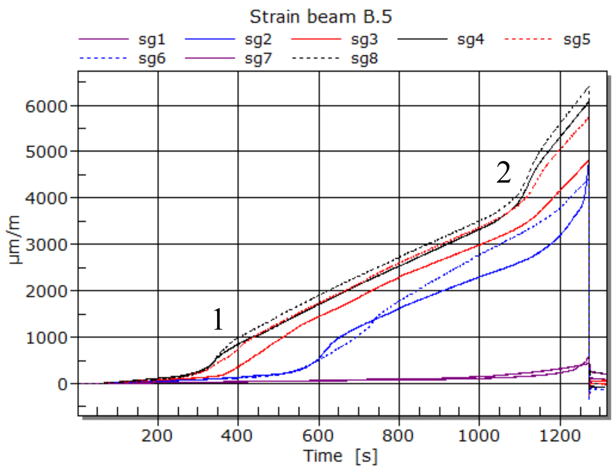


Figure 4.16 B.5 Strain development

For the unloaded beams, A.2 and B.5, the load response behavior can be related to the corresponding strain development in the CFRP plates. Both the Load vs. displacement graph and the strain development displays two notable gradient changes in the curve, which represents the change in sectional properties, cracking of concrete and yielding of steel respectively.

**30% preload**

Beam A.4

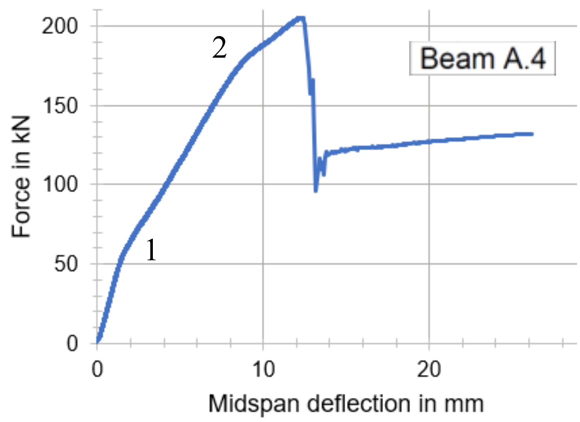


Figure 4.17 A.4 Load vs. deflection

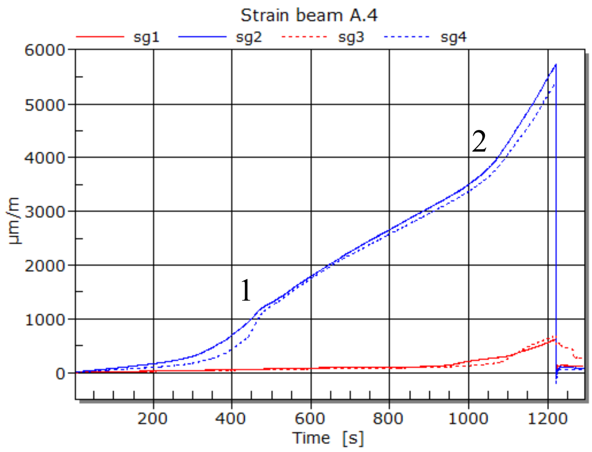


Figure 4.18 A.4 Strain development

Beam B.4

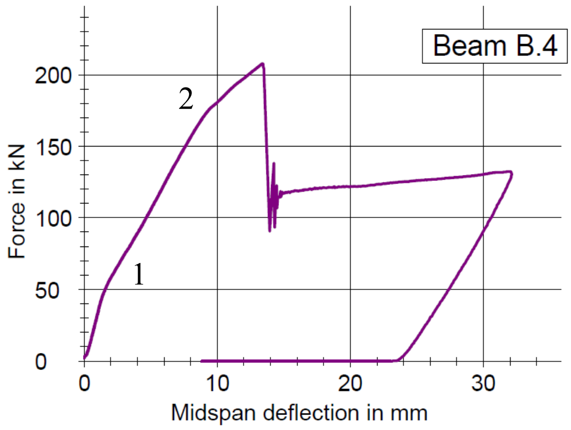


Figure 4.19 B.4 Load vs. deflection

The beams subjected to 30% preload shows a similar load response and strain development as presented for the unloaded beams. Since only few cracks were detected after pre-loading prior to strengthening no large difference in behavior can be expected.

**50% preload**

Beam A.3

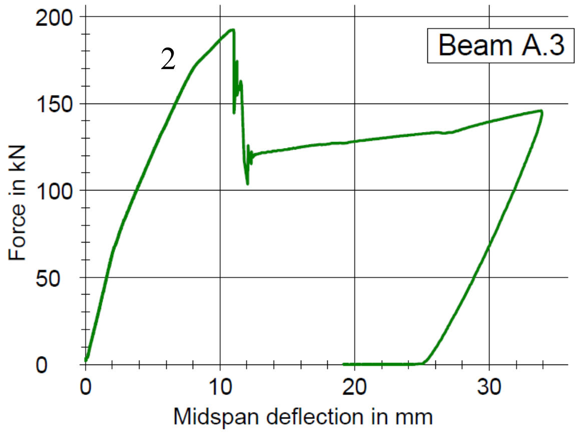


Figure 4.20 A.3 Load vs. deflection

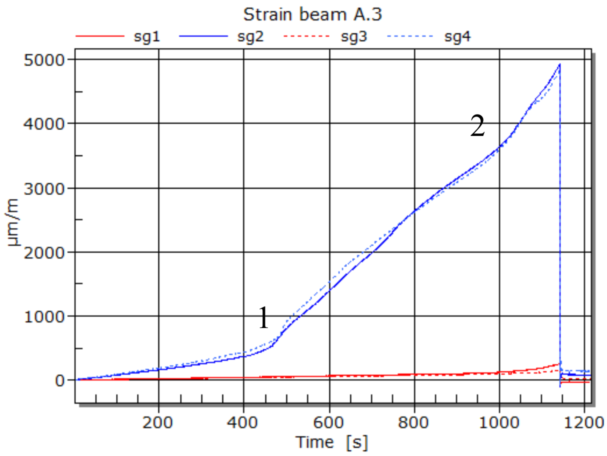


Figure 4.21 A.3 Strain development

Beam B.3

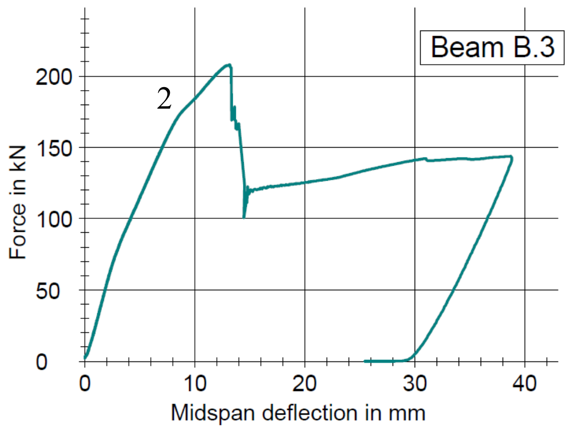


Figure 4.22 B.3 Load vs. deflection

The beams subjected to 50% preload had a relatively large extent of crack formation, especially within constant bending zone, prior to strengthening. By graphical evaluation the load vs. displacement curve for beam A.3 and B.3, a clear gradient change representing the cracking of concrete are not displayed. A slight change in curvature are found at a higher load compared to the uncracked beam. This corresponds to the observed behavior with crack propagation in existing cracks prior to formation of new cracks. However, the strain development graph still displays a distinguished gradient change which might relate to crack expansion or new crack formation in proximity to the location of the strain gauges.

**70% preload**

Beam A.5

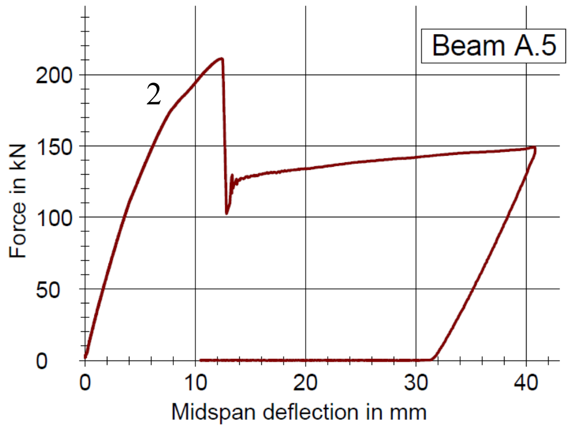


Figure 4.23 A.5 Load vs. deflection

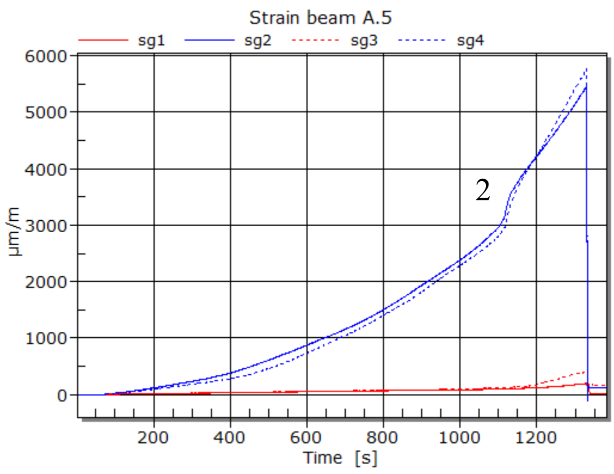


Figure 4.24 A.5 Strain development

Beam B.6

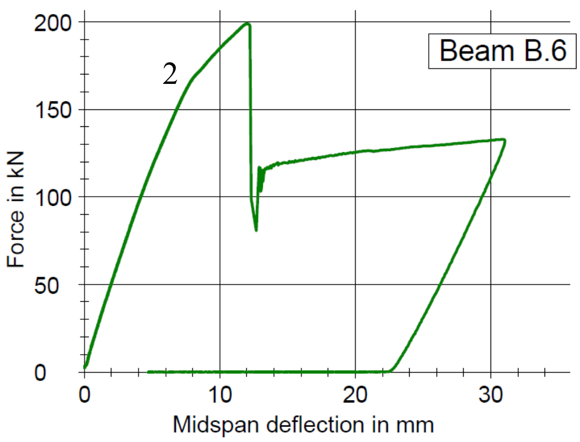


Figure 4.25 B.6 Load vs. deflection

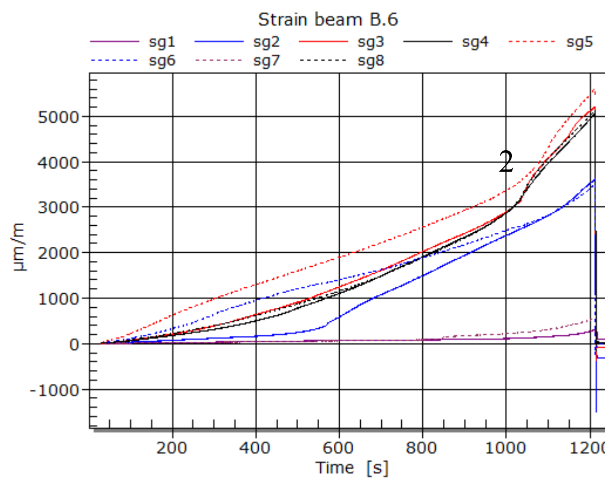


Figure 4.26 B.6 Strain development

For the beams subjected to 70% preload prior to strengthening the gradient change in the curves representing crack formation can no longer be detected. Both the load vs. defection curves and the corresponding strain development displays a relative linear curve up to the second gradient change, which indicated that the majority of cracks have already been formed in the sections.

## 4.3 Summary of results

The summarized test result is presented in Table 4.2, where failure load and the measured maximum strain for each beam are presented.

Table 4.2 Result from experiment

| **Test** | **Preload** | **Beam** | **Failure load [kN]** | **Max strain [μm/m]** | **Location of max strain** |
|---|---|---|---|---|---|
| 3.0 | 0% | A.2 | 208.37 | 5948 | Midspan |
| | | B.5 | 203.88 | 6408 | Midspan |
| 3.3 | 30% | A.4 | 205.43 | 5731 | Midspan |
| | | B.4 | 207.63 | - | - |
| 3.5 | 50% | A.3 | 192.39 | 4925 | Midspan |
| | | B.3 | 207.85 | - | - |
| 3.7 | 70% | A.5 | 211.10 | 5763 | Midspan |
| | | B.6 | 199.02 | 5610 | Under point load |

Comparison of the theoretical calculations and the experimental findings are demonstrated in Table 4.3 – 4.4 below, derived in Appendix E.

First the capacity for the unstrengthen beams are evaluated. The mean failure load found for the reference beams, presented in Chapter 3.9.1, are evaluated against the theoretical capacity derived in Chapter 3.9.3. Theoretical and experimental failure load are denoted $P_t$ and $P_e$ respectively.

Table 4.3 Theoretical and experimental result unstrengthen beam

| | **Experimental result** | | **Theoretical values** | | **Ratio** |
|---|---|---|---|---|---|
| | $P_e$ $[kN]$ | $M_{Rd,ex}$ $[kNm]$ | $P_t$ $[kN]$ | $M_{Rd,us}$ $[kNm]$ | $P_e/P_t$ |
| Test 1 Unstrengthen section | 116 | 44.44 | 108.3 | 41.56 | 1.07 |

Evaluating the result from the 4-point bending test of the strengthened beams with the theoretical capacity derived in Chapter 3.13, following relations are found.

Table 4.4 Theoretical and experimental result strengthen beam

| | | Experimental result | | Theoretical values | | Ratio | |
|---|---|---|---|---|---|---|---|
| Preload | Beam | $P_e$ $[kN]$ | $\varepsilon_e$ $[\mu m/m]$ | $P_t$ $[kN]$ | $\varepsilon_t = \varepsilon_{f,lim}$ $[\mu m/m]$ | $P_e/P_t$ | $\varepsilon_e/\varepsilon_t$ |
| 0% | A.2 | 208.37 | 5948 | 224 | 8000 | 0.93 | 0.74 |
| | B.5 | 203.88 | 6408 | " | " | 0.91 | 0.80 |
| 30% | A.4 | 205.43 | 5731 | " | " | 0.91 | 0.72 |
| | B.4 | 207.63 | - | " | " | 0.92 | - |
| 50% | A.3 | 192.39 | 4925 | " | " | 0.86 | 0.62 |
| | B.3 | 207.85 | - | " | " | 0.93 | - |
| 70% | A.5 | 211.10 | 5763 | " | " | 0.94 | 0.72 |
| | B.6 | 199.02 | 5610 | " | " | 0.89 | 0.70 |

The strength increase and increased flexural capacity are found for each specimen by evaluating the respective failure load and corresponding moment at failure for the strengthen beams against the mean failure load of the unstrengthen member with the corresponding moment at failure. The results are demonstrated in Table 4.5.

Table 4.5 Increased moment capacity

| | | Unstrengthen capacity | | Strengthen capacity | | Increased flexural capacity |
|---|---|---|---|---|---|---|
| Preload | Beam | $P_e$ $[kN]$ | $M_{Rd,ex}$ $[kNm]$ | $P_e$ $[kN]$ | $M_{Rd,ex}$ $[kNm]$ | $\frac{\Delta M}{M_{Rd,ex}} \cdot 100\%$ |
| 0% | A.2 | 116 | 44.44 | 208.37 | 79.08 | 78% |
| | B.5 | " | " | 203.88 | 77.39 | 74% |
| 30% | A.4 | " | " | 205.43 | 77.97 | 75% |
| | B.4 | " | " | 207.63 | 78.80 | 77% |
| 50% | A.3 | " | " | 192.39 | 73.08 | 64% |
| | B.3 | " | " | 207.85 | 78.88 | 77% |
| 70% | A.5 | " | " | 211.10 | 80.10 | 80% |
| | B.6 | " | " | 199.02 | 75.57 | 70% |

By visual observation the load at first crack first or crack propagation of existing cracks of the beams were documented. At failure, the distance from support to first visual crack was measured to estimate the available development length for the bond force at failure. The results are found in Table 4.6. The corresponding crack development documented during preloading included within brackets to compare the crack propagation.

Table 4.6 Crack formation

| **Test** | **Preload** | **Beam** | **First crack [kN]** | **Distance Left support to first crack [cm]** | **Distance Right support to first crack [cm]** |
|---|---|---|---|---|---|
| 3.0 | 0% | A.2 | 52 | 37 | 36 |
| | | B.5 | 46 | 28 | 28 |
| 3.3 | 30% | A.4 | 45 (34.8) | 33 (89) | 49 (82) |
| | | B.4 | 48 (29) | 30 (88) | 24 (75) |
| 3.5 | 50% | A.3 | 61 (35.5) | 41 (47) | 34 (59) |
| | | B.3 | 47 (32.6) | 27 (41) | 26 (47) |
| 3.7 | 70% | A.5 | 81 (37) | 42 (55) | 41 (45) |
| | | B.6 | 58 (28) | 29 (42) | 35 (35) |

## 4.4 Discussion regarding experimental result

Evaluating the result given above, no correlation between the degree of preload and capacity are found. Crack propagation of the beams were closely monitored with respect to first crack initiation and crack propagation, but regardless of precondition and crack propagation in the beams, all the beams displayed similar behavior after tension steel is yielded.

By comparing the load vs. deflection curves of unloaded and uncracked beam B.5 with beam B.6 subjected to 70% preload with extensive crack formation, the slight difference in load response can be considered negligible. Graphical comparison of B.5 and B.6 are illustrated in Figure 4.27 below.

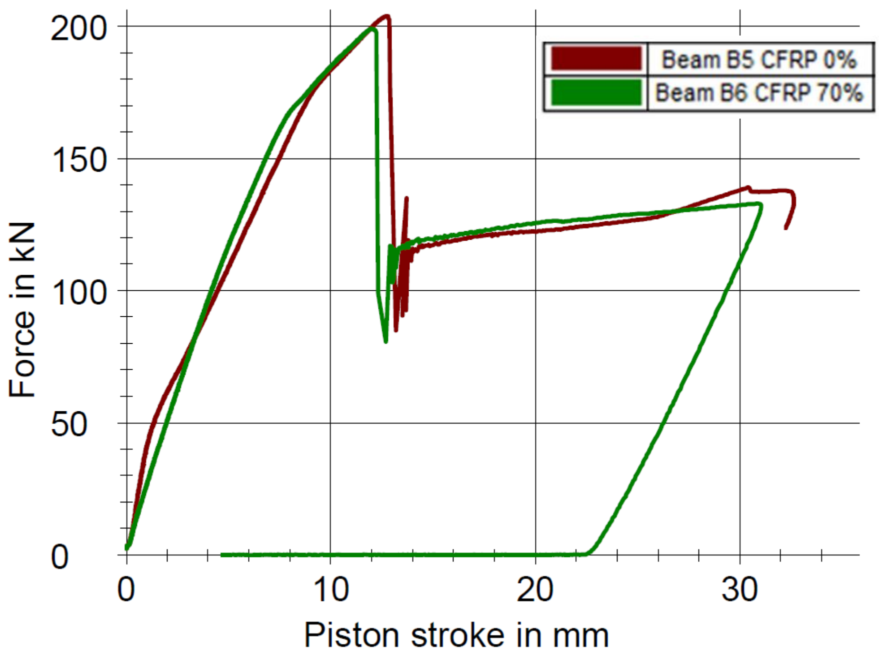


Figure 4.27 Comparison of uncracked and pre-cracked beam

The failure load for all the beams are within a range of approximately 200-210 kN, with no distinct difference in capacity between the different preloaded specimens. One deviating result is found for beam A.3 with a failure load of 192 kN. The lower capacity of this beam can be related to the bond deficiencies found during visual inspection. The poor bond condition is confirmed by observation after failure, where both plates were debonded from side with detected voids in bond. The corresponding maximum strain recorded for beam A.3 are also found notably lower than the other readings. The result from beam A.3 will therefore be disregarded, since poor bond condition of the CFRP plates were confirmed prior to test.

The other beam with potentially compromised bond quality due to the voids detected during visual inspection, beam B.3, does not display any reduced capacity with one of the highest recorded failure loads, bond quality of beam B.3 can therefore be considered satisfactory.

The importance of the concrete quality of the substrate were also emphasized by the test result, as both of the repaired beams A.3 and A.4, delaminated from the repaired side. This might relate to poorly executed repair work, however, with only two specimens, no conclusion can be made, but should nonetheless be remarked.

From Table 4.3 where theoretical and experimental results for the unstrengthen beams are presented, the experimental result displays a slightly higher capacity than the theoretical prediction for the unstrengthen reinforced concrete beam. A ratio of 1.07 are found when evaluating experimental result over theoretical.

Evaluating the results given in Table 4.4, where theoretical and experimental results of the CFRP strengthened beams are presented, the experimental results are found lower than theoretical predicted values. Displayed with the ratio of experimental over theoretical, neither theoretical failure load nor the strain used for the derivation of theoretical capacity are reached.

As the theoretical capacity are determined neglecting all partial factors for the material, the theoretical capacity is based on assumption of ideal material behavior and full composite action without margin for deficiencies in any of the materials in the composite. With the confirmed bond defects from visual inspection the assumption of full composite action is no longer reliable. To determine the cause of the premature debonding, the FRP separation criteria discussed in Chapter 2.2.5 are evaluated in chapter below.

## 4.5 Interpretation of raw data from strain gauges

When analyzing the raw data from the strain gauges some anomalies and unreasonable peak values were found at failure.

Evaluating the strain curves up to failure, the strain curve displays a relatively constant and steady strain increase prior to failure, corresponding to the load increase of the applied load. Unreasonable peak values at moment of failure, as illustrated in Figure 4.28 can be related to turbulence and vibrations at delamination of the plates. Peak values with a duration of milliseconds prior to failure will therefore not be considered reliable. Strain gauges displaying anomalies and sudden peaks are therefore modified and presented with highest value prior to peak, as illustrated in Figure 4.28.

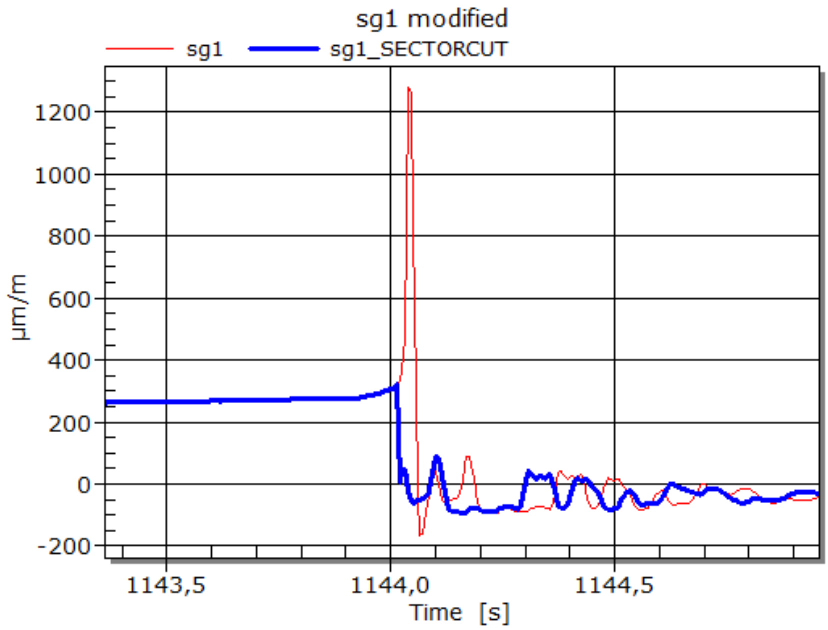


Figure 4.28 Anomalies in raw data from strain gauges

# 5 Evaluation of experimental results

Given that the governing failure mode for all the beams was delamination of the CFRP plates, the criterion for FRP separation from Chapter 2.2.5 are evaluated to assess the initiation mechanism resulting in delamination.

## 5.1 Verification of FRP separation criteria

Since the failure load of the different beams did not display any consistent difference between unloaded beams and beams subjected to preloading, the average failure load from all beams are used as the applied load in below derivation.

Due to the confirmed poor bond of beam A.3, both from visual bond inspection and the results of the failure test, this result was neglected. The resulting average failure load and average maximum strain for the beams are found in Table 5.1.

Table 5.1 Average failure load and strain

| **Beam** | **Failure load** [kN] | **Maximum strain** [µm/m] |
|---|---|---|
| A.2 | 208.37 | 5948 |
| B.5 | 203.88 | 6408 |
| A.4 | 205.43 | 5731 |
| B.4 | 207.63 | - |
| B.3 | 207.85 | - |
| A.5 | 211.10 | 5763 |
| B.6 | 199.02 | 5610 |
| Average | $P = \sum \frac{P_i}{n} = 206\ kN$ | $\varepsilon_{avg} = \sum \frac{\varepsilon_i}{n} = 5892\ \mu m/m$ |

## 5.2 Debonding criteria

The evaluation of FRP separation failure are performed based on the theoretical guideline given by TR55, described in Chapter 2.2.5. However, since TR55 does not provide analytical expression for all the parameters used, the derivation of the parameters has been performed based on assumed material behavior, with comparison to approach used by Arya et al [16]. Since approach by Arya et al. (2002) are based on an older version of TR55, some definitions and equations are slightly different, this paper have therefore been used to get an understanding of the behavior rather than definition of the parameters.

Derivation of parameters are performed similarly to the theoretical moment capacity, by omitting partial factors and replacing design properties with actual strength found in test or the characteristic properties. $f_{ck}$ are replaced with $f_{cm}$ from compression test and $f_{ctk}$ are replaced with $f_{ctm}$ derived from tensile splitting test. Complete calculation of below procedure is found in Appendix F.

**A. Surface irregularity induced FRP separation**

Since the beams are unloaded when the strengthening system is applied, curvature and deflection of the beam soffit are neglectable. No additional transverse tensile stresses will be induced due to curvature.

**B. Shear-crack induced FRP separation**

Check

$V_{Ed} \leq V_{Rd,crack}$

Determination of $V_{Rd,crack}$

For beam specimen used in the flexural test, no shear strengthening has been performed. The governing equations for determining $V_{Rd,crack}$ are therefore based on below criterion.

- $V_{Rd,crack}$ should be no greater than $V_{Rd,c} + V_{S,eff}$
- For members with shear reinforcement but no shear strengthening, $V_{Rd,crack}$ should be no greater than $0.67V_{Rd,s}$

The first criterion consider the combined effect of the shear strength of the concrete section without shear reinforcement $V_{Rd,c}$, calculated according to EN 1992-1-1 6.2.2, and the effective shear resistance and $V_{S,eff}$ calculated according to TR55 6.3.3 (B) eq. 6.2

To define coefficient $\alpha_{flex}$ in equation for $V_{S,eff}$, moment of inertia for the strengthen and unstrengthen section, $I_{cs}$ and $I_{cc}$ were derived with cracked section properties transformed to concrete equivalent properties by modular ratio $\alpha_s$ and $\alpha_f$ for the reinforcement. Results are demonstrated below.

$$V_{Rd,c} = \left[C_{Rd,c}k(100\rho_1 f_{ck})^{\frac{1}{3}} + k_1\sigma_{cp}\right]b_w d \qquad V_{Rd,c} = 68.30\ kN$$

$$\geq (v_{min} + k_1\sigma_{cp})b_w d$$

$$V_{S,eff} = \frac{d}{s}A_{sw}E_s\varepsilon_{sv,eff} \qquad V_{S,eff} = 16.86\ kN$$

$$V_{Rd,c} + V_{S,eff} = 85.16\ kN$$

The second criterion consider the shear strength of the concrete section including shear reinforcement $V_{Rd,s}$ calculated according to EN 1992-1-1 6.2.3.

$$V_{Rd,s} = \frac{A_{sw}}{s}zf_{ywd}\,cot(\theta)$$

Evaluating $0.67V_{Rd,s}$ with different angle $\theta$ within range $1 \leq \cot(\theta) \leq 2.5$ the different criterion for $V_{Rd,crack}$ are evaluated, results demonstrated in Table 5.2.

Table 5.2 Governing definition of $V_{Rd,crack}$

| $(\boldsymbol{\theta})$ | $\mathbf{0.67 \cdot V_{Rd,s}}$ | $\boldsymbol{V_{Rd,c} + V_{S,eff}}$ |
|---|---|---|
| 22 ° | $0.67 \cdot V_{Rd,s} = 171.18\ kN$ | $85.16\ kN$ |
| 39 ° | $0.67 \cdot V_{Rd,s} = 85.41\ kN$ | $85.16\ kN$ |
| 40 ° | $0.67 \cdot V_{Rd,s} = 82.42\ kN$ | $85.16\ kN$ |
| 45 ° | $0.67 \cdot V_{Rd,s} = 69.16\ kN$ | $85.16\ kN$ |

Since $V_{Rd,c} + V_{S,eff}$ are the limiting criterion for crack angles up to 40°, this criterion will be assumed as governing definition of $V_{Rd,crack}$.

$$V_{Rd,crack} = V_{Rd,c} + V_{S,eff} = 85.16\ kN$$

Maximum applied shear force $V_{Ed}$ are determined at the support.

$$P = 206\ kN$$
$$q = \gamma * A_c = 1.875\ kN/m$$
$$L = 2\ m$$

$$V_{Ed} = R_A = \frac{P}{2} + \frac{qL}{2} = 104.875\ kN$$

Verification

For applied load $P = 206\ kN$ the corresponding shear force exceeds the capacity of the section to resist formation of significant shear cracks $V_{Ed} > V_{Rd,crack}$. Shear crack induced debonding can therefore be assumed to be one of the debonding mechanism resulting in lower capacity compared to the theoretical in the experiment.

According to the design requirement given in TR55, for situations when $V_{Ed}$ exceeds $V_{Rd,crack}$, additional anchorage of the CFRP plates should be provided to increase the shear resistance on the section [3, p.79].

## C. Longitudinal shear stress in yield zone

Check

$\tau_t \leq \tau_{lim,y}$

Determination of $\tau_t$

The stepwise procedure described in Chapter 2.2.5 were followed to determine $\tau_t$.

$\tau_t = \tau_m + \tau_{sc}$

Where

$\tau_m = t_f \left[\frac{\sigma_{fmax} - \sigma_{fy}}{\Delta x}\right]$

$\tau_{sc} = 7.8\left[1.1 - \frac{M_y}{M_{Ed}}\right] f_{ctk}$

Determination of parameters:

1. Derivation of moment at which the steel reinforcement reaches yield stress, $M_y$, are not defined in TR55. $M_y$ are therefore determined by assuming elastic sectional properties and triangular stress distribution when steel reaches yield strain $\varepsilon_y$. Neutral axis depth at load when steel reaches yield stress is estimated by taking first moment of area for the transformed, concrete equivalent cracked section. Corresponding strain in CFRP can then be derived using yield strain of steel and neutral axis depth.

| | |
|---|---|
| $\frac{bx^2}{3} = \alpha_s A_s(d-x) + \alpha_f A_f(h-x)$ | $x = 61\ mm$ |
| $\varepsilon_y = \frac{f_{yk}}{E_s}$ | $\varepsilon_y = 0.0025$ |
| $\varepsilon_f = \frac{(h-x)}{(d-x)}\varepsilon_y$ | $\varepsilon_f = 0.00314$ |
| $M_y = A_s f_{yk}\left(d - \frac{1}{3}x\right) + \varepsilon_f E_f A_f(h - \frac{1}{3}x)$ | $M_y = 56.5\ kNm$ |
| $\sigma_{fy} = \varepsilon_f E_f$ | $\sigma_{fy} = 519\ MPa$ |

2. The maximum moment $M_{Ed}$ are derived with the average failure load found from the experiment $P = 206\,kN$. Since theoretical moment capacity is derived based on assumption that CFRP reaches debonding strain limit $\varepsilon_{f,lim} = 0.008$, but the tested specimen failed before reaching maximum capacity, the stress and strain are derived based in the experimental failure load.

To define $\varepsilon_{fmax}$ and $\sigma_{fmax}$ associated to $M_{Ed}$, the system of equations demonstrated below was solved to find the unknown variables $x$ and $\varepsilon_f$.

1. $M_{Ed} = f_{yk}A_s(d - \delta_G x) + \varepsilon_f E_f A_f(h - \delta_G x)$
2. $\psi x b f_{cm} = f_{yk}A_s + \varepsilon_f E_f A_f$

Above system have four unknown parameters $x, \varepsilon_f, \delta_G$ and $\psi$. To get a system of two equations with two unknowns, the concrete strain, $\varepsilon_c$, in the expressions for $\delta_G$ and $\psi$ are substituted with the corresponding expresses in terms of $\varepsilon_f$ and $x$, defined through triangular strain relation between $\varepsilon_c$, $\varepsilon_f$ and neutral axis depth $x$ demonstrated below.

$$\varepsilon_c = \varepsilon_f \frac{x}{h - x}$$

$$\psi = 1000\varepsilon_c\left(0.5 - \frac{1000}{12}\varepsilon_c\right) \rightarrow 1000\left(\varepsilon_f \frac{x}{h-x}\right)\left(0.5 - \frac{1000}{12}\left(\varepsilon_f \frac{x}{h-x}\right)\right)$$

$$\delta_G = \frac{8 - 1000\varepsilon_c}{4(6 - 1000\varepsilon_c)} \rightarrow \frac{8 - 1000\left(\varepsilon_f \frac{x}{h-x}\right)}{4\left(6 - 1000\left(\varepsilon_f \frac{x}{h-x}\right)\right)}$$

The resulting system of equations are reduced to two unknown variables: $x$ and $\varepsilon_f$.

1. $M_{Ed} = f_{yk}A_s(d - \delta_G x) + \varepsilon_f E_f A_f(h - \delta_G x)$
2. $\psi x b f_{cm} = f_{yk}A_s + \varepsilon_f E_f A_f$

Solving equation 2. with respect to $\varepsilon_f$, two roots are found, expressed in terms of $x$. Both roots are evaluated and used to solve equation 1. for $x$.

Evaluating the solution given for the system of equations, neutral axis depth can be determined by omitting imaginary and negative values of neutral axis depth $x$. Since neutral axis depth should be in proximity to the neutral axis depth derived for the theoretical capacity defined in Chapter 3.12, Table 3.25, the real value of $x$ can be determined.

Neutral axis depth is determined as the real, positive root found from solving equation 1. with first root of $\varepsilon_f$ from equation 2. Detailed demonstration of the solution of the system of equations are demonstrated in Appendix F. Corresponding strain in CFRP are found by evaluating the expression of $\varepsilon_f$ with respect to defined $x$ value.

To verify the solution, the variables are compared to corresponding variables derived for maximum theoretical capacity defined in Chapter 3.12. Results are found in Table 5.3 below.

Table 5.3 Result based on actual failure load compared to theoretical failure load

| **Variables** | **Actual failure load** | **Theoretical failure load** (Result from Table 3.28) |
|---|---|---|
| $P$ | 206 kN | 224 kN |
| $x$ | 43.39 mm | 42.33 mm |
| $\varepsilon_f$ | 0.006784 | 0.008 |
| $\varepsilon_c$ | 0.001147 | 0.001314 |
| $\psi$ | 0.4639 | 0.5132 |
| $\delta_G$ | 0.3530 | 0.3567 |

The results yield a slightly higher depth of neutral axis and lower strain which are reasonable considering the lower applied load. Associated strain and stress for the applied failure load can then be defined.

$$\varepsilon_{fmax} = 0.006784$$

$$\sigma_{fmax} = \varepsilon_{fmax} E_f = 1119\ MPa$$

3. Distance $\Delta_x$ are found by consider a linear bending moment diagram, neglecting self-weight, up to point load. Analytical expression of this parameter is not defined in TR55, therefore below derivation is based on assumed relation:

$$\Delta_x = 750 - \left(\frac{M_y}{M_{Ed}} \cdot 750\right)$$

With defined variables, the total combined longitudinal shear stress in the yield zone $\tau_t$ can be determined. The shear stress should be lower than limiting shear stress $\tau_{\text{lim,y}}$ to ensure enough capacity in areas with high shear stresses.

$$\tau_m = t_f \left[\frac{\sigma_{fmax} - \sigma_{fy}}{\Delta x}\right] \qquad \tau_m = 3.464\ MPa$$

$$\tau_{sc} = 7.8\left[1.1 - \frac{M_y}{M_{Ed}}\right] f_{ctk} \qquad \tau_{sc} = 8.770\ MPa$$

$$\tau_t = \tau_m + \tau_{sc} \qquad \tau_t = 12.234\ MPa$$

$$\tau_{lim,y} = 4.5\frac{f_{ctk}}{\gamma_c} \qquad \tau_{lim,y} = 13.41\ MPa$$

Verification

For applied load $P = 206\ kN$, and parameters determined omitting partial factors, the longitudinal shear forces are within allowable limit.

$$\tau_t < \tau_{lim,y}$$

**D. Strain in FRP**

The strain in the CFRP are checked with respect to localized stress increase at cracks to verify strain levels are below rupture strain of the CFRP. Since failure mode for the test specimen were not governed by rupture of CFRP plates this verification is not essential. Although to assess the maximum developed strain at locations of flexural cracks in the yield zone, the corresponding maximum strain are calculated.

Check

$\varepsilon_{mt} \leq \varepsilon_{fd}$

Maximum strain at locations of cracks in the yield zone, $\varepsilon_{mt}$, are derived with $\varepsilon_{fmax}$ and $\tau_{sc}$ defined in C. Rupture strain are derived neglecting partial factors and are therefore equal to characteristic strain $\varepsilon_{fd} = \varepsilon_{fk}$.

$$\varepsilon_{mt} = \varepsilon_{fmax} + 0.114 \frac{\tau_{sc}}{\sqrt{E_{fd} t_f}} \qquad \varepsilon_{mt} = 0.00903$$

$$\varepsilon_{fd} = \frac{\varepsilon_{fk}}{\gamma_{FRP,\varepsilon} \gamma_{FRP,m}} \qquad \varepsilon_{fd} = \varepsilon_{fk} = 0.00176$$

Verification

Maximum strain $\varepsilon_{mt}$ derived based on the applied load $P = 206\ kN$ are below rupture strain $\varepsilon_{fk}$ for the CFRP plates.

$\varepsilon_{mt} \leq \varepsilon_{fk}$

## E. Longitudinal shear stress near ends of FRP

Check

$\tau \leq \tau_{\mathrm{lim,c}}$

Determination of $\tau$

$$\tau = \frac{V_{add} \alpha_f A_f (h - x)}{I_{cs} b_a}$$

Since no load are applied during strengthening of the beams, $V_{add}$ is the applied point load. Resulting shear stress at end of CFRP plates $\tau$ and the limiting shear stress $\tau_{lim,c}$ are derived below.

$$\tau = \frac{V_{add}\alpha_f A_f(h-x)}{I_{cs}b_a} \qquad \tau = 1.135\ MPa$$

$$\tau_{lim,c} = 0.8\frac{f_{ctk}}{\gamma_c} \qquad \tau_{lim,c} = 2.384\ MPa$$

Verification

According to above definition, shear stresses near ends of CRFP plates are within allowable limits.

$$\tau < \tau_{lim,c}$$

## F. Anchorage design

Using the TR.55 definition of anchorage design, the corresponding force in the CFRP plates, $T_{CFRP}$, at the location where applied moment $M_{Ed}$ exceeds original moment capacity $M_{Rd,us}$, are determined and verified towards the characteristic bond force failure, $T_{k,max}$. Sufficient anchorage is provided by extending the CFRP plates a length $l_{t,max}$ beyond this point.

To determine location in the span where applied moment exceeds original moment capacity, the bending moment diagram are evaluated up to location of point load. Distance $x$ are found from similar triangles. Available anchorage length $l_t$ are derived by deducting to 50 mm, the distance from support to start of CFRP plates.

$$x = \frac{M_{Rd,us}}{M_{Ed}} \cdot 750$$

$$l_t = x - 50\ mm$$

Since the unstrengthen moment capacity are lower than the yield moment of the strengthened section, $M_{Rd,us} < M_y$, elastic sectional properties can be assumed. Corresponding force in the CFRP plates at distance $x$ are found from flexure formula with transformed area of CFRP by modular ratio $\alpha_f$.

$$T_{CFRP} = \frac{M_{Rd,us}\alpha_f A_f (h - x)}{I_{cs}} \qquad T_{CFRP} = 45.80\ kN$$

$$T_{k,max} = 0.5 k_b b_f \sqrt{E_{fd} t_f f_{ctk}} \qquad T_{k,max} = 46.06\ kN$$

$$l_{t,max} = 0.7 \sqrt{\frac{E_{fd} t_f}{f_{ctk}}} \geq 500\ mm \qquad l_{t,max} = 180\ mm < 500\ mm$$

$$\therefore l_{t,max} = 500\ mm$$

$$x = \frac{M_{Rd,us}}{M_{Ed}} \cdot 750 \qquad x = 399\ mm$$

$$l_t = x - 50\ mm \qquad l_t = 349\ mm$$

From the derived forces above, the resulting force in CFRP are smaller than the ultimate anchorage capacity $T_{CFRP} < T_{k,max}$, sufficient anchorage design are performed by extending the CFRP plates by an anchorage length $l_{t,max}$ beyond this length.

However, available anchorage length $l_t$ are smaller than the required anchorage length $l_{t,max}$, $l_t = 348\ mm < l_{t,max} = 500\ mm$. By theoretical definition, the provided anchorage length is not sufficient to develop the ultimate bond force $T_{k,max}$. Reduced bond force $T_k$ should thereby be derived with formula below.

$$T_k = \left(\frac{T_{k,max} l_t}{l_{t,max}}\right)\left(\frac{2 - l_t}{l_{t,max}}\right) \qquad T_k = 41.84\ kN$$

By above definition, the resulting force in the CRFP are larger than the available bond force, $T_{CFRP} > T_k$, and sufficient anchorage are therefore not available when the beams are loaded to failure.

## 5.3 Summary FRP separation failure

Summarized result from the FRP separation verification are found in Table 5.4.

Table 5.4 Result from FRP separation verification

| | **Criterion** | **Verification** | |
|---|---|---|---|
| B. Shear crack induced FRP separation | $V_{Ed} \leq V_{Rd,crack}$ | $104.875\ kN > 85.16\ kN$ | ✗ |
| C. Longitudinal shear stress in yield zone | $\tau_t \leq \tau_{lim,y}$ | $12.234\ MPa < 13.41\ MPa$ | ✓ |
| D. Stain in FRP | $\varepsilon_{mt} \leq \varepsilon_{fd}$ | $0.00903 < 0.00176$ | ✓ |
| E. Longitudinal shear stress near ends of FRP | $\tau \leq \tau_{lim,c}$ | $1.135\ MPa < 2.384\ MPa$ | ✓ |
| F. Anchorage design | $T_{CFRP} \leq T_k$ | $45.80\ kN > 41.84\ kN$ | ✗ |

## 5.4 Verification of approach used for theoretical calculations

Due to difficulties regarding the interpretation of all the parameters used for theoretical evaluation of FRP strengthened structures, assumed material behavior have been used to perform the above procedure when parameters have not been clearly defined.

To verify the approach used to determine the theoretical capacity of the CFRP strengthened beams, a comparison between the performed calculations and corresponding result from Sika CarboDur FRP Design software are performed.

The Sika CarboDur FRP design software is compliant with different international guidelines, for comparable results, the TR55 and Eurocode default was used.

To evaluate the beam with respect to actual material strength and unfactored load, user-defined combination of partial factors for the material and load combinations were applied. To demonstrate the user-defined modifications used in software Figure 5.1 below demonstrated the partial factors for steel and concrete set to 1.0, compared to the Eurocode defined default setting used for ULS verification illustrated in Figure 5.2.

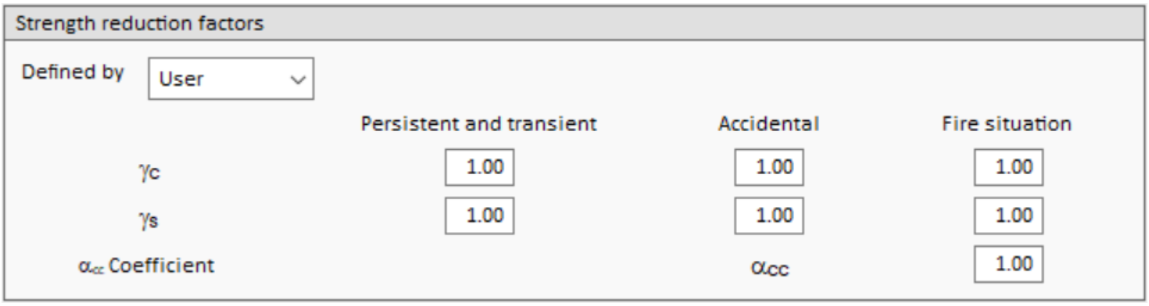


Figure 5.1 User-defined partial factors for material

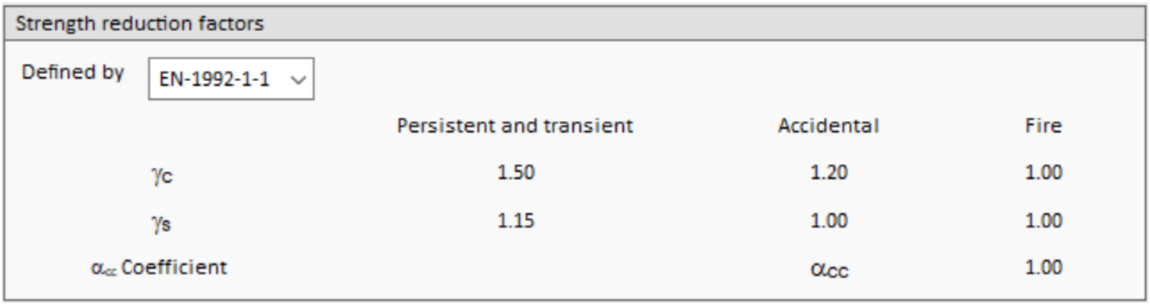


Figure 5.2 Default setting for partial factors in accordance with EN 1992-1-1

The load factors were user-defined in a similar manner, to evaluate the beam with respect to actual failure load. The load combinations for verification of FRP reinforcement failure and fire situation illustrated in Figure 5.3 and 5.4, have not been considered. Since load situation for the experiment are based on very high imposed load compared to dead load, these verifications are neglected due to the unrealistic combination of loads. The user-defined combinations are illustrated in Figure 5.3 while default settings for ULS verification are demonstrated in Figure 5.4.

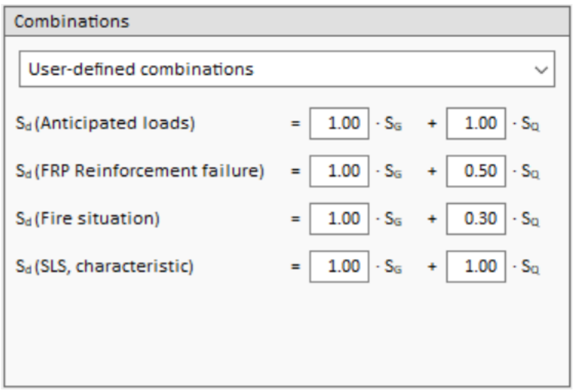


Figure 5.3 User defined load factors

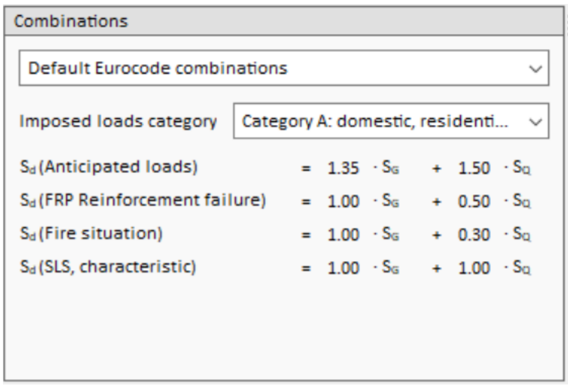


Figure 5.4 Default setting for load combination according to Eurocode

Remark: Safety factors for FRP materials cannot be altered in the software, expression containing the E-modulus and strain of the CFRP plate will therefore be derived with design value to get results derived on same parameters. Corresponding results will therefore be lower than the theoretical values derived in Chapter 5.2 and should therefore only be used to verify the approach. Table 5.5 below demonstrates the parameters used for the comparison.

Table 5.5 Parameters used for comparison

| | | | |
|---|---|---|---|
| **CFRP** | | | |
| $E_{fk} = 165\ GPa$ | | $\varepsilon_{fk} = 0.00176$ | |
| $\gamma_{FRP,m} = 1.05$ | | $\varepsilon_{f,lim} = 0.008$ | |
| $\gamma_{FRP,E} = 1.1$ | | $\gamma_{FRP,\varepsilon} = 1.25$ | |
| $E_{fd} = \dfrac{E_{fk}}{\gamma_{FRP,m}\gamma_{FRP,E}}$ | $E_{fd} = 142857\ MPa$ | $\varepsilon_{fd} = \dfrac{\varepsilon_{fk}}{\gamma_{FRP,m}\gamma_{FRP,\varepsilon}}$ | $\varepsilon_{fd} = 0.0134$ |
| **Concrete** | | | |
| $f_{ck} = f_{cm}$ | $f_{ck} = 60.4\ MPa$ | | |
| $f_{ctk} = f_{ctm}$ | $f_{ctk} = 2.98\ MPa$ | | |
| $\gamma_c$ | $\gamma_c = 1.0$ | | |
| **Steel** | | | |
| $f_{yk}$ | $f_{yk} = 500M\ MPa$ | | |
| $f_{ywd}$ | $f_{ywd} = 500\ MPa$ | | |
| $\gamma_s$ | $\gamma_s = 1.0$ | | |
| **Load** | | | |
| Applied load | $P = 206\ kN$ | | |
| Self-weight | $q = 1.875\ kN/m$ | | |
| Shear span | $a = 0.75\ m$ | | |

First a verification of the calculated theoretical moment capacity is performed with the corresponding neutral axis depth and resulting strain state in the section. The results from calculated values and corresponding results from Sika CarboDur FRP Design software are presented in Table 5.6 below.

Table 5.6 Comparison of result of strengthened moment capacity

| | **Calculated value** | **Sika CarboDur software** |
|---|---|---|
| $M_{Ed}$ | $78.187\ kNm$ | $78.19\ kNm$ |
| $M_{Rd}$ | $79.23\ kNm$ | $79.15\ kNm$ |
| $\varepsilon_f$ | $0.008$ | $0.008$ |
| $\varepsilon_c$ | $0.0012599$ | $0.00126$ |
| $x$ | $40.82\ mm$ | $40.89\ mm$ |

Based on above comparison, the approach used to derive the theoretical capacity can be considered consistent with the software approach given the small deviation between the results. The approach used do derive the concrete compression force according to FiB Bulletin 14 [7, p.36] will therefore be considered a suitable approach given the similar results.

The results from calculated values and corresponding results from Sika CarboDur FRP Design software regarding FRP separation failure are presented in Table 5.7 below.

Table 5.7 Comparison of result of FRP separation verification

| | **Calculated value** | | **Sika CarboDur software** | |
|---|---|---|---|---|
| | | | | |
| $V_{Ed} \leq V_{Rd,crack}$ | $104.87\ kN > 87.73\ kN$ | × | $104.14\ kN > 86.39\ kN$ | × |
| $\tau_t \leq \tau_{lim,y}$ | $13.07\ MPa < 13.41\ MPa$ | ✓ | $12.42\ MPa < 13.42\ MPa$ | ✓ |
| $\varepsilon_{mt} \leq \varepsilon_{fd}$ | $0.0106 < 0.01341$ | ✓ | $0,01022 < 0.01341$ | ✓ |
| $\tau \leq \tau_{lim,c}$ | $1.023\ MPa < 2.38\ MPa$ | ✓ | $1.00\ MPa < 2.38\ MPa$ | ✓ |
| $T_{CFRP} \leq T_k$ | $41.28\ kN > 38.93\ kN*$ | × | $39.16\ kN < 42.86\ kN$ | ✓ |
| | $*T_k = 38.92\ kN$<br>$T_{k,max} = 42.86\ kN$ | | | |
| *Reduced bond force due to insufficient anchorage length | | | | |

From above comparison, larger deviations between calculated value and software results are found compared to result demonstrated in Table 5.6. This indicates some errors in performed calculation. Although, since the largest deviation are within approximately 5% the performed calculations can be considered satisfactory. Demonstration of the performed calculation are found in Appendix G with the corresponding report from Sika CarboDur software in Appendix H.

### 5.4.1 Conflict in results

However, one distinguished difference is found when considering anchorage design.

Software result indicates satisfactory anchorage design as developed force in CFRP at location where applied moment exceeds unstrengthen moment capacity are lower than the ultimate bond force, $T_{CFRP} \leq T_{k,max}$. In Figure 5.5 below, the bond check from the software are illustrated.

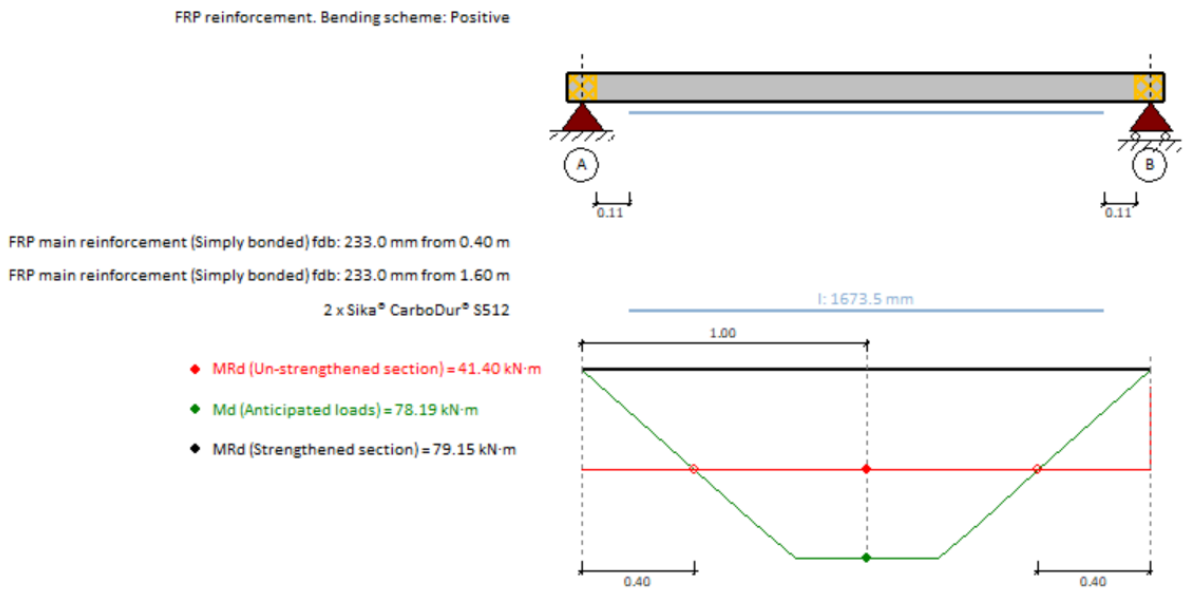


Figure 5.5 Bond check in Sika CarboDur FRP Design software

Evaluating the figure, the location where the applied moment exceeds the unstrengthen capacity $x = 0.4\ m$ corresponds to calculated value.

$$x = \frac{M_{Rd,us}}{M_{Ed}} \cdot 0.75 = 0.398\ m$$

The length the CFRP plate extended beyond this location are given with notation "$f_{bd}$: $233\ mm\ from\ 0.4\ m\ and\ 1.6\ m$", illustrated in Figure 5.5. This length does not correspond to code defined anchorage length given in TR55, $l_{t,max}$, nor does it satisfy the recommended minimum anchorage length of 500 mm. Derived anchorage length $l_{t,max}$ are demonstrated below.

$$l_{t,max} = 0.7\sqrt{\frac{E_{fd}t_f}{f_{ctk}}} = 0.7\sqrt{\frac{\left(\frac{165000}{1.1 \cdot 1.05}\right) \cdot 1.2}{2.98}}\ 168\ mm$$

Further, the notation $f_{bd}$ are not found in chapter describing anchorage design of TR55. It is unclear if $f_{bd}$ refers to the ultimate bond stress defined in EN 1992-1-1 clause 8.4.2, and if so, how the length 233mm have been derived. Uncertainties regarding the definitions have led to difficulties interpreting the software approach for anchorage design.

For the theoretical approach used to verify anchorage design, the bond force is derived with respect to the reduced bond force $T_k$, with expression below. Reduced bond force is assumed to be governing, since required anchorage length are not available $l_t < l_{t,max}$.

$$T_k = \left(\frac{T_k l_t}{l_{t,max}}\right)\left(\frac{2 - l_t}{l_{t,max}}\right)$$

Using this expression for bond force, the developed force in the CFRP exceeds the available bond force $T_{CFRP} > T_k$ resulting in unsatisfactory anchorage of the CFRP plates.

However, since shear force exceeds the capacity to resist shear crack $V_{Ed} > V_{Rd,crack}$, the section should be anchored with additional transverse U-Wrap in accordance with section 6.3.3 (B) in TR55. In Appendix H, a report of the results from Sika CarboDur FRP Design software are demonstrated. Following remark are given in the report:

*"5.6 Remarks*
*Shear- crack-induced FRP separation. The presence of shear crack in the member can lead to the initiation of FRP separation failure. Transverse U-Wrap must be applied, both sides (TR55, fig.26)"*

Since no additional anchorage was applied for the experiment, and result from Sika CarboDur FRP Design software specifies that transverse U-anchorage must be applied, the results cannot be compared due to the different prerequisites

## 5.5 Discussion about CFRP separation

From the result given in Table 5.4, verification for both anchorage design and shear capacity are violated. From a theoretical approach, shear crack induced delamination as well as insufficient anchorage length can be considered the reason for delamination of the CFRP plates and a lower failure load found in the experiment compared to the theoretical prediction.

However, the uncertainties regarding the interpretation of anchorage design with respect to TR55 definitions should be considered. Due to the contradictive result found when comparing the theoretical approach with the Sika CarboDur FRP Design software the verification of anchorage length is inconclusive.

By consider the definition of anchorage length by the other guidelines reviewed, discussed in chapter 2.2.6.2, a quantitative evaluation of anchorage capacity can be determined with the measured distance to first crack recorded for the specimen, presented in Table 4.6.

From the results in Table 4.6, shortest distance recorded from support to first crack is 24 cm. Minimum provided anchorage length are determined by deducting the distance from support to start of CFRP plate, 50 mm, from this recorded value.

$$l_{provided} = 240mm - 50mm = 190\ mm$$

Using the strength parameters determined from compression and tensile splitting test, the provided anchorage length exceeds the required anchorage length for all the codes reviewed, demonstrated in Table 5.8.

Table 5.8 verification of provided anchorage length

| **Guideline** | **Anchorage length** | **Verification** | |
|---|---|---|---|
| ACI 440.2R-17 [2, p.44] | $l_{df} = \sqrt{\frac{nE_f t_f}{\sqrt{f_c'}}} = 159\ mm$ | $l_{provided} > l_{df}$ | ✓ |
| FiB bulletin 14 Approach 1 [7, p.51] | $l_{b,max} = \sqrt{\frac{E_f t_f}{c_2 f_{ctm}}} = 182\ mm$ | $l_{provided} > l_{df}$ | ✓ |
| FiB bulletin 14 Approach 2 [7, p.54] | $l_{b,max} = c_2 \sqrt{\frac{E_f t_f}{\sqrt{f_{ck} f_{ctm}}}} = 175\ mm$ | $l_{provided} > l_{df}$ | ✓ |
| Kompositförstärkning av betong [12, p.48] | $l_{ef} = \sqrt{\frac{E_f t_f}{2 f_{ctm}}} = 182\ mm$ | $l_{provided} > l_{df}$ | ✓ |
| **Material properties used in above derivation** | | | |
| $E_f = 165\ GPa$<br>$t_f = 1.2\ mm$<br>$f_{ck} = f_c' = f_{cm} = 60.4\ MPa$<br>$f_{ctm} = 2.98\ MPa$<br>$c_2 = 2$ (Approach 1)<br>$c_2 = 1.44$ (Approach 2) | | | |

By the results given in table above, and from evaluation of the failed beam specimen, sufficient anchorage length is provided to support the development of ultimate bond force when considering anchorage with respect to last crack in the beam.

The actual reason for the debonding of the CFRP plates is hard to determine since failure and delamination of the test specimen happened very suddenly. Whether debonding initiated from the ends of the CFRP plates or from crack initiation in span of the beams, could not be confirmed from visual observation, as failure occurred in a matter of seconds. For the theoretical FRP verification regarding the shear resistance, the applied force exceeds the capacity significant. Shear crack induced delamination should therefore be considered a governing contribution to the debonding. However, by examination of the failed specimens, illustrated in Figure 4.4-4.6, the crack formation in the beam are dominated by significant flexural cracks within constant bending zone and the distribution of shear cracks are sparse.

Some discrepancies are also found when evaluating the theoretical derived parameters and the observed behavior and recorded data. Since the theoretical prediction are derived based on various assumptions and simplifications, these predictions might not be adequate to describe a detailed failure analysis of the specimens.

In debonding criteria C, the moment at yielding of steel was determined. $M_y$ was derived by a simplified approach, considering triangular stress distribution, the corresponding load at this moment is shown below.

$M_y = 56.5\ kNm$

$$P = \frac{M_y}{a} \cdot 2 - \frac{qL^2}{8} = 150\ kN$$

From the load vs. deflection graph illustrated in Figure 4.27, and the graphs illustrated in Chapter 4.2, the load at which the graph displays change in curvature, associated with the yielding of steel occurs at approximately 170 kN.

By comparing the theoretically derived yield load $P = 150\ kN$, with the behavior demonstrated in graphs, $P = 170\ kN$, the theoretically derived yield moment displays deviation from actual behavior of the specimen.

In step 2. of debonding criteria C**,** the associated strain due to applied load $P = 206\ kN$ are derived. The value of resulting strain $\varepsilon_{fmax} = 0.006784$ found from this derivation are closer to the measured strain from the strain gauges, demonstrated in Table 5.1, with a maximum recorded strain of 0.0064 and a mean value of 0.0059

| Strain from strain gauges | Theoretical strain due to load $P = 206\ kN$ |
|---|---|
| $\varepsilon_{max} = 0.0064$ | $\varepsilon_{fmax} = 0.006784$ |
| $\varepsilon_{avg} = 0.0059$ | |

The data from the strain gauges should however be used as an indicative value, as the readings from the strain gauges depends on the accuracy of alignment of the measuring grid of the strain gauge with the fibers in the CFRP plate [26]. Also found from the results in Table 4.2, the maximum strain was not recorded at same location in the span for all the beams, therefore the maximum strain recorded might not display the maximum strain developed in the CFRP plates. More strain gauges should have been installed within the constant bending zone of the specimen for a more accurate data procurement.

Nevertheless, the recorded valued of maximum strain at debonding are significantly lower than the code defined debonding strain given in TR55.

$\varepsilon_{avg} = 0.0059 < \varepsilon_{f,lim} = 0.008$

From two sources [16] [13], referring to an older version of TR55(2000), a different debonding limit are referred to:

*"(...) laboratory test shows that FRP rupture is a rare event and plate separation due to debonding is more likely. Limiting the strain in the FRP to 0.8% when the load is uniformly distributed, or 0.6% if combined high shear forces and bending moment are present, can prevent this mode of failure"* [16, p.892].

This statement could not be found in the 3rd edition of TR55(2012). A strain limit of 0.006 are defined for axially loaded members [3, p.127], but not found related to flexural strengthened members.

Given the result from the flexural test and the measured strain development in the CFRP plates, a strain limit of 0.006 would have yielded a more conservative theoretical prediction of capacity.

Comparing the different debonding limits discussed in chapter 2.2.6.1, the corresponding moment capacity and failure load derived by different definition of debonding strain are demonstrated in Table 5.9 below. Same procedure to determine moment capacity demonstrated in Chapter 3.12 are used, with strength parameters determined from compression and tensile splitting test and neglecting partial factors. Derivation demonstrated in Appendix I.

Table 5.9 Moment capacity derived by different debonding strain definitions

| **Guideline** | **Debonding strain limit** | $M_{Rd}$ $[kNm]$ | $P_{max}$ $[kN]$ |
|---|---|---|---|
| TR55 [3, p.72] | $\varepsilon_{f.lim} = 0.008$ | 85.1 | 224 |
| ACI 440.2R-17 [2 p.24] | $\varepsilon_{fd} = 0.41\sqrt{\frac{f_c'}{nE_f t_f}} = 0.007159$ | 80.3 | 212 |
| FiB bulletin 14 [7, p.51] Lower limit | $\varepsilon_{f,lim} = 0.0065$ | 76.6 | 201 |
| FiB bulletin 14 [7, p.51] Higher limit | $\varepsilon_{f,lim} = 0.0085$ | 87.9 | 232 |
| Kompositförstärkning av betong [12, p.43] | $\varepsilon_{fd,ic} = 0.41\sqrt{\frac{f_{cd}}{nE_f t_f}} = 0.007159$ | Same value as derived for ACI (when partial factors are neglected) | |

By above comparison, the importance of the limiting value of FRP strain for the theoretical prediction of moment capacity for a strengthened member are demonstrated.

If considering the bond behavior described by J.F. Chen and J.G. Teng [17], discussed in Chapter 2.6.2, and relate this behavior to the crack surface of the failed beam in the experiment, localized debonding in proximity of flexural cracks can be a reasonable assumption. Since the calculated value of maximum strain in yield zone $\varepsilon_{mt}$, derived with the combined effect of bending stresses and flexural cracks, demonstrated in debonding criteria D, exceeds the debonding strain, this assumption is strengthened.

# 6 Conclusion

The aim of the experiment was to determine the effect of existing cracks in a specimen strengthened with externally bonded CFRP plates. By subjecting the specimen to different degree of preload prior to strengthening, different degree of damage levels was simulated, with corresponding different degree of crack formation in the specimens. From the experimental findings, no indication of reduced capacity is found for the beams subjected to higher preload.

Disregarding one of the results due to confirmed poor bond quality, the resulting failure load for all the specimen are within range of 200-210 kN with no distinguished difference with respect to the precondition of the specimen. Two control beams were included in the test program to be used as reference value of failure load for uncracked beams. Since the failure load of all the preloaded specimen are found within same range, the effect of the degree of preloading are insignificant for the performed experiment.

The result from the testing displayed no difference in ultimate capacity of the beams. However, this type of experiment is limited to equipment available and by consideration to the practical feasibility of the performed experiment. Since preloading of the beams were performed on the same load machine, no permanent load scenario could be maintained during installation of the strengthening system and since the beams were not loaded to inflict permanent deformation, no deflection or curvature of the beam soffit were persistent after the load was removed.

The initiated cracks during preloading will be closed when the load is removed. Hence, no substantial cracks will be present during installation of the strengthened system. The installation of the CFRP plates are therefore performed on an approximately plane substrate.

If the corresponding preload of the specimen could be maintained while the strengthening system was installed, the test result could have a different outcome since both initial strain and deflection would be present in the member. From the theoretical derivation of flexural capacity, both of these conditions need to be considered as they affect the theoretical result.

However, the result did display a significant capacity increase of the reinforced concrete members strengthened with externally bonded CFRP plates. Table 4.5 demonstrated a capacity increase between 70-80% compared to the unstrengthen member. The test result demonstrates the vast potential of capacity enhancement possible to attain by externally bonded CFRP reinforcement.

Consistent for all the results, however, is the lower experimental result compared to the theoretical. Ideally, when evaluating the capacity of a section based on actual strength parameters. the theoretical prediction should be close to the actual behavior of the section.

The cause of the lower experimental results is hard to determine and can be related to various different factors mentioned in previous discussion where debonding criteria and strain limits for the CFRP have been evaluated. From the result of the recorded strain, one can argue for a too unconservative strain limit used for the theoretical prediction.

Reflecting over the failure behavior of the specimen and the brittle failure observed, the importance of strengthening limits are emphasized. After delamination of the CFRP plates, the resulting deflection of the delaminated beam was severe.

For a complete design of a strengthened member, both serviceability limit state and ultimate limit state must be verified. Partial factors of safety for both the material and load are used to determine the design capacity of the structure and the allowable loads on the member in ultimate limit state. In addition, strengthening limits are implemented to account for the associated risk of loss of damage to the strengthened system and loss of composite action. These verifications effectively limit the additional loads above unstrengthen capacity.

The 70-80% capacity increase found from the experimental testing demonstrates the potential of the CFRP reinforced member, for a design situation however, additional loads over the capacity of the unstrengthen member  must be limited in order to maintain the safety and integrity of the structure.

## References

[1] A. Stacey, G. Ersdal and J. V. Sharp, *Ageing and life extension of offshore structures: the challenge of managing structural integrity*, 1st edition, Hoboken, NJ, USA: Wiley, 2019.

[2] *Guide for the Design and Construction of Externally Bonded FRP Systems for Strengthening Concrete Structures*, ACI 440.2R-17, 2017 [Online] Available: https://www.concrete.org/publications/internationalconcreteabstractsportal.aspx?m=details&id=51700867

[3] B. Bell et al., «TR55 Design guidance for strengthening concrete structures using fibre composite materials», Concrete Society, Surrey, UK, Technical Report No.55, 3. Edition, 2012.

[4] A. Baier, «Method Statement Sika CarboDur System», Sika Services AG, Pfäffikon ZH, Switzerland, VERSION 2.0, 15.01.2014.

[5] Sika, PRODUCT DATA SHEET: Sika Carbodur S, September 2017, Version 05.01 [Online] Available: https://gbr.sika.com/dms/getdocument.get/02772e0b-de83-3f22-8d08-71f4352432ce/SikaCarboDurS_en_GB_(09-2017)_5_1.pdf

[6] Sika, PRODUCT DATA SHEET: Sikadur 30, February 2020, Version 03.01 [Online] Available: https://gbr.sika.com/content/dam/dms/gb01/w/sikadur_-30.pdf

[7] T.Triantafillou et al., «Externally bonded FRP reinforcement for RC structures», International Federation for Structural Concrete *(fib)*, Lausanne, Switzerland, Technical report Fib Bulletin 14, July 2001.

[8] L.A. Bisby et al., « ISIS Educational Module 2: An introduction to FRP Composites for Construction», ISIS Canada, March 2006.

[9] B. Täljsten, *FRP strengthening of Existing Concrete Structured Design Guideline,* Luleå, Sweden: Luleå University printing office, 2006.

[10] E. Thorenfeldt et al., «Forsterkning av betongkonstruksjoner», Norsk Betongforening, Sandvika, Norway, Publikasjon nr. 36, April 2006.

[11] L. Ascione et al., «Prospect for new guidance in the design of FRP», EC JRC, Italy, JRC99714/EUR 27666 EN, 2016 [Online] Available: DOI: 10/2788/22306.

[12] B. Täljsten, T. Blankssvärd, G. Sas, *Kompositförstärkning av betong*, Halmstad, Sweden: AB Svensk Byggtjänst, 2016.

[13] H.-W. Wu, C.D. Eamon, *Strengthening of Concrete Structures Using Fiber Reinforced Polymers (FRP) Design, Construction and Practical Applications*, Cambridge, USA: Woodhead publishing, 2017.

[14] D. Vázquez, «USER GUIDE Sika CarboDur calculation software», Sika Services AG, V1.2, January 2017. [Online] Available: https://gilar.co.il/wp-content/uploads/2020/11/User-Guide-Sika-Carbodur-TR55Eurocode2-English.pdf

[15] *Eurocode 2: Design of concrete structures-Part 1-1: General rules and rules for buildings*, EN 1992-1-1:2004 + AI:2014 + NA:2018, 2018.

[16] C. Arya, J.L. Clarke, E.A. Kay, P.D. O'Regan, «TR 55: Design guidance for strengthening concrete structures using fibre composite material: a review», *Engineering Structures*, Volume 24, Issue 7, p. 889-900, 2002. [Online] Available: https://doi.org/10.1016/S0141-0296(02)00027-5

[17] J.F. Chen, J.G Teng, «Anchorage strength models for FRP and steel plates bonded to concrete», *Journal of Structural Engineering*, Volume 127, Issue 7, p.784-791, July, 2001. [Online] Available: https://doi.org/10.1061/(ASCE)0733-9445(2001)127:7(784)

[18] W. Choi, H.-D Yun, «21 Non-destructive evaluation (NDE) of composites: use of acoustic emission (AE) techniques», *Non-Destructive evaluation (NDE) of polymer matrix composites*, Woodhead Publishing series in Composites Science and Engineering, p.557-573, 2013. [Online] Available: https://doi.org/10.1533/9780857093554.4.557

[19] B. Mosley, J.Bungey, R. Hulse, *Reinforced Concrete Design to Eurocode 2*, 6th edition, New York, N.Y, USA: Palgrave Macmillian, 2007.

[20] E, Sunder er al., «Armering - Prosjektering og utførelse», Norsk Betongforening, Oslo, Norway, Publikasjon nr. 28 Høringsutkast 26, Oktober, 2018.

[21] Sola Betong AS, «ALMINNELIGE SALGS- OG LEVERINGSBETINGELSER for fabrikkblandet betong», Website, Avaliable: http://sola-betong.no/wp-content/uploads/2019/12/Salgs-og-Leveringsbetingelser-for-fabrikkblandet-betong.pdf 29.02.2021

[22] S. Jacobsen et al., «Chapter 11 – Curing Technology», *Concrete Technology*, Trondheim, Norway: NTNU, Jan 2016.

[23] *Prøvning an herdet betong – Del 3: Prøvelegemers trykkfasthet*, NS-EN 12390-3, 2019.

[24] *Prøving av herdet betong -Del 13: Bestemmelser av sekantmodulus for elastisitet under trykk*, NS-EN 12390-13, 2013.

[25] *Prøving av herdet betong – Del 6: Prøvelegemers spaltestrekkfasthet*, NS-EN 12390-6, 2009.

[26] HBM, «Installing Strain Gauges on Fiber-Reinforced Plastics» Website, Available: https://www.hbm.com/en/3180/tips-and-tricks-strain-gage-installation-on-fiber-reinforced-plastics/ 29.03.21

Appendix:

A: Initial design RC beam

B: Concrete recipe Sola Betong

C: Unstrengthen moment capacity

D: Strengthened moment capacity

E: Comparison experimental and theoretical reault

F: FRP debonding

G: Comparison with Sika Software

H: Report Sika Software

I: Moment capacity with different strain limits

J: Compression test

K: Splitting tensile test

L: E-modulus test

M: 4-point bending test

# Appendix A

>

## Initial design

>

> $restart:$

>

Derived by omitting partial factors

>

> $f_{ck} := 35:$

> $f_{yk} := 500:$

> $b := 250:$

> $h := 300:$

> $c_{nom} := 35:$

> $Ø_L := 12:$

> $A_{12} := \frac{\mathrm{Pi}\cdot Ø_L^2}{4}:$

> $Ø_s := 8:$

> $d := h - c_{nom} - Ø_s - \frac{Ø_L}{2};$

$$d := 251 \tag{1}$$

> $A_s := evalf(3\cdot A_{12});$

$$A_s := 339.2920066 \tag{2}$$

>

**Neutral axis, top reinforcement neglected**

> $x := \frac{f_{yk}\cdot A_s}{0.8\cdot b\cdot f_{ck}};$

$$x := 24.23514332 \tag{3}$$

>

> $M_{Rd} := (0.8\cdot x\cdot f_{ck}\cdot b\cdot (d - (0.4\cdot x)))\cdot 10^{-6};$

$$M_{Rd} := 40.93658873 \tag{4}$$

>

Check if section requires compression reinforcement according to:
Reinforced Concrete Design to Eurocode 2, Mosley et al. 6th edition p.65

>

Applied load equal maximum capasity

> $M_{Ed} := M_{Rd}:$

>

> $k := evalf\left(\frac{M_{Ed} \cdot 10^6}{b \cdot d^2 \cdot f_{ck}}\right)$; #

$$k := 0.07426020671 \quad \textbf{(5)}$$

> **if** $(k \leq 0.167)$ **then** *print*(*Singly reinforced, no compression reinforcement required*)
> **else** *print*(*Doubly reinforced, compression reinforcement required*) **end if**;

*Singly reinforced, no compression reinforcement required* **(6)**

>

Singly reinforced cross section, top reinforcement included to keep Stirrup in place

Unstrengthened capacity

> $M_{Rd,\, us} := M_{Rd}$;

$$M_{Rd,us} := 40.93658873 \quad \textbf{(7)}$$

>

Check to ensure yielding of steel, ductile failure according to:
Reinforced Concrete Design to Eurocode 2, Mosley et al. 6th edition p.63

>

> **if** $(x \leq 0.617 \cdot d)$ **then** *print*(*Yielding of tensile steel, ductile failure*)
> **else** *print*(*No yielding of tensile steel, brittle failure*) **end if**;

*Yielding of tensile steel, ductile failure* **(8)**

>

Check with minimum reinforcement EC2 9.2.1.1 (1)

Corresponding tension strength for B35 concrete according to table 3.1 EN 1992-1-1

> $f_{ctm} := 3.2$ :

> $A_{s,\, \min} := \max\left(0.26 \cdot \frac{f_{ctm}}{f_{yk}} \cdot b \cdot d,\ 0.0013 \cdot b \cdot d\right)$;

$$A_{s,min} := 104.4160000 \quad \textbf{(9)}$$

>

> **if** $(A_s \geq A_{s,\, \min})$ **then** *print*(*Provided reinforcement satisfied*)
> **else** *print*(*Provided reinforcement unsatisfied*) **end if**;

*Provided reinforcement satisfied* **(10)**

**Spacing for stirrups**

Check crushing strength $V_{Rd,max}$ with θ=22. Partial factors neglected. EN 1992-1-1 clause (6.2.3(3))

>

> $V_{Rd,\, \max} = \frac{\alpha_{cw} \cdot b_w \cdot z \cdot v_1 \cdot f_{cd}}{(\cot(\theta) + \tan(\theta))}$ :

>

> $v_1 := 0.6 \cdot \left(1 - \frac{f_{ck}}{250}\right)$ : *#NA 6.2.3(3)*

Degrees converted to radians

> $\theta := \frac{22 \cdot \mathrm{Pi}}{180}$ :

>

>

> $V_{Rd,\,\max} := evalf\left(\dfrac{b\cdot 0.9\cdot d\cdot v_1\cdot f_{ck}}{\left(\dfrac{\cos(\theta)}{\sin(\theta)}+\tan(\theta)\right)}\right)\cdot 10^{-3};$

$$V_{Rd,max} := 354.2544081 \quad \textbf{(11)}$$

High shear capacity when derived without partial factors. Spacing will be governed by maximum longitudinal spacing $s_{l,max}$ (9.2.2 (6))

>

> $A_{Ø_s} := \dfrac{\mathrm{Pi}\cdot(8^2)}{4}$ :

> $A_{sw} := 2\cdot A_{Ø_s}$ :

**Clause 6.2.3(3) Shear links required**

> $V_{Rd,\,s} = \dfrac{A_{sw}}{s}\cdot z\cdot f_{ywd}\cdot\cot(\theta)$ :

Applied load for CFRP strengthened beams unknown.
Assume high shear force for conservetive estimation required shear links.
Maximum capacity of 4 point load machine: 400 kN
Conservative estimation of $V_{Ed}$: 200 kN

>

> $V_{Ed} := 200$ :

> $V_{Rd,\,s} := V_{Ed}$ :

>

> $s_2 := evalf\left(\dfrac{A_{sw}\cdot 0.9\cdot d\cdot f_{yk}\cdot\left(\dfrac{\cos(\theta)}{\sin(\theta)}\right)}{V_{Rd,\,s}\cdot 10^3}\right);$

$$s_2 := 140.5227157 \quad \textbf{(12)}$$

>

**Clause 9.2.2(5) mimimum reinforcement**

> $\rho_w = \dfrac{A_{sw}}{(s\cdot b_w\cdot\sin(\alpha))}$ :

> $\rho_{w,\,\min} := \dfrac{0.1\cdot\mathrm{sqrt}(f_{ck})}{f_{yk}}$ :

> $s_1 := evalf\left(\dfrac{A_{sw}}{\rho_{w,\,\min}\cdot b\cdot 1.0}\right);$

$$s_1 := 339.8566909 \quad \textbf{(13)}$$

>

**N.A 9.2.2(6) Max longitudinal spacing**

> $\varnothing_{L,\,top} := 10$ :

> $d_{top} := c_{nom} + \varnothing_s + \frac{\varnothing_{L,\,top}}{2}$ :

>

> $s_{l,\,\max} := 0.6 \cdot \left(d - d_{top}\right);$

$$s_{l,max} := 121.8 \tag{14}$$

**Spacing between stirups**

> $s := \min\left(s_1, s_2, s_{l,\,\max}\right);$

$$s := 121.8 \tag{15}$$

>

**Suitable spacing**

> $L := 2200$ :

> $no_{stirups} := \frac{L}{s};$

$$no_{stirups} := 18.06239737 \tag{16}$$

**20 stirups over 2200mm gives even and suitable spacing**

> $s_{suitable} := \frac{L}{20};$

$$s_{suitable} := 110 \tag{17}$$

**Stirups Ø8c110**

>

**Failure load**

Failure load dependent on length of shear span, a

>

> $P_{\max} := (a) \rightarrow \frac{M_{Rd,\,us} \cdot 2}{a};$

$$P_{\max} := a \mapsto \frac{2 \cdot M_{Rd,us}}{a} \tag{18}$$

Distance for experimental setup

> $a := 0.75$ :

>

Failure load

> $P_{fail} := P_{\max}(a);$

$$P_{fail} := 109.1642366 \tag{19}$$

**Anchorage length**

Cracking moment

Concrete equivalent transformed section

>

> $E_s := 200$ :

> $E_{cm} := 34$ : *#Corresponding E modulus B35 concrete*

> $\alpha_s := \dfrac{E_s}{E_{cm}}$ :

Neutral axis, uncracked section

> $y_0 := evalf\left(\dfrac{b \cdot h \cdot \left(\frac{h}{2}\right) + (\alpha_s - 1) \cdot A_s \cdot d}{b \cdot h + (\alpha_s - 1) \cdot A_s}\right);$

$$y_0 := 152.1826039 \qquad (20)$$

> $y_t := h - y_0;$

$$y_t := 147.8173961 \qquad (21)$$

Moment of inertia, uncracked section

> $I_{uc} := \dfrac{b \cdot h^3}{12} + b \cdot h \cdot \left(y_0 - \dfrac{h}{2}\right)^2 + (\alpha_s - 1) \cdot A_s \cdot (d - y_0)^2;$

$$I_{uc} := 5.790332251\ 10^8 \qquad (22)$$

Cracking moment

> $M_{cr} := \dfrac{f_{ctm} \cdot I_{uc}}{y_t} \cdot 10^{-6};$

$$M_{cr} := 12.53510323 \qquad (23)$$

**Avaliable anchorage length**

>

Distance from support to last crack (x) derived with likesided triangles with relation below.
Distance to last crack dependent on applied moment $M_{Ed}$ and shear span a

> $\dfrac{x}{M_{cr}} = \dfrac{a}{M_{Ed}}$ :

>

**Evaluation of avaliable anchorage length with respect to unstrengthened moment capacity $M_{Rd,us}$**

> $x := (a) \rightarrow \dfrac{a}{M_{Rd,us}} \cdot M_{cr} \cdot 10^3 \mathrm{mm}$ :

Test with different length of shear span.

>

> $a_{0.6} := 0.6$ :

> $a_{0.7} := 0.7$ :

> $a_{0.75} := 0.75$ :

> $a_{0.8} := 0.8$ :

>

Distance to $M_{cr}$

> $x_{0.6} := x(a_{0.6});$

$$x_{0.6} := 183.7246867\ \mathrm{mm} \qquad (24)$$

> $x_{0.7} := x(a_{0.7});$

(25)

$$x_{0.7} := 214.3454678\ \text{mm} \tag{25}$$

> $x_{0.75} := x(a_{0.75});$

$$x_{0.75} := 229.6558583\ \text{mm} \tag{26}$$

> $x_{0.8} := x(a_{0.8});$

$$x_{0.8} := 244.9662489\ \text{mm} \tag{27}$$

>

Anchorage length

> $l_b := (x) \rightarrow x - 50\text{mm} :$

> 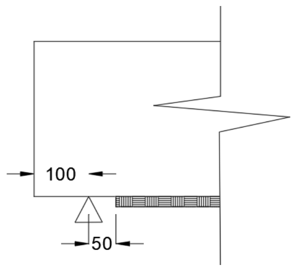


>

> $l_{b_{0.6}} := l_b(x_{0.6});$

$$l_{b_{0.6}} := 133.7246867\ \text{mm} \tag{28}$$

> $l_{b_{0.7}} := l_b(x_{0.7});$

$$l_{b_{0.7}} := 164.3454678\ \text{mm} \tag{29}$$

> $l_{b_{0.75}} := l_b(x_{0.75});$

$$l_{b_{0.75}} := 179.6558583\ \text{mm} \tag{30}$$

> $l_{b_{0.8}} := l_b(x_{0.8});$

$$l_{b_{0.8}} := 194.9662489\ \text{mm} \tag{31}$$

**Corresponding result with 20% increase in applied load**

> $x := (a) \rightarrow \dfrac{a}{1.2 \cdot M_{Rd,us}} \cdot M_{cr} \cdot 10^3\,\text{mm} :$

Distance to Mcr

>

> $x_{0.6} := x(a_{0.6});$

$$x_{0.6} := 153.1039055\ \text{mm} \tag{32}$$

> $x_{0.7} := x(a_{0.7});$

$$x_{0.7} := 178.6212232\ \text{mm} \tag{33}$$

> $x_{0.75} := x(a_{0.75});$

$$x_{0.75} := 191.3798820\ \text{mm} \tag{34}$$

> $x_{0.8} := x(a_{0.8});$

$$x_{0.8} := 204.1385408\ \text{mm} \tag{35}$$

>

Anchorage length

>

> $l_{b_{0.6}} := l_b(x_{0.6});$

$$l_{b_{0.6}} := 103.1039055\ \text{mm} \tag{36}$$

> $l_{b_{0.7}} := l_b(x_{0.7});$

$$l_{b_{0.7}} := 128.6212232\ \text{mm} \tag{37}$$

> $l_{b_{0.75}} := l_b(x_{0.75});$

$$l_{b_{0.75}} := 141.3798820\ \text{mm} \tag{38}$$

> $l_{b_{0.8}} := l_b(x_{0.8});$

$$l_{b_{0.8}} := 154.1385408\ \text{mm} \tag{39}$$

>

**Code defined anchorage length**

>

**Carbodur s512**

> $t_f := 1.2 :$

> $b_f := 50 :$

> $A_f := 2 \cdot t_f \cdot b_f :$

> $E_{fk} := 165000 :$

> $\varepsilon_{fk} := 0.0176 :$

**ACI 440.2R-17**

>

> $l_{df} = \operatorname{sqrt}\left(\frac{n \cdot E_f \cdot t_f}{\operatorname{sqrt}(f_c')}\right) :$

>

> $n := 1 :$ *#layers of plates*

> $f_c' = f_{ck} :$

>

> $l_{df} := evalf\left(\operatorname{sqrt}\left(\frac{n \cdot E_{fk} \cdot t_f}{\operatorname{sqrt}(f_{ck})}\right)\right) \text{mm};$

$$l_{df} := 182.9429104\ \text{mm} \tag{40}$$

>

**FiB Bulletin**

>

**Approach 1**

>

> $l_{b,max} = \mathrm{sqrt}\left(\frac{E_f \cdot t_f}{c_2 \cdot f_{ctm}}\right)$ :

>

> $c_2 := 2$ :

> $f_{ctm} := 3.2$ :

>

> $l_{b,\,\mathrm{max}} := \mathrm{sqrt}\left(\frac{E_{fk} \cdot t_f}{c_2 \cdot f_{ctm}}\right) \mathrm{mm};$

$$l_{b,max} := 175.8905910 \text{ mm} \tag{41}$$

>

**Approach 2**

>

> $l_{b,max} = c_2 \cdot \mathrm{sqrt}\left(\frac{E_f \cdot t_f}{\mathrm{sqrt}(f_{ck} \cdot f_{ctm})}\right)$ :

> $c_2 := 1.44$ :

>

> $l_{b,\,\mathrm{max}} := c_2 \cdot \mathrm{sqrt}\left(\frac{E_{fk} \cdot t_f}{\mathrm{sqrt}(f_{ck} \cdot f_{ctm})}\right) \mathrm{mm};$

$$l_{b,max} := 196.9656899 \text{ mm} \tag{42}$$

**Kompositförstärkning av betong**

>

> $l_{ef} := \mathrm{sqrt}\left(\frac{E_{fk} \cdot t_f}{2 \cdot f_{ctm}}\right) \mathrm{mm};$

$$l_{ef} := 175.8905910 \text{ mm} \tag{43}$$

>

Tel.: +47 51 64 49 49
W..:  - @..: post@sola-betong.no

BR ANEL

## Resept opplysninger

| | | | |
|---|---|---|---|
| Resept | : 251 ~ B35 M45 SKB dmax 16 std FA SF2 | | |
| Opprettet av | : Rune | Dato | : 18-10-2016 13:02:41 |
| Redigert av | : proces | Dato | : 12-11-2019 09:53:51 |
| Resepttype | : Fast verdi | Status | : Aktiv |
| Konsistenstype | : Synkudbredningsmål | | |
| Varepris navn | : | Varepris | : B23516003000 |
| Familie | : B | Familie navn | : standard fa u/luft |
| Tilslagsspec. | : 11 SKB ~ SKB 16 | | |
| Bindemiddel spec. | : 71 ~ Std Fa 90 10 Flyveaske 3,3% SILICA | | |
| Vannspec. | : 01 ~ Kaldt Vann | | |
| Kjemispec. | : 31  B35 SKB ~ SX 23 1,0 %+ luft 0,1% | | |

## Standard : NS206

| | | | |
|---|---|---|---|
| VC spec.nr. | : | V/C-Forhold | : 0,447 |
| Bestandighetsklasse | : M45 | Ameringstål | : Ingen valgt |
| Kloridklasse | : Cl 0,10 | Kontrollklasse | : Ingen valgt |
| Modenhetsminutter | : | Klassifikasjon | : Designet |
| Fasthetsklasse | : B35 | Manuel børverdi | : 60 |
| M³ siden sidste prøve(fam.) | : 91,15 | M³ siden siste prøve | : 19,00 |
| Rct.prv.hyp. i periode | : 30,76 | | |
| Eksponeringsklasse | : X0, XC1, XC2, XC3, XC4, XF1, XD1, XS1, XA1, XA2, XA4 | | |

## Stamopplysninger

| | | | |
|---|---|---|---|
| Min. sement innhold | : Nei | | |
| Min. sement innhold | : | Max | : |
| Min. filler innhold | : | Max | : |
| Synkutbredelsesinterval | : 500 - 700 | Betongtype | : |
| Bruk tilstrebt synkutbredels | : Ja | Tilstræbt synkmål | : 630 |
| Ekstra Specifikationer | : | Sertifiseringsorgan | : |
| Auto % andel af vann ved fl | : 100,00 | | |

## Prøvning

| | | | |
|---|---|---|---|
| Uttak prøve | : Nei | Dato | : 07-10-2016 |
| Prøvehyppighet | : | | |
| Uttak prøve bemerkninger | : | | |
| Forprøve gruppenr. | : Ingen valgt | Foræld. | : |
| Dato for siste prøve | : 21-09-2020 | Dato for siste produksjon | : 03.12.2020 |
| Siste forprøve | : 45580 | | |

## Blanderdata

| Blandernavn | Blandetid | Tømmetid | Deltatid | Blander korr. |
|---|---|---|---|---|
| 1 (Blander 1) | 40,00 | 7,00 | 0,00 | 0,00 |
| 2 (Blander 2) | 40,00 | 7,00 | 0,00 | 0,00 |

## Vekt forsinkelse

**Blander: Blander 1**

| Vækt: | A1-Tilslag 1 | A1-Tilslag 2 | A1-Pulver | A1-Vann | A1-Kjemi 1 | A1-Kjemi 2 | A1-Fiber |
|---|---|---|---|---|---|---|---|
| Sek: | 0 | 0 | 10 | 15 | 16 | 16 | 0 |

## Resept flyt synkmål:

| Install: | 550 | 600 | 650 | 700 |
|---|---|---|---|---|
| VannBehov: | 176,00 | 179,00 | 183,00 | 187,00 |
| Luftinnhold %: | 2,00 | 2,00 | 2,00 | 2,00 |

## Tilslag

Synkmål

| Materialer | Alle |
|---|---|
| Velde 8-16mm | 36,00 |
| Velde 08mm sand | 48,00 |
| Velde 02mm fin sand | 16,00 |

Tel.: +47 51 64 49 49
W..: - @..: post@sola-betong.no

## Bindemiddel

Synkmål

| Materiale | Alle |
|---|---|
| Silika | 3,30 |
| K-verdi | 2,00 |
| Tyrkisk flyveaske | 6,00 |
| K-verdi | 0,70 |
| Standard sement FA | 90,70 |
| K-verdi | 1,00 |

## Vann

| Materiale | Procent |
|---|---|
| varmt vann | |
| Kaldt vann | 100,00 |

## Kjemi

Synkudbredningsmå

| Materiale: | Av materiale | Forsinkelse | 550 | 600 | 650 | 700 |
|---|---|---|---|---|---|---|
| Mapeair 25 1:19 | % av bindemiddel | | 0,10 | 0,10 | 0,10 | 0,10 |
| Mapepump oil | % av bindemiddel | | 0,20 | 0,20 | 0,20 | 0,20 |
| Dynamon SX-23 | % av bindemiddel | 10,00 | 1,00 | 1,05 | 1,10 | 1,15 |

## Proporsjonering

Synkudbredningsmål : 200
Luft : 2,0
Ekv. sement : 346,756
Samlet vannbehov : 155,000

| Materialer | Kilo/m³ VOT | Vanninnhold | Kilo/m³ | Pris/Kg | Pris/m3 | CO2/m³ |
|---|---|---|---|---|---|---|
| Velde 8-16mm | 672,184 | 0,50 | 675,532 | 0,1146 | | 2,39 |
| Velde 08mm sand | 896,246 | 1,50 | 909,556 | 0,1146 | | 3,18 |
| Velde 02mm fin sand | 302,143 | 1,50 | 306,613 | 0,1146 | | 1,07 |
| Silika | 11,274 | 0,00 | 11,274 | 2,9000 | | 0,00 |
| Tyrkisk flyveaske | 20,498 | 0,00 | 20,498 | 0,9735 | | 0,00 |
| Standard sement FA | 309,860 | 0,00 | 309,860 | 0,9155 | | 189,40 |
| Kaldt vann | 152,272 | 100,00 | 131,145 | 0,0000 | | 0,00 |
| varmt vann | 0,000 | 100,00 | 0,000 | 0,0000 | | 0,00 |
| Mapeair 25 1:19 | 0,342 | 99,70 | 0,342 | 0,7300 | | 0,01 |
| Mapepump oil | 0,683 | 99,10 | 0,683 | 6,8000 | | 0,00 |
| Dynamon SX-23 | 2,221 | 77,00 | 2,221 | 9,9000 | | 0,00 |
| | 2367,723 | | | 2367,723 | | 196,05 |

Min/max sementinnhold er anvendt under proporsjoneringen

Proporsjoneringsfeil: Prod. synkmål utenfor grenser (500-700)

## NS206

| | Resultat | Krav | Ok |
|---|---|---|---|
| **Vannbehov (Fri)** | 155,000 | - | |
| **Effektiv bindemiddel (Fri)** | 346,756 | - | |
| **V/C fri beregning** | 0,447 | - | |
| **Vannbehov (EN206)** | 155,000 | - | |
| **Effektiv Bindemiddel (EN206)** | 346,756 | 300,000 | ✓ |
| **V/C i henhold til EN206** | 0,447 | 0,454 | ✓ |
| **Eff. Bindemiddel mængde fratrukket k** | 0,000 | - | |
| **Bindemiddel (total kg)** | 341,632 | - | |
| **Luft %** | 2,000 | - | |
| **Beregnet m³** | 1,000 | - | |
| **Kloridinnhold** | 0,078 | 0,100 | ✓ |
| **Andel reaktiv tilslag %** | 0,000 | - | |
| **Alkaliinnhold** | 4,384 | - | |
| **Flyveaske/bindemiddel forhold** | 0,223 | 0,350 | ✓ |
| **Silika/bindemiddel forhold** | 0,033 | 0,110 | ✓ |
| **Flyveaske, Ren sement andel** | 70,746 | 65,000 | ✓ |
| **Slagg, Ren sement andel** | 0,000 | - | |
| **Matriksvolum eks. luft (l)** | 383,871 | - | |
| **Sementpastavolum (l)** | 272,323 | - | |
| **Samlet vurdering** | | | ✓ |

Tel.: +47 51 64 49 49
W..:  - @..: post@sola-betong.no

BR ANEL

## Blanket

| | |
|---|---|
| Resept nr. | : 251 ~ B35 M45 SKB dmax 16 std FA SF2 |
| Familie | : B |
| Anvendelse 1 | : |
| Anvendelse 2 | : |

## Klassifikasjon

| | | | |
|---|---|---|---|
| Bestandighetsklasse | : M45 | Eksponeringsklasse | : X0, XC1, XC2, XC3, XC4, XF1, XD1, XS1,<br>: XA1, XA2, XA4 |
| Fasthetsklasse | : B35 | Tilstræbt kons. | : 630 |
| Kontrollklasse | : Ingen valgt | Ekstra Specifikationer | : |
| Max. Steinstørrelse | : 16 | Sertifiseringsorgan | : |

## Materiale sammensetning

| Forkortelse | Materiale | Densitet Kg/m³ | Mengde Kg/m³ | Volum Liter m³ | Dekl.dato |
|---|---|---|---|---|---|
| V16 | Velde 8-16mm | 2640,000 | 672,184 | 254,615 | 17-10-2016 |
| V08 | Velde 08mm sand | 2640,000 | 896,246 | 339,487 | 17-10-2016 |
| V02 | Velde 02mm fin sand | 2670,000 | 302,143 | 113,162 | 17-10-2016 |
| silika | Silika | 2200,000 | 11,274 | 5,124 | 07-10-2016 |
| flyveaske | Tyrkisk flyveaske | 2300,000 | 20,498 | 8,912 | 07-10-2016 |
| Standard FA | Standard sement FA | 3000,000 | 309,860 | 103,287 | 07-10-2016 |
| K-Vann | Kaldt vann | 1000,000 | 152,272 | 152,272 | 17-10-2016 |
| V-Vann | varmt vann | 1000,000 | 0,000 | 0,000 | 17-10-2016 |
| Luft | Mapeair 25 1:19 | 1000,000 | 0,342 | 0,342 | 07-10-2016 |
| Pump oil | Mapepump oil | 1000,000 | 0,683 | 0,683 | 07-10-2016 |
| SX-23 | Dynamon SX-23 | 1050,000 | 2,221 | 2,115 | 07-10-2016 |
| Tilstræbt luft i betong (2,0 Vol %) | | | | 20,000 | |
| | | | 2367,723 | 1000,000 | |

| Sand | V08 | V02 | Stein | V16 |
|---|---|---|---|---|
| Materialeklasse | | | Materialeklasse | |
| Humus | | | Lette korn < 2200 kg/m³ | |
| Kjemisk svind Ml/kg | | | Lette korn < 2400 kg/m³ | |
| Innhold av reaktive korn | | | Lette korn < 2500 kg/m³ | |
| Mørtelekspansjon % Uge | | | Kritisk absorbtion av 10 Pct. | |
| Acc. mørtelekspansion % Ug | | | Acc. mørtelekspansion % Ug | |
| Absorbtsjon % | 1,00 | 1,40 | Absorbtsjon % | 0,40 |
| $D_{Lower}$ | | | $D_{Lower}$ | |
| $D^{Upper}$ | | | $D^{Upper}$ | |

| Sement | Sulfatres. |
|---|---|
| Standard sement FA | Nei |

| Andre tilsetninger | Tilsetningsstoffer | Luft | Pump oil | SX-23 |
|---|---|---|---|---|
| Tørstofinnhold % | Tørstofinnhold % | 0,30 | 0,90 | 23,00 |

| Fibre | Vann | K-Vann | V-Vann |
|---|---|---|---|
| Type | Materialeklasse | | |
| Fiber tversnit | Tørstofinnhold % | 0,00 | 0,00 |
| Fiber lengde | | | |

| Klorid/Alkali regnskab | | Kloridberegning | | Alkaliberegning | |
|---|---|---|---|---|---|
| Innhold av delmaterialer | Kg/m³ | % cl | Kg/m³ | % Ekv. Alk | Kg/m³ |
| Velde 8-16mm | 672,184 | 0,000 | 0,000 | | |
| Velde 08mm sand | 896,246 | 0,000 | 0,000 | | |
| Velde 02mm fin sand | 302,143 | 0,000 | 0,000 | | |
| Silika | 11,274 | 0,000 | 0,000 | 0,000 | 0,000 |
| Tyrkisk flyveaske | 20,498 | 0,000 | 0,000 | 0,000 | 0,000 |
| Standard sement FA | 309,860 | 0,085 | 0,263 | 1,400 | 4,338 |
| Kaldt vann | 152,272 | 0,000 | 0,000 | 0,000 | 0,000 |
| varmt vann | 0,000 | 0,000 | 0,000 | 0,000 | 0,000 |
| Mapeair 25 1:19 | 0,342 | 0,050 | 0,000 | 0,200 | 0,001 |
| Mapepump oil | 0,683 | 0,050 | 0,000 | 0,100 | 0,001 |
| Dynamon SX-23 | 2,221 | 0,050 | 0,001 | 2,000 | 0,044 |
| Total | | | 0,265 | | 4,384 |

Tel.: +47 51 64 49 49
W..: - @..: post@sola-betong.no

| **KornKurver, gjennomgang i %** | | | | |
|---|---|---|---|---|
| | **V16** | **V08** | **V02** | **Total** |
| **Mengde, Kg** | 672,184 | 896,246 | 302,143 | 1870,573 |
| **Vol.-%** | 36,000 | 48,000 | 16,000 | 100,000 |
| **Sikt, mm** | | | | |
| 64,000 | 100,000 | 100,000 | 100,000 | 100,000 |
| 32,000 | 100,000 | 100,000 | 100,000 | 100,000 |
| 16,000 | 99,324 | 100,000 | 100,000 | 99,757 |
| 8,000 | 89,654 | 97,800 | 100,000 | 95,220 |
| 4,000 | 78,578 | 75,300 | 100,000 | 80,432 |
| 2,000 | 67,461 | 63,300 | 94,000 | 69,710 |
| 1,000 | 56,313 | 45,600 | 71,000 | 53,521 |
| 0,500 | 45,138 | 29,700 | 50,000 | 38,506 |
| 0,250 | 33,934 | 16,900 | 32,000 | 25,448 |
| 0,125 | 22,699 | 9,400 | 19,300 | 15,772 |
| 0,063 | 11,425 | 5,300 | 10,000 | 8,257 |
| 0,000 | 0,000 | 0,000 | 0,000 | 0,000 |

## Siktekurve

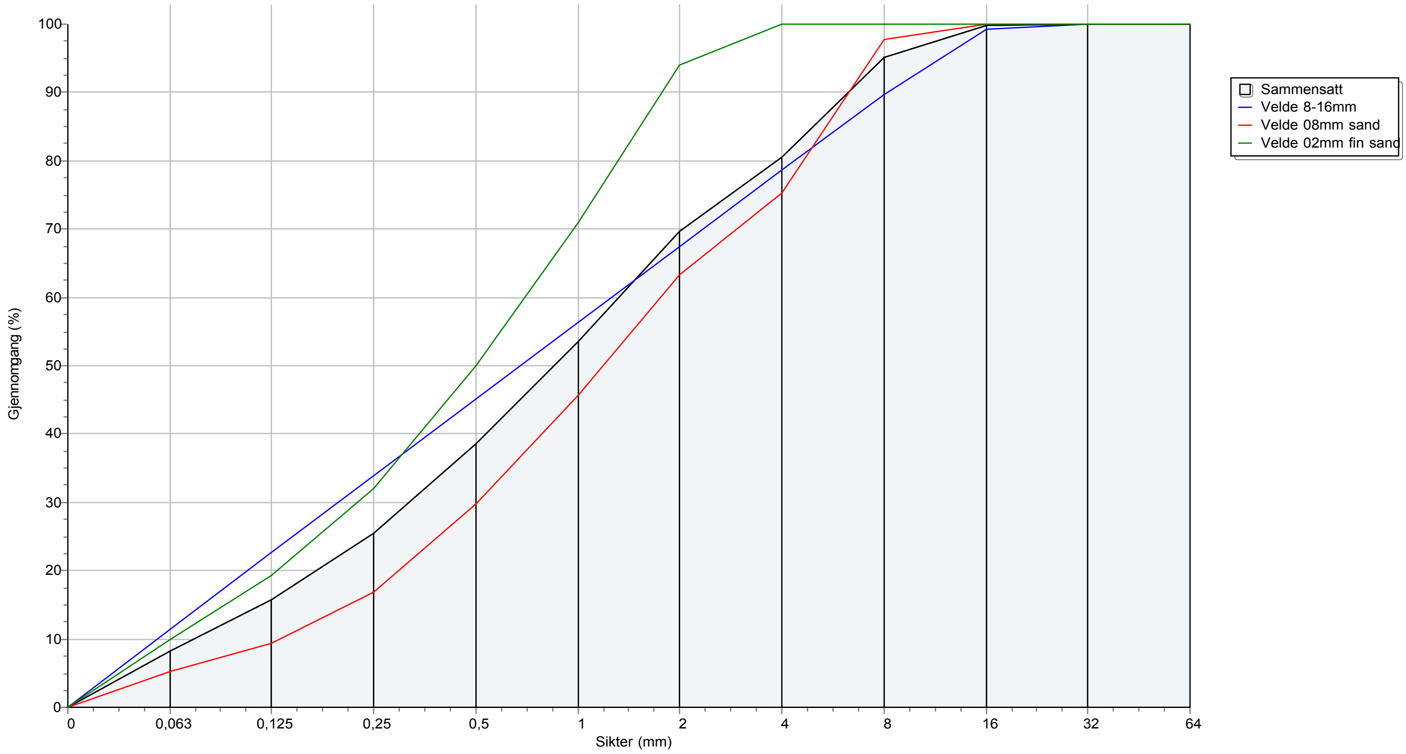


Finhed (Sammensat) : 2,8

Tel.: +47 51 64 49 49
W..: - @..: post@sola-betong.no



## Prøvedata

| Flg nr. | Datotid | Luft % | Konsistens | V/C forhold | T 2 | T 7 | T 28 |
|---|---|---|---|---|---|---|---|
| 48887 | 21-09-2020 09:04 | 2,00/0,00 | 580/640 | 0,447/0,444/0,00( | 0,0 | 0,0 | 60,0/61,6 |
| 47705 | 20-08-2020 12:21 | 2,00/0,00 | 630/640 | 0,447/0,447/0,00( | 0,0 | 0,0 | 60,0/64,0 |
| 45630 | 19-06-2020 09:00 | 2,00/0,00 | 630/620 | 0,447/0,447/0,00( | 0,0 | 0,0 | 60,0/53,4 |
| 45580 | 18-06-2020 10:42 | 2,00/0,00 | 630/640 | 0,447/0,448/0,449 | 0,0 | 0,0 | 60,0/59,3 |
| 43021 | 21-04-2020 11:30 | 2,00/0,00 | 630/680 | 0,447/0,448/0,44( | 0,0 | 0,0 | 60,0/60,6 |
| 40123 | 13-02-2020 14:42 | 2,00/0,00 | 630/650 | 0,447/0,452/0,452 | 0,0 | 0,0 | 60,0/56,5 |
| 36958 | 13-11-2019 08:28 | 2,00/0,00 | 630/660 | 0,447/0,457/0,453 | 0,0 | 0,0 | 60,0/57,5 |
| 32746 | 04-07-2019 11:36 | 2,00/0,00 | 630/660 | 0,447/0,447/0,00( | 0,0 | 0,0 | 60,0/62,1 |
| 32549 | 01-07-2019 13:12 | 2,00/0,00 | 630/640 | 0,447/0,450/0,45( | 0,0 | 0,0 | 60,0/66,2 |
| 31139 | 03-06-2019 07:01 | 2,00/0,00 | 630/630 | 0,447/0,449/0,00( | 0,0 | 0,0 | 60,0/64,7 |
| **Gennemsnit** | | **0,00/0,00** | **625/646** | **0,447/0,449/0,45(** | **0,0** | **0,0** | **60,0/60,6** |

# Appendix C

>

**Unstrengthened capacity**

>

> $restart;$

>

Test results, cube compression 18.03. Time of unstrengthened capacity test

>

> $\sigma_{A1} := 73.95 :$

> $\sigma_{A2} := 73.10 :$

> $\sigma_{A3} := 73.59 :$

> $\sigma_{B1} := 68.62 :$

> $\sigma_{B2} := 67.16 :$

> $\sigma_{B3} := 67.01 :$

>

Mean strength, cube transformed to sylinder by factor 0.8.

> $$f_{cm} := \frac{0.8 \cdot \left(\sigma_{A1} + \sigma_{A2} + \sigma_{A3} + \sigma_{B1} + \sigma_{B2} + \sigma_{B3}\right)}{6};$$

$$f_{cm} := 56.45733331 \tag{1}$$

> $f_{yk} := 500 :$

> $b := 250 :$

> $h := 300 :$

> $c_{nom} := 35 :$

> $$\varnothing_{L_b} := 12 : A_{12} := \frac{\mathrm{Pi} \cdot {\varnothing_{L_b}}^2}{4} :$$

> $$\varnothing_{L_t} := 10 : A_{10} := \frac{\mathrm{Pi} \cdot {\varnothing_{L_t}}^2}{4} :$$

> $\varnothing_s := 8 :$

> $$d := h - c_{nom} - \varnothing_s - \frac{\varnothing_{L_b}}{2} :$$

> $$d_{top} := c_{nom} + \varnothing_s + \frac{\varnothing_{L_t}}{2} :$$

> $A_s := evalf\left(3 \cdot A_{12}\right) :$

> $A_{s_{top}} := evalf\left(2 \cdot A_{10}\right) :$

>

**Case. 1.1 Moment capacity w.r.t fcm, neglection top reinforcement**

>

> $x_{1.1} := \frac{f_{yk} \cdot A_s}{0.8 \cdot b \cdot f_{cm}};$

$$x_{1.1} := 15.02426641 \quad (2)$$

> $M_{Rd_{1.1}} := \left(0.8 \cdot x_{1.1} \cdot f_{cm} \cdot b \cdot \left(d - \left(0.4 \cdot x_{1.1}\right)\right)\right) \cdot 10^{-6};$

$$M_{Rd_{1.1}} := 41.56162412 \quad (3)$$

> $\#M_{ed} = \frac{P}{2} \cdot 0.75 + \frac{q \cdot L^2}{8}$

> #q=self weight of beam

> $q := 0.25 \cdot 0.3 \cdot 25 :$

> $L := 2 :$

>

> $P_{1.1} := \frac{\left(M_{Rd_{1.1}} - \frac{q \cdot L^2}{8}\right) \cdot 2}{0.75};$

$$P_{1.1} := 108.3309976 \quad (4)$$

Evaluation of capacity with top reinforcement included in calculations.

>

**Case 1.2 Moment capacity w.r.t fcm, including top reinforcement**

>

> $x_{1.2} := \frac{f_{yk} \cdot A_s - f_{yk} \cdot A_{s_{top}}}{0.8 \cdot b \cdot f_{cm}};$

$$x_{1.2} := 8.068587516 \quad (5)$$

N.A over top reinforcement, top reinforcement in tension. Recalculate N.A

> $x_{1.2} := \frac{f_{yk} \cdot A_s + f_{yk} \cdot A_{s_{top}}}{0.8 \cdot b \cdot f_{cm}};$

$$x_{1.2} := 21.97994530 \quad (6)$$

However, this approach are based on yield stress in top reinforcement, which is not correct. Corresponding stress in top steel found by itterative approach.

>

Yield strain

>

> $\sigma_y := 500 :$

> $E_s := 200 \cdot 10^3 :$

> $\varepsilon_y := evalf\left(\frac{\sigma_y}{E_s}\right);$

$$\varepsilon_y := 0.002500000000 \tag{7}$$

>

Start with x from calculation without top reinforcemen, initial value

>

> $x_i := x_{1.2};$

$$x_i := 21.97994530 \tag{8}$$

Iteration

> **for** *i* **from** 1 **to** 5 **do**
*print*(' ') :
*print*('*Iteration*', *i*);

$$\varepsilon_i := \frac{\varepsilon_y \cdot (d_{top} - x_i)}{(d - x_i)} :$$

$$\sigma_i := \varepsilon_i \cdot E_s :$$

$$x_i := \frac{f_{yk} \cdot A_s + \sigma_i \cdot A_{s_{top}}}{0.8 \cdot b \cdot f_{cm}} :$$

**od**;

*Iteration*, 1

$$\varepsilon_i := 0.0002840368580$$

$$\sigma_i := 56.80737160$$

$$x_i := 15.81453409$$

*Iteration*, 2

$$\varepsilon_i := 0.0003421285600$$

$$\sigma_i := 68.42571200$$

$$x_i := 15.97616098$$

*Iteration*, 3

$$\varepsilon_i := 0.0003406445827$$

$$\sigma_i := 68.12891654$$

$$x_i := 15.97203215$$

*Iteration*, 4

$$\varepsilon_i := 0.0003406825169$$

$$\sigma_i := 68.13650338$$

$$x_i := 15.97213769$$

*Iteration*, 5

$$\varepsilon_i := 0.0003406815473$$

$$\sigma_i := 68.13630946$$

$$x_i := 15.97213499 \tag{9}$$

>

Considered converged after 5 iterations

>

> $x_{1.2} := x_i;$

$$x_{1.2} := 15.97213499 \tag{10}$$

> $\sigma_{s_{top}} := \sigma_i;$

$$\sigma_{s_{top}} := 68.13630946 \tag{11}$$

Moment capacity including top reinforcement

>

> $M_{Rd_{1.2}} := \left(f_{yk} \cdot A_s \cdot (d - 0.4 \cdot x_{1.2}) + \sigma_{s_{top}} \cdot A_{s_{top}} \cdot (d_{top} - 0.4 \cdot x_{1.2})\right) \cdot 10^{-6};$

$$M_{Rd_{1.2}} := 41.94266015 \tag{12}$$

> $P_{1.2} := \dfrac{\left(M_{rd_{1.2}} - \dfrac{q \cdot L^2}{8}\right) \cdot 2}{0.75};$

$$P_{1.2} := 109.3470937 \tag{13}$$

>

Difference between approaches

>

> $\Delta M := M_{Rd_{1.2}} - M_{Rd_{1.1}};$

$$\Delta M := 0.38103603 \tag{14}$$

>

# Appendix D

>

**Procedure according to TR55**

>

> *restart*;

>

**Material properties and dimensions**

Test result, cube compression 10.04

>

> $\sigma_{A1} := 79.22 :$

> $\sigma_{A2} := 79.09 :$

> $\sigma_{A3} := 78.34 :$

> $\sigma_{B1} := 71.76 :$

> $\sigma_{B2} := 73.04 :$

> $\sigma_{B3} := 71.35 :$

>

Mean strength, cube transformed to sylinder by factor 0.8.

> $f_{cm} := \dfrac{0.8 \cdot \left(\sigma_{A1} + \sigma_{A2} + \sigma_{A3} + \sigma_{B1} + \sigma_{B2} + \sigma_{B3}\right)}{6};$

$$f_{cm} := 60.37333331 \quad \textbf{(1)}$$

> $E_{cm} := 22 \cdot \left(\dfrac{f_{cm}}{10}\right)^{0.3} \cdot 10^{3};$ *#EC2 Table 3.1*

$$E_{cm} := 37729.08104 \quad \textbf{(2)}$$

> $f_{yk} := 500 :$

> $E_s := 200 \cdot 10^{3} :$

> $b := 250 : h := 300 : c_{nom} := 35 :$

> $\varnothing_{L_b} := 12 :$

>

> $\varnothing_s := 8 :$

> $d := h - c_{nom} - \varnothing_s - \dfrac{\varnothing_{L_b}}{2} :$

> $A_s := 339 :$

>

**Carbodur s512**

>

> $no := 2 :$ *#No of plates*

> $t_f := 1.2 :$

> $w_f := 50 :$

> $A_f := no \cdot t_f \cdot w_f :$ #mm^2

> $E_f := 165 \cdot 10^3 :$ #MPa

> $\varepsilon_{fk} := 0.0176 :$

> $\varepsilon_{f,\,\lim} := 0.008 :$

>

**Strengthened capacity**

>

Initial strain

>

> $$\varepsilon_{c0} = \frac{M_0 x_0}{E_c I_{cc}}$$
> $$\varepsilon_0 = \varepsilon_{c0} \frac{(h - x_0)}{x_0}$$

> $\varepsilon_{c0} := 0 :$

> $\varepsilon_0 := 0 :$

>

Step 1: Assume maximim compressive strain

>

> $\varepsilon_{cu} := 0.0035 :$

>

Step 2: Assume neutral axis

Choosen after ACI sugesttion

>

> $x_i := 0.2 \cdot d;$

$$x_i := 50.2 \tag{3}$$

Step 3: define strain in FRP by implementing linear strain relation and deduct initial strain

>

> $\varepsilon_f := \varepsilon_{cu} \cdot \frac{(h - x_i)}{x_i} - \varepsilon_0;$

$$\varepsilon_f := 0.01741633466 \tag{4}$$

> $'\varepsilon_f > \varepsilon_{f,\,\lim}'$

$$\varepsilon_f > \varepsilon_{f,lim} \tag{5}$$

From above derivation, with assumed neutral axis depth x=0.2d, strain exceeds debonding strain

Apply itterative process to determine neutral axis depth and verify the strain.

>

Step 4: Calculate forces in section

Force concrete

> $F_{ci} := 0.8 \cdot x_i \cdot b \cdot f_{cm};$

$$F_{ci} := 606148.2664 \quad (6)$$

Force tension

> $F_f := \varepsilon_f \cdot E_f \cdot A_f;$

$$F_f := 344843.4263 \quad (7)$$

> $F_s := f_{yk} \cdot A_s;$

$$F_s := 169500 \quad (8)$$

> $F_t := F_f + F_s;$

$$F_t := 514343.4263 \quad (9)$$

Section is not in force equlibrium

>

Step 5: iterative adjust location of N.A until force balance is achieved

>

> $x_i := 0.2 \cdot d;$

$$x_i := 50.2 \quad (10)$$

> **for** $i$ **from** 1 **to** 50 **do**

$\#print(\text{' '}):$

$\#print(\text{'Iteration'}, i):$

$\varepsilon_i := \dfrac{\varepsilon_{cu} \cdot (h - x_i)}{x_i}:$

$F_f := \varepsilon_i \cdot E_f \cdot A_f : F_s := f_{yk} \cdot A_s : F_t := F_f + F_s; F_c := 0.8 \cdot x_i \cdot b \cdot f_{cm};$

$x_i := \dfrac{F_t}{0.8 \cdot b \cdot f_{cm}};$

**od**:

>

Result after 50 iterations

>

> $x := x_i$

$$x := 45.85072125 \quad (11)$$

> $F_c := F_c;$

$$F_c := 553627.0550 \quad (12)$$

> $F_t := F_t;$

$$F_t := 553632.1752 \quad (13)$$

Can be considered converged, Force balance achieved

>

Check the calculates stresses and strains against following criteria:

>

i) Concrete strain should not exceed maximum strain.
Due to assumption of maximum concrete compression strain the section is subjected to compressive strain of 0.0035.

ii) FRP strain should not exceed debonding or rupture strain

Corresponding strain in FRP for force equlibrium are:

>

> $\varepsilon_f := \varepsilon_i;$

$$\varepsilon_f := 0.01940061491 \tag{14}$$

> $'\varepsilon_f > \varepsilon_{f,\,\mathrm{lim}}';$

$$\varepsilon_f > \varepsilon_{f,lim} \tag{15}$$

Corresponding strain in FRP exceeds both rupture strain and limiting debonding strain.

Failure mode will therefore NOT be governed by concrete crushing, but by strain limit in FRP

>

Process repeated from Step 2 assumption of neutral axis. Iterate until force equlibrium is achieved.

In this case, concrete will not reach its limiting strain since maximum FRP strain will govern the design.

Strain in concrete will be governed by the FRP strain and the loaction of neutral axis.

>

TR55 states rectangular stress blocks should not be used, but does not provide method of to determine area of concrete in compression.

>

Both ACI and FiB bulletin 14 provide numeric expression for appropriate stress block factors when strain limit of concrete have not been reached.

>

Since ACI have a different design approach of reinforced concrete in general compared to concrete design according to Eurocode, the definition in FiB bulletin 14 will be used to determine truncated parameters for the concrete compression area.

>

$\psi$ = stress block area coefficient

$\delta_G$ = stress block centroid coefficient

> 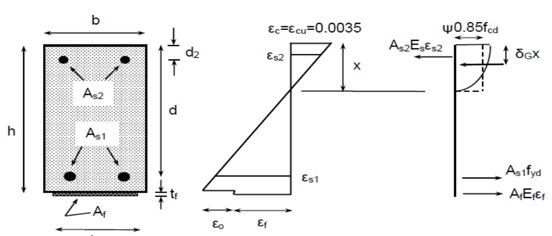


>

According to FiB, in failure modes goverened by steel yielding and FRP fracture, stress block factors $\psi$ and $\delta_G$ should be modified.
Since FRP debonding will occur prior to FRP fracture, the debonding limit of FRP will be the governing parameter.

>

Stress block factors are defined with formulas below.

>

$$\psi = \begin{cases} 1000\varepsilon_c\left(0.5 - \frac{1000}{12}\varepsilon_c\right) & \text{for } \varepsilon_c \le 0.002 \\ 1 - \frac{2}{3000\varepsilon_c} & \text{for } 0.002 \le \varepsilon_c \le 0.0035 \end{cases} \qquad \text{(4-11)}$$

>

$$\delta_G = \begin{cases} \frac{8 - 1000\varepsilon_c}{4(6 - 1000\varepsilon_c)} & \text{for } \varepsilon_c \le 0.002 \\ \frac{1000\varepsilon_c(3000\varepsilon_c - 4) + 2}{2000\varepsilon_c(3000\varepsilon_c - 2)} & \text{for } 0.002 \le \varepsilon_c \le 0.0035 \end{cases} \qquad \text{(4-12)}$$

>

Step 2. Start by assuming an initial neutral axis, choose value close to previous result. FRP strain limit 0.008

>

> $\varepsilon_f := 0.008$ :

> $x_i := 0.2 \cdot d$ :

>

Step 3: Corresponding concrete strain.

> $\varepsilon_c := \varepsilon_f \cdot \frac{x_i}{(h - x_i)}$;

$$\varepsilon_c := 0.001607686149 \qquad \textbf{(16)}$$

>

> $\#\varepsilon_c < 0.002$

>

Step 4: Internal forces, iteration procedure

>

Display of first 5 iterations

> **for** $i$ **from** 1 **to** 5 **do**

*print*(' ') :

*print*('*Iteration*', $i$) :

$\varepsilon_i := \frac{\varepsilon_f \cdot x_i}{(h - x_i)}$ :

$\psi := 1000 \cdot \varepsilon_i \cdot \left(0.5 - \frac{1000}{12} \cdot \varepsilon_i\right)$ : $\delta_G := \frac{8 - 1000 \cdot \varepsilon_i}{4 \cdot (6 - 1000 \cdot \varepsilon_i)}$ : $F_f := \varepsilon_f \cdot E_f \cdot A_f$: $F_s := f_{yk} \cdot A_s$:

$F_t := F_f + F_s$: $F_c := \psi \cdot x_i \cdot b \cdot f_{cm}$:

$x_i := \frac{F_t}{\psi \cdot b \cdot f_{cm}}$;

**od**;

*Iteration*, 1

$$\varepsilon_i := 0.001607686149$$
$$\psi := 0.5884551784$$
$$\delta_G := 0.3638352170$$
$$F_f := 158400.0000$$
$$F_s := 169500$$
$$F_t := 327900.0000$$
$$F_c := 445863.8579$$
$$x_i := 36.91839945$$

*Iteration*, 2
$$\varepsilon_i := 0.001122644818$$
$$\psi := 0.4562947934$$
$$\delta_G := 0.3525145763$$
$$F_f := 158400.0000$$
$$F_s := 169500$$
$$F_t := 327900.0000$$
$$F_c := 254257.3645$$
$$x_i := 47.61137679$$

*Iteration*, 3
$$\varepsilon_i := 0.001509144943$$
$$\psi := 0.5647792666$$
$$\delta_G := 0.3613373719$$
$$F_f := 158400.0000$$
$$F_s := 169500$$
$$F_t := 327900.0000$$
$$F_c := 405858.5026$$
$$x_i := 38.46604260$$

*Iteration*, 4
$$\varepsilon_i := 0.001176628625$$
$$\psi := 0.4729430691$$
$$\delta_G := 0.3536619329$$

$$F_f := 158400.0000$$
$$F_s := 169500$$
$$F_t := 327900.0000$$
$$F_c := 274581.6667$$
$$x_i := 45.93538789$$

*Iteration*, 5
$$\varepsilon_i := 0.001446415934$$
$$\psi := 0.5488647124$$
$$\delta_G := 0.3598036169$$
$$F_f := 158400.0000$$
$$F_s := 169500$$
$$F_t := 327900.0000$$
$$F_c := 380537.8510$$
$$x_i := 39.58138105 \tag{17}$$

>

Iteration until convergece

> $\varepsilon_f := 0.008$ :

> $x_i := 0.2 \cdot d$ :

> **for** $i$ **from** 1 **to** 70 **do**
#*print*(' ') :
#*print*('*Iteration*', $i$) :

$\varepsilon_i := \dfrac{\varepsilon_f \cdot x_i}{(h - x_i)}$ :

$\psi := 1000 \cdot \varepsilon_i \cdot \left(0.5 - \dfrac{1000}{12} \cdot \varepsilon_i\right)$ : $\delta_G := \dfrac{8 - 1000 \cdot \varepsilon_i}{4 \cdot \left(6 - 1000 \cdot \varepsilon_i\right)}$ : $F_f := \varepsilon_f \cdot E_f \cdot A_f$ : $F_s := f_{yk} \cdot A_s$ :

$F_t := F_f + F_s$ : $F_c := \psi \cdot x_i \cdot b \cdot f_{cm}$ :

$x_i := \dfrac{F_t}{\psi \cdot b \cdot f_{cm}}$;

**od**:

>

>

Step 6: Parameters at force equilibrium

>

> $\varepsilon_c := \varepsilon_i$;

(18)

$$\varepsilon_c := 0.001314304460 \tag{18}$$

> $\psi := \psi;$

$$\psi := 0.5132025455 \tag{19}$$

> $\delta_G := \delta_G;$

$$\delta_G := 0.3567077439 \tag{20}$$

> $F_f := F_f;$

$$F_f := 158400.0000 \tag{21}$$

> $F_s := F_s;$

$$F_s := 169500 \tag{22}$$

> $F_c := F_c;$

$$F_c := 327899.5132 \tag{23}$$

> $F_t := F_t;$

$$F_t := 327900.0000 \tag{24}$$

> $F_c \approx F_t;$

$$327899.5132 \approx 327900.0000 \tag{25}$$

> $x := x_i;$

$$x := 42.33186978 \tag{26}$$

> $\varepsilon_s := \left(\varepsilon_f - \varepsilon_{c0}\right) \cdot \frac{(d - x)}{(h - x)};$

$$\varepsilon_s := 0.006478663235 \tag{27}$$

Moment capacity, CFRP strengthened section

>

> $M_{Rd,\,CFRP} := \left(f_{yk} \cdot A_s \cdot \left(d - \delta_G \cdot x\right) + \varepsilon_f \cdot E_f \cdot A_f \left(h - \delta_G \cdot x\right)\right) \cdot 10^{-6};$

$$M_{Rd,st} := 85.11317531 \tag{28}$$

> $q := 0.25 \cdot 0.3 \cdot 25 :$

> $L := 2 :$

>

> $P_{fail} := \left(M_{Rd,\,st} - \frac{q \cdot L^2}{8}\right) \cdot \frac{2}{0.75};$

$$P_{fail} := 224.4684675 \tag{29}$$

>

# Appendix E

>

Comparison of results

>

> $restart:$

>

**Strengthened capacity, Theoretical values**

> $M_{Rd,\,CFRP} := 85.11317531:$

> $P_{fail} := 224.4684675:$

>

**Unstrengthen capacity, from failure load**

> $P_{fail,\,us} := 116;$

$$P_{fail,us} := 116 \tag{1}$$

> $q := 0.25 \cdot 0.3 \cdot 25:$

> $L := 2:$

>

> $M_{Rd,\,us,\,ex} := \frac{P_{fail,\,us}}{2} \cdot 0.75 + \frac{q \cdot L^2}{8};$

$$M_{Rd,us,ex} := 44.43750000 \tag{2}$$

>

**Ratio Experimental over theoretical values**

> $M_{us} := M_{Rd,\,us,\,ex};$

$$M_{us} := 44.43750000 \tag{3}$$

> $M := (P) \rightarrow \frac{P}{2} \cdot 0.75 + \frac{q \cdot L^2}{8}:$

> $\varepsilon_{f,\,\lim} := 0.008:$

>

**Beam A.2**

> $P_{A.2} := 208.37 : \varepsilon_{A.2} := 5948 \cdot 10^{-6}:$

> $\Delta P := \frac{P_{A.2}}{P_{fail}}; \Delta\varepsilon := \frac{\varepsilon_{A.2}}{\varepsilon_{f,\,\lim}};$

$$\Delta P := 0.9282818309$$

$$\Delta\varepsilon := 0.7435000000 \tag{4}$$

Increased flexural capacity

> $M_{A.2} := M(P_{A.2}); \Delta_M := M_{A.2} - M_{us}; increase := \frac{\Delta_M}{M_{us}} \cdot 100;$

$$M_{A.2} := 79.07625000$$

$$\Delta_M := 34.63875000$$

$$increase := 77.94936709 \quad (5)$$

**Beam B.5**

$> P_{B.5} := 203.88 : \varepsilon_{B.5} := 6408 \cdot 10^{-6} :$

$> \Delta P := \frac{P_{B.5}}{P_{fail}}; \Delta\varepsilon := \frac{\varepsilon_{B.5}}{\varepsilon_{f,\lim}};$

$$\Delta P := 0.9082790214$$

$$\Delta\varepsilon := 0.8010000000 \quad (6)$$

Increased flexural capacity

$> M_{B.5} := M(P_{B.5}); \Delta_M := M_{B.5} - M_{us}; increase := \frac{\Delta_M}{M_{us}} \cdot 100;$

$$M_{B.5} := 77.39250000$$

$$\Delta_M := 32.95500000$$

$$increase := 74.16033755 \quad (7)$$

**Beam A.4**

$> P_{A.4} := 205.43 : \varepsilon_{A.4} := 5731 \cdot 10^{-6} :$

$> \Delta P := \frac{P_{A.4}}{P_{fail}}; \Delta\varepsilon := \frac{\varepsilon_{A.4}}{\varepsilon_{f,\lim}};$

$$\Delta P := 0.9151842229$$

$$\Delta\varepsilon := 0.7163750000 \quad (8)$$

Increased flexural capacity

$> M_{A.4} := M(P_{A.4}); \Delta_M := M_{A.4} - M_{us}; increase := \frac{\Delta_M}{M_{us}} \cdot 100;$

$$M_{A.4} := 77.97375000$$

$$\Delta_M := 33.53625000$$

$$increase := 75.46835443 \quad (9)$$

**Beam B.4**

$> P_{B.4} := 207.63 :$

$> \Delta P := \frac{P_{B.4}}{P_{fail}};$

$$\Delta P := 0.9249851541 \quad (10)$$

Increased flexural capacity

$> M_{B.4} := M(P_{B.4}); \Delta_M := M_{B.4} - M_{us}; increase := \frac{\Delta_M}{M_{us}} \cdot 100;$

$$M_{B.4} := 78.79875000$$

$$\Delta_M := 34.36125000$$

$$increase := 77.32489451 \quad \textbf{(11)}$$

**Beam A.3**

> $P_{A.3} := 192.39 : \varepsilon_{A.3} := 4925 \cdot 10^{-6} :$

> $\Delta P := \dfrac{P_{A.3}}{P_{fail}}; \Delta\varepsilon := \dfrac{\varepsilon_{A.3}}{\varepsilon_{f,\lim}};$

$$\Delta P := 0.8570914309$$

$$\Delta\varepsilon := 0.6156250000 \quad \textbf{(12)}$$

Increased flexural capacity

> $M_{A.3} := M(P_{A.3}); \Delta_M := M_{A.3} - M_{us}; increase := \dfrac{\Delta_M}{M_{us}} \cdot 100;$

$$M_{A.3} := 73.08375000$$

$$\Delta_M := 28.64625000$$

$$increase := 64.46413502 \quad \textbf{(13)}$$

**Beam B.3**

> $P_{B.3} := 207.85 :$

> $\Delta P := \dfrac{P_{B.3}}{P_{fail}};$

$$\Delta P := 0.9259652472 \quad \textbf{(14)}$$

Increased flexural capacity

> $M_{B.3} := M(P_{B.3}); \Delta_M := M_{B.3} - M_{us}; increase := \dfrac{\Delta_M}{M_{us}} \cdot 100;$

$$M_{B.3} := 78.88125000$$

$$\Delta_M := 34.44375000$$

$$increase := 77.51054852 \quad \textbf{(15)}$$

**Beam A.5**

> $P_{A.5} := 211.10 : \varepsilon_{A.5} := 5763 \cdot 10^{-6} :$

> $\Delta P := \dfrac{P_{A.5}}{P_{fail}}; \Delta\varepsilon := \dfrac{\varepsilon_{A.5}}{\varepsilon_{f,\lim}};$

$$\Delta P := 0.9404438955$$

$$\Delta\varepsilon := 0.7203750000 \quad \textbf{(16)}$$

Increased flexural capacity

> $M_{A.5} := M(P_{A.5})$; $\Delta_M := M_{A.5} - M_{us}$; $increase := \dfrac{\Delta_M}{M_{us}} \cdot 100$;

$$M_{A.5} := 80.10000000$$

$$\Delta_M := 35.66250000$$

$$increase := 80.25316456 \tag{17}$$

**Beam B.6**

> $P_{B.6} := 199.02 : \varepsilon_{B.6} := 5610 \cdot 10^{-6} :$

> $\Delta P := \dfrac{P_{B.6}}{P_{fail}}$; $\Delta\varepsilon := \dfrac{\varepsilon_{B.6}}{\varepsilon_{f,\,\mathrm{lim}}}$;

$$\Delta P := 0.8866278735$$

$$\Delta\varepsilon := 0.7012500000 \tag{18}$$

Increased flexural capacity

> $M_{B.6} := M(P_{B.6})$; $\Delta_M := M_{B.6} - M_{us}$; $increase := \dfrac{\Delta_M}{M_{us}} \cdot 100$;

$$M_{B.6} := 75.57000000$$

$$\Delta_M := 31.13250000$$

$$increase := 70.05907173 \tag{19}$$

# Appendix F

>

**FRP separation failure according to TR55**

>

> $restart;$

>

Material properties and dimensions

>

> $f_{cm} := 60.37333331 :$

> $E_{cm} := 22 \cdot \left(\frac{f_{cm}}{10}\right)^{0.3} \cdot 10^3;$ *#EC2 Table 3.1*

$$E_{cm} := 37729.08104 \qquad (1)$$

> $f_{yk} := 500 :$

> $E_s := 200 \cdot 10^3 :$

> $b := 250 : h := 300 : c_{nom} := 35 :$

> $\varnothing_{L_b} := 12 :$

>

> $\varnothing_s := 8 :$

> $d := h - c_{nom} - \varnothing_s - \frac{\varnothing_{L_b}}{2} :$

> $A_s := 339 :$

>

**Carbodur s512**

>

> $no := 2 :$ *#No of plates*

> $t_f := 1.2 :$

> $w_f := 50 :$

> $A_f := no \cdot t_f \cdot w_f :$ *#mm*$^2$

> $E_f := 165 \cdot 10^3 :$ *#MPa*

> $\varepsilon_f := 0.0176 :$

> $\varepsilon_{f,\lim} := 0.008 :$

>

**(A) Surface irregularity induced FRP separation**

>

Allowable curvature while strengthening: 3 mm in 1m

>

Since beams are unloaded at moment of strengthening, the curvature of the profile are within allowable limits.

>

>

**(B) Shear crach induced FRP separation**

>

Calculation of $V_{Rd,crack}$

>

**Determination of $V_{Rd,c}$ according to EC2 6.2.2**

>

$$> \; V_{Rd,\,c} := \left(\left(C_{Rd,c} \cdot k \cdot \left(100 \cdot \rho_1 \cdot f_{ck}\right)^{\frac{1}{3}} + k_1 \cdot \sigma_{cp}\right) \cdot b_w \cdot d\right) \geq \left(v_{\min} + k_i \cdot \sigma_{cp}\right) \cdot b_w \cdot d :$$

>

$$> \; \sigma_{cp} := 0 :$$

Partial factors neglected,

$$> \; \gamma_c := 1.0 :$$

$$> \; k_2 := 0.18 :$$

$$> \; C_{Rd,\,c} := \frac{k_2}{\gamma_c} :$$

$$> \; k := evalf\left(\min\left(\left(1 + \operatorname{sqrt}\left(\frac{200}{d}\right)\right), 2\right)\right);$$

$$k := 1.892643685 \qquad (2)$$

Using measured compression strength

$$> \; f_{ck} := f_{cm};$$

$$f_{ck} := 60.37333331 \qquad (3)$$

$$> \; b_w := b :$$

$$> \; \rho_1 := evalf\left(\frac{A_s}{b_w \cdot d}\right);$$

$$\rho_1 := 0.005402390438 \qquad (4)$$

>

$$> \; V_{Rd,\,c1} := evalf\left(\left(C_{Rd,\,c} \cdot k \cdot \left(100 \cdot \rho_1 \cdot f_{ck}\right)^{\frac{1}{3}}\right) \cdot b_w \cdot d\right);$$

$$V_{Rd,c1} := 68301.79797 \qquad (5)$$

$$> \; v_{\min} := 0.0035 \cdot \left(k^{\frac{3}{2}}\right) \cdot f_{ck}^{\frac{1}{2}};$$

$$v_{\min} := 0.07080988862 \qquad (6)$$

>

$$> \; V_{Rd,\,c2} := evalf\left(v_{\min} \cdot b_w \cdot d\right);$$

$$(7)$$

$$V_{Rd,c2} := 4443.320512 \quad (7)$$

>

> $V_{Rd,\,c} := \max\left(V_{Rd,\,c1}, V_{Rd,\,c2}\right);$

$$V_{Rd,c} := 68301.79797 \quad (8)$$

**Determination of Vs,eff according to TR55**

> $\varepsilon_{sv,\,eff} := \dfrac{10^{-5}}{\mathrm{sqrt}\left(\alpha_{flex} \cdot \alpha_{w} \cdot \left(\dfrac{E_{fd}}{E_{s}}\right) \cdot \left(\dfrac{t_{f}}{d}\right)^{1.3}\right)}:$

>

> $\alpha_{flex} := \dfrac{I_{cs} - I_{cc}}{I_{cc}}:$

> $\alpha_{w} := \min\left(\dfrac{b}{b_{f}}, 3\right):$

**Moment of inertia, unstrengthened, cracked, equivalent cross section**

>

> $\alpha_{s} := \dfrac{E_{s}}{E_{cm}};$

$$\alpha_{s} := 5.300950738 \quad (9)$$

> $\alpha_{f} := \dfrac{E_{f}}{E_{cm}};$

$$\alpha_{f} := 4.373284359 \quad (10)$$

> $y_1 := evalf\left(solve\left(\dfrac{b \cdot x_1^{\,2}}{2} = \alpha_{s} \cdot A_{s} \cdot \left(d - x_1\right), x_1\right)\right);$

$$y_1 := 53.31058355,\ -67.68676195 \quad (11)$$

> $x_1 := \max\left(y_1\right);$

$$x_1 := 53.31058355 \quad (12)$$

> $I_{cc} := \dfrac{1}{3} \cdot b \cdot x_1^{\,3} + \alpha_{s} \cdot A_{s} \cdot \left(d - x_1\right)^2;$

$$I_{cc} := 8.285542242\ 10^{7} \quad (13)$$

**Moment of inertia, strengthened cracked section**

>

> $y_2 := evalf\left(solve\left(\dfrac{b \cdot x_2^{\,2}}{2} = \alpha_{s} \cdot A_{s} \cdot \left(d - x_2\right) + \alpha_{f} \cdot A_{f} \cdot \left(h - x_2\right), x_2\right)\right);$

$$y_2 := 61.09867024,\ -79.67320163 \quad (14)$$

> $x_2 := \max\left(y_2\right);$

(15)

$$x_2 := 61.09867024 \quad \textbf{(15)}$$

> $I_{cs} := \frac{1}{3} \cdot b \cdot x_2^{\,3} + \alpha_s \cdot A_s \cdot \left(d - x_2\right)^2 + \alpha_f \cdot A_f \left(h - x_2\right)^2;$

$$I_{cs} := 1.137641823\ 10^8 \quad \textbf{(16)}$$

>

> $\alpha_{flex} := \frac{I_{cs} - I_{cc}}{I_{cc}};$

$$\alpha_{flex} := 0.3730445030 \quad \textbf{(17)}$$

> $b_f := 2 \cdot w_f:$

> $\alpha_w := \min\left(\frac{b}{b_f}, 3\right);$

$$\alpha_w := \frac{5}{2} \quad \textbf{(18)}$$

Neglecting partial factors for FRP E-modulus

> $\varepsilon_{sv,eff} := \frac{10^{-5}}{\operatorname{sqrt}\left(\alpha_{flex} \cdot \alpha_w \cdot \left(\frac{E_f}{E_s}\right) \cdot \left(\frac{t_f}{d}\right)^{1.3}\right)};$

$$\varepsilon_{sv,eff} := 0.0003674877003 \quad \textbf{(19)}$$

Conservative lower bound

> $\#\varepsilon_{sv,\,eff} := 0.00025:$

>

> $s := 110:$

> $A_{sw} := 32 \cdot \mathrm{Pi}:$

> $V_{S,\,eff} := \frac{d}{s} \cdot A_{sw} \cdot E_s \cdot \varepsilon_{sv,\,eff};$

$$V_{S,eff} := 16859.84940 \quad \textbf{(20)}$$

> $V_{Rd,\,c} + V_{S,\,eff};$

$$85161.64737 \quad \textbf{(21)}$$

>

**Determination of 0.67$V_{Rd,s}$ according to EC2 6.2.3**

>

> $V_{Rd,\,s} := \frac{A_{sw}}{s} \cdot z \cdot f_{ywd} \cdot \cot(\theta):$

>

**Crack angle θ=22**

>

> $\theta := \frac{22 \cdot \mathrm{Pi}}{180}:$

> $\gamma_s := 1.0:$

> $f_{ywd} := \frac{f_{yk}}{\gamma_s}:$

> $z := 0.9 \cdot d:$

> $V_{Rd,\,s,\,\theta 22} := evalf\left(\frac{A_{sw}}{s} \cdot z \cdot f_{ywd} \cdot \frac{\cos(\theta)}{\sin(\theta)}\right);$

$$V_{Rd,s,\theta 22} := 255495.8466 \qquad (22)$$

**Crack angle θ=45**

>

> $\theta := \frac{45 \cdot \mathrm{Pi}}{180}:$

> $V_{Rd,\,s,\,\theta 45} := evalf\left(\frac{A_{sw}}{s} \cdot z \cdot f_{ywd} \cdot \frac{\cos(\theta)}{\sin(\theta)}\right);$

$$V_{Rd,s,\theta 45} := 103227.0226 \qquad (23)$$

**Crack angle θ=39**

>

> $\theta := \frac{39 \cdot \mathrm{Pi}}{180}:$

> $V_{Rd,\,s,\,\theta 39} := evalf\left(\frac{A_{sw}}{s} \cdot z \cdot f_{ywd} \cdot \frac{\cos(\theta)}{\sin(\theta)}\right);$

$$V_{Rd,s,\theta 39} := 127474.7566 \qquad (24)$$

**Crack angle θ=40**

>

> $\theta := \frac{40 \cdot \mathrm{Pi}}{180}:$

> $V_{Rd,\,s,\,\theta 40} := evalf\left(\frac{A_{sw}}{s} \cdot z \cdot f_{ywd} \cdot \frac{\cos(\theta)}{\sin(\theta)}\right);$

$$V_{Rd,s,\theta 40} := 123021.1751 \qquad (25)$$

>

**Results**

>

> $0.67 \cdot V_{Rd,s,\theta 22};$

$$171182.2172 \qquad (26)$$

> $0.67 \cdot V_{Rd,\,s,\,\theta 39};$

$$85408.08692 \qquad (27)$$

> $0.67 \cdot V_{Rd,\,s,\,\theta 40};$

$$82424.18732 \qquad (28)$$

> $0.67 \cdot V_{Rd,s,\theta 45};$

(29)

$$69162.10514 \quad (29)$$

> $V_{Rd,c} + V_{S,eff};$

$$85161.64737 \quad (30)$$

For angled up to 40 degrees the $V_{Rd,c} + V_{S,eff}$ are governing. Assumed governing value for $V_{Rd,crack}$

>

> $V_{Rd,\,crack} := V_{Rd,\,c} + V_{S,\,eff};$

$$V_{Rd,crack} := 85161.64737 \quad (31)$$

$V_{Ed}$ are determined at the support

> $P := 206 :$

> $q := 0.25 \cdot 0.3 \cdot 25 :$

> $L := 2 :$

> $V_{Ed} := \left( \frac{P}{2} + \frac{q \cdot L}{2} \right) \cdot 10^3;$

$$V_{Ed} := 104875.0000 \quad (32)$$

> **if** $(V_{Ed} \geq V_{Rd,\,crack})$ **then** *print*( Not *OK*) **else** *print*(*OK*) **end if**;

$$\text{Not } OK \quad (33)$$

>

When $V_{Ed}$ is larger than $V_{Rd,crack}$ Transverse U-wrap must be applied to ensure no shear crack induced separation.

>

**(C) Longitudinal shear stress in yield zone**

>

**1) Deteermine My, the moment which the steel first yields of the strengthened section and associated stress in FRP σfy**

>

When steel reaches yielding we can expect cracked section, derive $M_y$ using triangular stress distribution for concrete in compression.

Ref. figure 10.6 ACI 440.2R-08 For stress and strain under service load

> 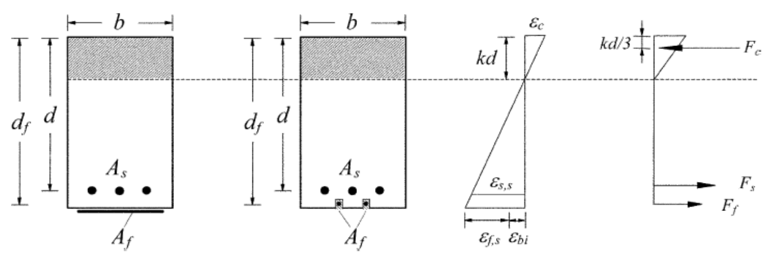


Fig. 10.6—Elastic strain and stress distribution.

> $\varepsilon_y := \frac{f_{yk}}{E_s} :$

> $\varepsilon_f := \frac{(h - x_c)}{(d - x_c)} \cdot \varepsilon_y :$

>

Neutral axis found from second moment of area of transformed, concrete equivalent cracked section.

>

> $x_{NA} := solve\left(\frac{b \cdot x^2}{2} = \alpha_s \cdot A_s \cdot (d - x) + \alpha_f \cdot A_f \cdot (h - x), x\right);$

$$x_{NA} := 61.09867024, -79.67320163 \quad \textbf{(34)}$$

> $x_c := \max(x_{NA});$

$$x_c := 61.09867024 \quad \textbf{(35)}$$

> $\varepsilon_f := \frac{(h - x_c)}{(d - x_c)} \cdot \varepsilon_y;$

$$\varepsilon_f := 0.003145071840 \quad \textbf{(36)}$$

> $M_y := \left(f_{yk} \cdot A_s \cdot \left(d - \frac{1}{3} \cdot x_c\right) + \left(\varepsilon_f \cdot E_f \cdot A_f \cdot \left(h - \frac{1}{3} \cdot x_c\right)\right)\right) \cdot 10^{-6};$

$$M_y := 56.50589779 \quad \textbf{(37)}$$

>

Associated stress in FRP

>

> $\sigma_{fy} := \varepsilon_f \cdot E_f;$

$$\sigma_{fy} := 518.9368536 \quad \textbf{(38)}$$

>

**(2) Determine Med with accosiated σfmax and εfmax**

Using load at actual failure from experimental test Pavg=206

>

> $P := 206 :$

>

> $M_{Ed} := \left(\frac{P}{2} \cdot 0.75 + \frac{q \cdot L^2}{8}\right) \cdot 10^6;$

$$M_{Ed} := 7.818750000\ 10^7 \quad \textbf{(39)}$$

>

Determine associated neutral axis depth and developed strain in CFRP for applied load

Unsubscribe x and εf

> $x :='x':$

> $\varepsilon_f :='\varepsilon_f':$

>

Known relation

> *# equation for moment capacity*

> *#1.* $\boldsymbol{M_{Ed} = f_{yk} \cdot A_s \cdot (d - \delta_G \cdot x) + \varepsilon_f \cdot E_f \cdot A_f \cdot (h - \delta_G \cdot x) :}$

> *#3 unknown parameters* $\varepsilon_f$, $\delta_G$ and $x$

> *#Evaluate definition of* $\delta_G$

> $\#\delta_G := \dfrac{8 - 1000\cdot\varepsilon_c}{4\cdot\left(6 - 1000\cdot\varepsilon_c\right)}$

> *#concrete strain derived with similar triangles dependen on x and* $\varepsilon_f$

> $\#\varepsilon_c := \varepsilon_f\cdot\dfrac{x}{h-x}$

> *#Rewrite* $\delta_G$ *as expression of* $\varepsilon_c$ and $x$

>

> $\#\delta_G := \dfrac{8 - 1000\cdot\left(\varepsilon_f\cdot\dfrac{x}{h-x}\right)}{4\cdot\left(6 - 1000\cdot\left(\varepsilon_f\cdot\dfrac{x}{h-x}\right)\right)}$

> *#Rewrite equation 1. with expression for* $\delta_G$

> $\#1.1.\ \ M_{Ed} = f_{yk}\cdot A_s\cdot\left(d - \left(\dfrac{8 - 1000\cdot\left(\varepsilon_f\cdot\dfrac{x}{h-x}\right)}{4\cdot\left(6 - 1000\cdot\left(\varepsilon_f\cdot\dfrac{x}{h-x}\right)\right)}\right)\cdot x\right) + \varepsilon_f\cdot E_f\cdot A_f\cdot\left(h - \left(\dfrac{8 - 1000\cdot\left(\varepsilon_f\cdot\dfrac{x}{h-x}\right)}{4\cdot\left(6 - 1000\cdot\left(\varepsilon_f\cdot\dfrac{x}{h-x}\right)\right)}\right)\cdot x\right)$

> *#We now have 1 equation, 2 unknowns,* $\varepsilon_f$ and $x$

>

> *#Force equlibrium*

> $\boldsymbol{\#2.\ \psi\cdot x\cdot b\cdot f_{cm} = f_{yk}\cdot A_s + \varepsilon_f\cdot E_f\cdot A_f}$

> *#3 unknown parameters* $\varepsilon_f$, $\psi$ and $x$

> $\#\psi := 1000\cdot\varepsilon_c\cdot\left(0.5 - \dfrac{1000}{12}\cdot\varepsilon_c\right)$

> *#Rewrite with expression for* $\varepsilon_c$

> $\#\psi = 1000\cdot\left(\varepsilon_f\cdot\dfrac{x}{h-x}\right)\cdot\left(0.5 - \dfrac{1000}{12}\cdot\left(\varepsilon_f\cdot\dfrac{x}{h-x}\right)\right)$

> *#Rewrite 2. with expression for* $\psi$

> $\#2.\ 2\ \left(1000\cdot\left(\varepsilon_f\cdot\dfrac{x}{h-x}\right)\cdot\left(0.5 - \dfrac{1000}{12}\cdot\left(\varepsilon_f\cdot\dfrac{x}{h-x}\right)\right)\right)\cdot x\, b\, f_{cm} = f_{yk}\cdot A_s + \varepsilon_f\cdot E_f\cdot A_f$

>

> *#We now have two equations, 2 unknowns can solve for* $\varepsilon_f$ and $x$

>

> $\#1.\ \ M_{Ed} = f_{yk}\cdot A_s\cdot\left(d - \left(\dfrac{8 - 1000\cdot\left(\varepsilon_f\cdot\dfrac{x}{h-x}\right)}{4\cdot\left(6 - 1000\cdot\left(\varepsilon_f\cdot\dfrac{x}{h-x}\right)\right)}\right)\cdot x\right) + \varepsilon_f\cdot E_f\cdot A_f\cdot\left(h\right.$

$$-\left(\frac{8-1000\cdot\left(\varepsilon_f\cdot\frac{x}{h-x}\right)}{4\cdot\left(6-1000\cdot\left(\varepsilon_f\cdot\frac{x}{h-x}\right)\right)}\right)\cdot x\Bigg)$$

>

> #2. $\left(1000\cdot\left(\varepsilon_f\cdot\frac{x}{h-x}\right)\cdot\left(0.5-\frac{1000}{12}\cdot\left(\varepsilon_f\cdot\frac{x}{h-x}\right)\right)\right)\cdot x\cdot b\cdot f_{cm}=f_{yk}\cdot A_s+\varepsilon_f\cdot E_f\cdot A_f$

>

>

>

Solving equation 2 with respect to εf we get two roots

> $w := solve\left(\left(1000\cdot\left(\varepsilon_f\cdot\frac{x}{h-x}\right)\cdot\left(0.5-\frac{1000}{12}\cdot\left(\varepsilon_f\cdot\frac{x}{h-x}\right)\right)\right)\cdot x\cdot b\cdot f_{cm}=\left(f_{yk}\cdot A_s+\varepsilon_f\cdot E_f\cdot A_f\right),\ \varepsilon_f\right);$

$$w := \frac{1}{x^3}\Big(1.987632509\ 10^{-12}\Big(-1.509333333\ 10^{9}\ x^2-3.960000000\ 10^{9}\ x + 1.188000000\ 10^{12} + \left(2.278087110\ 10^{18}\ x^4-2.215701333\ 10^{19}\ x^3-3.570494399\ 10^{21}\ x^2-9.408960000\ 10^{21}\ x + 1.411344000\ 10^{24}\right)^{1/2}\Big)\ (-300.+x)\Big),$$
$$-\frac{1}{x^3}\Big(1.987632509\ 10^{-12}\Big(1.509333333\ 10^{9}\ x^2 + \left(2.278087110\ 10^{18}\ x^4-2.215701333\ 10^{19}\ x^3-3.570494399\ 10^{21}\ x^2-9.408960000\ 10^{21}\ x + 1.411344000\ 10^{24}\right)^{1/2} + 3.960000000\ 10^{9}\ x-1.188000000\ 10^{12}\Big)\ (-300.+x)\Big) \tag{40}$$

>

Fiest root

> $\varepsilon_{f.1} := w[1];$

$$\varepsilon_{f.1} := \frac{1}{x^3}\Big(1.987632509\ 10^{-12}\Big(-1.509333333\ 10^{9}\ x^2-3.960000000\ 10^{9}\ x + 1.188000000\ 10^{12} + \left(2.278087110\ 10^{18}\ x^4-2.215701333\ 10^{19}\ x^3-3.570494399\ 10^{21}\ x^2-9.408960000\ 10^{21}\ x + 1.411344000\ 10^{24}\right)^{1/2}\Big)\ (-300.+x)\Big) \tag{41}$$

>

Second root

> $\varepsilon_{f.2} := w[2];$

$$\varepsilon_{f.2} := -\frac{1}{x^3}\Big(1.987632509\ 10^{-12}\Big(1.509333333\ 10^{9}\ x^2 \tag{42}$$

$$+\left(2.278087110\ 10^{18}\,x^4-2.215701333\ 10^{19}\,x^3-3.570494399\ 10^{21}\,x^2-9.408960000\ 10^{21}\,x+1.411344000\ 10^{24}\right)^{1/2}+3.960000000\ 10^{9}\,x-1.188000000\ 10^{12}\Big)\ (-300.+x)\Big)$$

>

Replacing the εf term in equation 1 we can solve for x

>

Trial with first root of above equation

Defining εf

> $\varepsilon_f := \varepsilon_{f.1}:$

>

> $$u_1 := solve\left(M_{Ed}=f_{yk}\cdot A_s\cdot\left(d-\left(\frac{8-1000\cdot\left(\varepsilon_f\cdot\frac{x}{h-x}\right)}{4\cdot\left(6-1000\cdot\left(\varepsilon_f\cdot\frac{x}{h-x}\right)\right)}\right)\cdot x\right)+\varepsilon_f\cdot E_f\cdot A_f\cdot\left(h-\left(\frac{8-1000\cdot\left(\varepsilon_f\cdot\frac{x}{h-x}\right)}{4\cdot\left(6-1000\cdot\left(\varepsilon_f\cdot\frac{x}{h-x}\right)\right)}\right)\cdot x\right),x\right);$$

$$u_1 := 43.39125030,\ -48.69895478+166.7713088\,\mathrm{I},\ -46.06514759,\ -622.2709805,\ -48.69895478-166.7713088\,\mathrm{I} \tag{43}$$

>

We know result are not negative or imaginary, therfore x derived by first root for εf can be defined

> $x_1 := u_1[1];$

$$x_1 := 43.39125030 \tag{44}$$

>

Trial with second root for εf

Defining εf

>

> $\varepsilon_f := w[2]:$

>

> $$u_2 := solve\left(M_{Ed}=f_{yk}\cdot A_s\cdot\left(d-\left(\frac{8-1000\cdot\left(\varepsilon_f\cdot\frac{x}{h-x}\right)}{4\cdot\left(6-1000\cdot\left(\varepsilon_f\cdot\frac{x}{h-x}\right)\right)}\right)\cdot x\right)+\varepsilon_f\cdot E_f\cdot A_f\cdot\left(h-\left(\frac{8-1000\cdot\left(\varepsilon_f\cdot\frac{x}{h-x}\right)}{4\cdot\left(6-1000\cdot\left(\varepsilon_f\cdot\frac{x}{h-x}\right)\right)}\right)\cdot x\right),x\right);$$

$$u_2 := 3.584922149\ 10^{-9},\ 90.94166216,\ -702.9585826 \tag{45}$$

We know x should be close to x derived for theoretical moment capacity: #42.33186978 therfore solutions for second root of εf are not realistic.

>

Defining x as the real, positive root found from first root of εf, the other variables can be determined.

>

> $x := x_1;$

$$x := 43.39125030 \tag{46}$$

Using derived x values as input in first root of εf we get correspoding strain

>

> $\varepsilon_f := \varepsilon_{f.1};$

$$\varepsilon_f := 0.006784027933 \tag{47}$$

Verification when using x as input in expression 2, we get the corresponding roots.

> $\varepsilon_f :='\varepsilon_f';$

$$\varepsilon_f := \varepsilon_f \tag{48}$$

> $w := solve\left(\left(1000 \cdot \left(\varepsilon_f \cdot \frac{x}{h-x}\right) \cdot \left(0.5 - \frac{1000}{12} \cdot \left(\varepsilon_f \cdot \frac{x}{h-x}\right)\right)\right) \cdot x \cdot b \cdot f_{cm} = \left(f_{yk} \cdot A_s + \varepsilon_f \cdot E_f \cdot A_f\right), \varepsilon_f\right);$

$$w := 0.006784027921, 0.01601085731 \tag{49}$$

Same result as given in (47), solution ok!

>

εfmax and σfmax can then be determined for the associated maximum moment

> $\varepsilon_f := \varepsilon_{f.1}:$

> $\varepsilon_{fmax} := \varepsilon_f;$

$$\varepsilon_{fmax} := 0.006784027933 \tag{50}$$

> $\sigma_{fmax} := \varepsilon_{fmax} \cdot E_f;$

$$\sigma_{fmax} := 1119.364609 \tag{51}$$

>

Verification of the other variables to compare to theoretical capacity

>

> $\varepsilon_c := \varepsilon_f \cdot \frac{x}{h-x};$

$$\varepsilon_c := 0.001147145039 \tag{52}$$

> $\psi := 1000 \cdot \varepsilon_c \cdot \left(0.5 - \frac{1000}{12} \cdot \varepsilon_c\right);$

$$\psi := 0.4639107078 \tag{53}$$

> $\delta_G := \frac{8 - 1000 \cdot \varepsilon_c}{4 \cdot \left(6 - 1000 \cdot \varepsilon_c\right)};$

$$\delta_G := 0.3530321335 \tag{54}$$

>

**(3) For the applied load, determine distance Δx along the beam between the moment at yield My and max moment Med.**

>

Applying a linear approach of bending moment diagram, defining Δx with likesided triangles.

>

Rewrite My to Nmm

> $M_y := M_y \cdot 10^6 :$

>

> $\dfrac{M_y}{M_{Ed}}$

$$0.7226973338 \tag{55}$$

> $x_{dif} := \dfrac{M_y}{M_{Ed}} \cdot 750;$

$$x_{dif} := 542.0230004 \tag{56}$$

> $\Delta_x := 750 - x_{dif};$

$$\Delta_x := 207.9769996 \tag{57}$$

**(4) Calculate $\tau_m$, the mean longitudinal shear stress due to the gradient of the nominal axial stress in the FRP between minimun and maximum moment loactions along the yield zone.**

>

> $\tau_m := t_f \cdot \left( \dfrac{\sigma_{fmax} - \sigma_{fy}}{\Delta_x} \right);$

$$\tau_m := 3.464389369 \tag{58}$$

**(5) Calculate $\tau_{sc}$, the additional longitudinal shear stress due to stress concentration at the positions of flexural cracks in the yield zone**

>

> $f_{ctk} := 2.98 :$ *#From tensile splitting test*

> $\tau_{sc} := 7.8 \cdot \left( 1.1 - \left( \dfrac{M_y}{M_{Ed}} \right) \right) \cdot f_{ctk};$

$$\tau_{sc} := 8.770023171 \tag{59}$$

**(6) Determine $\tau_t$, the total combined longitudinal shear stress in the yields zone.**

>

> $\tau_t := \tau_m + \tau_{sc};$

$$\tau_t := 12.23441254 \tag{60}$$

**(7) Longitudinal shear strength must fullfill below criteria**

> $\tau_t \leq \tau_{lim,y} = 4.5 \dfrac{f_{ctk}}{\gamma_C}$

>

> $\tau_{\lim,\,y} := \frac{4.5 \cdot f_{ctk}}{\gamma_c};$

$$\tau_{lim,y} := 13.41000000 \quad (61)$$

> **if** $\left(\tau_t \le \tau_{\lim,\,y}\right)$ **then** *print*(*OK*! *Longitudinal shear stress within allowable limits*)
> **else** *print*(Not *OK*! *Longitudinal shear stress exceeds allowable limit*) **end if**;

*OK*! *Longitudinal shear stress within allowable limits* **(62)**

>

**(D) Strain in FRP**

Should be checked to ensure strain in FRP does not exceed rupture strain of FRP. Since rupture rarely is goverened failure mode for beams, this verification is not neccesary.

>

Partial factors for E-modulus omitted

> $\varepsilon_{mt} := \varepsilon_{fmax} + 0.114 \cdot \frac{\tau_{sc}}{\mathrm{sqrt}\left(E_f \cdot t_f\right)};$

$$\varepsilon_{mt} := 0.009030872331 \quad (63)$$

Criterion:

> $\varepsilon_{mt} \le \varepsilon_{fd}:$

Neglecting partial factors

> $\varepsilon_{fk} := 0.0176:$

> $\varepsilon_{fd} := \varepsilon_{fk};$

$$\varepsilon_{fd} := 0.0176 \quad (64)$$

> **if** $\left(\varepsilon_{mt} \le \varepsilon_{fd}\right)$ **then** *print*('*OK*! *below rupture strain*') **end if**;

*OK*! *below rupture strain* **(65)**

> $'\varepsilon_{mt} \le \varepsilon_{fd}'$

$$\varepsilon_{mt} \le \varepsilon_{fd} \quad (66)$$

**(E) Longitudinal shear stress near ends of FRP**

For surface mounted reinforcement, near the ends of the plates the concrete and steel reinforcement can be assumed to behave linearly elastic (i.e outside regions where the reinforcement has yielded).

>

Verification

>

> $\tau \le \tau_{\lim,\,c}:$

>

Longitudinal shear stress at end of the FRP reinforcement are defined

>

> $\tau := \frac{V_{add} \cdot \alpha_f \cdot A_f \cdot (h - x)}{I_{cs} \cdot b_a}:$

>

> $\#V_{add}$ = difference between the ultimate shear force and the applied shear force when strengthening is installed.

> $\#I_{cs}$ = moment of inertia of strengthened equivalent cracked concrete section.

> $\#x$= depth of neutral axis of strengthened section

>

Since no load are applied while strengthening, $V_{add}$ is the applied point load

>

> $V_{add} := 103 \cdot 10^3$ :

> $b_a := 2 \cdot w_f$:

> $\alpha_f := \frac{E_f}{E_{cm}}$ :

> $y := evalf\left(solve\left(\frac{b \cdot x_i^2}{2} = \alpha_s \cdot A_s \cdot \left(d - x_i\right) + \alpha_f \cdot A_f \cdot \left(h - x_i\right), x_i\right)\right)$ :

> $x := \max(y)$;

$$x := 61.09867024 \tag{67}$$

> $I_{cs} := \frac{1}{3} \cdot b \cdot x^3 + \alpha_s \cdot A_s \cdot (d - x)^2 + \alpha_f \cdot A_f \cdot (h - x)^2$;

$$I_{cs} := 1.137641823\ 10^8 \tag{68}$$

> $\tau := \frac{V_{add} \cdot \alpha_f \cdot A_f \cdot (h - x)}{I_{cs} \cdot b_a}$;

$$\tau := 1.135113282 \tag{69}$$

Limiting shear stress

>

> $\tau_{lim,c} := 0.8 \cdot \frac{f_{ctk}}{\gamma_c}$;

$$\tau_{lim,c} := 2.384000000 \tag{70}$$

>

> $\tau \le \tau_{\mathrm{lim},\, c}$;

$$1.135113282 \le 2.384000000 \tag{71}$$

> **if** $\left(\tau \le \tau_{\mathrm{lim},\, c}\right)$ **then** *print*(*OK*! *Longitudinal shear stress near ends of FRP within allowable limits*) **else** *print*·(Not *OK*! *Longitudinal shear stress near ends of FRP exceeds allowable limit*) **end if**;

*OK*! *Longitudinal shear stress near ends of FRP within allowable limits* **(72)**

**(F) Anchorage design**

>

The maximum ultimate bond force $T_{kmax}$, and the corresponding maximum anchorage length $l_{tmax}$ are calculated with following expression.

> $T_{k,\,\max} := 0.5 \cdot k_b \cdot b_f \cdot \mathrm{sqrt}\left(E_{fd} \cdot t_f \cdot f_{ctk}\right)$ :

> $k_b := evalf\left(\max\left(1.06 \cdot \mathrm{sqrt}\left(\frac{2 - \frac{b_f}{b}}{1 + \frac{b_f}{400}}\right), 1\right)\right)$;

$$k_b := 1.199253101 \tag{73}$$

> $T_{k,max} := 0.5 \cdot k_b \cdot b_f \cdot \mathrm{sqrt}\left(E_f \cdot t_f \cdot f_{ctk}\right) \cdot 10^{-3}$;

$$T_{k,max} := 46.05975056 \tag{74}$$

> $l_{t,\,\max} := 0.7 \cdot \mathrm{sqrt}\left(\frac{E_f \cdot t_f}{f_{ctk}}\right)$;

$$l_{t,max} := 180.4357143 \tag{75}$$

> $l_{t,\,\max} := 500$ :

The anchorage zone starts at the intersection when the strengthned moment exceeds the unstrengthened capacity.

Unstrengthened capacity

> $M_{Rd,\,us} := 41.56162412 \cdot 10^6$ :

Location of intersection

> $x_{loc} := \frac{M_{Rd,\,us}}{M_{Ed}} \cdot 750$;

$$x_{loc} := 398.6726534 \tag{76}$$

Find corresponding force in FRP at point of intersection x

> $M_{Rd,\,us} \leq M_y$;

$$4.156162412\ 10^7 \leq 5.650589779\ 10^7 \tag{77}$$

$M_{Rd,us}$ is lower than yielding moment $M_y$, linear elastic region.
Steel has not reaches yield stress

Force in FRP at point in span where moment exceeds the original moment

> $T_{FRP} := \frac{M_{Rd,us} \cdot \alpha_f \cdot A_f \cdot \left(h - x_{cs}\right)}{I_{cs}} \cdot 10^{-3}$ :

> $NA := evalf\left(solve\left(\frac{b \cdot x_i^2}{2} = \alpha_s \cdot A_s \cdot (d - x_i) + \alpha_f \cdot A_f \cdot (h - x_i), x_i\right)\right):$

> $x_{cs} := \max(NA);$

$$x_{cs} := 61.09867024 \qquad (78)$$

> $I_{cs} := \frac{1}{3} \cdot b \cdot x_{cs}^3 + \alpha_s \cdot A_s \cdot (d - x_{cs})^2 + \alpha_f \cdot A_f \cdot (h - x_{cs})^2;$

$$I_{cs} := 1.137641823\ 10^8 \qquad (79)$$

> $T_{FRP} := \frac{M_{Rd,\ us} \cdot \alpha_f \cdot A_f \cdot (h - x_{cs})}{I_{cs}} \cdot 10^{-3};$

$$T_{FRP} := 45.80305974 \qquad (80)$$

Developed force in FRP are less than $T_{k,max}$

> $T_{FRP} < T_{k,\ \max};$

$$45.80305974 < 46.05975056 \qquad (81)$$

>

Avaliable anchorage length

> $l_{avaliable} := x_{loc};$

$$l_{avaliable} := 398.6726534 \qquad (82)$$

CFRP plates terminates 50 mm from support, this gives an avaliable anchorage length, $l_t$

>

> $l_t := x_{loc} - 50;$

$$l_t := 348.6726534 \qquad (83)$$

Avaliable anchorage length less than minimum anchorage length

> $l_t < l_{t,\ \max}$

$$348.6726534 < 500 \qquad (84)$$

>

Reduction in bond bond force

> $T_k := \left(\frac{T_{k,max} \cdot l_t}{l_{t,max}}\right) \cdot \left(2 - \frac{l_t}{l_{t,max}}\right);$

$$T_k := 41.84068369 \qquad (85)$$

> $'T_{FRP} \geq T_k'$

$$T_{FRP} \geq T_k \qquad (86)$$

>

> **if** $(T_k \leq T_{FRP})$ **then** *print*(*Bond force exceeded, risk of anchorage failure*)
> **else** *print*(*Bond force sufficient, anchorage OK*) **end if**;

*Bond force exceeded, risk of anchorage failure* **(87)**

Anchorage not sufficient for applied load

>

# Appendix G

>

**Comparison of procedure and result from Sika CarboDur software**
**Using design parameters for CFRP**

>

> $restart;$

>

Material properties and dimensions

> $f_{cm} := 60.37333331 :$

> $E_{cm} := 22 \cdot \left(\frac{f_{cm}}{10}\right)^{0.3} \cdot 10^3 :$ *#EC2 Table 3.1*

> $f_{yk} := 500 :$

> $E_s := 200 \cdot 10^3 :$

> $b := 250 : h := 300 : c_{nom} := 35 :$

> $\varnothing_{L_b} := 12 :$

> $\varnothing_s := 8 :$

> $d := h - c_{nom} - \varnothing_s - \frac{\varnothing_{L_b}}{2} :$

> $A_s := 339 :$

>

**Carbodur s512**

> $no := 2 :$ *#No of plates*

> $t_f := 1.2 :$

> $w_f := 50 :$

> $A_f := no \cdot t_f \cdot w_f :$ *#mm²*

> $E_f := 165 \cdot 10^3 :$ *#MPa*

> $\varepsilon_f := 0.0176 :$

> $\varepsilon_{f,\,\mathrm{lim}} := 0.008 :$

> $\gamma_{FRP,\,m} := 1.05 :$

> $\gamma_{FRP,\,E} := 1.1 :$

> $\gamma_{FRP,\,\varepsilon} := 1.25 :$

>

> $E_{fd} := \frac{E_f}{\gamma_{FRP,\,m} \cdot \gamma_{FRP,\,E}};$

$$E_{fd} := 142857.1428 \qquad (1)$$

> $\varepsilon_{fd} := \dfrac{\varepsilon_f}{\gamma_{FRP,\,m} \cdot \gamma_{FRP,\,\varepsilon}};$

$$\varepsilon_{fd} := 0.01340952381 \quad \textbf{(2)}$$

First moment capacity is reduced when calculated with design E modulus. Therfore derivation on moment capacity must be performed. Same procedure as before with Ef replaced with Efd.

>

Start by assuming an initial neutral axis, choose value close to previous result. FRP strain limit 0.008

>

> $\varepsilon_f := 0.008 :$

> $x_i := 0.2 \cdot d :$

>

Strain compatibility then gives correspondin concrete strain.

> $\varepsilon_c := \varepsilon_f \cdot \dfrac{x_i}{(h - x_i)};$

$$\varepsilon_c := 0.001607686149 \quad \textbf{(3)}$$

> $\#\varepsilon_c < 0.002$

>

> **for** $i$ **from** 1 **to** 70 **do**
$\#\, print(\text{' '}) :$
$\#print(\text{'Iteration'}, i) :$

$\varepsilon_i := \dfrac{\varepsilon_f \cdot x_i}{(h - x_i)} :$

$\psi := 1000 \cdot \varepsilon_i \cdot \left(0.5 - \dfrac{1000}{12} \cdot \varepsilon_i\right) : \delta_G := \dfrac{8 - 1000 \cdot \varepsilon_i}{4 \cdot (6 - 1000 \cdot \varepsilon_i)} : F_f := \varepsilon_f \cdot E_{fd} \cdot A_f : F_s := f_{yk} \cdot A_s :$

$F_t := F_f + F_s : F_c := \psi \cdot x_i \cdot b \cdot f_{cm} :$

$x_i := \dfrac{F_t}{\psi \cdot b \cdot f_{cm}};$

**od**:

>

Considered converged

>

> $F_c \approx F_t;$

$$306641.3767 \approx 306642.8570 \quad \textbf{(4)}$$

> $\varepsilon_c := \varepsilon_i;$

$$\varepsilon_c := 0.001259994806 \quad \textbf{(5)}$$

> $x := x_i;$

(6)

$$x := 40.82078601 \quad \textbf{(6)}$$

> $\varepsilon_s := (\varepsilon_f) \cdot \frac{(d-x)}{(h-x)};$

$$\varepsilon_s := 0.006487533032 \quad \textbf{(7)}$$

> $M_{Rd,st} := \left(f_{yk} \cdot A_s \cdot (d - \delta_G \cdot x) + \varepsilon_f \cdot E_{fd} \cdot A_f \cdot (h - \delta_G \cdot x)\right) \cdot 10^{-6};$

$$M_{Rd,st} := 79.23760683 \quad \textbf{(8)}$$

Applied load

>

> $q := 0.25 \cdot 0.3 \cdot 25 :$

> $L := 2 :$

> $P := 206 :$

> $M_{Ed} := \left(\frac{P}{2} \cdot 0.75 + \frac{q \cdot L^2}{8}\right);$

$$M_{Ed} := 78.18750000 \quad \textbf{(9)}$$

**(A) Surface irregularity induced FRP separation**

>

Allowable curvature while strengthening: 3 mm in 1m

Since beams are unloaded at moment of strengthening, the curvature of the profile are within allowable limits.

>

**(B) Shear crach induced FRP separation**

>

Check #$V_{Ed} \leq V_{Rd,crack}$:

>

Calculation of $V_{Rd,crack}$

**Determination of $V_{Rd,c}$ according to EC2 6.2.2**

Partial factors neglected for steel and concrete negelcted.

> $\gamma_c := 1.0 :$

> $k_2 := 0.18 :$

> $C_{Rd,\,c} := \frac{k_2}{\gamma_c} :$

> $k := evalf\left(\min\left(\left(1 + \mathrm{sqrt}\left(\frac{200}{d}\right)\right), 2\right)\right) :$

Using measured compression strength

> $f_{ck} := f_{cm} :$

> $b_w := b :$

> $\rho_1 := evalf\left(\frac{A_s}{b_w \cdot d}\right) :$

> $V_{Rd,\,c1} := evalf\left(\left(\left(C_{Rd,\,c}\cdot k\cdot\left(100\cdot\rho_1\cdot f_{ck}\right)^{\frac{1}{3}}\right)\cdot b_w\cdot d\right)\right):$

> $v_{\min} := 0.0035\cdot\left(k^{\frac{3}{2}}\right)\cdot f_{ck}^{\frac{1}{2}}:$

>

> $V_{Rd,\,c2} := evalf\left(v_{\min}\cdot b_w\cdot d\right):$

> $V_{Rd,\,c} := \max\left(V_{Rd,\,c1}, V_{Rd,\,c2}\right);$

$$V_{Rd,c} := 68301.79797 \tag{10}$$

**Determination of VS,eff according to TR55**

> $\varepsilon_{sv,\,eff} := \dfrac{10^{-5}}{\mathrm{sqrt}\left(\alpha_{flex}\cdot\alpha_w\cdot\left(\frac{E_{fd}}{E_s}\right)\cdot\left(\frac{t_f}{d}\right)^{1.3}\right)}:$

>

**Moment of inertia, unstrengthened equivalent cross section**

>

> $\alpha_s := \dfrac{E_s}{E_{cm}};$

$$\alpha_s := 5.300950738 \tag{11}$$

> $\alpha_f := \dfrac{E_{fd}}{E_{cm}};$

$$\alpha_f := 3.786393383 \tag{12}$$

> $y_1 := evalf\left(solve\left(\dfrac{b\cdot x_1^{\,2}}{2} = \alpha_s\cdot A_s\cdot\left(d - x_1\right), x_1\right)\right);$

$$y_1 := 53.31058355, -67.68676195 \tag{13}$$

> $x_1 := \max\left(y_1\right);$

$$x_1 := 53.31058355 \tag{14}$$

> $I_{cc} := \dfrac{1}{3}\cdot b\cdot x_1^{\,3} + \alpha_s\cdot A_s\cdot\left(d - x_1\right)^2;$

$$I_{cc} := 8.285542242\ 10^7 \tag{15}$$

>

**Moment of inertia, strengthened cracked section**

>

> $y_2 := evalf\left(solve\left(\dfrac{b\cdot x_2^{\,2}}{2} = \alpha_s\cdot A_s\cdot\left(d - x_2\right) + \alpha_f\cdot A_f\cdot\left(h - x_2\right), x_2\right)\right);$

$$y_2 := 60.13200158, -78.14311763 \tag{16}$$

> $x_2 := \max\left(y_2\right);$

$$x_2 := 60.13200158 \quad \textbf{(17)}$$

> $I_{cs} := \frac{1}{3} \cdot b \cdot x_2^{3} + \alpha_s \cdot A_s \cdot (d - x_2)^2 + \alpha_f \cdot A_f \cdot (h - x_2)^2;$

$$I_{cs} := 1.097284206\ 10^{8} \quad \textbf{(18)}$$

> $\alpha_{flex} := \frac{I_{cs} - I_{cc}}{I_{cc}};$

$$\alpha_{flex} := 0.3243360229 \quad \textbf{(19)}$$

> $b_f := 2 \cdot w_f:$

> $\alpha_w := \min\left(\frac{b}{b_f}, 3\right);$

$$\alpha_w := \frac{5}{2} \quad \textbf{(20)}$$

> $\varepsilon_{sv,eff} := \frac{10^{-5}}{\mathrm{sqrt}\left(\alpha_{flex} \cdot \alpha_w \cdot \left(\frac{E_{fd}}{E_s}\right) \cdot \left(\frac{t_f}{d}\right)^{1.3}\right)};$

$$\varepsilon_{sv,eff} := 0.0004235615504 \quad \textbf{(21)}$$

Conservative lower bound

> $\#\varepsilon_{sv,\ eff} := 0.00025 :$

> $s := 110 :$

> $A_{sw} := 32 \cdot \mathrm{Pi} :$

> $V_{S,\ eff} := \frac{d}{s} \cdot A_{sw} \cdot E_s \cdot \varepsilon_{sv,\ eff};$

$$V_{S,eff} := 19432.44344 \quad \textbf{(22)}$$

> $V_{Rd,\ c} + V_{S,\ eff};$

$$87734.24141 \quad \textbf{(23)}$$

>

**Determination of 0.67VRd,s according to EC2 6.2.3**

>

>

**Crack angle θ=22**

>

> $\theta := \frac{22 \cdot \mathrm{Pi}}{180} :$

> $\gamma_s := 1.0 :$

> $f_{ywd} := \frac{f_{yk}}{\gamma_s} :$

> $z := 0.9 \cdot d :$

> $V_{Rd,\,s,\,\theta22} := evalf\left(\frac{A_{sw}}{s} \cdot z \cdot f_{ywd} \cdot \frac{\cos(\theta)}{\sin(\theta)}\right);$

$$V_{Rd,s,\theta22} := 255495.8466 \quad (24)$$

>

**Crack angle θ=45**

>

> $\theta := \frac{45 \cdot \mathrm{Pi}}{180}$ :

> $V_{Rd,\,s,\,\theta45} := evalf\left(\frac{A_{sw}}{s} \cdot z \cdot f_{ywd} \cdot \frac{\cos(\theta)}{\sin(\theta)}\right);$

$$V_{Rd,s,\theta45} := 103227.0226 \quad (25)$$

>

**Crack angle θ=39**

>

> $\theta := \frac{39 \cdot \mathrm{Pi}}{180}$ :

> $V_{Rd,\,s,\,\theta39} := evalf\left(\frac{A_{sw}}{s} \cdot z \cdot f_{ywd} \cdot \frac{\cos(\theta)}{\sin(\theta)}\right);$

$$V_{Rd,s,\theta39} := 127474.7566 \quad (26)$$

**Crack angle θ=38**

>

> $\theta := \frac{38 \cdot \mathrm{Pi}}{180}$ :

> $V_{Rd,\,s,\,\theta38} := evalf\left(\frac{A_{sw}}{s} \cdot z \cdot f_{ywd} \cdot \frac{\cos(\theta)}{\sin(\theta)}\right);$

$$V_{Rd,s,\theta38} := 132124.5638 \quad (27)$$

>

**Results**

>

> $0.67 \cdot V_{Rd,s,\theta22};$

$$171182.2172 \quad (28)$$

> $0.67 \cdot V_{Rd,s,\theta45};$

$$69162.10514 \quad (29)$$

> $0.67 \cdot V_{Rd,\,s,\,\theta39};$

$$85408.08692 \quad (30)$$

> $0.67 \cdot V_{Rd,\,s,\,\theta38};$

$$88523.45775 \quad (31)$$

> $V_{Rd,c} + V_{S,eff};$

$$87734.24141 \quad (32)$$

For angled up to 38 degrees $V_{Rd,c} + V_{S,eff}$ are governing. Assumed governing value for $V_{Rd,crack}$

>

> $V_{Rd,\,crack} := V_{Rd,\,c} + V_{S,\,eff};$

$$V_{Rd,crack} := 87734.24141 \tag{33}$$

$V_{Ed}$ are determined at the support

> $P := 206:$

> $q := 0.25 \cdot 0.3 \cdot 25:$

> $L := 2:$

> $V_{Ed} := \left(\frac{P}{2} + \frac{q \cdot L}{2}\right) \cdot 10^3;$

$$V_{Ed} := 104875.0000 \tag{34}$$

> **if** $\left(V_{Ed} \geq V_{Rd,\,crack}\right)$ **then** *print*( Not *OK*) **else** *print*(*OK*) **end if**;

Not *OK* **(35)**

>

When $V_{Ed}$ is larger than $V_{Rd,crack}$ Transverse U-wrap must be applied to ensure no shear crack induced separation.

>

**(C) Longitudinal shear stress in yield zone**

>

**1) Deteermine My, the moment which the steel first yields of the strengthened section and associated stress in FRP σfy**

>

> $\varepsilon_y := evalf\left(\frac{f_{yk}}{E_s}\right):$

> $\varepsilon_f := \frac{(h - x)}{(d - x)} \cdot \varepsilon_y:$

>

Neutral axis found from second moment of area of transformed, concrete equivalent cracked section.

> $x :=$'x':

> $x_{NA} := solve\left(\frac{b \cdot x^2}{2} = \alpha_s \cdot A_s \cdot (d - x) + \alpha_f \cdot A_f \cdot (h - x), x\right);$

$$x_{NA} := 60.13200158,\ -78.14311763 \tag{36}$$

> $x_c := \max(x_{NA});$

$$x_c := 60.13200158 \tag{37}$$

> $\varepsilon_f := \frac{(h - x_c)}{(d - x_c)} \cdot \varepsilon_y;$

$$\varepsilon_f := 0.003141804812 \tag{38}$$

> $M_y := \left(f_{yk} \cdot A_s \cdot \left(d - \frac{1}{3} \cdot x_c\right) + \left(\varepsilon_f \cdot E_{fd} \cdot A_f \cdot \left(h - \frac{1}{3} \cdot x_c\right)\right)\right) \cdot 10^{-6};$

$$M_y := 54.22533517 \tag{39}$$

>

Associated nominal stress in FRP

> $\sigma_{fy} := \varepsilon_f \cdot E_{fd};$

$$\sigma_{fy} := 448.8292587 \quad \textbf{(40)}$$

**(2) Determine Med with accosiated σfmax and εfmax**

Using load at actual failure from experimental test Pavg=206 with maximum developed strain and corresponding stress in FRP

Since difference from MRd and MEd are small, maxumin theoretical stress and strain for FRP are used.

>

> $M_{Ed} := \left(\frac{P}{2} \cdot 0.75 + \frac{q \cdot L^2}{8}\right) \cdot 10^6;$

$$M_{Ed} := 7.818750000\ 10^7 \quad \textbf{(41)}$$

> $\varepsilon_{fmax} := 0.008 :$

> $\sigma_{fmax} := \varepsilon_{fmax} \cdot E_{fd};$

$$\sigma_{fmax} := 1142.857142 \quad \textbf{(42)}$$

>

**(3) For the applied load, determine distance Δx along the beam between the sections of first yield My and max moment Med.**

>

Applying a linear approach of bending moment diagram, defining Δx with likesided triangles.

>

Rewrite My to Nmm

> $M_y := M_y \cdot 10^6;$

$$M_y := 5.422533517\ 10^7 \quad \textbf{(43)}$$

> $\frac{M_y}{M_{Ed}}$

$$0.6935294666 \quad \textbf{(44)}$$

> $x_{dif} := \frac{M_y}{M_{Ed}} \cdot 750;$

$$x_{dif} := 520.1471000 \quad \textbf{(45)}$$

> $\Delta_x := 750 - x_{dif};$

$$\Delta_x := 229.8529000 \quad \textbf{(46)}$$

**(4) Calculate τm, the mean longitudinal shear stress due to the gradient of the nominal axial stress in the FRP between minimun and maximum moment loactions along the yield zone.**

> $\tau_m := t_f \cdot \left(\frac{\sigma_{fmax} - \sigma_{fy}}{\Delta_x}\right);$

**(47)**

$$\tau_m := 3.623332401 \tag{47}$$

**(5) Calculate τsc, the additional longitudinal shear stress due to stress concentration at the positions of flexural cracks in the yield zone**

> $f_{ctk} := 2.98$ : *#From tensile splitting test*

> $\tau_{sc} := 7.8 \cdot \left(1.1 - \left(\frac{M_y}{M_{Ed}}\right)\right) \cdot f_{ctk};$

$$\tau_{sc} := 9.448001082 \tag{48}$$

**(6) Determine τt, the total combined longitudinal shear stress in the yields zone.**

> $\tau_t := \tau_m + \tau_{sc};$

$$\tau_t := 13.07133348 \tag{49}$$

**(7) Longitudinal shear strength must fullfill below criteria**

> $\tau_t \le \tau_{\text{lim,y}} = 4.5 \frac{f_{\text{ctk}}}{\gamma_C}$

> $\tau_{\text{lim}, y} := \frac{4.5 \cdot f_{ctk}}{\gamma_c};$

$$\tau_{lim,y} := 13.41000000 \tag{50}$$

> **if** $\left(\tau_t \le \tau_{\text{lim}, y}\right)$ **then** *print*(*OK*! *Longitudinal shear stress within allowable limits*)
**else** *print*(Not *OK*! *Longitudinal shear stress exceeds allowable limit*) **end if**;

*OK*! *Longitudinal shear stress within allowable limits* **(51)**

>

**(D) Strain in FRP**

>

> $\varepsilon_{mt} := \varepsilon_{fmax} + 0.114 \cdot \frac{\tau_{sc}}{\text{sqrt}\left(E_{fd} \cdot t_f\right)};$

$$\varepsilon_{mt} := 0.01060137632 \tag{52}$$

Criterion:

> $\varepsilon_{mt} \le \varepsilon_{fd}$ :

>

> $\varepsilon_{fk} := 0.0176$ :

> $\gamma_{FRP,\varepsilon} := 1.25$ :

> $\gamma_{FRP, m} := 1.05$ :

> $\varepsilon_{fd} := \frac{\varepsilon_{fk}}{\gamma_{FRP, \varepsilon} \cdot \gamma_{FRP, m}};$

$$\varepsilon_{fd} := 0.01340952381 \tag{53}$$

> if $\left(\varepsilon_{mt} \le \varepsilon_{fd}\right)$ **then** *print*('*OK*! *below rupture strain*') **end if**;

$$\text{OK! below rupture strain} \tag{54}$$

> $'\varepsilon_{mt} \le \varepsilon_{fd}'$

$$\varepsilon_{mt} \le \varepsilon_{fd} \tag{55}$$

**(E) Longitudinal shear stress near ends of FRP**

Verification

> $\tau \le \tau_{\mathrm{lim},\,c}$ :

Longitudinal shear stress at end of the FRP reinforcement are defined

>

> $\tau := \dfrac{V_{add} \cdot \alpha_f \cdot A_f \cdot (h - x)}{I_{cs} \cdot b_a}$ :

> $V_{add} := 103 \cdot 10^3$ :

> $b_a := 2 \cdot w_f$:

>

**Modular ratio $\alpha_f$ defined with design E-modulus in TR55**

> $\alpha_f := \dfrac{E_{fd}}{E_{cm}}$ :

> $x :='x'$:

> $y := evalf\left(solve\left(\dfrac{b \cdot x^2}{2} = \alpha_s \cdot A_s \cdot (d - x) + \alpha_f \cdot A_f \cdot (h - x), x\right)\right)$;

$$y := 60.13200158,\ -78.14311763 \tag{56}$$

> $x := \max(y)$ :

> $I_{cs} := \dfrac{1}{3} \cdot b \cdot x^3 + \alpha_s \cdot A_s \cdot (d - x)^2 + \alpha_f \cdot A_f \cdot (h - x)^2$;

$$I_{cs} := 1.097284206\ 10^{8} \tag{57}$$

> $\tau := \dfrac{V_{add} \cdot \alpha_f \cdot A_f \cdot (h - x)}{I_{cs} \cdot b_a}$;

$$\tau := 1.023051240 \tag{58}$$

>

**Limiting shear stress**

>

> $\tau_{lim,c} := 0.8 \cdot \dfrac{f_{ctk}}{\gamma_c}$;

$$\tau_{lim,c} := 2.384000000 \tag{59}$$

> $\tau \le \tau_{\mathrm{lim},\,c}$;

$$1.023051240 \le 2.384000000 \tag{60}$$

> **if** $\left(\tau \le \tau_{\mathrm{lim},\,c}\right)$ **then** *print*(*OK*! *Longitudinal shear stress near ends of FRP within allowable limits*) **else** *print*·(Not *OK*! *Longitudinal shear stress near ends of FRP exceeds allowable limit*) **end if**;

*OK*! *Longitudinal shear stress near ends of FRP within allowable limits* **(61)**

>

**(F) Anchorage design**

>

The maximum ultimate bond force Tkmax, and the corresponding maximum anchorage length ltmax are calculated with following expression.

>

> $T_{k,\,\max} := 0.5 \cdot k_b \cdot b_f \cdot \mathrm{sqrt}\left(E_{fd} \cdot t_f \cdot f_{ctk}\right)$ :

>

> $k_b := evalf\left(\max\left(1.06 \cdot \mathrm{sqrt}\left(\frac{2 - \frac{b_f}{b}}{1 + \frac{b_f}{400}}\right), 1\right)\right)$;

$$k_b := 1.199253101 \quad \textbf{(62)}$$

> $T_{k,max} := 0.5 \cdot k_b \cdot b_f \cdot \mathrm{sqrt}\left(E_{fd} \cdot t_f \cdot f_{ctk}\right) \cdot 10^{-3}$;

$$T_{k,max} := 42.85787062 \quad \textbf{(63)}$$

> $l_{t,\,\max} := 0.7 \cdot \mathrm{sqrt}\left(\frac{E_{fd} \cdot t_f}{f_{ctk}}\right)$;

$$l_{t,max} := 167.8925831 \quad \textbf{(64)}$$

>

> $l_{t,\,\max} := 500$ :

>

Unstrengthened capacity

> $M_{Rd,\,us} := 41.56162412 \cdot 10^6$;

$$M_{Rd,us} := 4.156162412\ 10^7 \quad \textbf{(65)}$$

Location of intersection

> $x_{loc} := \frac{M_{Rd,\,us}}{M_{Ed}} \cdot 750$;

$$x_{loc} := 398.6726534 \quad \textbf{(66)}$$

Find corresponding force in FRP at point of intersection x

>

> $M_{Rd,\,us} \le M_y$;

$$4.156162412\ 10^7 \le 5.422533517\ 10^7 \quad \textbf{(67)}$$

$> \; T_{CFRP} := \frac{M_{Rd,us} \cdot \alpha_f \cdot A_f \cdot (h - x_{cs})}{I_{cs}} \cdot 10^{-3} :$

$> \; \alpha_f := \frac{E_{fd}}{E_{cm}} :$

$> \; x := 'x':$

$> \; y := evalf\left( solve\left( \frac{b \cdot x^2}{2} = \alpha_s \cdot A_s \cdot (d - x) + \alpha_f \cdot A_f \cdot (h - x), x \right) \right) :$

$> \; x_{cs} := \max(y);$

$$x_{cs} := 60.13200158 \qquad (68)$$

$> \; I_{cs} := \frac{1}{3} \cdot b \cdot x_{cs}^{\;3} + \alpha_s \cdot A_s \cdot (d - x_{cs})^2 + \alpha_f \cdot A_f \cdot (h - x_{cs})^2;$

$$I_{cs} := 1.097284206\ 10^8 \qquad (69)$$

Force in FRP at point in span where moment exceeds the original moment

$>$

$> \; T_{CFRP} := \frac{M_{Rd,\,us} \cdot \alpha_f \cdot A_f \cdot (h - x_{cs})}{I_{cs}} \cdot 10^{-3};$

$$T_{CFRP} := 41.28123409 \qquad (70)$$

CFRP plates terminates 50 mm from support, this gives an avaliable anchorage length, lt

$> \; l_t := x_{loc} - 50;$

$$l_t := 348.6726534 \qquad (71)$$

Avaliable anchorage length less than minimum anchorage length

$> \; l_t < l_{t,\,\max}$

$$348.6726534 < 500 \qquad (72)$$

$>$

Reduced bond force

$>$

$> \; T_k := \left( \frac{T_{k,max} \cdot l_t}{l_{t,max}} \right) \cdot \left( 2 - \frac{l_t}{l_{t,max}} \right);$

$$T_k := 38.93209553 \qquad (73)$$

$>$

$> \; T_k < T_{CFRP};$

$$38.93209553 < 41.28123409 \qquad (74)$$

$>$ **if** $(T_k \le T_{CFRP})$ **then** *print*(*Bond force exceeded, risk of anchorage failure*)
**else** *print*(*Bond force sufficient, anchorage OK*) **end if**;

*Bond force exceeded, risk of anchorage failure* **(75)**

Anchorage not sufficient for applied load

$>$

$>$

BUILDING TRUST

# SIKA® CARBODUR® CALCULATION SOFTWARE

## PROJECT: Beam EC

## ELEMENT:

INDEX

## 1. DESIGN CRITERIA AND REGULATIONS

Flexural FRP strengthening of beam

Concrete Society Technical Report No. 55 (TR 55): design guidance for strengthening concrete structures using fibre composite materials, Third Edition 2012.

EN 1992-1-1. Eurocode 2: Design of concrete structures - Part 1-1: General rules and rules for buildings.

Country: Norway

## 2. CALCULATION ASSUMPTIONS

### 2.1. Beam definition

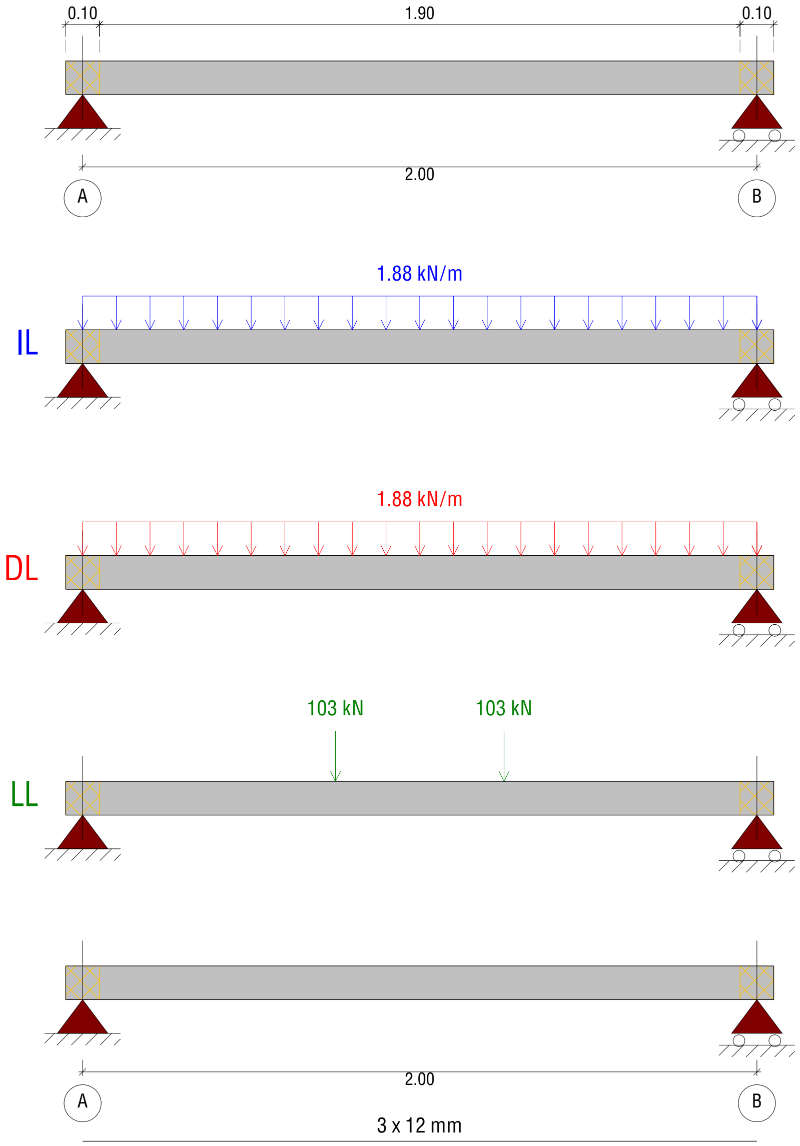


### 2.2. Geometry

Cross section = Rectangled

Width = 250 mm

Height = 300 mm

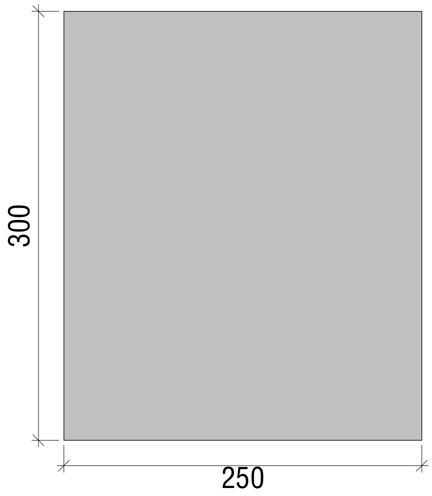


2.3. Concrete

Compressive strength of concrete

Concrete strength ($f_{ck}$) = 60 MPa

Cylinder specimen = 60 MPa

Cube specimen = 75 MPa

2.4. Reinforcing steel

Reinforcement layers

| Bottom layer | $d_1$ mm | Steel $f_{yk}$ (MPa) | $E_s$ (MPa) | Number x Ø (mm) |
|---|---|---|---|---|
| 1. | 49 | (B500C) 500 | 205000 | 3 x 12.0 |

2.5. Strength reduction factors

Defined by (User)

Concrete

$\gamma_c$ (Persistent and transient) = 1.00

$\gamma_c$ (Accidental) = 1.00

$\gamma_c$ (Fire) = 1.00

$\alpha_{cc}$ = 1.00

Steel

$\gamma_s$ (Persistent and transient) = 1.00

$\gamma_s$ (Accidental) = 1.00

$\gamma_s$ (Fire) = 1.00

2.6. Load factors

| User values | Permanent loads | Imposed loads |
|---|---|---|
| Anticipated loads | 1.00 | 1.00 |
| FRP Reinforcement failure | 1.00 | 0.50 |
| Fire situation | 1.00 | 0.30 |
| SLS, characteristic | 1.00 | 1.00 |

3. FRP STRENGTH

3.1. Main FRP reinforcement

Simply bonded. Sika CarboDur® S

| Sika® CarboDur® S512 | Fiber type | Strength reduction factors | $\varepsilon_{fk}$ | $E_{fk}$ (MPa) | $t_f$ (mm) | Number | Width (mm) |
|---|---|---|---|---|---|---|---|
| Layer: 1 | Carbon | $\gamma_{FRP,E}$: 1.10, $\gamma_{FRP,m}$: 1.05, $\gamma_{FRP,\varepsilon}$: 1.25, $\gamma_A$: 4.00 | 0.0176 | 165000.00 | 1.200 | 2 | 50.00 |

4. ANTICIPATED COMBINATIONS OF LOADS

4.1. Beam loads

Initial loads

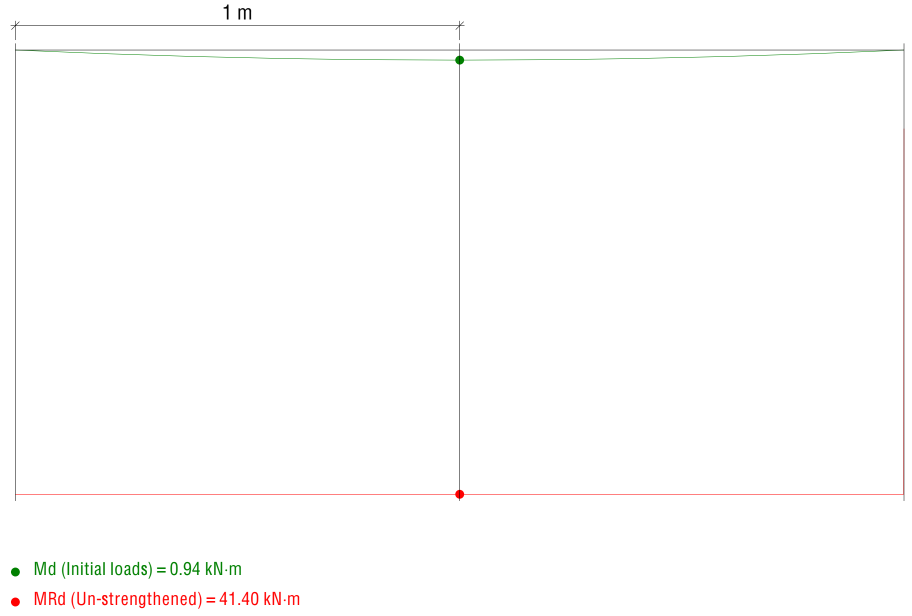

## FRP Reinforcement failure

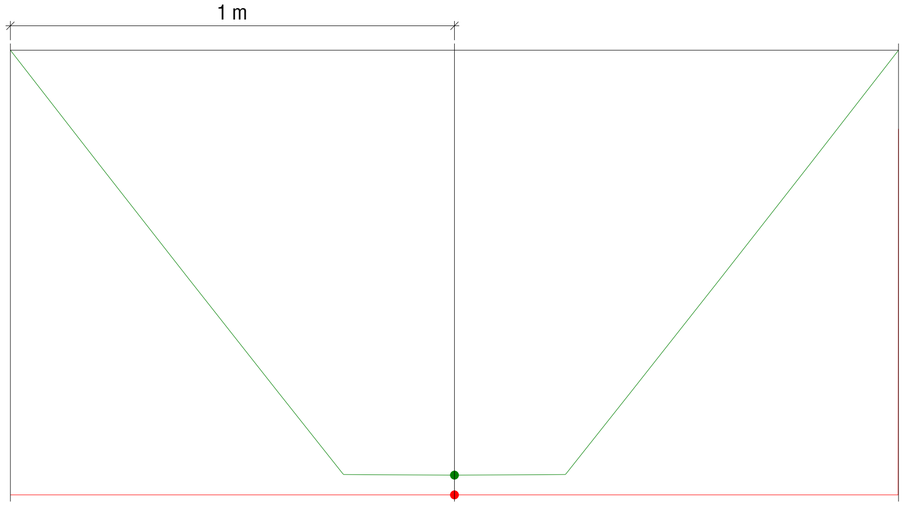


- Md (FRP Reinforcement failure) = 39.57 kN·m
- MRd (Un-strengthened) = 41.40 kN·m

## Anticipated loads

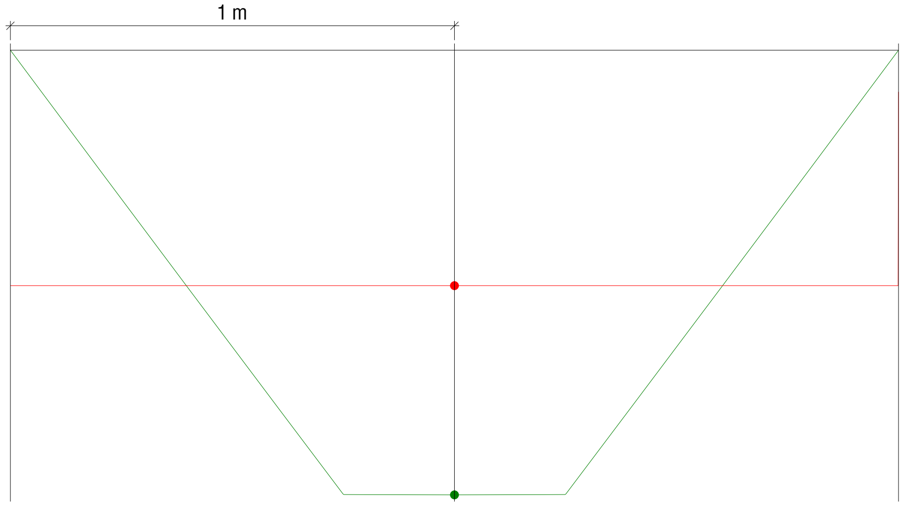


- Md (Anticipated loads) = 78.19 kN·m
- MRd (Un-strengthened) = 41.40 kN·m

Fire situation

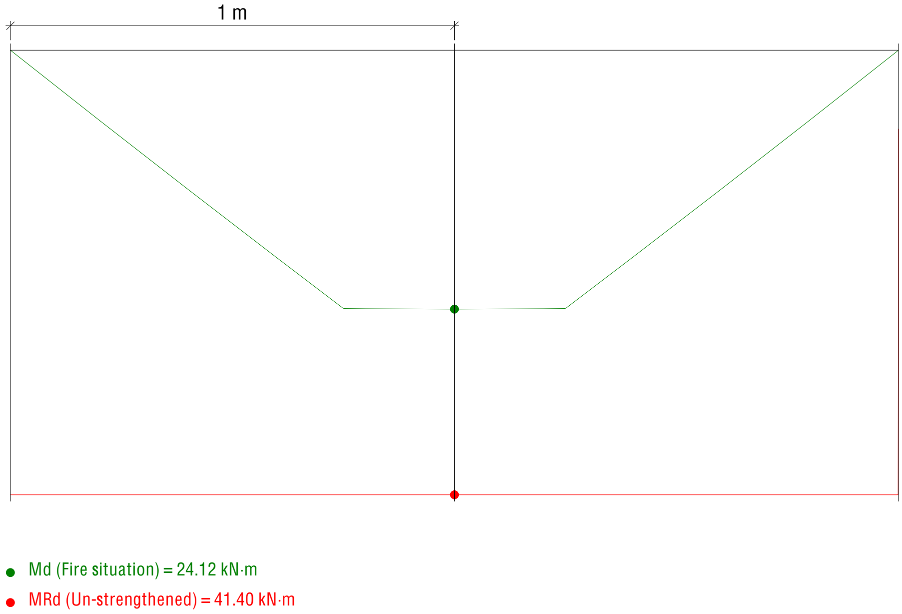


5. RESULTS

5.1. Summary of results

| ULS Anticipated loads | | | |
|---|---|---|---|
| loading | $M_{Ed}$ (kN·m) | $M_{Rd}$ (kN·m) | $M_{Rd} \geq M_{Ed}$ ($N_{Ed} = N_{Rd}$) |
| $S_{Ed} = 1.00 \cdot S_G + 1.00 \cdot S_Q$ | 78.19 | 79.15 | Strengthened section 79.15 kN·m ≥ 78.19 kN·m ✓ |

| ULS Reinforcement failure | | | |
|---|---|---|---|
| loading | $M_{Ed}$ (kN·m) | $M_{Rd}$ (kN·m) | $M_{Rd} \geq M_{Ed}$ ($N_{Ed} = N_{Rd}$) |
| $S_{Ed} = 1.00 \cdot S_G + 0.50 \cdot S_Q$ | 39.57 | 41.40 | Un-strengthened section 41.40 kN·m ≥ 39.57 kN·m ✓ |

| Serviceability limit states | |
|---|---|
| loading | Service stresses |
| $S_{Ed} = 1.00 \cdot S_G + 1.00 \cdot S_Q$ | $\sigma_s \leq 0.8 \cdot f_{yk}$<br>500.00 MPa ≤ 400.00 MPa ✗ |

| Fire resistance (t=0 min.) | | | |
|---|---|---|---|
| loading | $M_{Ed}$ (kN·m) | $M_{Rd}$ (kN·m) | $M_{Rd} \geq M_{Ed}$ ($N_{Ed} = N_{Rd}$) |
| $S_{Ed} = 1.00 \cdot S_G + 0.30 \cdot S_Q$ | 24.12 | 41.40 | Un-strengthened section 41.40 kN·m ≥ 24.12 kN·m ✓ |

5.2. Ultimate limit states

When analysing a cross-section to determine its ultimate moment of resistance, the following assumptions should be made:

> The strain distribution in the concrete in compression and the strains in the reinforcement, whether in tension or compression, are derived from the assumption that plane sections remain plane and that no longitudinal slip occurs between or within the components of the section.

The stresses in the concrete in compression are derived from the stress-strain curve in the section 3.1.7 of EN 1992-1-1.

$$\sigma_c = f_{cd} \cdot \left[1 - \left(1 - \frac{\varepsilon_c}{\varepsilon_{c2}}\right)^n\right] \quad \text{for} \quad 0 \le \varepsilon_c \le \varepsilon_{c2}$$

$$\sigma_c = f_{cd} \quad \text{for} \quad \varepsilon_{c2} < \varepsilon_c \le \varepsilon_{cu2}$$

with

$$f_{cd} = \alpha_{cc} \cdot \frac{f_{ck}}{\gamma_c}$$

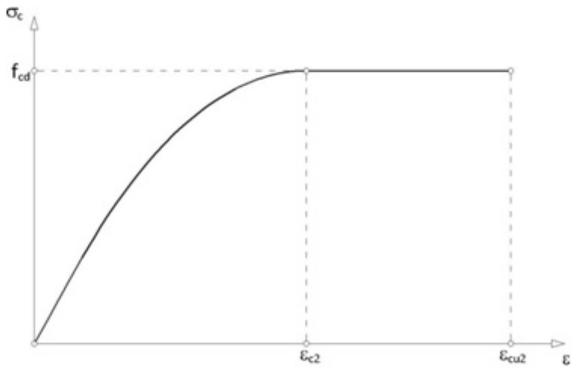


| $f_{cd}$ (MPa) | $\varepsilon_{c2}$ | $\varepsilon_{cu2}$ | n |
|---|---|---|---|
| 60.0 | 0.0020 | 0.0035 | 2 |

The tensile strength of the concrete is ignored.

The stresses in the steel reinforcement are derived from the stress-strain curves in the section 3.2 of EN 1992-1-1.

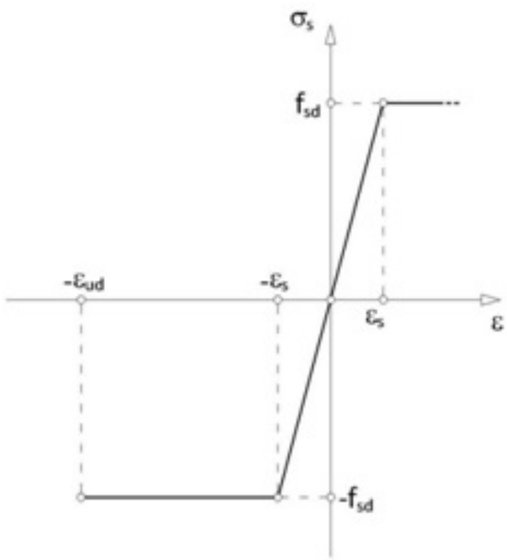


The strains in the cross-section should take into account the strains present in the existing structure at the time of application of the FRP reinforcement.

The stresses in the FRP reinforcement are derived from the assumption that the FRP has a linear elastic characteristic until rupture.

Force balance of section. Initial loads
$M_i = 0.94$ kN·m

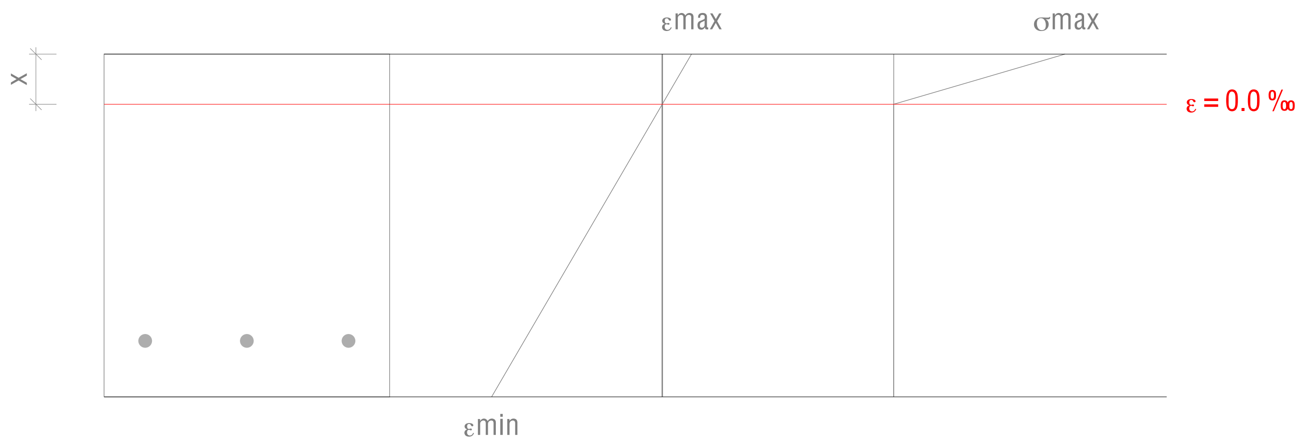


| | |
|---|---|
| Maximum and minimum strain | $\varepsilon_{max} = 0.01$ ‰ |
| | $\varepsilon_{min} = -0.07$ ‰ |
| Maximum stress in concrete | $f_c = 0.72$ MPa |
| Distance from extreme compression fiber to neutral axis | $x = 43.87$ mm |

| Stress and strain of reinforcement | | | |
|---|---|---|---|
| Ref. | Y Coord. (mm) | f (MPa) | ε (‰) |
| No. 12 | -101 | -11.72 | -0.06 |

FRP Reinforcement failure. Minimum combination of loads to be resisted by the un-strengthened member.
$S_{Ed} = 1.00 \cdot S_G + 0.50 \cdot S_Q$

$M_{Rd} \geq M_{Ed}$ 41.40 kN·m ≥ 39.57 kN·m ✓

$M_{Rd}$ : 41.40 kN·m

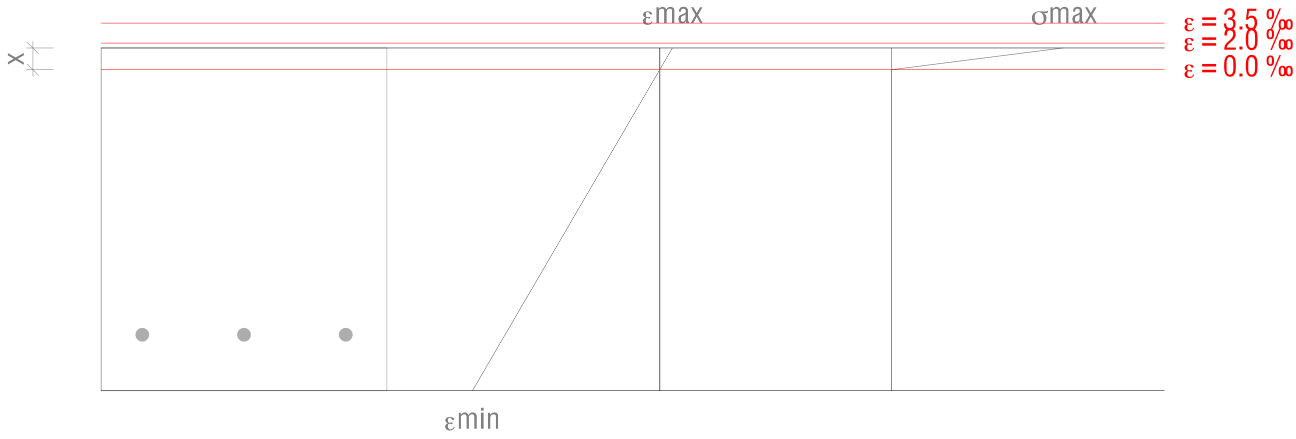


Maximum and minimum strain $\varepsilon_{max} = 1.63$ ‰

$\varepsilon_{min} = -24.10$ ‰

Maximum stress in concrete $f_c = 57.98$ MPa

Distance from extreme compression fiber to neutral axis $x = 19.03$ mm

| Stress and strain of reinforcement | | | |
|---|---|---|---|
| Ref. | Y Coord. (mm) | f (MPa) | ε (‰) |
| No. 12 | -101 | -500.00 | -19.90 |

Strengthened section and expected loads.

$S_{Ed} = 1.00 \cdot S_G + 1.00 \cdot S_Q$

$M_{Rd} \geq M_{Ed}$ 79.15 kN·m ≥ 78.19 kN·m ✓

$M_{Rd}$ : 79.15 kN·m

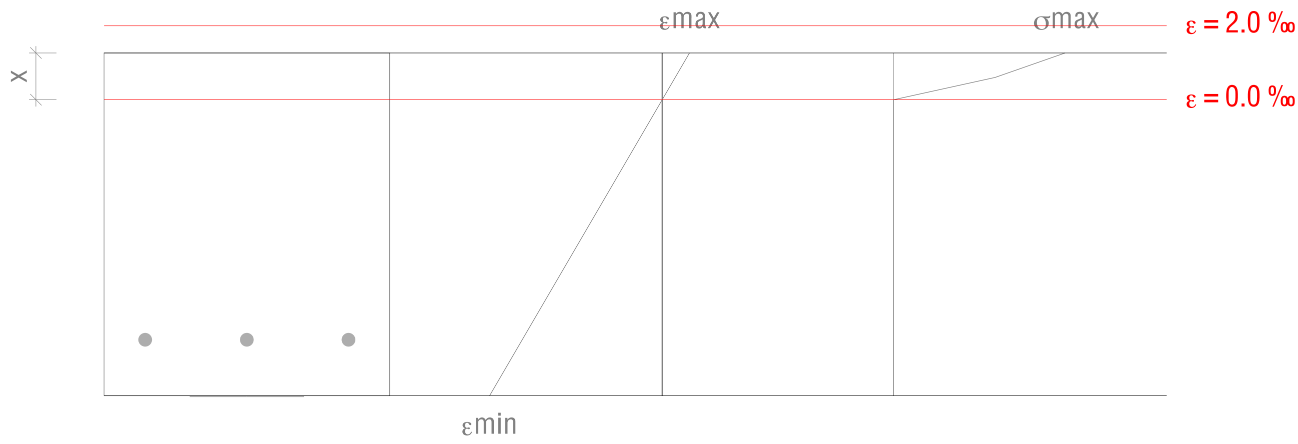


Maximum and minimum strain $\varepsilon_{max} = 1.26$ ‰

$\varepsilon_{min} = -8.01$ ‰

Maximum stress in concrete $f_c = 51.89$ MPa

Distance from extreme compression fiber to neutral axis $x = 40.89$ mm

| Stress and strain of reinforcement | | | |
|---|---|---|---|
| Ref. | Y Coord. (mm) | f (MPa) | ε (‰) |
| No. 12 | -101 | -500.00 | -6.50 |
| FRP | -151 | -1137.14 | -7.96 |

Fire situation. Un-strengthened section.

$S_{Ed} = 1.00 \cdot S_G + 0.30 \cdot S_Q$

$M_{Rd} \geq M_{Ed}$ 41.40 kN·m ≥ 24.12 kN·m ✓

$M_{Rd}$ : 41.40 kN·m

The strength of the un-strengthened member is enough to support the combination of loads corresponding to the fire situation. The FRP strengthening is therefore not necessary during a fire situation, and does not need to be protected. If a certain fire rating is necessary, the designer must evaluate the need for a protection of the RC element (concrete and steel reinforcement) according to the local codes.

5.3. Serviceability limit states

SLS stresses in the steel reinforcement at the characteristic combination of actions should not exceed the relevant design limits in Eurocode 2, part 1-1.

Force balance of section. SLS Characteristic combination of loads

$S_{Ed} = 1.00 \cdot S_G + 1.00 \cdot S_Q$

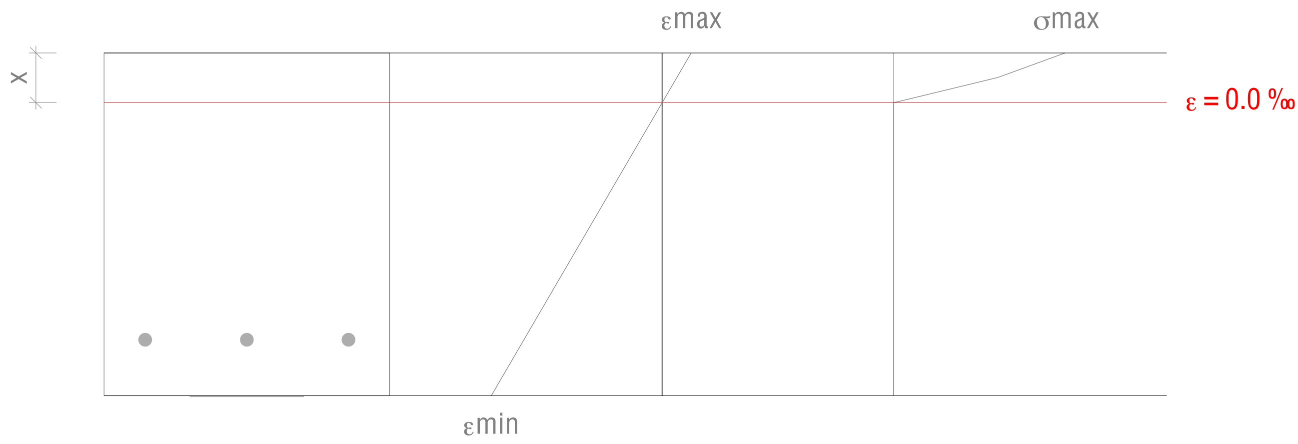


| | |
|---|---|
| Maximum and minimum strain | $\varepsilon_{max} = 1.15$ ‰ |
| | $\varepsilon_{min} = -6.82$ ‰ |
| Maximum stress in concrete | $f_c = 49.27$ MPa |
| Distance from extreme compression fiber to neutral axis | $x = 43.42$ mm |

| Stress and strain of reinforcement | | | |
|---|---|---|---|
| Ref. | Y Coord. (mm) | f (MPa) | ε (‰) |
| No. 12 | -101 | -500.00 | -5.52 |
| FRP | -151 | -1116.24 | -6.77 |

In the case of significant non-static live loads during the hardening of the adhesive, the reduced adhesive strength cannot be determined according to tabulated data as indicated in TR55, 6.9.4, considering that the acting loads during that period correspond to the quasi-permanent load combination.

$\varepsilon_{fe,curing} = 0.001244 > 0.000200$

5.4. Additional check

In addition, if the ultimate moment of resistance is less than 1.15 times the required value, the section should be proportioned such that the strain at the centroid of the tensile steel reinforcement is not less than $0.002 + f_{yk}/(E_s\gamma_s)$.

$$M_{Rd} \leq 1{,}15 \cdot M_{Ed} \quad ; \quad \varepsilon_s \geq 0{,}002 + \frac{f_{yk}}{E_s \cdot \gamma_s}$$

0.00650 ≥ 0.00444 ✓

5.5. FRP separation failure and anchorage design

| | | | | |
|---|---|---|---|---|
| Shear crack induced FRP separation | $V_{Ed} \le V_{Rd,crack}$ | 104.14 kN ≤ 86.39 kN | ✗ | x = 1.60 m |
| Longitudinal shear stress in the yield zone | $\tau_t \le \tau_{lim,y}$ | 12.42 MPa ≤ 13.41 MPa | ✓ | x = [0.64, 0.72] m |
| Strain in the FRP | $\varepsilon_{mt} \le \varepsilon_{fd}$ | 0.01022 ≤ 0.01341 | ✓ | x = 1.00 m |
| Longitudinal shear stress near ends of FRP | $\tau \le \tau_{lim,c}$ | 1.00 MPa ≤ 2.38 MPa | ✓ | x = [1.52, 1.60] m |
| Anchorage | $T_d \le T_k$ | 39.16 kN ≤ 42.86 kN | ✓ | x = 0.40 m |

5.6. Remarks

Shear-crack-induced FRP separation. The presence of shear crack in the member can lead to the initiation of FRP separation failure. Transverse U-Wrap must be applied, both sides (TR55, fig. 26)

5.7. FRP arrangement

The previous results correspond to the following FRP scheme:
FRP main reinforcement: 2 (Sika® CarboDur® S512)

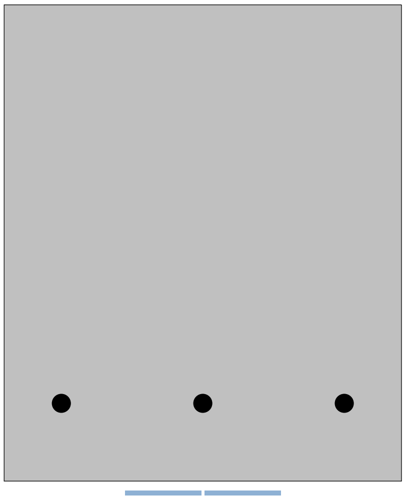

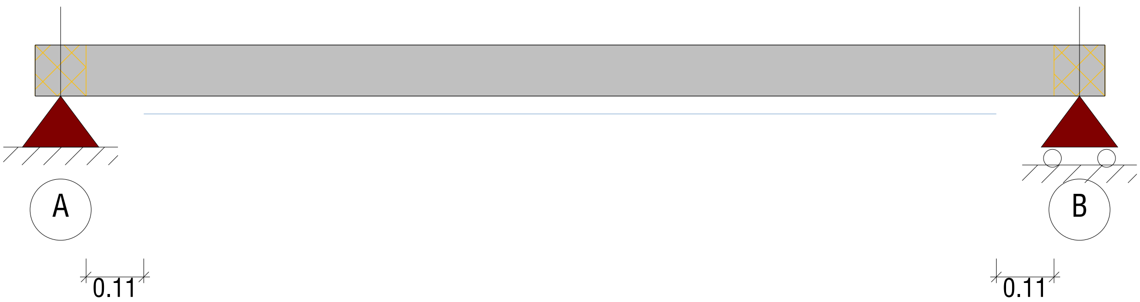

## 6. PRODUCT SPECIFICATION

### 6.1. Bonded Sika CarboDur® plates

The strengthening shall be achieved using pultruded Carbodur plates reinforced polymer laminate, externally bonded to the structure with epoxy adhesive Sikadur®-30.

The material shall be a pultruded, unidirectional CFRP plate, and exhibit a fibre volume content >68%.

The plates shall be straight, flat and free of torsion.

The material shall have a long track record (> 25 years) for structural strengthening.

Test reports regarding reaction of adhesive joint to artificial weathering after 100 days shall be provided.

#### 6.1.1. Concrete surface preparation

Any unsound material shall be removed and removed concrete shall be repaired as described above. Large blowholes and honeycombing shall be filled with a suitable repair mortar.

Repair materials shall be fully compatible with the adhesive.

The actual strength of the concrete substrate shall be verified with at least three pull-off tests.

The concrete shall be older than 28 days.

The laitance layer on the substrate surface shall be removed and an open-textured surface shall be created.

The substrate surface shall be cleaned so that it is free from oil, grease and any other contaminants as well as loose particles and dust.

The substrate moisture content shall be less than 4% pbw.

#### 6.1.2. Sika CarboDur® plates

The materials shall comply with the performance characteristics described as follows:

##### 6.1.2.1. Typical Properties of Sika CarboDur® S plates:

| | | |
|---|---|---|
| Fibre volume content | | > 68% |
| Glass transition temp. | | > 100°C |
| E-Modulus | EN 2561/ASTM D3039 | ≈ 170000 N/mm² (MPa) |
| Tensile Strength | EN 2561/ASTM D3039 | ≈ 3100 N/mm² (MPa) |
| Strain at break | EN 2561/ASTM D3039 | > 1.7% |

#### 6.1.3. Epoxy Adhesive

The material shall be epoxy based, and combine primer, putty and adhesive in one product.

The material shall not release substances dangerous to health, hygiene and the environment.

The material shall be long-term creep resistant proven by independent report.

The material shall meet the requirements of EN 1504-4 as structural bonding product for bonded plate reinforcement.

### 6.1.3.1. Typical Properties of Sikadur®-30 adhesive:

The adhesive must comply with EN 1504-4.

| | |
|---|---|
| Density (parts A+B mixed) at +23°C | 1.65 kg/l + 0.1 kg/l |
| Slant shear strength at steel: | 50° ≥ 50 N/mm² |
| | 60° ≥ 60 N/mm² |
| | 70° ≥ 70 N/mm² |
| Bond/adhesion strength: | ≥ 14 N/mm² |
| Shear strength: | ≥ 12 N/mm² |
| Compressive strength: | ≥ 30 N/mm² |
| Shrinkage / expansion: | ≤ 0.1% |
| Workability: | 85 min. at 23°C |
| Sensitivity to water | Pass |
| Modulus of elasticity: | ≥ 2000 N/mm² |
| Coefficient of thermal expansion: | ≤ 100 x 10-6 |
| Glass transition temperature: | ≥ 40°C |
| Durability | Pass |

Compliance with FIP requirement

| | |
|---|---|
| Sag flow | Non sag up to 3 -5 mm in vertical |
| Squeezability | 4000 m2 at +15°C at 15 kg |
| Volume change | 0.04% |
| Shear strength at 15°C | >14 N/mm² |
| Shear strength at 35°C | >26 N/mm² |
| E-modulus in compression | 9600 N/mm² |
| E-modulus in tensile | 11200 N/mm² |

### 6.1.4. Application procedure

The plates shall be cut to length using either a rotary disc cutter or a hacksaw.

The plates shall be cleaned and degreased with Sika® Colma® Cleaner or an Isopropyl alcohol based cleaner.

The adhesive shall be applied to the plates in a way that it is approximately 1 mm thick on the sides and 2 mm thick in the middle of the plate.

A very thin layer of the adhesive shall be applied to the prepared substrate surface to fill any small voids and irregularities.

The plate shall be placed on the prepared area and pressed onto the substrate, first gently by hand and second with a hard rubber roller, until adhesive material is squeezed out on both sides of the plate. The excess material shall be removed.

In case of plate intersections, the surface of the underlying plate shall be cleaned from dirt and grease and an adhesive ramp shall be applied on both sides of the underlying plate so the top plate is connected to the substrate on the entire area.

The freshly bonded system shall not be disturbed for at least 24 hours and any vibrations shall be kept at a minimum during the curing period of the adhesive.

If necessary, the applied system shall be protected with a suitable coating (compatibility tests between the coating and the laminate shall be available).

## 7. LEGAL DISCLAIMER

THIS SOFTWARE APPLICATION AND THE RESULTS DERIVED FROM ITS UTILIZATION ARE INTENDED ONLY FOR USE BY PROFESSIONAL USERS WITH EXPERT KNOWLEDGE IN THE AREA OF THE INTENDED APPLICATION. USERS MUST INDEPENDENTLY VERIFY THE RESULTS BEFORE ANY USE AND TAKE INTO ACCOUNT THE SITE AND APPLICATION CONDITIONS, PRODUCT DATA SHEET AND PRODUCT LITERATURE, TECHNICAL STATE OF THE ART AS WELL AS LOCAL APPLICABLE STANDARDS AND REGULATIONS.

With respect to the software application and results derived from its use, SIKA MAKES NO WARRANTIES OF ACCURACY, RELIABILITY, COMPLETENESS, MERCHANTABILITY OR FITNESS FOR ANY PURPOSE. THE SOFTWARE APPLICATION IS PROVIDED ON AN "AS-IS" BASIS AND SIKA EXPRESSLY DISCLAIMS ANY WARRANTIES WITH RESPECT TO THE SOFTWARE APPLICATION AND RESULTS DERIVED FROM ITS USE.

Sika shall not be liable for any consequential, punitive, incidental, exemplary, or special damages (including but not limited to loss of business opportunity or loss of profit) arising out of the evaluation or use of the software application and results derived from its use.

The information, and, in particular, the recommendations relating to the application and end-use of Sika products, are given in good faith based on Sika's current knowledge and experience of the products when properly stored, handled and applied under normal conditions in accordance with Sika's recommendations. In practice, the differences in materials, substrates and actual site conditions are such that no warranty in respect of merchantability or of fitness for a particular purpose, nor any liability arising out of any legal relationship whatsoever, can be inferred either from this information, or from any written recommendations, or from any other advice offered. The user of the product must test the product's suitability for the intended application and purpose. Sika reserves the right to change the properties of its products. The proprietary rights of third parties must be observed. All orders are accepted subject to our current terms of sale and delivery. Users must always refer to the most recent issue of the local Product Data Sheet for the product concerned, copies of which will be supplied on request.

Except as indicated otherwise, all information, text, graphic images, features, functions, and layout contained in this software are the exclusive property of Sika and may not be copied or distributed, in whole or in part, without the Company's express written consent.

By transmitting information to Sika, you grant to the Company the unrestricted irrevocable license to use, reproduce, display, modify, distribute and perform such information. Personal identity information is used by Sika only to process a request for information by you or for marketing our products and services.



## 8. ABOUT SIKA® CARBODUR® CALCULATION SOFTWARE

Engineered by:

cype

Cype Software - Eusebio Sempere, 5 - 03003 Alicante (Spain)

www.cype.com

# Appendix I

>

**Moment capacity derived with differeent debonding strain limits**

>

> $restart;$

> $f_{cm} := 60.37333331 : E_{cm} := 22 \cdot \left(\frac{f_{cm}}{10}\right)^{0.3} \cdot 10^3 :$

> $f_{yk} := 500 : E_s := 200 \cdot 10^3 :$

> $b := 250 : h := 300 :$

> $d := 251 :$

> $A_s := 339 :$

> $t_f := 1.2 :$

> $A_f := 120 :$

> $E_f := 165 \cdot 10^3 :$

>

> $q := 0.25 \cdot 0.3 \cdot 25 :$

> $L := 2 :$

>

**TR55**

> $\varepsilon_{f,\,\mathrm{lim}} := 0.008 :$

>

Start by assuming an initial neutral axis

> $x_i := 0.2 \cdot d :$

> $\varepsilon_f := \varepsilon_{f,lim} :$

>

> **for** $i$ **from** 1 **to** 70 **do**

$\# print(' ') :$

$\# print('Iteration', i) :$

$$\varepsilon_i := \frac{\varepsilon_f \cdot x_i}{(h - x_i)} :$$

$$\psi := 1000 \cdot \varepsilon_i \cdot \left(0.5 - \frac{1000}{12} \cdot \varepsilon_i\right) : \delta_G := \frac{8 - 1000 \cdot \varepsilon_i}{4 \cdot (6 - 1000 \cdot \varepsilon_i)} : F_f := \varepsilon_f \cdot E_f \cdot A_f : F_s := f_{yk} \cdot A_s : F_t := F_f + F_s : F_c := \psi \cdot x_i \cdot b \cdot f_{cm} :$$

$$x_i := \frac{F_t}{\psi \cdot b \cdot f_{cm}};$$

**od**:

>

Considered converged

>

> $F_c \approx F_t$;

$$327899.5132 \approx 327900.000 \quad (1)$$

> $\varepsilon_c := \varepsilon_i$:

> $x := x_i$:

>

> $M_{Rd,st} := \left(f_{yk} \cdot A_s \cdot \left(d - \delta_G \cdot x\right) + \varepsilon_f \cdot E_f \cdot A_f \cdot \left(h - \delta_G \cdot x\right)\right) \cdot 10^{-6}$;

$$M_{Rd,st} := 85.11317531 \quad (2)$$

> $P_{fail} := \left(M_{Rd,\,st} - \frac{q \cdot L^2}{8}\right) \cdot \frac{2}{0.75}$;

$$P_{fail} := 224.4684675 \quad (3)$$

**ACI and Kompositförstärkning av betong**

Same debonding strain if partial factors are omitted

>

> $n := 1$ :

> $\varepsilon_{fd} := 0.41 \cdot \mathrm{sqrt}\left(\frac{f_{cm}}{n \cdot E_f \cdot t_f}\right)$;

$$\varepsilon_{fd} := 0.007159354031 \quad (4)$$

Start by assuming an initial neutral axis

> $x_i := 0.2 \cdot d$ :

> $\varepsilon_f := \varepsilon_{fd}$:

>

> **for** $i$ **from** 1 **to** 80 **do**

\# *print*(' ') :

\#*print*('*Iteration*', $i$) :

$\varepsilon_i := \frac{\varepsilon_f \cdot x_i}{(h - x_i)}$ :

$\psi := 1000 \cdot \varepsilon_i \cdot \left(0.5 - \frac{1000}{12} \cdot \varepsilon_i\right)$ : $\delta_G := \frac{8 - 1000 \cdot \varepsilon_i}{4 \cdot \left(6 - 1000 \cdot \varepsilon_i\right)}$ : $F_f := \varepsilon_f \cdot E_f \cdot A_f$: $F_s := f_{yk} \cdot A_s$ : $F_t :=$

$F_f + F_s$ : $F_c := \psi \cdot x_i \cdot b \cdot f_{cm}$ :

$x_i := \frac{F_t}{\psi \cdot b \cdot f_{cm}}$;

**od**:

>

Considered converged

> 

> $F_c \approx F_t$;

$$311252.6823 \approx 311255.2098 \quad (5)$$

> $\varepsilon_c := \varepsilon_i$:

> $x := x_i$:

> 

> $M_{Rd,st} := \left(f_{yk} \cdot A_s \cdot \left(d - \delta_G \cdot x\right) + \varepsilon_f \cdot E_f \cdot A_f \cdot \left(h - \delta_G \cdot x\right)\right) \cdot 10^{-6}$;

$$M_{Rd,st} := 80.33023829 \quad (6)$$

> $P_{fail} := \left(M_{Rd,\,st} - \frac{q \cdot L^2}{8}\right) \cdot \frac{2}{0.75}$;

$$P_{fail} := 211.7139688 \quad (7)$$

**FiB using lower limit 0.0065**

> $\varepsilon_f := 0.0065$ :

> $x_i := 0.2 \cdot d$ :

> 

> **for** $i$ **from** 1 **to** 100 **do**
> $\# print(\text{' '})$ :
> $\# print(\text{'Iteration'}, i)$ :
>
> $\varepsilon_i := \frac{\varepsilon_f \cdot x_i}{(h - x_i)}$ :
>
> $\psi := 1000 \cdot \varepsilon_i \cdot \left(0.5 - \frac{1000}{12} \cdot \varepsilon_i\right) : \delta_G := \frac{8 - 1000 \cdot \varepsilon_i}{4 \cdot \left(6 - 1000 \cdot \varepsilon_i\right)} : F_f := \varepsilon_f \cdot E_f \cdot A_f : F_s := f_{yk} \cdot A_s : F_t := F_f + F_s : F_c := \psi \cdot x_i \cdot b \cdot f_{cm}$ :
>
> $x_i := \frac{F_t}{\psi \cdot b \cdot f_{cm}}$;
>
> **od**:

> 

Converged

> 

> $F_c \approx F_t$;

$$298195.9795 \approx 298200.0000 \quad (8)$$

> $\varepsilon_c := \varepsilon_i$:

> $x := x_i$:

> 

> $M_{Rd,st} := \left(f_{yk} \cdot A_s \cdot \left(d - \delta_G \cdot x\right) + \varepsilon_f \cdot E_f \cdot A_f \cdot \left(h - \delta_G \cdot x\right)\right) \cdot 10^{-6}$;

(9)

$$M_{Rd,st} := 76.56278628 \quad \textbf{(9)}$$

>

> $P_{fail} := \left(M_{Rd,\,st} - \frac{q \cdot L^2}{8}\right) \cdot \frac{2}{0.75}$;

$$P_{fail} := 201.6674301 \quad \textbf{(10)}$$

**FiB using lower limit 0.0085**

> $\varepsilon_f := 0.0085$ :

> $x_i := 0.2 \cdot d$ :

>

> **for** $i$ **from** 1 **to** 70 **do**

\# *print*(' ') :

\#*print*('*Iteration*' , $i$) :

$\varepsilon_i := \frac{\varepsilon_f \cdot x_i}{(h - x_i)}$ :

$\psi := 1000 \cdot \varepsilon_i \cdot \left(0.5 - \frac{1000}{12} \cdot \varepsilon_i\right)$ : $\delta_G := \frac{8 - 1000 \cdot \varepsilon_i}{4 \cdot (6 - 1000 \cdot \varepsilon_i)}$ : $F_f := \varepsilon_f \cdot E_f \cdot A_f$ : $F_s := f_{yk} \cdot A_s$ : $F_t := F_f + F_s$ : $F_c := \psi \cdot x_i \cdot b \cdot f_{cm}$ :

$x_i := \frac{F_t}{\psi \cdot b \cdot f_{cm}}$;

**od**:

>

Considered converged

>

> $F_c \approx F_t$;

$$337799.9300 \approx 337800.0000 \quad \textbf{(11)}$$

> $\varepsilon_c := \varepsilon_i$:

> $x := x_i$:

>

> $M_{Rd,st} := \left(f_{yk} \cdot A_s \cdot \left(d - \delta_G \cdot x\right) + \varepsilon_f \cdot E_f \cdot A_f \cdot \left(h - \delta_G \cdot x\right)\right) \cdot 10^{-6}$;

$$M_{Rd,st} := 87.94758345 \quad \textbf{(12)}$$

>

> $P_{fail} := \left(M_{Rd,\,st} - \frac{q \cdot L^2}{8}\right) \cdot \frac{2}{0.75}$;

$$P_{fail} := 232.0268892 \quad \textbf{(13)}$$

>

# Parameter table:

Test protocol :
Tester :
Customer :
Test standard :
Strength grade :
Creation date :
Age : 0 T
Other :

Type strain extensometer :
Machine data : Controller TT0322
PistonStroke
LoadCell 3 MN

# Results:

| Nr | Date | ID | a mm | b mm | A mm² |
|---|---|---|---|---|---|
| 1 | 24.02.2021 | Test A1 28 days | 100,0 | 100,0 | 10000,0 |
| 2 | 24.02.2021 | Test A1 28 days | 100,0 | 100,0 | 10000,0 |
| 3 | 24.02.2021 | Test A1 28 days | 100,0 | 100,0 | 10000,0 |
| 4 | 25.02.2021 | Test B1 28 days | 100,0 | 100,0 | 10000,0 |
| 5 | 25.02.2021 | Test B1 28 days | 100,0 | 100,0 | 10000,0 |
| 6 | 25.02.2021 | Test B1 28 days | 100,0 | 100,0 | 10000,0 |
| 7 | 18.03.2021 | Test A2 Test 1 reference beams | 100,0 | 100,0 | 10000,0 |
| 8 | 18.03.2021 | Test A2 Test 1 reference beams | 100,0 | 100,0 | 10000,0 |
| 9 | 18.03.2021 | Test A2 Test 1 reference beams | 100,0 | 100,0 | 10000,0 |
| 10 | 18.03.2021 | Test B2 Test 1 reference beams | 100,0 | 100,0 | 10000,0 |
| 11 | 18.03.2021 | Test B2 Test 1 reference beams | 100,0 | 100,0 | 10000,0 |
| 12 | 18.03.2021 | Test B2 Test 1 reference beams | 100,0 | 100,0 | 10000,0 |
| 13 | 10.04.2021 | Test A3 CFRP beams | 100,0 | 100,0 | 10000,0 |
| 14 | 10.04.2021 | Test A3 CFRP beams | 100,0 | 100,0 | 10000,0 |
| 15 | 10.04.2021 | Test A3 CFRP beams | 100,0 | 100,0 | 10000,0 |
| 16 | 10.04.2021 | Test B3 CFRP beams | 100,0 | 100,0 | 10000,0 |
| 17 | 10.04.2021 | Test B3 CFRP beams | 100,0 | 100,0 | 10000,0 |
| 18 | 10.04.2021 | Test B3 CFRP beams | 100,0 | 100,0 | 10000,0 |

| Nr | h mm | $F_m$ kN | $\sigma_m$ N/mm² |
|---|---|---|---|
| 1 | 100,0 | 647,29 | 64,73 |
| 2 | 100,0 | 643,97 | 64,40 |
| 3 | 100,0 | 656,25 | 65,63 |
| 4 | 100,0 | 594,63 | 59,46 |
| 5 | 100,0 | 591,36 | 59,14 |
| 6 | 100,0 | 595,35 | 59,53 |
| 7 | 100,0 | 739,45 | 73,95 |
| 8 | 100,0 | 731,00 | 73,10 |
| 9 | 100,0 | 735,94 | 73,59 |
| 10 | 100,0 | 686,21 | 68,62 |
| 11 | 100,0 | 671,60 | 67,16 |
| 12 | 100,0 | 670,13 | 67,01 |
| 13 | 100,0 | 792,17 | 79,22 |
| 14 | 100,0 | 790,91 | 79,09 |
| 15 | 100,0 | 783,40 | 78,34 |
| 16 | 100,0 | 717,59 | 71,76 |
| 17 | 100,0 | 730,41 | 73,04 |
| 18 | 100,0 | 713,51 | 71,35 |

# Series graphics:

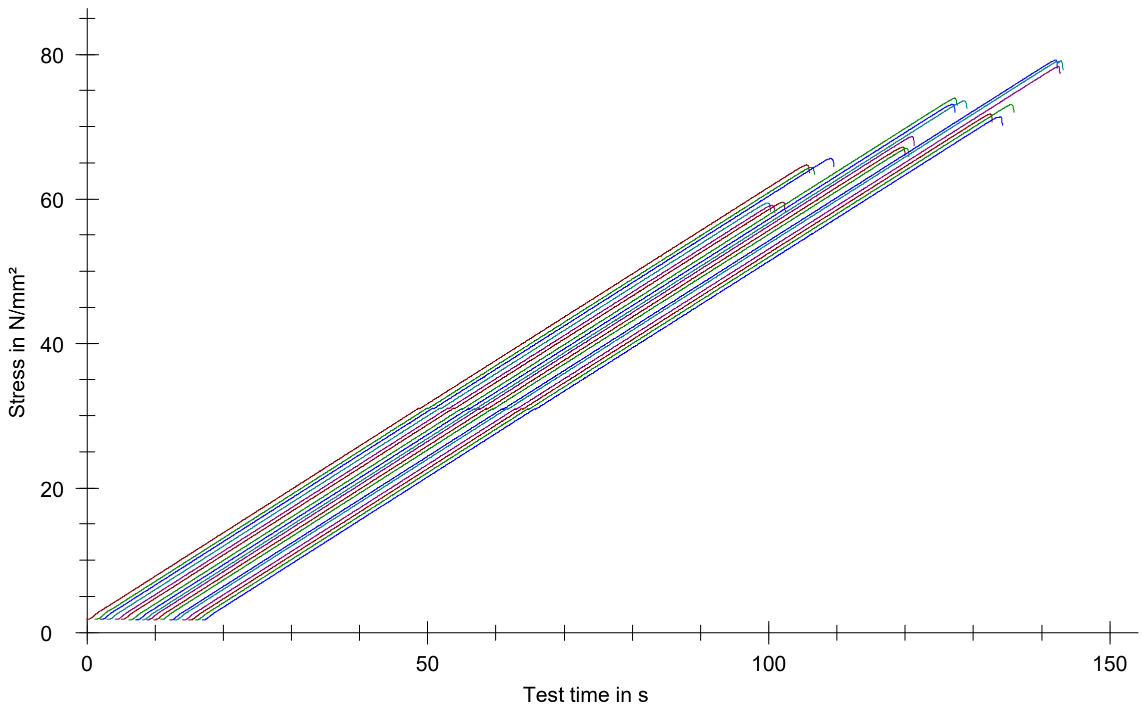


# Statistics:

| Series n = 18 | a mm | b mm | A mm² | h mm | $F_m$ kN | $\sigma_m$ N/mm² |
|---|---|---|---|---|---|---|
| $\bar{x}$ | 100,0 | 100,0 | 10000,0 | 100,0 | 693,96 | 69,40 |
| s | 0,0 | 0,0 | 0,0 | 0,0 | 65,02 | 6,50 |
| $\nu$ | 0,00 | 0,00 | 0,00 | 0,00 | 9,37 | 9,37 |

# Parameter table:

Test protocol :
Tester :
Customer :
Test standard :
Strength grade :
Creation date :
Age : 0 T
Other :

Type strain extensometer :
Machine data : Controller TT0322
PistonStroke
LoadCell 3 MN

# Results:

| Nr | Date | ID | d mm | A mm² | h mm | $F_m$ kN | $\sigma_m$ N/mm² |
|---|---|---|---|---|---|---|---|
| 1 | 24.02.2021 | Test A1 | 150,0 | 17671,5 | 300,0 | 250,99 | 14,20 |
| 2 | 24.02.2021 | Test A1 | 150,0 | 17671,5 | 300,0 | 210,96 | 11,94 |
| 3 | 25.02.2021 | Test B1 | 150,0 | 17671,5 | 300,0 | 234,15 | 13,25 |
| 4 | 25.02.2021 | Test B1 | 150,0 | 17671,5 | 300,0 | 239,81 | 13,57 |

# Series graphics:

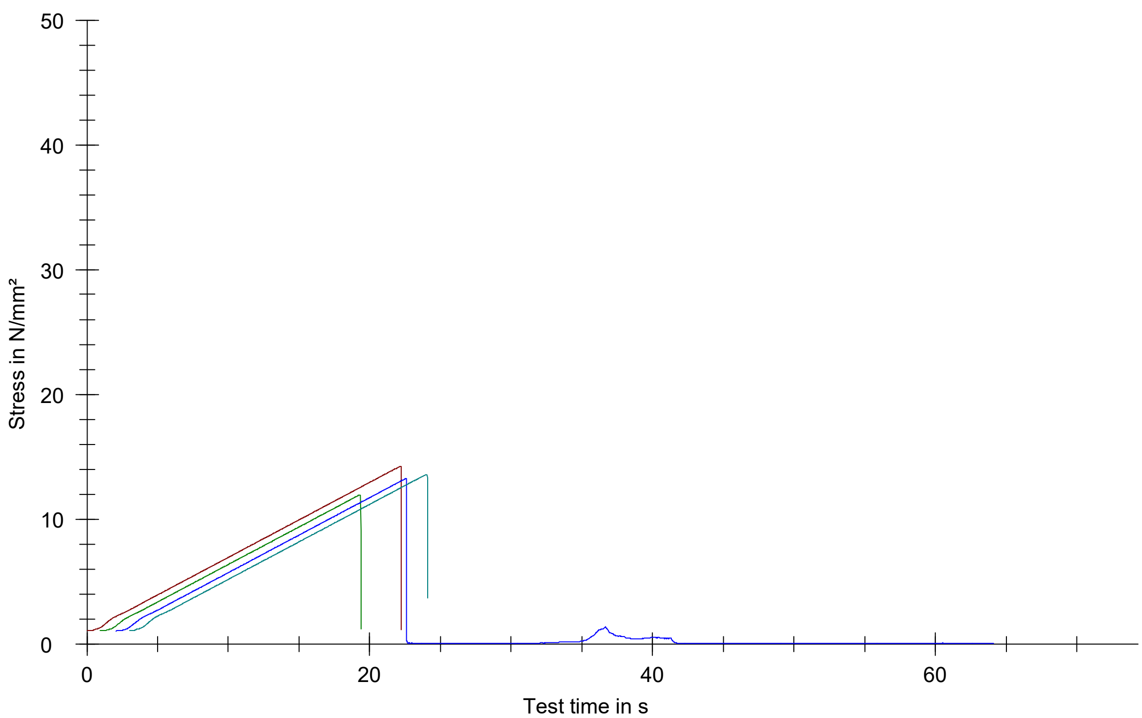


# Statistics:

| Series n = 4 | d mm | A mm² | h mm | $F_m$ kN | $\sigma_m$ N/mm² |
|---|---|---|---|---|---|
| $\bar{x}$ | 150,0 | 17671,5 | 300,0 | 233,98 | 13,24 |
| s | 0,0 | 0,0 | 0,0 | 16,86 | 0,95 |
| ν | 0,00 | 0,00 | 0,00 | 7,21 | 7,21 |

# Parameter table:

Test protocol :
Tester :
Customer :
Test standard : EN12390-13 method A
Strength grade :
Creation date :
Age : 0 T
Other :

Type strain extensometer :
Machine data : Controller TT0322
PistonStroke
LoadCell 3 MN
Extensometer
Extensometer2

# Results:

| Nr | $\varepsilon_{b2,E1}$ mm | $\varepsilon_{b2,E2}$ mm | $\varepsilon_{b3,E1}$ mm | $\varepsilon_{b3,E2}$ mm | $\Delta\varepsilon_{b23,E}$ % | $\Delta\varepsilon_{b23,E}$ % | $\Delta\varepsilon_{b3,E1}$ % | $\sigma_{m\,a,1}$ N/mm | $\sigma_{m\,b,0}$ N/mm | $\varepsilon_{a,1}$ mm | $\varepsilon_{b,0}$ mm | $E_{C,0}$ N/mm | $\sigma_{m\,a,3}$ N/mm | $\sigma_{m\,b,2}$ N/mm | $\varepsilon_{a,3}$ mm | $\varepsilon_{b,2}$ mm | $E_{C,S}$ N/mm |
|---|---|---|---|---|---|---|---|---|---|---|---|---|---|---|---|---|---|
| max. | | | | | 10,0( | 10,0( | 20,0 | | | | | | | | | | |
| min | | | | | -10,0( | -10,0( | -20,0 | | | | | | | | | | |
| 1 | 0,173 | 0,081 | 0,174 | 0,080 | 0,12 | 0,08 | 18,3 | 17,02 | 6,04 | 0,222 | 0,080 | 15492 | 17,05 | 5,96 | 0,217 | 0,088 | 17145 |
| 2 | 0,182 | 0,058 | 0,184 | 0,058 | 0,28 | 0,11 | >26,0 | - | - | - | - | - | - | - | - | - | - |
| 3 | 0,204 | 0,059 | 0,205 | 0,052 | 0,08 | 3,04 | >29,6 | 17,03 | 6,03 | 0,220 | 0,046 | 12614 | 17,05 | 5,94 | 0,224 | 0,067 | 14197 |
| 4 | 0,163 | 0,049 | 0,163 | 0,048 | 0,1( | 0,24 | >27,2 | - | - | - | - | - | - | - | - | - | - |
| 5 | 0,133 | 0,052 | 0,133 | 0,052 | 0,01 | 0,24 | >22,0 | 16,04 | 6,05 | 0,167 | 0,050 | 17041 | 16,04 | 5,92 | 0,173 | 0,068 | 19319 |
| 6 | 0,132 | 0,080 | 0,135 | 0,080 | 0,56 | 0,09 | 12,7 | 16,03 | 6,03 | 0,260 | 0,080 | 11089 | 16,03 | 5,96 | 0,269 | 0,118 | 13348 |

# Series graphics:

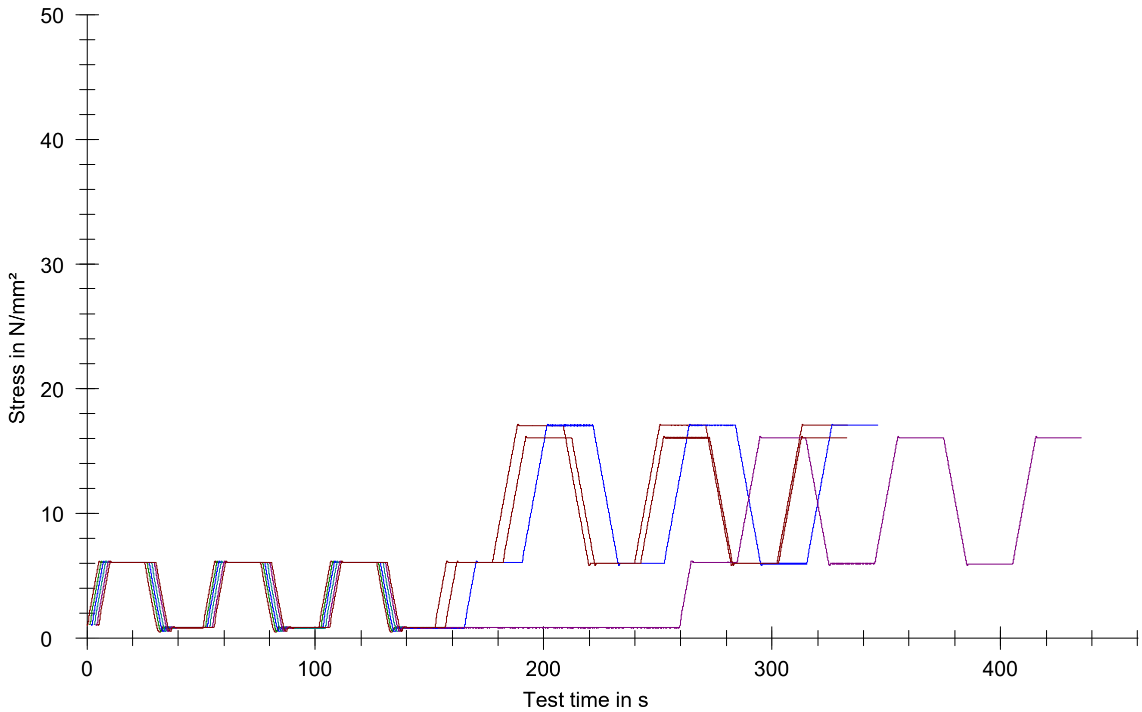


# Statistics:

| Series n = 6 | $\sigma_m$ N/mm² | $E_{C,0}$ N/mm² | $E_{C,S}$ N/mm² |
|---|---|---|---|
| $\bar{x}$ | 13,15 | 14059,42 | 16002,64 |
| s | 5,44 | 2699,23 | 2745,46 |
| ν | 41,34 | 19,20 | 17,16 |

# Parameter table:

Test protocol : Masterthesis
Tester : Test 1 Capasity
Creation date : 1.12.2015

Type strain extensometer :
Machine data : Controller TT0322
PistonStroke
LoadCell 400 kN
Extensometer
Extensometer2

# Results:

| Date | ID | a mm | b mm | h mm | $F_m$ kN |
|---|---|---|---|---|---|
| 18.03.2021 | Beam B2 | 250,0 | 2200,0 | 300,0 | 132,07 |
| 18.03.2021 | Beam A6 | 250,0 | 2200,0 | 300,0 | 132,31 |
| 18.03.2021 | Beam B1 | 250,0 | 2200,0 | 300,0 | 129,41 |
| 18.03.2021 | Beam A1 | 250,0 | 2200,0 | 300,0 | 131,18 |
| 06.04.2021 | Beam A2 CFRP 0% | 250,0 | 2200,0 | 300,0 | 208,37 |
| 06.04.2021 | Beam A5 CFRP 70% | 250,0 | 2200,0 | 300,0 | 211,10 |
| 07.04.2021 | Beam A3 CFRP 50% | 250,0 | 2200,0 | 300,0 | 192,39 |
| 07.04.2021 | Beam A4 CFRP 30% | 250,0 | 2200,0 | 300,0 | 205,43 |
| 08.04.2021 | Beam B3 CFRP 50% | 250,0 | 2200,0 | 300,0 | 207,85 |
| 08.04.2021 | Beam B4 CFRP 30% | 250,0 | 2200,0 | 300,0 | 207,63 |
| 12.04.2021 | Beam B5 CFRP 0% | 250,0 | 2200,0 | 300,0 | 203,88 |
| 12.04.2021 | Beam B6 CFRP 70% | 250,0 | 2200,0 | 300,0 | 199,02 |

# Series graphics:

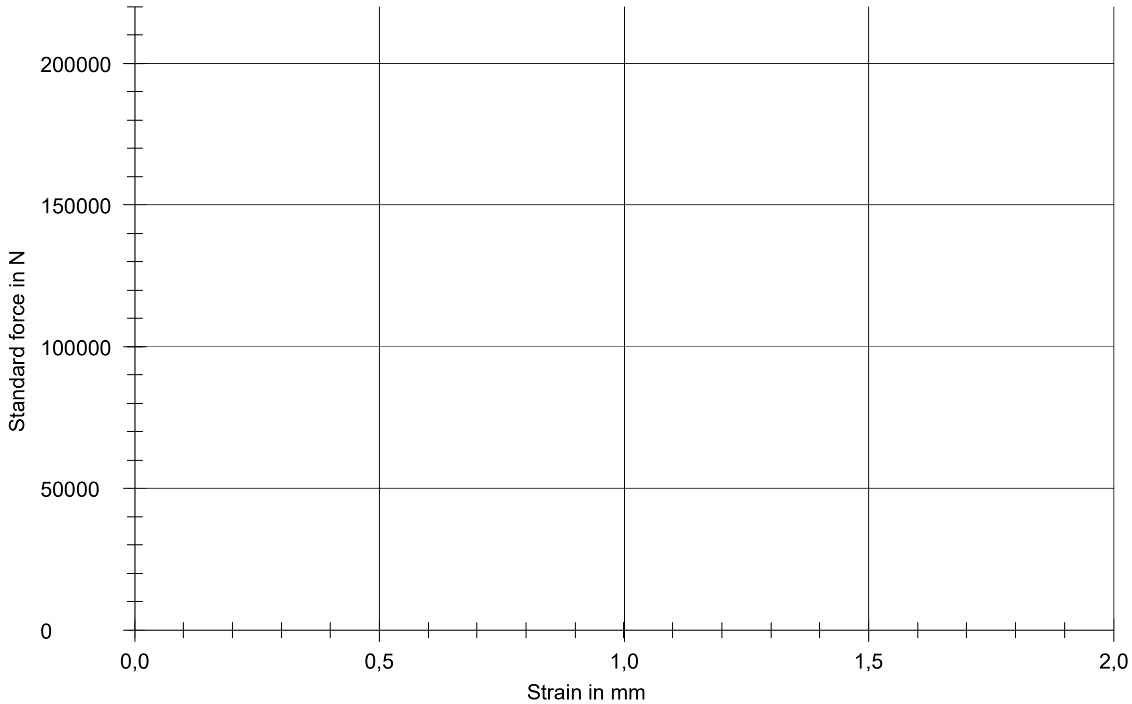


# Statistics:

| Series n = 12 | a mm | b mm | h mm | $F_m$ kN |
|---|---|---|---|---|
| $\bar{x}$ | 250,0 | 2200,0 | 300,0 | 180,05 |
| s | 0,0 | 0,0 | 0,0 | 36,38 |
| $\nu$ | 0,00 | 0,00 | 0,00 | 20,20 |